# UC Riverside

## UC Riverside Electronic Theses and Dissertations

### Title

Sensitivity of Classic and Novel Proxies to Oxygen Minimum Zone Variability of the Eastern Tropical North Pacific

### Permalink

https://escholarship.org/uc/item/3fp5q7p8

### Author

Choumiline, Konstantin

### Publication Date

2019

Peer reviewed|Thesis/dissertation

eScholarship.org Powered by the California Digital Library
University of California

UNIVERSITY OF CALIFORNIA
RIVERSIDE

# Sensitivity of Classic and Novel Proxies to Oxygen Minimum Zone Variability of the Eastern Tropical North Pacific

A Dissertation submitted in partial satisfaction
of the requirements for the degree of

Doctor of Philosophy

in

Geological Sciences

by

Konstantin Choumiline

December 2019

Dissertation Committee:
Dr. Timothy W. Lyons, Chairperson
Dr. Gordon D. Love
Dr. Sandra Kirtland Turner

Copyright by
Konstantin Choumiline
2019

The Dissertation of Konstantin Choumiline is approved:

_____

_____

_____

Committee Chairperson

University of California, Riverside

# ACKNOWLEDGMENTS

First, I want to thank my qualifying exam and dissertation committee members: Timothy W. Lyons, Gordon Love, Sandra Kirtland Turner, Richard Minnich, and James Sickman for taking the time to read my proposals and/or dissertation and for all the life lessons and advice. Tim, thank you for immediately believing in me and for showing interest in my research goals. There is a chance that I would have done a completely different study if you did not encourage me to apply to UCR as your grad student after I first showed you my research plan. I truly value all the insights and the feedback, reassurance, and most importantly the independence to wander towards pretty much any scientific path I wanted to. Thank you also, for teaching me your unique way of selling science. This skill has truly opened many doors to summer schools, workshops, and collaborations.

Multiple people contributed, directly and indirectly, to make this work a reality: Ligia Perez-Cruz, Morten B. Andersen, Jose D. Carriquiry, Steven M. Bates, Stephen J. Romaniello, Kimberly Lau, Geoff Gilleaudeau, Rob Raiswell, Fernando Aguirre-Bahena, and many others. All the wonderful and friendly folks at UCR whom I interacted with including staff, fellow grad students, and faculty. I learned valuable lessons from you all. Being able to teach was a privilege and an enriching experience. My students taught me how fulfilling could mentoring be. I also thank all my friends and loved ones for keeping me sane in this journey. Morten B. Andersen, you truly are the mentor and co-advisor of my isotope work! I am forever grateful for the clean lab training and for making me feel at

home in Cardiff. I hope to continue this collaboration endlessly. Ligia, you have an exclusive dedication here and special place in my heart. I am forever grateful for all the unconditional support you have provided me. Thank you for sharing valuable samples, inviting me to unique collaborations and expeditions, and for opening your heart to a true friendship. I will never forget those extended shifts in the middle of the ocean subsampling muddy sediments of the Gulf of California. Gracias por todo y en especial por tu amistad tan genuina.

Thank you, Mom and Dad, for fostering essential values. I especially dedicate this to my father from whom I learned how truly challenging, but also genuinely exciting and rewarding the life of an academic can be. He has been and will always be my true inspiration and one of the reasons I became the scientist I am today.

Importantly, I would like to thank all the taxpayers who contributed towards the funding agencies that sponsored my tuition, fees, stipend, and research. Scientific advancement should have no borders and international collaborations are the only way towards this goal. Truly thankful to UC MEXUS – CONACYT Doctoral Fellowship, UCR Dean's Distinguished Fellowship, UC MEXUS Dissertation Grant, and NASA Astrobiology Institute.

Ultimately, I would have loved to say that completing a Ph.D. program was a smooth and easy task, but as for most people, it was not. Nonetheless, more than ever I feel that I could not have picked a better profession. The desire to learn and share this knowledge kept me motivated even in the long days and nights of lab work and dissertation writing.

ABSTRACT OF THE DISSERTATION

Sensitivity of Classic and Novel Proxies to Oxygen Minimum Zone Variability of the Eastern Tropical North Pacific

by

Konstantin Choumiline

Doctor of Philosophy, Graduate Program in Geological Sciences
University of California, Riverside, December 2019
Dr. Timothy W. Lyons, Chairperson

Accurately recreating how Oxygen Minimum Zones (OMZs) changed through time requires the combined use of classic and novel proxy approaches. Short-term proxy trends are often deemphasized in favor of the major patterns despite having the potential to capture environmental shifts in the OMZs. To address this problem decadal-to-millennial OMZ variations were reconstructed over the last 70 kyr BP in a major OMZ—the Eastern Tropical North Pacific (ETNP). Specifically, sedimentary material collected from basinal settings with diverse levels of restriction and nutrient availability in the Gulf of California were analyzed: Alfonso, La Paz, and Pescadero. This dissertation emphasizes a broad range of classic and novel paleoredox and paleoproductivity proxies ($CaCO_3$, C-S-Fe relationships, Ba, Cd, Cu, Mo, Mn, Ni, V, Zn, as well as U concentrations and isotope ratios).

Global circulation effects on the availability of nutrients and deep-water oxygenation are the main controls for OMZ variability over glacial-interglacial time scales. Newly-generated data reveal that the ETNP OMZ achieved its peak strength during warm Marine Isotope Stages (MIS) accompanied by sea-level highstands (MIS3 and Holocene) exposed by high Mo, V, authigenic U ($U_{auth}$) and higher $\delta^{238}U$. Conversely, the cold sea-level lowstands (MIS4, LGM) often manifested as low Mo, V, and Fe/Al values indicating exposure of the marine basins to oxygenated waters. When it comes to submillennial variability, Heinrich events and cold Dansgaard-Oeschger phases enhanced the ventilation of the ETNP, as fingerprinted in low Mo, V, U, and lower $\delta^{238}U$ values. The mechanisms that control decadal-to-centennial oxygen variability in the ETNP remain in the shadows but are likely influenced by solar forcing indirectly driving the intensity changes of the Pacific Walker Circulation (PWC). During the Little Ice Age, solar irradiance was at its lowest for the past millennium, which strengthened the PWC. The latter created more frequent La Niña-like conditions that enhanced upwelling of nutrient-rich waters of the west coast of North America, driving productivity and reducing bottom oxygen levels, as seen in the ETNP records.

This research brings new insights into the biogeochemistry of U in OMZs, revealing the sources and causes of its isotopic fractionation and enrichment mechanisms.

**TABLE OF CONTENTS**

## LIST OF FIGURES

## LIST OF TABLES

# INTRODUCTION AND MOTIVATION

## INTRODUCTION

Many studies have recognized the importance of climate on oxygen availability in the oceans. A tight metabolic balance between photosynthesis and respiration in the ocean creates a surplus or deficit of dissolved oxygen at greater depths, usually starting below the photic zone. The shortage of $O_2$ causes the formation of Oxygen Minimum Zones (OMZs). Such zones are abundant in certain coastal regions of the ocean, with one of the largest being the Eastern Tropical North Pacific (ETNP). In the ETNP, the OMZ varies broadly between 100 and 900 m (Karstensen et al., 2008) and reaches $O_2$ concentrations below 0.1 ml/L – a condition called oceanic anoxia. The spatial extent of OMZs directly impacts the availability of marine resources to coastal populations, especially relevant for developing nations that rely on fisheries (Levin, 2018). While OMZs are commonly thought to expand in response to increasing climate (Oschlies et al., 2018; Shaffer et al., 2009; Praetorius et al., 2015; Breitburg et al., 2018), more studies are needed to properly predict the consequences of this phenomenon across various spatiotemporal scales.

Our ability to reconstruct OMZ variability of the past depends on the resolution of our records; reliability of age models; and, most importantly, the proper understanding of our paleoproxies. Most of these proxies rely on authigenic elemental enrichments that are usually microbially mediated. Several classic and novel geochemical proxies for paleoproductivity and paleoxygenation will be mentioned throughout the dissertation, with particular emphasis on U and its isotopes (Dymond et al., 1992; Calvert and Pedersen, 1993; Calvert et al., 1996; Morford and Emerson, 1999; Eagle et al., 2003; Tribovillard et al., 2006; Weyer et al., 2008; Brennecka et al., 2010; Andersen et al., 2014; Schoepfer et al., 2015). This dissertation provides new insights into the geochemistry of this element, which will be discussed in detail in every chapter. Across the dissertation I will focus on climatic and oceanographic processes that control productivity and oxygenation of marine basins on annual, decadal, millennial, and multimillennial timescales.

Additionally, I will assess the contribution of redox-sensitive trace elements through marine snow aggregates, being via detrital supply or authigenic enrichments. The latter has important implications for the way we interpret paleoceanographic records using elements like U in the geologic past.

This dissertation will focus on providing mechanistic explanations for OMZ variability in the ETNP, mostly manifested in changes in oxygenation. Chapter 1 outlines a reconstruction of ETNP OMZ variability of the last millennium on a decadal timescale and proposes the core climatic triggers of deoxygenation and reoxygenation events in coastal regions. Chapter 2 focuses on the multimillennial OMZ variability over Marine Isotope Stages (MIS) as the world transitioned from a colder MIS4 to significantly warmer MIS3 (Lisiecki and Raymo, 2005). This chapter also addresses the effect of short-scale events like Heinrich and Dansgaard–Oeschger on productivity and oxygenation of marine basins (Bond et al., 1992; 1993; Alley, 1998). Chapter 3 summarizes the study of sources that contribute different amounts of U into coastal marine basins. This chapter provides new insights on water column processes that can trigger authigenic U enrichments in marine snow aggregates associated with redox microniches. It also evaluates the differences between the abundances of $^{238}U$, $^{235}U$, and $^{234}U$ isotopes in settling particles and establishes the potential sources of variability and fractionation mechanisms. Importantly, in this chapter, the use of geochemical toolboxes involving both major and trace element ratios and U isotope relationships is suggested as a way of separating biotic and abiotic processes that can lead to authigenic U formation.

To accomplish my paleoceanographic reconstructions, I use sediment cores collected during the PALEOMAR-I and DIPAL-III expeditions on R/V El Puma (UNAM, Mexico) and IMAGES VIII / MD126 MONA aboard R/V Marion Dufresne (IPEV, France). The following cores were used to produce geochemical records described in this dissertation: MD02-2510, DIPAL-III T2,

PALEOMAR-I C37A, C42A, and C52A. Basic stratigraphic description and other supporting data on the studied cores were taken from Beaufort et al. (2003), Choumiline (2011), Escorza-Reyes (2013), Staines-Urías et al. (2015), and Choumiline et al. (2019). The sediment trap material used in this research was collected between 2002 and 2012 by members of the Cuenca Alfonso Time Series (CATS), initiated in CICIMAR-IPN (La Paz, Baja California Sur, Mexico). In addition to the new data of this study, some appear in Aguirre-Bahena (2007), Rodríguez-Castañeda (2008), Choumiline et al. (2010), Choumiline (2011), Rochín-Bañaga (2014), and Silverberg et al. (2014). The above references will be cited in each chapter accordingly.

Most of the sample preparation and analyses were performed at the University of California Riverside. Selected samples were analyzed for U isotopes at Cardiff University and Arizona State University.

**REFERENCES**


Aguirre-Bahena, F. (2007). Cambios temporales en los componentes y flujos de la materia en hundimiento en Cuenca Alfonso, Bahía de La Paz, durante el periodo 2002-2005. Master's Thesis, Centro Interdisciplinario de Ciencias Marinas - Instituto Politécnico Nacional.

Alley, R.B. (1998). Icing the North Atlantic. Nature 392, 335-337.
Andersen, M.B., Romaniello, S., Vance, D., Little, S.H., Herdman, R., and Lyons, T.W. (2014). A modern framework for the interpretation of 238U/235U in studies of ancient ocean redox. Earth and Planetary Science Letters 400, 184-194.

Anderson, R.F., Sachs, J.P., Fleisher, M.Q., Allen, K.A., Yu, J., Koutavas, A., and Jaccard, S.L. (2019). Deep-Sea Oxygen Depletion and Ocean Carbon Sequestration During the Last Ice Age. Global Biogeochemical Cycles 33, 301-317.

Beaufort, L., et al. (2002), Cruise report MD126 MONA (Marges Ouest Nord Américaines) – IMAGESVIII, 452 pp., Inst. Polaire Fr. Paul-Emile Victor, Plouzaneé, France.

Bond, G., Broecker, W., Johnsen, S., McManus, J., Labeyrie, L., Jouzel, J., and Bonani, G. (1993). Correlations between climate records from North Atlantic sediments and Greenland ice. Nature 365, 143-147.

Bond, G., Heinrich, H., Broecker, W., Labeyrie, L., McManus, J., Andrews, J., Huon, S., Jantschik, R., Clasen, S., Simet, C., Tedesco, K., Klas, M., Bonani, G., and Ivy, S. (1992). Evidence for massive discharges of icebergs into the North Atlantic ocean during the last glacial period. Nature 360, 245-249.

Breitburg, D., Levin, L.A., Oschlies, A., Grégoire, M., Chavez, F.P., Conley, D.J., Garçon, V., Gilbert, D., Gutiérrez, D., Isensee, K., Jacinto, G.S., Limburg, K.E., Montes, I., Naqvi, S.W.A., Pitcher, G.C., Rabalais, N.N., Roman, M.R., Rose, K.A., Seibel, B.A., Telszewski, M., Yasuhara, M., and Zhang, J. (2018). Declining oxygen in the global ocean and coastal waters. Science 359.

Brennecka, G.A., Borg, L.E., Hutcheon, I.D., Sharp, M.A., and Anbar, A.D. (2010). Natural variations in uranium isotope ratios of uranium ore concentrates: Understanding the 238U/235U fractionation mechanism. Earth and Planetary Science Letters 291, 228-233.

Calvert, S.E., Bustin, R.M., and Ingall, E.D. (1996). Influence of water column anoxia and sediment supply on the burial and preservation of organic carbon in marine shales. Geochimica et Cosmochimica Acta 60, 1577-1593.

Calvert, S.E., and Pedersen, T.F. (1993). Geochemistry of Recent oxic and anoxic marine sediments: Implications for the geological record. Marine Geology 113, 67-88.

Choumiline, K. (2011). Geoquímica de la materia particulada en hundimiento y de los sedimentos recientes de Cuenca Alfonso, Bahía de La Paz. Master's Thesis, Centro Interdisciplinario de Ciencias Marinas - Instituto Politécnico Nacional.

Choumiline, K., Rodríguez-Castañeda, A.P., Silverberg, N., Aguirre-Bahena, F., Sapozhnikov, D., and Pérez-Cruz, L. (2010). "Arsenic and uranium in the settling particulate matter and sediments of Alfonso Basin, La Paz Bay", in: Proceedings of the 13th International Conference on Water-Rock Interaction. (Guanajuato).

Dymond, J., Suess, E., and Lyle, M. (1992). Barium in deep-sea sediment. A geochemical proxy for paleoproductivity. Paleoceanography 7, 163-181.

Eagle, M., Paytan, A., Arrigo, K.R., Van Dijken, G., and Murray, R.W. (2003). A comparison between excess barium and barite as indicators of carbon export. Paleoceanography 18, 1021.

Escorza-Reyes, M. (2013). Reconstrucción paleoceanográfica y paleoclimática de los últimos 18,000 años en la región suroriental del golfo de California a partir de la interpretación de indicadores geoquímicos Master's Thesis, Universidad Nacional Autónoma de México.

Karstensen, J., Stramma, L., and Visbeck, M. (2008). Oxygen minimum zones in the eastern tropical Atlantic and Pacific oceans. Progress in Oceanography 77, 331-350.
Levin, L.A. (2018). Manifestation, Drivers, and Emergence of Open Ocean Deoxygenation. Annual Review of Marine Science.

Lisiecki, L.E., and Raymo, M.E. (2005). A Pliocene-Pleistocene stack of 57 globally distributed benthic $\delta^{18}O$ records. Paleoceanography 20.

Morford, J.L., and Emerson, S. (1999). The geochemistry of redox sensitive trace metals in sediments. Geochimica et Cosmochimica Acta 63, 1735-1750.

Oschlies, A., Brandt, P., Stramma, L., and Schmidtko, S. (2018). Drivers and mechanisms of ocean deoxygenation. Nature Geoscience 11, 467-473.

Praetorius, S.K., Mix, A.C., Walczak, M.H., Wolhowe, M.D., Addison, J.A., and Prahl, F.G. (2015). North Pacific deglacial hypoxic events linked to abrupt ocean warming. Nature 527, 362-366.

Rochin-Bañaga, H. (2014). Contribución de cocolitóforos y foraminíferos al flujo de carbonato de calcio en Cuenca Alfonso, B.C.S. Master's Thesis, Centro Interdisciplinario de Ciencias Marinas - Instituto Politécnico Nacional.

Rodríguez-Castañeda, A.P. (2008). Variación de flujos de los elementos particulados en Cuenca Alfonso, Bahía de La Paz, en el periodo 2002-2005. Ph.D. Thesis, Centro Interdisciplinario de Ciencias Marinas - Instituto Politécnico Nacional.

Schoepfer, S.D., Shen, J., Wei, H., Tyson, R.V., Ingall, E., and Algeo, T.J. (2015). Total organic carbon, organic phosphorus, and biogenic barium fluxes as proxies for paleomarine productivity. Earth-Science Reviews 149, 23-52.

Shaffer, G., Olsen, S.M., and Pedersen, J.O.P. (2009). Long-term ocean oxygen depletion in response to carbon dioxide emissions from fossil fuels. Nature Geoscience 2, 105-109.

Silverberg, N., Aguirre-Bahena, F., and Mucci, A. (2014). Time-series measurements of settling particulate matter in Alfonso Basin, La Paz Bay, southwestern Gulf of California. Continental Shelf Research 84, 169-187.

Staines-Urías, F., González-Yajimovich, O., and Beaufort, L. (2015). Reconstruction of past climate variability and ENSO-like fluctuations in the southern Gulf of California (Alfonso Basin) since the last glacial maximum. Quaternary Research 83, 488-501.

Tribovillard, N., Algeo, T.J., Lyons, T., and Riboulleau, A. (2006). Trace metals as paleoredox and paleoproductivity proxies: An update. Chemical Geology 232, 12-32.

Weyer, S., Anbar, A.D., Gerdes, A., Gordon, G.W., Algeo, T.J., and Boyle, E.A. (2008). Natural fractionation of 238U/235U. Geochimica et Cosmochimica Acta 72, 345-359.

# CHAPTER 1:

# SCENARIOS OF DEOXYGENATION OF THE EASTERN TROPICAL NORTH PACIFIC DURING THE PAST MILLENNIUM AS A WINDOW INTO THE FUTURE OF OXYGEN MINIMUM ZONES

## PREFACE

The contents of this chapter have been published as:

Choumiline, K., Pérez-Cruz, L., Gray, A.B., Bates, S.M., and Lyons, T.W. (2019). Scenarios of Deoxygenation of the Eastern Tropical North Pacific During the Past Millennium as a Window Into the Future of Oxygen Minimum Zones. Frontiers in Earth Science 7.

## ABSTRACT

Diverse studies predict global expansion of Oxygen Minimum Zones (OMZs) as a consequence of anthropogenic global warming. While the observed dissolved oxygen concentrations in many coastal regions are slowly decreasing, sediment core paleorecords often show contradictory trends. This is the case for numerous high-resolution reconstructions of oxygenation in the Eastern Tropical North Pacific (ETNP). While major shifts in redox conditions of the ETNP are dominated by glacial-interglacial cycling, important fluctuations also occur in response to minor climatic and oceanographic perturbations. It is important to understand these scenarios of past redox variation, as they are the closest analog for near future climate and oceanographic change. We present recently collected sediment core proxy records from the Gulf of California in which we reproduce the variability of productivity and oxygenation of the ETNP OMZ during the past millennium. We emphasize paleoproductivity ($C_{org}$, Ni, $B_{aexcess}$) and paleoredox indicators (Mo, Cd, V, $U_{auth}$) in sediment cores collected in Alfonso and La Paz basins and compare these OMZ records with other archives of the Eastern Pacific. Our findings indicate that the OMZ expanded in response to increased upwelling and productivity during cold intervals of the early 1400s, early 1500s, late 1600s, and early 1800s AD (evidenced by higher Ni, V, Cd, Mo, and $U_{auth}$). The most hypoxic times corresponded to the beginning of the Little Ice Age (expressed in elevated Mo). Significant OMZ contractions occurred around late 1300s, early 1700s,

and late 1900s AD after reoxygenation events that were instigated by low productivity (lower Ni, V, Cd, Mo, and $U_{auth}$). The mechanisms that control decadal-to-centennial oxygen variability in the ETNP remain unidentified but are likely influenced by solar forcing not only driving migrations of the Intertropical Convergence Zone (ITCZ) but more importantly changes in the intensity of the Pacific Walker Circulation (PWC). During the Little Ice Age solar irradiance was at its lowest for the past millennium, which strengthened the PWC. This pattern contributed to more frequent La Niña-like conditions, which enhanced upwelling of nutrient-rich waters in the west coast of North America, driving productivity and reducing bottom oxygen levels, as seen in our ETNP records.

## 1.1. INTRODUCTION

Numerous experimental, observational, and numerical model studies predict global expansion of Oxygen Minimum Zones (OMZ) linked to human induced climate change (Keeling et al., 2010; Gilly et al., 2013; Howes et al., 2015; Praetorius et al., 2015; Levin, 2018). The Eastern Tropical North Pacific (ETNP) hosts the largest OMZ in the world, and its economic importance for the coastal regions of North and South America is indisputable (Levin, 2018). Numerous in-situ measurements during recurring oceanographic campaigns (e.g., CalCOFI, IMECOCAL; Lynn and Simpson, 1987; Bograd et al., 2003; Durazo-Arvizu and Gaxiola-Castro, 2010) revealed declining $O_2$ trends during the last few decades (Bograd et al., 2003, 2008; Lavín et al., 2013; Breitburg et al., 2018; Levin, 2018). It is important to note that some of the decreasing patterns could be biased by improvements in $O_2$ measurement technologies that have decreased minimum detection thresholds. Despite this caveat, high-resolution reconstructions of changes in dissolved oxygen in the ETNP OMZ over the past century yield contrasting observations, with warming and increasing extent of anoxia (<0.1 mL/L $O_2$) not always correlated (Choumiline, 2011; Deutsch et al., 2014; Tems et al., 2016; Fu et al., 2018; Ontiveros-Cuadras et al., 2019). Ongoing discussions about the causes of OMZ intensification over the past decades typically invoke decreased $O_2$ solubility due to warming of the upper ocean, increased stratification slowing ventilation (Oschlies et al., 2008; Shaffer et al., 2009; Moffitt et al., 2015; Praetorius et al., 2015; Fu et al., 2018), and the strong effect of enhanced marine productivity on the formation of settling organic matter that undergoes decay and consumes more $O_2$ during remineralization (Wright et al., 2012; Levin, 2018). The latter relationship is the main mechanism by which some OMZ basins in the Eastern Pacific become anoxic (Moffitt et al., 2015; Breitburg et al., 2018; Levin, 2018). However, what causes increases in primary productivity is still debated, with initial results pointing to a complex

interaction of factors involving increased upwelling rates and terrigenous discharge—both of which can provide the necessary nutrients for proliferation of primary producers (Howes et al., 2015).

Because the first analytical measurements of dissolved oxygen in seawater started in the late 1800s (Carpenter, 1965), data are not available for preceding portions of the nineteenth century. Nevertheless, multiple applications of well-established paleoceanographic proxies allow us to infer changes in earlier productivity and oxygenation by reconstructing past conditions preserved in the elemental composition of marine sedimentary records emphasizing organic carbon ($C_{org}$), Ba, Cd, Mo, Mn, Ni, U, and V (Calvert and Pedersen, 1993; Helz et al., 1996; Morford and Emerson, 1999; Zheng et al., 2000; Lyons and Severmann, 2006; Tribovillard et al., 2006; Algeo and Rowe, 2012; Schoepfer et al., 2015). Multiple lines of proxy evidence show that major oxygenation shifts in the ETNP are coupled to glacial-interglacial cycling, often leading to a decrease in dissolved $O_2$ concentrations in North Pacific Intermediate and North Pacific Deep waters during glacial stages (e.g., Last Glacial Maximum) as well as cold Dansgaard-Oeschger and/or Heinrich-like events (e.g., the Younger Dryas) (Ganeshram and Pedersen, 1998; Hendy and Kennett, 2000; Nameroff et al., 2004; Hendy and Pedersen, 2006; Tetard et al., 2017). Paleoceanographic changes are not only observed in sediment core records at OMZ-depths (400–1,000 m) but also in sediments collected at greater depths of the Pacific and shallower waters of the glacial Southern Ocean, which confirms the likelihood of widespread impacts on oxygenation far beyond intra-OMZ variability (Lu et al., 2016; Hoogakker et al., 2018). Important fluctuations of the upper OMZ also occurred. Rather than the traditional view of these fluctuations as lesser responses to minor climate perturbations, they may have dominated certain regions such as the ETNP. The Pacific Decadal Oscillation (PDO)—detected as decadal cyclic changes in climatic regime from warm to cold and vice versa—is one of these atmospheric effects with strong oceanographic implications (Mantua and Hare, 2002). The North Pacific Gyre Oscillation (NPGO) manifests in decadal fluctuations of nutrients, chlorophyll,

and consequentially primary productivity that very often go hand to hand with atmospheric PDO changes in the Pacific (Di Lorenzo et al., 2008). Despite the similarities between the PDO and NPGO, they do not always co-vary.

High-resolution variability in paleoceanographic records, previously categorized by the scientific community as regional background noise, is now elucidating decadal- and centennial-scale OMZ fluctuations (Dean et al., 2004; Barron and Bukry, 2007; Choumiline, 2011; Deutsch et al., 2014; Tems et al., 2015, 2016). In the ETNP, cold PDO and/or NPGO phases cause intense upwelling off the western mainland of North America and lead to enhanced productivity, denitrification, and extreme water column anoxia (Di Lorenzo et al., 2008). However, numerous reports of marine sedimentary records in the literature typically lack the highly resolved age models needed to study decadal phenomena, which coupled with the absence of published multi-proxy records for denitrification ($\delta^{15}N$) and water column redox (Cd, Mn, V, Mo, U) make ETNP-wide redox reconstructions challenging (Moffitt et al., 2015; Borreggine et al., 2017). The importance of reconstructing OMZ reoxygenation and deoxygenation events and mechanistically explaining their climatic causes is essential in light of current and potential future responses of the ocean to modern global warming. These efforts encounter further challenges as redox-sensitive data can be compromised when sediment cores from anoxic settings are not carefully sampled or stored with adequate care in core repositories (Zheng et al., 2000; McManus et al., 2006; Scholz et al., 2011; Costa et al., 2018).

Here we reconstruct changes in the ETNP OMZ based on sediment cores collected at various depths in the Gulf of California. To achieve an ETNP-wide reconstruction, we integrate our multiproxy record of paleoproductivity and paleoredox with published sediment cores from the region. Further, to avoid misinterpreting local variability as global patterns, we apply geostatistical and numerical approaches to existing datasets to unmix local from larger-scale controls.

### 1.1.1. Strengths and weaknesses of geochemical proxies as applied to Oxygen Minimum Zone reconstructions

In this section we provide background details for productivity and redox proxies as archived in marine sediments and as applied to OMZ reconstructions.

#### 1.1.1.1. Productivity proxies ($C_{org}$, $Ba_{excess,}$ Ni)

Organic carbon ($C_{org}$) has long been used as a proxy for exported organic matter because of its analytical simplicity and wide range of applications (Schoepfer et al., 2015). While $C_{org}$ could directly represent superficial primary productivity, this possibility is likely confounded by multiple controls on remineralization and burial that are tightly related to reactivity of organic matter, bioturbation, and oxygen availability (Calvert et al., 1996; Burdige, 2007; Bianchi et al., 2016).

Barite, Ba/Al, and excess barium ($Ba_{excess}$) have been used widely as productivity proxies (Dymond et al., 1992; Eagle et al., 2003; Anderson and Winckler, 2005; Schoepfer et al., 2015), although barite and $Ba_{excess}$ relationships with productivity may be complicated by post-burial reprecipitation (McManus et al.,1998; Riedinger et al., 2006; Schoepfer et al., 2015). In some well-oxygenated marine settings, sedimentary $Ba_{excess}$ corresponds well to changes in productivity established by other proxies (e.g., Ni, P, and biogenic silica) (Schoepfer et al., 2015). However, post-depositional diagenetic remobilization of Ba has been found both in regions with transient anoxia and where bottom waters are well-oxygenated (McManus et al., 1998; Riedinger et al., 2006; Schoepfer et al., 2015). Sedimentary records of $Ba_{excess}$ can be further compromised over glacial-interglacial cycles when significant reoxygenation can cause redissolution and reprecipitation of barite along reaction fronts (McManus et al., 1998; Riedinger et al., 2006; Schoepfer et al., 2015).

Nickel is actively involved in biological cycling related to diatom export (Dupont et al., 2010; Twining et al., 2012). Dissolved Ni is removed from the water column by organic matter and supplied to the bottom sediments through particle settling (Böning et al., 2015). In sediments, Ni is the best-known analog for fresh organic matter because it mirrors the input of chlorins—one of the degradation products of chlorophyll (Böning et al., 2015). An advantage of Ni over other biologically active trace elements is its detachment from Mn and S cycling, compared to Cd and Zn, which more readily form insoluble sulfides (Morse and Luther, 1999; Böning et al., 2015). Potential complications for Ni as a productivity proxy include its elevated concentration in the detrital fraction (Wedepohl, 1995) and the possibility of anthropogenic contribution of Ni to marine sediments (Reck et al., 2008).

1.1.1.2. Redox proxies (Mo, Cd, V, U)

Molybdenum enrichment processes are linked with incorporation into pyrite and associations with organic matter, which often require abundant hydrogen sulfide (Calvert and Pedersen, 1993; Tribovillard et al., 2008; Chappaz et al., 2014; Scholz et al., 2017). An important pathway for Mo enrichment is the transformation of molybdate to thiomolybdates ($MoO_xS_{4-x}^{2-}$, where x = 0~4), which are highly particle reactive (Helz et al., 1996; Erickson and Helz, 2000; Scholz et al., 2017). Additionally, Mo can be scavenged by Fe-Mo-S clusters (Helz et al., 2011) or adsorbed onto sulfide-rich organic matter (Helz et al., 1996). Molybdenum enrichments can occur diagenetically (within the sediments), in the water column, or in some cases near the sediment-water interface, which was reported for OMZs (Zheng et al., 2000). While widely used as an indicator of past anoxic and euxinic (anoxic and sulfidic) conditions, several complications have been reported for this proxy (Morford and Emerson, 1999; Chappaz et al., 2014), including localized Mo enriched in turbidites despite fully oxygenated water column conditions (McKay and Pedersen, 2014) and

uptake exclusively within the sediments when significant amounts of sulfide are present solely in pore waters (Zheng et al., 2000; Scholz et al., 2017; Hardisty et al., 2018)—although these enrichments tend to fall below those typical of euxinic settings (e.g., Scott and Lyons, 2012).

Cadmium is a biologically active trace element supplied to marine sediments in association with organic matter (Morford and Emerson, 1999). It has been used as a proxy for strongly reducing waters (Calvert and Pedersen, 1993; Tribovillard et al., 2006). Cadmium can be precipitated in the presence of $H_2S$, which makes it a particularly good indicator of euxinia (Morse and Luther, 1999).

Vanadium is present in well-oxygenated seawater in its V(+5) form, usually as $H_2VO_4^-$, which is reduced to V(+4) as $VO^{2+}$ under oxygen-deficient conditions (Calvert and Pedersen, 1993; Morford and Emerson, 1999). This V(+4) form is more effectively scavenged and can be adsorbed to Fe-(oxyhydr)oxides, which is one of its removal mechanisms from seawater (Bauer et al., 2017; Ho et al., 2018). Over sub-millennial and glacial-interglacial timescales, V is potentially one of the most reliable redox proxies, tightly following changes in oxygenation (Nameroff et al., 2004; Costa et al., 2018). The contribution of non-lithogenic V through particulate settling has not been fully constrained; however, slight enrichments in suspended and settling matter have been found (Rodríguez-Castañeda, 2008; Hakspiel-Segura et al., 2016; Bauer et al., 2017; Ho et al., 2018; Conte et al., 2019).

Uranium is widely used as paleoredox proxy; however, the pathways of its sedimentary enrichment are still not fully understood. Uranium is present in seawater in the dissolved U(+6) form as uranyl carbonate complexes $(UO_2)^{2+}$ that are reduced under anoxic conditions to the insoluble U(+4) form by inorganic and microbially mediated processes (Ku et al., 1977; Klinkhammer and Palmer, 1991; Dunk et al., 2002) resulting in the formation of solid particles. Uranium can also be adsorbed to organic matter and to Fe- and Mn-(oxyhydr)oxides (Anderson et al., 1989). While increases in particulate U are thought to mostly occur diagenetically in sediment

pore waters underlying strongly anoxic and sulfidic (euxinic) waters (Klinkhammer and Palmer, 1991), some particulate non-lithogenic U can form very slowly in the water column (Zheng et al., 2002; Holmden et al., 2015). The extent to which non-lithogenic U can be enriched in marine particles is not well-established and may be more common in highly productive OMZ-type settings than previously thought. We propose an updated model for the behavior of U in OMZs, which will be discussed further in the chapter.

## 1.2. METHODS

### 1.2.1. Depositional setting

The Gulf of California (GC) is located within the ETNP OMZ and is well-connected to the Eastern Pacific through its southern entrance (Lavín et al., 2013). Circulation is not known to be limited in most GC basins, including Guaymas, Pescadero, and La Paz. Alfonso Basin is the only partially restricted setting in the GC, with a bathymetric sill extending today to a depth of 250m (Nava-Sánchez et al., 2001). The sill restricts the incursion of North Pacific Intermediate Water (NPIW) and North Pacific Deep Water (NPDW) (Figures 1.1A,B). Primary productivity is higher on the eastern side of the GC because it is nourished by nutrients upwelled predominantly during dry and cold seasons with strong northwesterly winds (Lavín et al., 2013; Silverberg et al., 2014). Mesoscale eddies together with wind-driven coastal upwelling (primarily along the mainland margin during winter) promote primary productivity in the region (Badan-Dangon et al., 1991; Trasviña-Castro et al., 2003; Deutsch et al., 2014). A strong east-to-west gradient persists from autumn through spring (Lavín et al., 2013), which results in organic material produced in the upwelling system on the eastern margin being deposited as biogenic remains on the west side of the basin.

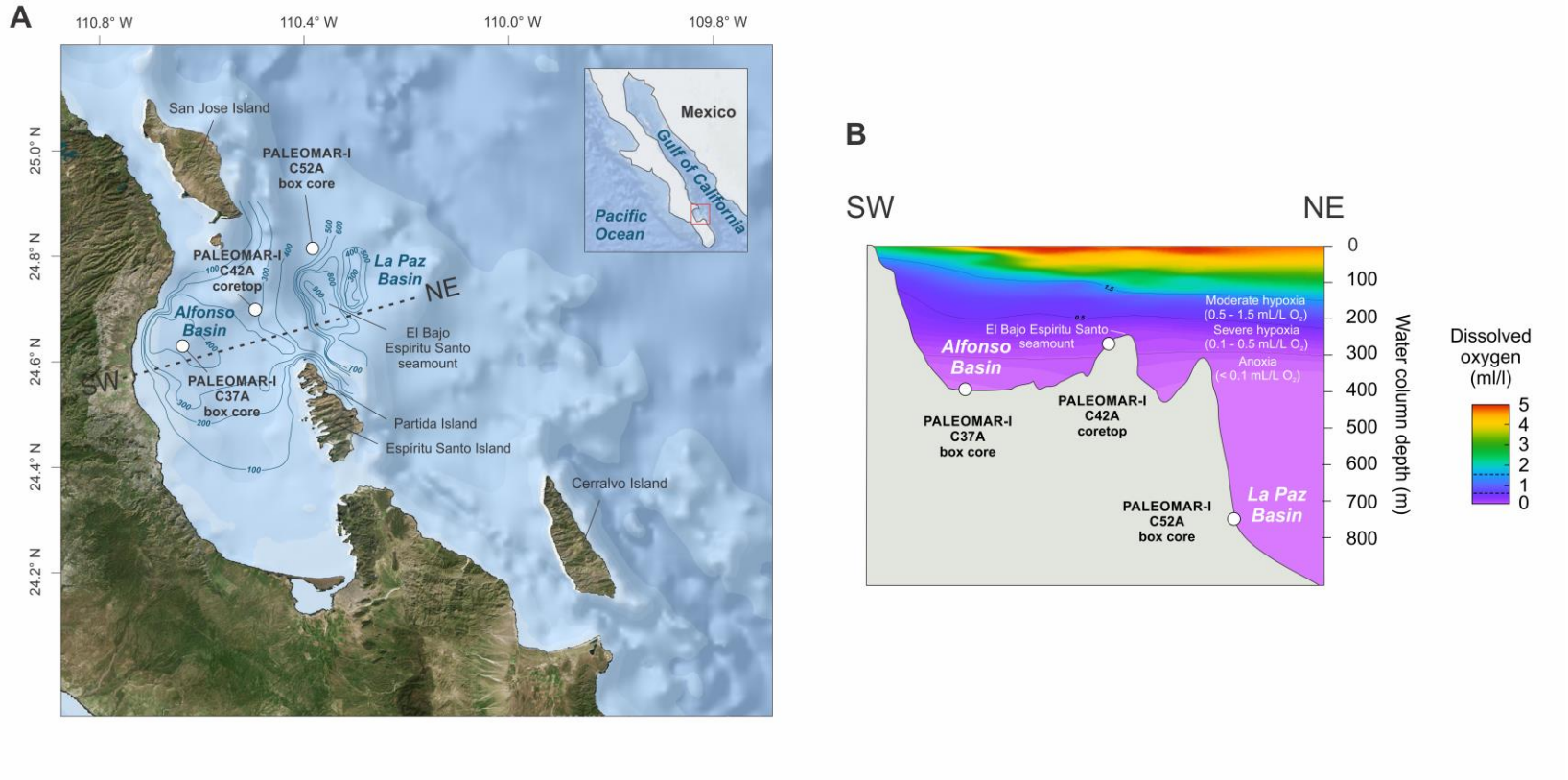


**Figure 1.1**. (A) Location of the studied marine setting in the eastern margin of the Gulf of California including the anoxic Alfonso and La Paz basins. The line between SW and NE represents a cross section shown in (B). (B) Cross section from the Baja California peninsula (SW) to the Gulf of California (NE) representing the basin morphology and dissolved oxygen (mL/L) concentrations spanning Alfonso and La Paz basins.

Particularly in Alfonso Basin, productivity is regulated by cyclonic flow that produces water divergence—transporting nutrients from the subsurface waters (>60m) into the photic zone. This cyclonic gyre is semi-permanent and has been linked by past researchers to the increase in productivity (Monreal-Gómez et al., 2001; Coria-Monter et al., 2014). Satellite and in-situ measurements of Net Primary Productivity (NPP) in Alfonso Basin range from 0.5 to 3.5 gC $m^{-2}d^{-1}$ over the last decade and show an inverse correlation with surface temperature. Mesoscale transport processes explain why the Gulf of California, like most of the Eastern Pacific, is influenced by ENSO, PDO, and/or NPGO phenomena (Mantua and Hare, 2002; Di Lorenzo et al., 2008). During cold La Niña years, the Walker Circulation triggers upwelling and productivity in the Eastern Pacific—weakening the typical upper ocean stratification that dominates during normal and El Niño years (Thunell, 1998; McPhaden, 2004; Bustos-Serrano and Castro-Valdez, 2006). Atmospheric circulation is also an important mechanism that seems to control upwelling in the Gulf of California and is dictated by the North American Monsoon (NAM) (Metcalfe et al., 2015). When the North Pacific High (NPH) and the Intertropical Convergence Zone (ITCZ) migrate southward, intense upwelling is triggered by northwesterly winds (Schneider et al., 2014; Metcalfe et al., 2015; Staines-Urías et al., 2015). Longer-scale variability of similar nature is attributed to cold PDO and sometimes NPGO phases, but the atmospheric and oceanographic links are still unclear.

The water columns of Alfonso and La Paz basins show a pronounced decrease in oxygen with depth, reaching values below 0.1 ml/L $O_2$ (Figure 1.1B). To avoid the imprecise term "suboxic" (Canfield and Thamdrup, 2009), we classify the water column using the threshold $O_2$ values from Hofmann et al. (2011) and Moffitt et al. (2015), which yielded the following categories: oxic ([bottom $O_2$] > 1.5 mL/L), moderately hypoxic (0.5 mL/L < [bottom $O_2$] < 1.5 mL/L), severely hypoxic (0.1 mL/L < [bottom $O_2$] < 0.5 mL/L), and anoxic ([bottom $O_2$] < 0.1 mL/L). According

to this classification, both Alfonso and La Paz basins fall within the “anoxic” category (Figure 1.1B).

Due to their locations near the open Pacific Ocean, the southern basins are a sensitive recorder of regional variation in the GC and the larger-scale climate circulation of the ETNP, capturing changes in productivity and redox conditions useful for tracking fluctuations of the OMZ (Dean et al., 2004; Barron and Bukry, 2007; Dean, 2007; Pérez-Cruz, 2013; Deutsch et al., 2014; Tems et al., 2015, 2016; Ontiveros-Cuadras et al., 2019).

### 1.2.2. Sampling

Laminated sediments from marine basins of the Gulf of California with varying degrees of deoxygenation were collected using a Reineck box corer during the PALEOMAR-I campaign in November 2014 aboard R/V “El Puma” owned by UNAM, Mexico (Figures 1.1A,B). The 50 cm sediment core PALEOMAR-I C37A was collected at 408m water depth in the silled Alfonso Basin. Core PALEOMAR-I C52A represents a sedimentary sequence of the upper 24 cm of La Paz Basin at 785 m depth. Both cores show a clear, continuously laminated fabric. Additionally, the core top of PALEOMAR-I C42A was sampled from the shallower part of Alfonso Basin (265m). This core did not show clear laminations. Poor recovery during retrieval limited its utility for paleoceanographic reconstructions. From this point forward, we will refer to these cores as C37A, C42A, and C52A.

Each core was extruded and subsampled immediately after collection, and pore waters were extracted from each section in a glove bag under $N_2$ atmosphere using CSS 5 cm Rhizon samplers attached to plastic syringes (Lyons and Berner, 1992; Dickens et al., 2007; Raiswell and Canfield, 2012; Riedinger et al., 2017). Each core segment yielded approximately 8 mL of pore waters, which were filtered at 0.2 μm, acidified with trace grade pure nitric acid (10 μL of acid per each 1 mL of

sample), and stored at 4°C (Riedinger et al., 2014, 2017). Prior to analysis, solid-phase samples were dried, weighed, and homogenized.

### 1.2.3. Age model

We use the present-day sedimentation rates previously reported in the literature for Alfonso Basin to generate the age model for the studied core C37A. Due to the extended timespan of the sedimentary section, the composite age model is based on $^{210}$Pb and $^{14}$C dating methods (Figure 1.2; Table 1.1). For this purpose, we selected box core DIPAL-II C44 (Choumiline, 2011) and gravity core DIPAL-III T43 (Pérez-Cruz, 2013). The dated materials were collected at the same location within the basin and span a matching sedimentary package (Supplementary Figure 1.1). High-resolution sections of the uppermost 10 cm (subsampled at <3mm) of core DIPAL-II C44

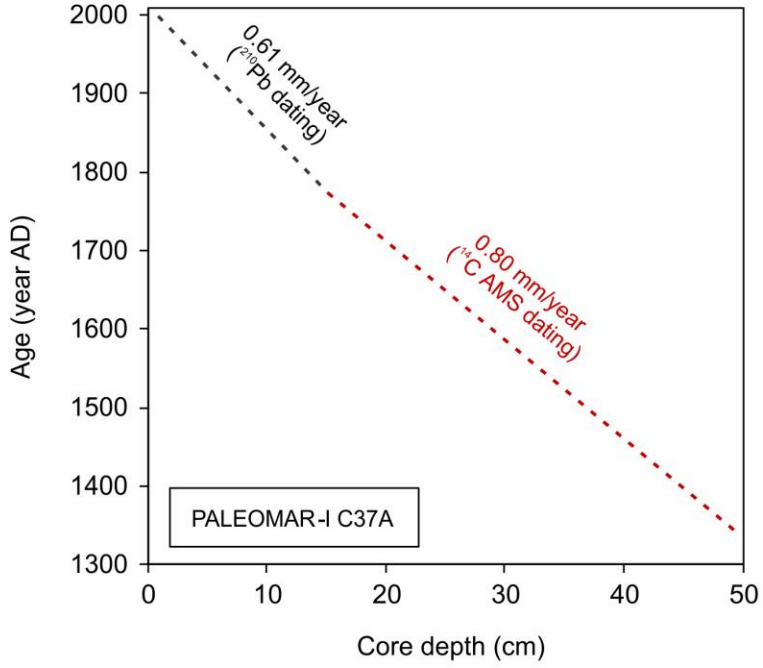


**Figure 1.2.** Age model of core PALEOMAR-I C37A from Alfonso Basin.

**Table 1.1.** Age model for core C37A, constructed by a combination of extrapolated average sedimentation rates produced using the $^{210}$Pb method on core DIPAL-II C44 (Choumiline et al., 2010; Choumiline, 2011) and acceleration mass spectrometry $^{14}$C on core DIPAL-III T43 (Pérez-Cruz, 2013). The cores were collected at the same location in Alfonso Basin.

| Depth range (cm) | Depth midpoint (cm) | Age in years AD | Dated material and method used | Corresponding sedimentation rate for C37A |
|---|---|---|---|---|
| 0-2 | 1 | 1999 | $^{210}$Pb dating of the uppermost 10 cm of bulk sediment from box core DIPAL-II C44 | 0.61 mm/year |
| 2-4 | 3 | 1967 | | |
| 4-6 | 5 | 1934 | | |
| 6-8 | 7 | 1902 | | |
| 8-10 | 9 | 1870 | | |
| 10-12 | 11 | 1837 | | |
| 12-14 | 13 | 1805 | | |
| 14-16 | 15 | 1772 | | |
| 14-16 | 15 | 1772 | AMS $^{14}$C dating with *Bolivina subadvena* in the following horizons of the gravity core DIPAL-III T43:<br><br>Code: BETA320950<br>Interval: 17-18 cm<br>Age: 1572 year AD<br><br>Code: BETA322689<br>Interval: 41-43 cm<br>Age: 1240 year AD | 0.8 mm/year |
| 16-18 | 17 | 1747 | | |
| 18-20 | 19 | 1722 | | |
| 20-22 | 21 | 1697 | | |
| 22-24 | 23 | 1672 | | |
| 24-26 | 25 | 1647 | | |
| 26-28 | 27 | 1622 | | |
| 28-30 | 29 | 1597 | | |
| 30-32 | 31 | 1572 | | |
| 32-34 | 33 | 1547 | | |
| 34-36 | 35 | 1522 | | |
| 36-38 | 37 | 1497 | | |
| 38-40 | 39 | 1472 | | |
| 40-42 | 41 | 1447 | | |
| 42-44 | 43 | 1422 | | |
| 44-46 | 45 | 1397 | | |
| 46-48 | 47 | 1372 | | |
| 48-50 | 49 | 1347 | | |

were analyzed for $^{210}$Pb at Flett Research Ltd. Laboratory (Winnipeg, Canada) (Supplementary Figure 1.2). The mean sedimentation rate for the upper 10 cm is 0.61 mm/year in Alfonso Basin (Choumiline et al., 2010; Choumiline, 2011). The sedimentary section of the gravity core DIPAL-III T43 corresponding to the lower part of C37 (between 15 and 50 cm) was dated using the $^{14}$C method (Pérez-Cruz, 2013). Measurements were performed in benthic foraminifera *Bolivina subadvena* by accelerator mass spectrometry at Beta Analytic (Pérez-Cruz, 2013) and the radiocarbon values were calibrated using the Marine13 curve (Reimer et al., 2013). This part of the core yielded a mean sedimentation rate of 0.8 mm/year (Pérez-Cruz, 2013). In our age model for C37A we extrapolate the sedimentation rate of 0.61 mm/year to the uppermost core section (0–15 cm) and use 0.8 mm/year for the lowermost segment (15–50 cm) as shown in Table 1.1 and Supplementary Figure 1.1. To demonstrate that the core sections are equivalent, we compared the total carbon ($C_{tot}$), calcium carbonate ($CaCO_3$) and Ca changes through time for cores C37A (this study), DIPAL-II C44 (Choumiline et al., 2010, 2017; Choumiline, 2011) and DIPAL-III T43 (Pérez-Cruz, 2013). The curves covary, confirming the consistency between age models for different core records (Supplementary Figure 1.1). Additionally, selected dry splits of sediment core C37A (Alfonso Basin) were dated using the $^{210}$Pb and $^{137}$Cs methods via gamma-ray spectroscopy in the Gray Lab (University of California, Riverside). The subsampling resolution of this core was too coarse to produce a robust age model using these methods. Despite known difficulties with radiocesium detection in the region (Ruiz-Fernández et al., 2009) it was still possible to find slightly elevated $^{137}$Cs activity values around the 2–4 cm core horizon, very likely corresponding to the mid-1960s peak of nuclear testing in the atmosphere (Foster and Walling, 1994). The resulting linear sedimentation rate using the radiocesium method for core C37A was roughly 0.6 mm/year. The sedimentation rates determined for Alfonso Basin from different age

models are consistent. Further, the age model for Alfonso Basin shows that the deepest sample of core C37A at 500 mm extends to 1300 AD (also called the Common Era or CE).

### 1.2.4. Analytical approaches

Total carbon ($C_{tot}$) and total inorganic carbon ($C_{inorg}$) in dry sediment subsamples were measured on an ELTRA CS-500. The $CO_2$ produced during subsample combustion at 1350°C ($C_{tot}$) or acidification with 20% HCl ($C_{inorg}$) was quantified with an infrared analyzer. The organic carbon ($C_{org}$) fraction was calculated by numerical difference: $C_{org} = C_{tot} - C_{inorg}$.

Prior to sample digestion, 100 mg splits were ashed in ceramic vessels for 8 h at 550°C in a high temperature oven. A two-step digestion procedure involved a mixture of $HNO_3$ and HF, followed by aqua regia (HCl and $HNO_3$) and acidification/drying cycles on temperature-controlled hot plates. A very low HF:$HNO_3$ ratio of 1:8 was employed during the first step to prevent insoluble fluoride formation. Careful evaluation of each sample revealed that no undissolved particles were detected, suggesting complete digestion (Durand et al., 2016). The final digested extracts were diluted in 2% $HNO_3$ and measured for major and trace elements (Al, Ba, Cd, Fe, Ni, Mo, V, U) on an Agilent 7900 Inductively Coupled Mass Spectrometer (ICP-MS).

Pore waters were analyzed for elemental composition on an Agilent 7900 ICP-MS, emphasizing dissolved Fe, Mn, and selected trace elements. The quality of our data was assessed by analyzing duplicates and certified reference materials USGS SGR-1B, USGS SDO-1, NIST 2702, AR4007, and AR4024. Analytical precision was always below 3%. Recoveries of measured sample relative to certified standard value ranged between 96 and 105%.

### 1.2.5. Numerical and statistical approaches

The productivity and redox proxy approaches used here rely heavily on authigenic enrichment of trace elements relative to detrital inputs through uptake in marine sediments during diagenesis and via scavenging from seawater during primary production and during particle settling. To assess enrichments relative to detrital contributions, each element was normalized to Al as a reliable crustal proxy (Wedepohl, 1995). Further, to account for dilution by $CaCO_3$, which can cause apparent elemental variability, we recalculated the data on a carbonate free basis (CFB) by dividing each concentration by the fraction of non-carbonate material. Elemental ratios were also calculated for selected elements. The authigenic uranium ($U_{auth}$) fraction was calculated as $U_{auth} = U_{total}$ - (Th/3) (Wignall and Myers, 1988).

Due to limited sample sizes, it was not possible to perform the barite sequential leach sometimes used as a productivity proxy in well-oxygenated marine settings (Dymond et al., 1992; Eagle et al., 2003; Schoepfer et al., 2015). Instead, we used our measurements for total Ba and Al to determine excess barium ($Ba_{excess}$) as the closest calculated alternative (Eagle et al., 2003; Anderson and Winckler, 2005): $Ba_{excess} = Ba_{total} - (Ba_{terrigenous}/Al_{terrigenous}) \times Al_{total}$. We assumed a $Ba_{terrigenous}/Al_{terrigenous}$ ratio of 0.0045 as suggested by Dymond et al. (1992) and Eagle et al. (2003).

In order to define proxy associations, we applied a multivariate statistical approach for the proxy datasets from Alfonso and La Paz basins. Specifically, we performed R-mode Factor Analysis with Varimax rotation using the software STATISTICA by StatSoft. The analysis included the following variables: $C_{org}$, $Ba_{excess}$, Ni, U, $U_{auth}$, Cd, Mo, and V.

Geostatistical analyses and data extraction techniques were performed using ArcGIS 10.6 software by ESRI. We combined our data with previously published geochemical records obtained in part from the EarthChem SedDB database via the Interdisciplinary Earth Data Alliance (IEDA) repository. Estimated oceanographic data (dissolved $O_2$ and chlorophyll) were obtained for each

core location in GIS and used in our statistical analysis. Global oceanic oxygen data are based on the World Ocean Atlas (2005) and Garcia et al. (2006); surficial chlorophyll estimates from the SeaWIFS satellite sensor were published by OBPG/NASA.

### 1.2.6. Paleoceanographic proxies used in this study

To interpret past OMZ conditions preserved in marine sediments we used a combination of proxies assuming $C_{org}$ as an indicator for organic carbon burial (Schoepfer et al., 2015); $Ba_{excess}$ (despite the caveats described above) and Ni for export production (Böning et al., 2015; Schoepfer et al., 2015); Cd, Mo, and V for bottom water anoxia (Calvert and Pedersen, 1993; McManus et al., 2006; Tribovillard et al., 2006; Lyons et al., 2009). Due to a strong contribution of $U_{auth}$ via settling particulates (Choumiline et al., 2010; Choumiline, 2011) potentially after its reduction or adsorption to organic matter, this proxy could trace both redox and productivity—as will be explained further in the text.

While each proxy has distinct biogeochemistry and enrichment pathways, they are all affected by a circular relationship between productivity and redox (Tribovillard et al., 2006; Schoepfer et al., 2015; Bianchi et al., 2016). In transiently anoxic settings high productivity often leads to the development of water column anoxia, which favors organic preservation and reduces the mobility of productivity proxies (Schoepfer et al., 2015). Due to the latter, it is often common to expect a covariance between productivity and redox proxies (Tribovillard et al., 2006; Bianchi et al., 2016). The differences in proxy relationships are often helpful to unravel more specific biogeochemical processes tied to preservation biases, such as organic matter reactivity and post-depositional diagenetic transformations.

## 1.3. RESULTS AND DISCUSSION

### 1.3.1. Geochemistry of modern sediments from the southwestern Gulf of California at various OMZ depths

The chemical compositions of core tops (upper 2 cm) represent the most recent sediments from Alfonso and La Paz basins (Table 1.2). A water depth transect from the 265 to 785 m through the study region revealed that dissolved $O_2$ values decreased from 0.3 mL/L (uppermost OMZ) to <0.1 mL/L (OMZ core) (Figure 1.1B). Most redox-sensitive elements increase in concentration in the deeper sites C37A and C52A relative to the shallower C42A. For all three sites the elemental concentrations range as follow: $C_{org}$ (2.96–6.41%), $Ba_{excess}$ (175.50–682.77 mg/kg), Ni (26.84–49.06 mg/kg), and Mo (0.75–6.75 mg/kg). In contrast, Cd and $U_{auth}$ are enriched at the shallow, more oxygenated site C42A—reaching 13.17 mg/kg for Cd and 5.34 mg/kg for $U_{auth}$, compared to 7.24 mg/kg for $U_{auth}$ in C52A and 2.48 mg/kg for Cd in C37A (Table 1.2). Although circulation in Alfonso Basin is slightly restricted due to the presence of a bathymetric sill at 250m depth,

**Table 1.2.** Composition of modern sedimentary material represented by core tops from different OMZ depths in Alfonso (C42A and C37A) and La Paz basin (C52A). The dissolved oxygen values presented here were obtained during the PALEOMAR-I oceanographic campaign.

| Marine basin | Water column depth | Redox condition and bottom dissolved $O_2$ (mL/L) | Core top proxy data | | | | | | | |
|---|---|---|---|---|---|---|---|---|---|---|
| | | | Productivity / Nutrients | | | Redox and/or Productivity | | Redox | | |
| | | | $C_{org}$ (%) | $Ba_{excess}$ (mg/kg) | Ni (mg/kg) | U (mg/kg) | $U_{auth}$ (mg/kg) | Cd (mg/kg) | Mo (mg/kg) | V (mg/kg) |
| Alfonso Basin (C42A) | uppermost OMZ (265 m) | Severe hypoxia (~ 0.3) | 2.96 | 175.70 | 26.84 | 14.31 | 13.17 | 5.34 | 0.75 | 26.05 |
| Alfonso Basin (C37A) | upper OMZ (408 m) | Anoxia (< 0.1) | 6.01 | 406.37 | 40.25 | 9.85 | 8.14 | 2.48 | 6.34 | 124.67 |
| La Paz Basin (C52A) | middle OMZ (785 m) | Anoxia (< 0.1) | 6.41 | 682.77 | 49.06 | 8.84 | 7.24 | 2.60 | 6.75 | 75.048 |

restriction was apparently not severe enough to limit trace element enrichments in La Paz Basin relative to the more open ocean. We calculated $U_{auth}$ values for the CFB fraction as 6.43 mg/kg in C42A, 7.26 mg/kg in C37A, and 7.24 mg/kg in C52A. Carbonate-free values were also calculated for the other proxies but did not produce major differences relative to either total or Al-normalized data (see Supplementary Material for this chapter).

### 1.3.2. Bioturbation and post-sampling effects as complicating overprints on primary proxy records

Visual observation confirmed that the sediments from Alfonso (C37A) and La Paz (C52A) basins are clearly laminated, with no evidence for bioturbation, which could obscure primary sedimentary features. Pore water profiles were used to establish the chemical zonation of electron acceptors at the time of sample collection (Canfield and Thamdrup, 2009). It is essential to evaluate diagenetic conditions before applying paleoreconstruction techniques because many proxies can be overprinted during diagenesis, obscuring records of primary water column conditions (Calvert and Pedersen, 1993; Tribovillard et al., 2006). Further, pore water data shed light on bioturbational overprints via burrow irrigation and sediment homogenization and disturbance during sediment collection and processing. At both Alfonso Basin (C37A) and La Paz Basin (C52A), concentrations of dissolved Fe ($Fe_{diss}$) and dissolved Mn ($Mn_{diss}$) show downcore decreases (Figure 1.3). The observed trend for $Fe_{diss}$ is similar to those from analogous OMZ settings of the Gulf of California (Guaymas Basin), offshore California (San Pedro and Catalina basins), and the Peruvian margin—that is, pore water $Fe_{diss}$ reaches its maximum a few centimeters below the sediment-water interface and gradually declines down core (Brumsack and Gieskes, 1983; McManus et al., 1997; Canfield and Thamdrup, 2009; Scholz et al., 2011; Scholz, 2018). Our recovery of expected trends suggests that proper techniques for sediment collection and preservation were employed in this study.

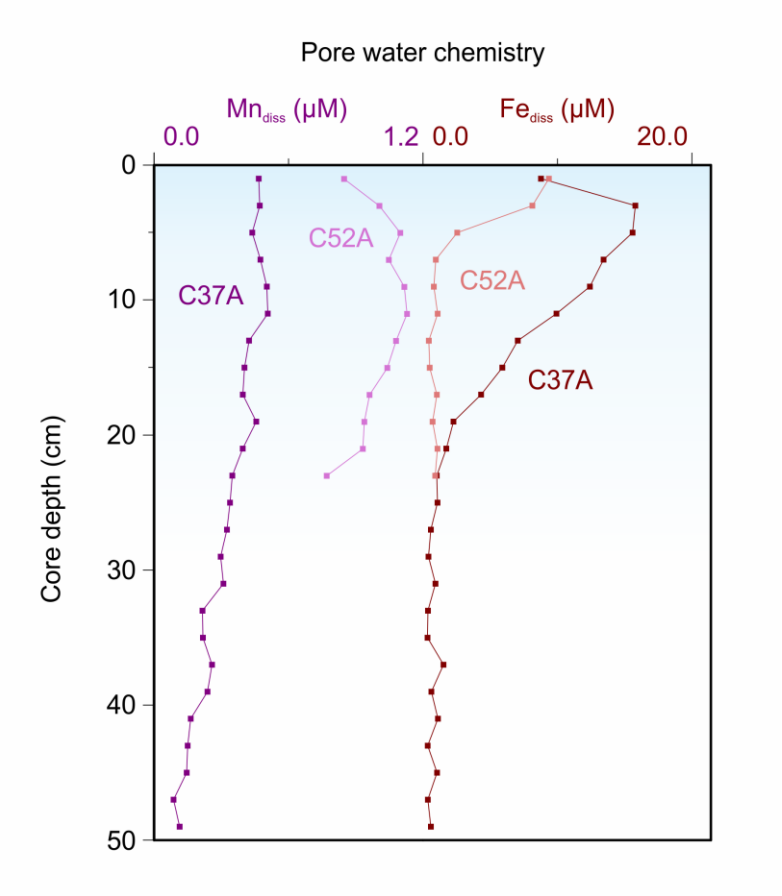


**Figure 1.3.** Pore water chemical profiles in cores PALEOMAR-I C37A from Alfonso Basin and PALEOMAR-I C52A from La Paz Basin (Data: Choumiline et al., 2017).

### 1.3.3. Downcore records of changing productivity and redox

Here we present downcore variations of productivity and redox proxies recorded in our sedimentary material from the ETNP (Figure 1.1). We found almost no difference between the trends for absolute concentrations and corrected data, so we present only absolute values. However, Al-normalized and CFB data are presented in Supplementary Materials for the interested reader.

1.3.3.1. Geochemistry of sediments from the upper OMZ in Alfonso Basin

Elemental profiles for C37A from Alfonso Basin are shown in Table 1.3. Data for $C_{org}$ are in good agreement with $Ba_{excess}$, Ni, $U_{auth}$, and V as proxies for past oxygenation and/or primary productivity. Values range from 5.60 to 6.76% for $C_{org}$, 372.22– 491.54 mg/kg for $Ba_{excess}$, 40.25–51.61 mg/kg for Ni, 9.23–14.15 mg/kg for U, 7.71–12.48 mg/kg for $U_{auth}$, and 115.81–172.40 mg/kg for V. Trends for Cd and Mo differ slightly from those for the other proxies and range from 2.48 to 7.04 mg/kg and 6.34–15.16 mg/kg, respectively (Figure 1.4).

1.3.3.2. Geochemistry of sediment from the mid-depth OMZ of La Paz Basin

Downcore concentrations for the productivity and redox proxies in core C52A from La Paz Basin are presented in Table 1.3. Despite differences in core length and depositional setting, the records for $C_{org}$, Ni, $U_{auth}$, V, and Cd in C52A are similar to those from core C37A (Supplementary Figure 1.3). These elements range as follow: 6.51–7.12% for $C_{org}$, 47.34–53.25 mg/kg for Ni, 5.97–9.32 mg/kg for $U_{auth}$, and 74.31–102.80 mg/kg for V. In C52A, $Ba_{excess}$ does not covary with Ni and $U_{auth}$, pointing to its potential remobilization during diagenesis. Excess-Ba concentrations range from 419.76 to 763.24mg/kg but are mostly uniform over the length of the core—averaging 670.89 mg/kg. The trends for Cd and Mo decrease down core in the upper 6 cm of laminated sediments (Supplementary Figure 1.3; Table 1.3) and range from 2.38 to 2.97 and 4.90 to 12.55 mg/kg, respectively.

The lowest concentrations for most proxy data are found in the upper 5 cm, at ~14 cm, and below 23 cm—perhaps corresponding to well-ventilated past conditions. The highest values, indicating enhanced anoxia, were registered around 20 cm for all proxies, while the second anoxic horizon close to 10 cm was only captured by $C_{org}$, Ni, $U_{auth}$, V, and more subtly by Cd and Mo.

**Table 1.3.** Elemental composition of the solid phase from cores C37A, C42A and C52A collected during PALEOMAR-I expedition to the Gulf of California.

| Core | Depth range (cm) | $C_{org}$ | Al | Fe | Ba | Cd | Mo | Ni | U | V | $Ba_{excess}$ | $U_{auth}$ |
|---|---|---|---|---|---|---|---|---|---|---|---|---|
| | | (%) | | | (mg/kg) | | | | | | | |
| C37A (Alfonso Basin) | 0-2 | 6.01 | 4.9 | 2.5 | 406.4 | 2.5 | 6.3 | 40.3 | 9.9 | 124.7 | 406.4 | 8.1 |
| | 2-4 | 6.18 | 5.1 | 2.6 | 419.3 | 2.6 | 6.4 | 41.9 | 10.1 | 115.8 | 419.2 | 8.3 |
| | 4-6 | 6.13 | 5.1 | 2.6 | 440.0 | 3.4 | 9.3 | 41.3 | 9.7 | 133.4 | 439.9 | 7.9 |
| | 6-8 | 6.42 | 5.0 | 2.5 | 454.3 | 3.4 | 10.2 | 44.2 | 10.1 | 137.1 | 454.3 | 8.4 |
| | 8-10 | | 4.7 | 2.3 | 439.9 | 3.5 | 9.9 | 44.0 | 11.3 | 139.6 | 439.9 | 9.6 |
| | 10-12 | 6.39 | 4.8 | 2.3 | 430.4 | 3.8 | 9.0 | 45.3 | 13.0 | 150.6 | 430.4 | 11.3 |
| | 12-14 | 6.65 | 5.0 | 2.5 | 476.6 | 4.1 | 9.5 | 47.9 | 13.5 | 156.8 | 476.6 | 11.7 |
| | 14-16 | 6.66 | 5.3 | 2.6 | 479.3 | 3.8 | 9.2 | 48.3 | 12.4 | 141.8 | 479.3 | 10.6 |
| | 16-18 | 6.76 | 4.3 | 2.1 | 416.0 | 3.8 | 9.2 | 41.2 | 9.2 | 117.0 | 415.9 | 7.7 |
| | 18-20 | 6.26 | 4.9 | 2.4 | 458.0 | 3.9 | 8.7 | 45.8 | 11.6 | 149.7 | 458.0 | 9.9 |
| | 22-24 | 6.43 | 5.0 | 2.6 | 480.5 | 4.8 | 12.7 | 49.5 | 10.9 | 167.1 | 480.5 | 9.1 |
| | 24-26 | 6.05 | 4.8 | 2.4 | 458.3 | 4.6 | 11.2 | 46.3 | 12.9 | 157.0 | 458.3 | 11.2 |
| | 26-28 | 6.56 | 4.9 | 2.4 | 459.1 | 4.7 | 8.2 | 50.4 | 12.4 | 154.9 | 459.1 | 10.7 |
| | 28-30 | 6.25 | 5.0 | 2.5 | 461.5 | 5.4 | 13.4 | 46.9 | 10.8 | 160.0 | 461.4 | 9.0 |
| | 30-32 | 5.93 | 5.0 | 2.5 | 485.5 | 5.0 | 13.0 | 46.4 | 11.2 | 164.2 | 485.5 | 9.5 |
| | 32-34 | 5.89 | 4.9 | 2.5 | 468.1 | 4.8 | 11.2 | 47.7 | 11.8 | 160.6 | 468.1 | 10.1 |
| | 34-36 | 6.53 | 5.1 | 2.6 | 488.8 | 5.3 | 12.9 | 51.6 | 11.9 | 172.4 | 488.7 | 10.1 |
| | 36-38 | 6.18 | 5.1 | 2.5 | 470.3 | 4.3 | 10.7 | 48.9 | 11.1 | 167.5 | 470.3 | 9.4 |
| | 38-40 | 6.04 | 5.1 | 2.5 | 441.8 | 3.7 | 9.3 | 46.1 | 11.3 | 146.4 | 441.8 | 9.5 |
| | 40-42 | 6.30 | 5.1 | 2.5 | 472.7 | 4.7 | 13.5 | 48.9 | 10.1 | 161.0 | 472.7 | 8.3 |
| | 42-44 | 6.65 | 4.7 | 2.4 | 481.5 | 7.0 | 14.2 | 51.4 | 14.2 | 170.8 | 481.5 | 12.5 |
| | 44-46 | 5.60 | 4.6 | 2.4 | 372.2 | 2.9 | 6.8 | 42.8 | 14.0 | 124.0 | 372.2 | 12.3 |
| | 46-48 | 6.62 | 4.6 | 2.3 | 440.1 | 5.0 | 13.3 | 46.3 | 9.9 | 148.5 | 440.1 | 8.2 |
| | 48-50 | | 4.8 | 2.4 | 491.6 | 5.2 | 15.2 | 50.0 | 12.9 | 165.9 | 491.5 | 11.2 |
| C52A (La Paz Basin) | 0-2 | 6.41 | 4.3 | 1.8 | 682.8 | 2.6 | 6.7 | 49.1 | 8.8 | 75.0 | 682.8 | 7.2 |
| | 2-4 | 6.58 | 4.3 | 1.9 | 681.1 | 2.4 | 4.9 | 49.4 | 7.5 | 76.0 | 681.1 | 6.0 |
| | 4-6 | 6.55 | 4.3 | 1.9 | 419.8 | 2.5 | 9.1 | 49.0 | 8.3 | 76.5 | 419.8 | 6.8 |
| | 6-8 | 6.68 | 4.3 | 1.9 | 580.4 | 2.5 | 10.7 | 49.9 | 8.4 | 86.8 | 580.4 | 6.8 |
| | 8-10 | 7.12 | 4.6 | 1.9 | 763.3 | 3.0 | 12.6 | 52.9 | 9.7 | 102.8 | 763.2 | 8.1 |
| | 10-12 | 6.61 | 4.4 | 1.8 | 689.6 | 2.8 | 11.8 | 50.7 | 10.4 | 93.4 | 689.5 | 8.8 |
| | 12-14 | 6.43 | 4.4 | 1.9 | 704.3 | 2.8 | 10.6 | 49.9 | 9.2 | 88.4 | 704.3 | 7.6 |
| | 14-16 | 6.54 | 4.6 | 1.9 | 723.0 | 2.8 | 9.9 | 51.7 | 9.6 | 83.9 | 722.9 | 8.0 |
| | 16-18 | 6.40 | 4.6 | 1.9 | 703.2 | 2.9 | 9.6 | 51.1 | 8.8 | 80.9 | 703.2 | 7.2 |
| | 18-20 | 6.49 | 4.8 | 2.0 | 728.1 | 2.9 | 10.3 | 53.2 | 11.1 | 94.7 | 728.1 | 9.3 |
| | 20-22 | 6.17 | 4.3 | 1.9 | 661.3 | 2.7 | 9.5 | 47.3 | 8.6 | 82.2 | 661.3 | 7.0 |
| | 22-24 | 6.10 | 4.5 | 2.0 | 714.1 | 2.4 | 10.9 | 50.2 | 9.1 | 74.3 | 714.1 | 7.5 |
| C42A | - | 2.96 | 2.3 | 1.0 | 175.7 | 5.3 | 0.8 | 26.8 | 14.3 | 26.0 | 175.7 | 13.2 |

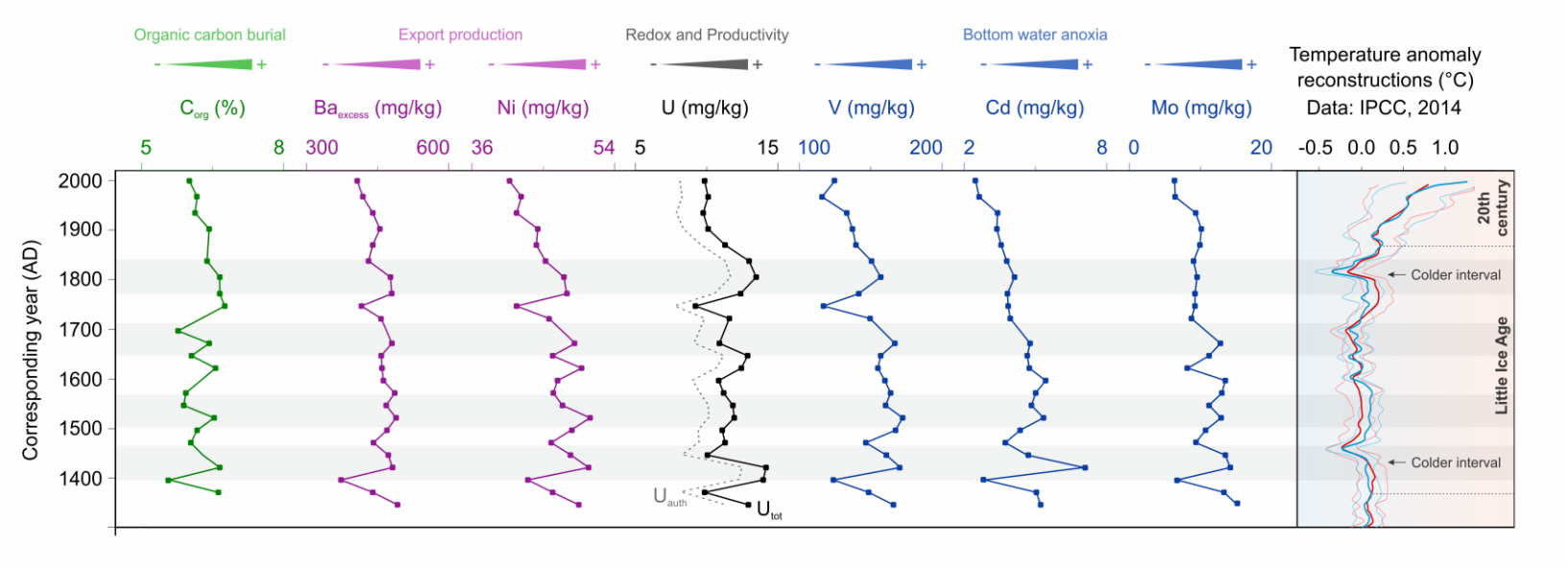


**Figure 1.4.** Organic carbon, productivity and redox proxies in core PALEOMAR-I C37A from Alfonso Basin. Data for temperature anomaly reconstructions of the last millennium taken from IPCC (2014).

### 1.3.4. Variability of the upper OMZ in Alfonso Basin over the last 700 years

We present down-core elemental concentrations in the context of the age model described earlier in the chapter. Due to multiple challenges during our efforts to date cores C42A and C52A, such as poor recovery, only core C37A from Alfonso Basin produced a robust age model. Core C37 will be emphasized for paleoceanographic reconstructions for the remainder of the report.

The geochemical profiles for C37A from Alfonso Basin record changes in the upper OMZ boundary dating back to 1300 AD (Figure 1.4; Table 1.3). Data for $C_{org}$ are in good agreement with $Ba_{excess}$, Ni, $U_{auth}$, and V as proxies for past oxygenation and/or primary productivity. Unlike our other proxies, Mo and Cd remain high from 1300 to 1700 AD and then slowly transition toward lower values after 1700 AD. This slight decrease toward the present corresponds to the uppermost 20 cm of the record in the Alfonso Basin. The lowest concentrations for our proxies are generally concurrent with the late 1900s, early 1700s, and late 1300s AD. These times correspond to warm periods of the past millennium as reconstructed by multiple records (IPCC, 2014), including the anthropogenically caused warming trend that started around the beginning of the nineteenth century and extends to present day (Figure 1.4). Lower proxy values indicate decreased primary productivity and correspond to slightly more oxygenated times. In contrast, high proxy values occurred in the early 1800s, late 1600s, early 1500s, and early 1400s, with maxima between roughly 1700 and 1400 AD are likely associated with the prolonged cold period of the Little Ice Age. Higher values usually correspond to increased primary productivity in surface waters and enhanced anoxia.

### 1.3.5. Multivariate statistical associations of paleoproxies in Alfonso and La Paz basins

Factor analysis results for the combined geochemical datasets from Alfonso Basin (core C37A) and La Paz Basin (C52A) distinguished three elemental associations between Factor 1 (48.23% variance) and Factor 2 (27.85% variance) (Table 1.4; Figure 1.5). The “productivity”

association is based on $C_{org}$, Ni and $Ba_{excess}$–elements related to organic matter production at shallow depths. The "redox with weak particulate contribution" defined by Cd and Mo, which require strongly reducing conditions in bottom waters for strong authigenic enrichments. The "redox with strong particulate contribution" links U, $U_{auth}$, and V—elements that can be supplied through particulate fluxes in oxygen-deficient water column depths and/or enriched diagenetically either under anoxic bottom waters or at the sediment-water interface.

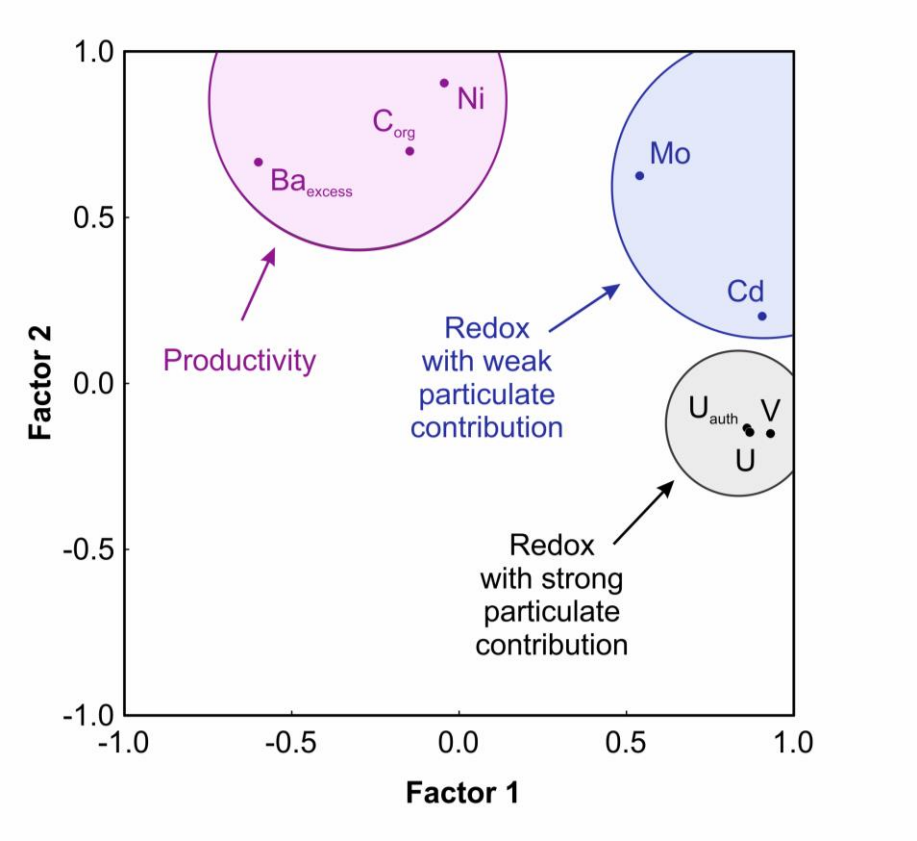


**Figure 1.5.** Productivity and redox proxy associations defined by R-mode Factor Analysis of a combined geochemical dataset from Alfonso Basin (core C37A) and La Paz Basin (C52A).

**Table 1.4.** Factor loadings of the R-mode Factor Analysis with Varimax rotation performed on a combined dataset of cores C37A (Alfonso Basin) and C52A (La Paz Basin).

| Proxy | Factor 1 | Factor 2 |
|---|---|---|
| $C_{org}$ | -0.1448 | 0.6978 |
| $Ba_{excess}$ | -0.5988 | 0.6615 |
| Ni | -0.0413 | 0.9013 |
| U | 0.8700 | -0.1489 |
| $U_{auth}$ | 0.8611 | -0.1366 |
| V | 0.9316 | -0.1517 |
| Cd | 0.9046 | 0.1995 |
| Mo | 0.5406 | 0.6226 |
| **Explained Variance** | 3.8581 | 2.2282 |
| **Proportion of Total Variance** | 48.23 % | 27.85 % |

### 1.3.6. Comparison of productivity and redox proxies in core tops across varying OMZ depths and productivity regimes in the ETNP

Here we present a compilation of data from core tops from this and previous studies (Table 1.5; Figure 1.6 and Supplementary Figure 1.4). Comparing core tops, most of the cores collected at upper- and mid-OMZ depths have significantly stronger $C_{org}$, $Ba_{excess}$, Ni, Mo, and V enrichments compared to shallower cores (e.g., core C42A)—with the latter perhaps representing the fluctuating upper OMZ boundary often exposed to high $O_2$ levels (Table 1.5). These enrichments correspond to regions where high chlorophyll is reported in the surface waters associated with eastern North Pacific upwelling (Table 1.5; Figure 1.6 and Supplementary Figure 1.4) (Badan-Dangon et al., 1991; Trasviña-Castro et al., 2003). The elevated $C_{org}$, $Ba_{excess}$, and Ni in these high-chlorophyll regions are likely to indicate enhanced primary productivity in the photic zone but could also reflect strong preservation of refractory organics delivered from land (Calvert et al., 1996; Burdige, 2007;

Bianchi et al., 2016) (Table 1.5). These productive coastal sectors correspond to severe hypoxia/anoxia in which trace element enrichments reach 75.05–149.08 mg/kg for V and 6.75–7.35 mg/kg for Mo in the deepest cores from La Paz and Pescadero basins, respectively (Table 1.5; Figure 1.6). Detrital contributions in such settings are relatively minor (Rodríguez-Castañeda, 2008; Choumiline, 2011). These enrichments are favored by oxygen-deficient conditions in the water column and, in the case of Mo, sulfide accumulation in seawater (Calvert and Pedersen, 1993; Zheng et al., 2000; Tribovillard et al., 2006). The studied core tops from the Eastern Pacific OMZ show Mo values sufficiently high to indicate anoxia but are too low to suggest euxinia (presence of $H_2S$) (Table 1.5; Figure 1.6A). For comparison, only certain places off the Peruvian margin, where water conditions are extremely reducing even for an OMZ, show Mo values as high as 70 mg/kg (McManus et al., 2006). In contrast, at 265m depth in the upper portion of the OMZ, core C42A displays low V and Mo values of 26.05 and 0.75 mg/kg, respectively, indicating the presence of some oxygen in the overlying waters and that V and Mo are mostly supplied through detrital inputs.

Uranium is the exception. The $U_{auth}$ concentrations are high in the shallower and more-oxygenated core (C42A), reaching 13.17 mg/kg—with values similar to those of the deeper, anoxic core tops (C37A and C52A). We hypothesize that the added contribution of uranium is through its uptake in settling particles and associated anoxic microenvironments. Under oxic and weakly oxic conditions, dissolved uranium is present in its +6 form but is reduced to the insoluble +4 form once oxygen declines further (moderate hypoxia) or disappears (anoxia). This authigenic U is preserved as the organic-rich marine aggregates settle through the water column, in the absence of $U_{auth}$ reoxidation even in ventilated waters. This exported authigenic uranium is delivered to the sediments—often showing a stronger correlation with $C_{org}$ compared to the relationships between the organic matter and V or Mo (Choumiline, 2011). Evidence for authigenic U enrichments in

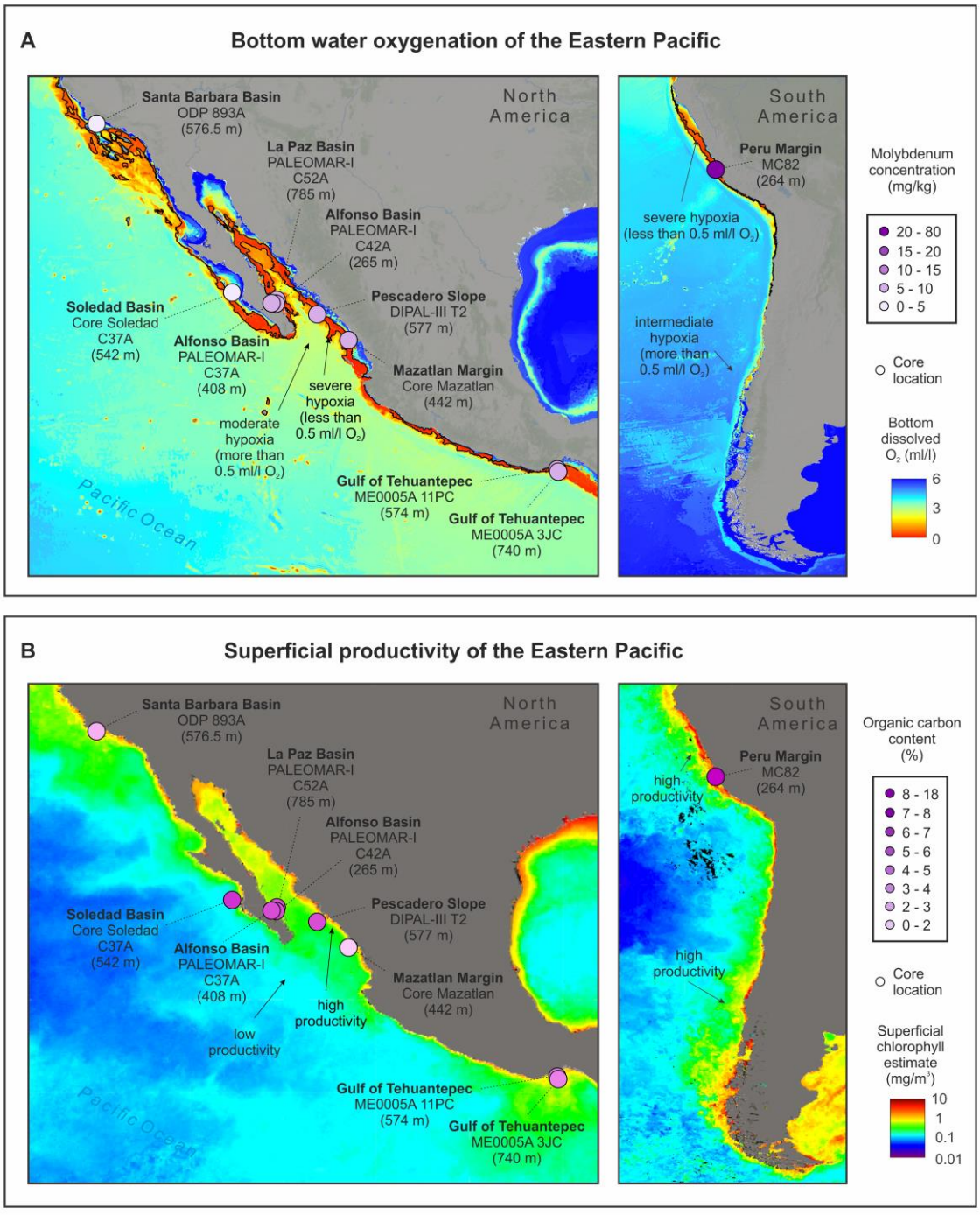


**Figure 1.6.** Molybdenum and organic carbon in core tops from various locations across the Gulf of California and adjacent Pacific, (A) bottom dissolved oxygen, and (B) superficial chlorophyll estimate from the studied marine OMZ settings of ETNP (Alfonso Basin and La Paz Basin) (Oxygen based on World Ocean Atlas, 2005, Garcia et al., 2006; superficial chlorophyll estimates by SeaWIFS satellite sensor published by OBPG/NASA).

**Table 1.5.** Comparison of productivity and/or redox proxy values for selected sedimentary material from different OMZ depths in the Eastern Pacific. The core top values represent the uppermost 2 cm of sedimentary record.

| Marine basin | Water column depth | Redox condition and bottom dissolved $O_2$ (mL/L) | Proxy data | | | | | | | |
|---|---|---|---|---|---|---|---|---|---|---|
| | | | Productivity / Nutrients | | | Redox and/or Productivity | | Redox | | |
| | | | $C_{org}$ (%) | $Ba_{excess}$ (mg/kg) | Ni (mg/kg) | U (mg/kg) | $U_{auth}$ (mg/kg) | Cd (mg/kg) | Mo (mg/kg) | V (mg/kg) |
| Alfonso Basin, Gulf of California (settling particles)[c] | upper OMZ (360 m) | Anoxia (< 0.1) | 7.80 [16.37] | 338.95* [2147.45] | 37.49 [107.99] | 4.65 [42.79] | 4.16 [42.70] | 1.42 [4.65] | 1.40 [7.92] | 38.96 [84.64] |
| Alfonso Basin, Gulf of California (core C42A)[a] | uppermost OMZ (265 m) | Severe hypoxia (~ 0.3) | 2.96 | 175.70 | 26.84 | 14.31 | 13.17 | 5.34 | 0.75 | 26.05 |
| Alfonso Basin, Gulf of California (core C37A)[a] | upper OMZ (408 m) | Anoxia (< 0.1) | 6.01 | 406.37 | 40.25 | 9.85 | 8.14 | 2.48 | 6.34 | 124.67 |
| La Paz Basin, Gulf of California (core C52A)[a] | middle OMZ (785 m) | Anoxia (< 0.1) | 6.41 | 682.77 | 49.06 | 8.84 | 7.24 | 2.60 | 6.75 | 75.048 |
| Pescadero Slope, Gulf of California (core DIPAL-III T2)[b] | upper OMZ (577 m) | Anoxia (< 0.1) | 6.42 | 654.95 | 54.10 | 8.09 | 5.05 | - | 7.35 | 149.08 |
| Santa Barbara Basin, Eastern Pacific, 34° N (core ODP 893A)[d] | upper OMZ (576.5 m) | Anoxia (< 0.1) | 3.00 | 513.2* | 51.00 | 2.90 | - | 2.80 | 4.70 | 186.70 |
| Mazatlan Margin, Eastern Pacific, 22.7 °N (core Mazatlan)[e] | upper OMZ (442 m) | Anoxia (< 0.1) | - | - | - | 4.29 | - | - | 6.26 | - |
| Soledad Basin, Eastern Pacific, 25.2° N (core Soledad)[e] | upper OMZ (542 m) | Anoxia (< 0.1) | 7.09 | - | - | 6.78 | - | - | 4.16 | - |
| Gulf of Tehuantepec, Eastern Pacific, 15.7° N (core ME0005A 11PC)[f] | upper OMZ (574 m) | Anoxia (< 0.1) | 4.74 | - | - | - | - | 3.05 | 6.51 | - |
| Gulf of Tehuantepec, Eastern Pacific, 15.7° N (core ME0005A 3JC)[f] | middle OMZ (740 m) | Anoxia (< 0.1) | 4.34 | - | - | - | - | 1.57 | 6.54 | - |
| Peru Margin Eastern Pacific, 13.7° S (core MC82)[e] | uppermost OMZ (264 m) | Anoxia (< 0.1) | 16.27 | - | - | 17.34 | - | - | 70.08 | - |
| Upper Continental Crust Average[g] | - | - | - | 668* | 18.6 | 2.5 | 2.5* | 0.102 | 1.4 | 53 |

*Total concentration value (not enough supplementary data to calculate authigenic or excess values)
[a] This study
[b] Gravity core (Choumiline, in prep)
[c] Sediment trap material; average and [maximum] values between 2002-2008 in 173 samples (Rodriguez-Castañeda, 2008; Choumiline, 2011; Silverberg et al., 2014)
[d] Drill core (Ivanochko and Pedersen, 2004)
[e] Multicore (McManus et al., 2006)
[f] Sediment core (Hendy and Pedersen, 2006)
[g] Wedepohl (1995)

settling particles was reported by Zheng et al. (2002) in marine basins of the California Margin and also from Alfonso Basin, with particulate U concentrations reaching 40 mg/kg (Choumiline et al., 2010; Choumiline, 2011)—more than an order of magnitude higher than the crustal average of 2.5 mg/kg (Wedepohl, 1995).

Like $U_{auth}$, V is enriched in sediments from regions of the Pacific where bottom water anoxia is present. Additionally, its concentration in suspended particles also peaks seasonally at depths of 150–250m in response to intra-annual changes in water column $O_2$ (Hakspiel-Segura et al., 2016). The contribution of V to the bottom via settling particles is usually lower than the average sedimentary concentration under low $O_2$ conditions but still within the same order of magnitude (Rodríguez-Castañeda, 2008).

To assess the contribution of authigenic U through settling, we contrast U and Mo sedimentary records published in the literature with ours from the ETNP (Ivanochko and Pedersen, 2004; McManus et al., 2006). Typically, Mo is used as an indicator for water euxinia (Calvert and Pedersen, 1993; Algeo and Lyons, 2006; Algeo and Tribovillard, 2009; Lyons et al., 2009; Algeo and Rowe, 2012; Scott and Lyons, 2012), but most of the enrichments in modern OMZs are likely tied to the presence of sulfide only in pore waters (Scholz et al., 2017; Hardisty et al., 2018). We are not using V because, like U, there could also be important contribution of the redox sensitive element through settling particles, associated to reducing microenvironments (Table 1.5; Choumiline, 2011). We expect good correlation between U and Mo records if both elements are enriched during burial (i.e., diagenetically or at the sediment-water interface; Klinkhammer and Palmer, 1991; Calvert and Pedersen, 1993; Zheng et al., 2002; Algeo and Tribovillard, 2009). A weak correlation is likely to be found for samples where significant amounts of non-lithogenic U are scavenged into particles and settle through the water column. In contrast, Mo uptake is typically limited to the sediments when oxygen is present in the water column. For the previously published

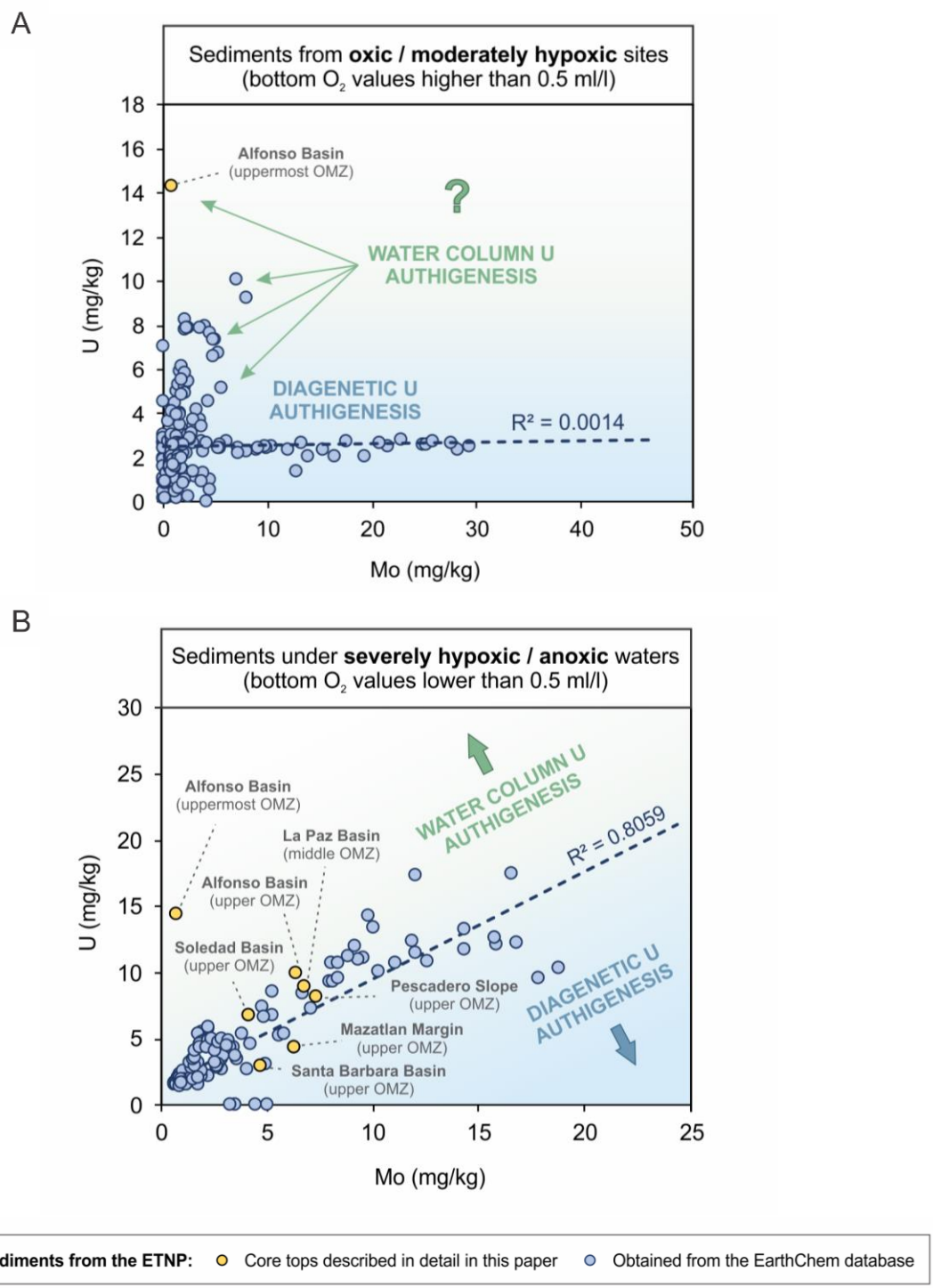


**Figure 1.7.** Correlation between U and Mo in sediments collected under (A) oxic or moderately hypoxic waters and (B) severely hypoxic or anoxic waters from different basins of the Eastern Tropical North Pacific (Data from: this study; Ivanochko and Pedersen, 2004; McManus et al., 2006; Choumiline et al., 2017; EarthChem database with $n$ = 183).

data, we estimated bottom $O_2$ values for each sediment core in a GIS using an interpolated global oxygen database (World Ocean Atlas, 2005; Garcia et al., 2006). This approach allowed us to classify data in two main groups depending on the dominant redox conditions: oxic to moderately hypoxic (0.5 mL/L < [bottom $O_2$] < 1.5 mL/L) (Figure 1.7A) and severely hypoxic (0.1 mL/L < [bottom $O_2$] < 0.5 mL/L) to anoxic ([bottom $O_2$] < 0.1 mL/L) (Figure 1.7B). We found that sediments underlying oxic–moderately hypoxic waters do not show correlation between U and Mo—with an $R^2$ value close to 0.00 (Figure 1.7A). Some samples do, however, show significant enrichment above crustal values of 2.5 mg/kg that could be due to water column U authigenesis (Zheng et al., 2002; Choumiline, 2011). In contrast, sediments deposited under severely hypoxic to anoxic waters show strong correlation between Mo and U, with an $R^2$ value of 0.80. While most of the U concentrations for the oxygen-deficient sites correlate with Mo, some reach even higher values of 17 mg/kg U with no significant Mo increase. In many cases, the lack of Mo enrichments could be attributed to bottom water redox potentials that were not sufficiently reducing, especially for sites in the upper OMZ. These observations of high U and low Mo could also indicate a water column supply of authigenic U through settling particles. In this context of U-Mo relationships, the studied sites from Alfonso and La Paz basins fall above the trend line, showing potential surpluses in $U_{auth}$ enrichments perhaps tied to high levels of productivity and associated particle scavenging (Figure 1.7).

### 1.3.7. Chronology of reoxygenation and deoxygenation events over the past millennium in a predominantly anoxic marine setting

In the following discussing, we use the term reoxygenation to imply a relative increase in dissolved $O_2$ at OMZ depths, usually corresponding to deepening of the upper OMZ boundary. Reoxygenation need not indicate disappearance of the OMZ, as no proxy record indicates fully

oxygenated water conditions (Tems et al., 2016), including the data produced in our study—specifically, Mo, V, and U values are several times higher than their crustal average values (Wedepohl, 1995). The oxygenation chronology of the last millennium starts with the predominantly warm climatic trends of the Medieval Warm Period (or Medieval Climate Optimum), which ended as cooling began with gradual change in the insolation regime after the Wolf Minimum (Figure 1.8). This cooling transitioned the planet into the colder Little Ice Age, which started around 1300 AD (Bard et al., 2000; IPCC, 2014; Griffiths et al., 2016) and was the most anoxic period of the last millennium as indicated by our V, Cd, Mo, and $U_{auth}$ data from Alfonso. The Little Ice Age coincides with the highest values of the SOI index, indicating more La Niña-like years and enhanced upwelling (Yan et al., 2011; Griffiths et al., 2016). Most marine basins of the ETNP experienced short-term reoxygenation events and corresponding decreases in water column denitrification during warm times around late 1300s, early 1700s, and the mid to late 1900s (Figure 1.8). These warm reoxygenation periods lasted from 100 to 150 years but reversed several times toward anoxic conditions in a matter of decades due to cooling and strengthening of the OMZ (Tems et al., 2016). During the Little Ice Age, denitrification, and bottom anoxia were the strongest during the Spörer Minimum, leading to OMZ expansion (this study; Tems et al., 2016). Subsequent periods of lower solar irradiance (Maunder and Dalton minimums) also corresponded with expanded OMZs but to a lesser degree than during the Spörer (Figure 1.8). The most recent stage was marked by a gradual reoxygenation during the twentieth century toward the mid-1990s, followed by a slight possible OMZ intensification over the last decade as shown by some of our proxy V and $U_{auth}$ data from Alfonso and La Paz basins in accordance with the findings of Tems et al. (2016), Ontiveros-Cuadras et al. (2019) and a high-resolution U record of the last century by Choumiline et al. (2010) and Choumiline (2011).

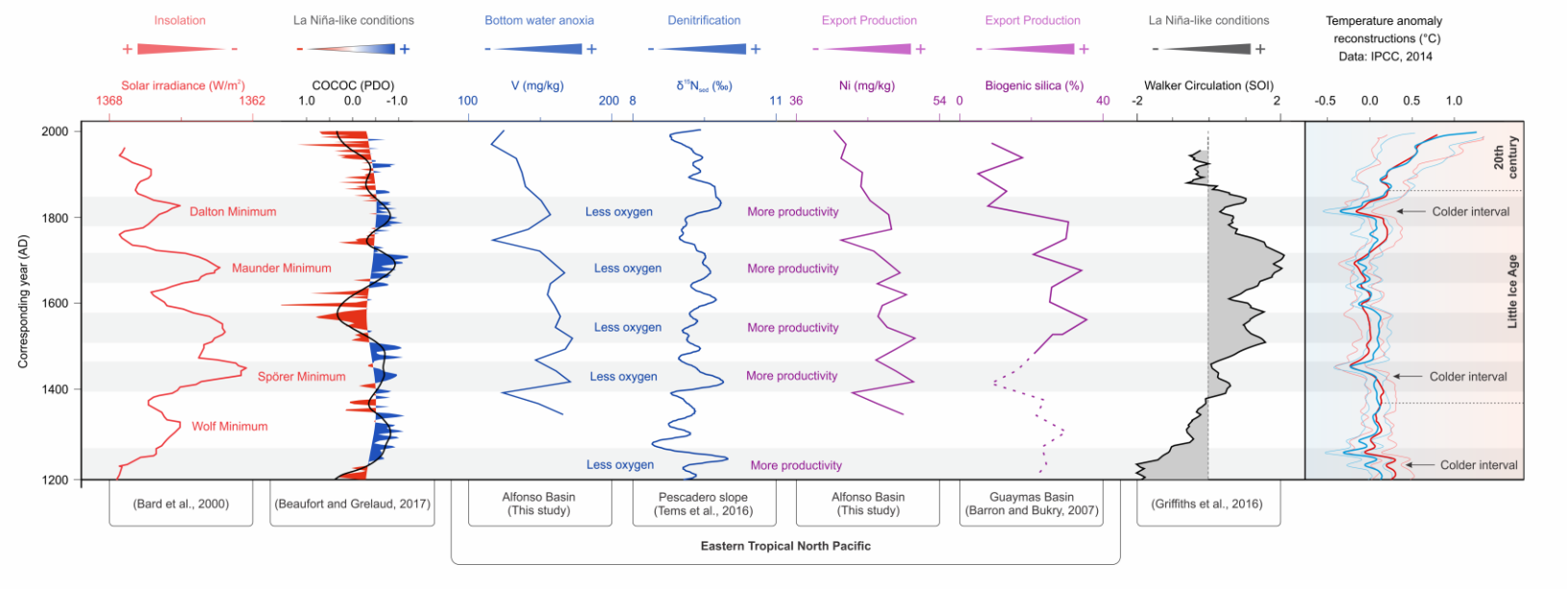


**Figure 1.8.** Reconstruction of OMZ variability of the Eastern Pacific during the last 800 years based on proxies for water column denitrification, redox and productivity compared to major climatic forcings. Note that the solar irradiance plot is inverted for better visualization.

### 1.3.8. Climatic drivers of historical OMZ fluctuations in the ETNP over the last millennium

As suggested by our data from marine basins of the southwestern Gulf of California, patterns of productivity tied to upwelling are one of the key drivers of oxygenation in coastal OMZs. Importantly, most of the variability in the ETNP is indirectly controlled by short and long-term variations of solar irradiance (Bard et al., 2000). La Niña years are known to positively impact productivity in coastal regions of the Eastern Pacific by increasing upwelling rates (Thunell, 1998; Chang et al., 2013). Atmospheric dynamics, also triggered by insolation changes, play a substantial role in controlling coastal wind-driven upwelling, caused by migrations of NPH and ITCZ (Schneider et al., 2014; Metcalfe et al., 2015; Staines-Urías et al., 2015). Southward position of the NPH and ITCZ would trigger more upwelling in the Eastern Pacific (Metcalfe et al., 2015). Our research suggests—based on the chronology of Ni, V, and $U_{auth}$ variability—that one of the most important controls on upwelling in the ETNP leading to OMZ fluctuations is the position of the Walker Circulation and its effect on El Niño or La Niña years on longer time scales (Figure 1.8). Evidence for long-term ENSO trends are manifested in PDO and/or NPGO variability in the Eastern Tropical North Pacific (Mantua and Hare, 2002; Moy et al., 2002; Di Lorenzo et al., 2010; Choumiline, 2011; Tems et al., 2016). These changes control delivery of nutrients to the marine basins of the Eastern Pacific, subsequently enhancing productivity and favoring oxygen loss (deoxygenation) of these oceanic settings (and OMZs). The mechanistic links between changes in PWC and PDO and their impacts on upwelling variability are still not clear, mainly due to difficulties in the paleoreconstruction of these phenomena.

Our record of productivity and redox over the last millennium can be compared to changes in COCOC (Composite Coccolith Proxy) presented by Beaufort and Grelaud (2017) in an attempt to reconstruct long-term variation in the PDO (Figure 1.8). The Southern Oscillation Index (SOI) presented by Yan et al. (2011) and Griffiths et al. (2016) is proposed to represent changes in Walker

Circulation through time (Figure 1.8). On decadal and centennial timescales, the driving force for the major and minor fluctuations in the PWC is solar irradiance (Bard et al., 2000). Colder periods corresponding to the solar irradiance minimums—known as Dalton, Maunder, Spörer, and Wolf minimums—are also times of higher productivity and lower oxygen concentrations (seen in the Alfonso, La Paz, and Pescadero records). Importantly, denitrification was also higher during times of low insolation, as evidenced by higher sedimentary $\delta^{15}N$ values on the Pescadero Slope (eastern side of the Gulf of California) published by Tems et al. (2016). Periods of high productivity are captured in records for $Ba_{excess}$, Ni, and $U_{auth}$ in Alfonso and La Paz basins during the Little Ice Age—with maximum peaks of productivity during Spörer, Maunder, and Dalton solar minimums (Bard et al., 2000; Barron and Bukry, 2007). Independent records of biogenic silica from Guaymas Basin, central Gulf of California, confirm elevated export production during colder solar episodes (Barron and Bukry, 2007). These productive times led to enhanced bottom water anoxia manifested in high V and $U_{auth}$ concentrations in marine sediments of Alfonso and La Paz basins (Figures 1.8, 1.9A). The drivers of climatic change over the last millennium remain unclear, but the leading theories involve a combination of factors from orbital change to periods of strong volcanism that triggered a cooling phase during the Little Ice Age (Atwood et al., 2016). That cooling phase affected the strength of the PWC and led to lesser El Niño years.

1.3.8.1. Drivers of redox in the Eastern Pacific and apparent contradictions with the glacial-interglacial model for OMZ expansions

The mechanisms that control decadal to centennial oxygen variability in the ETNP remain unresolved but are likely influenced by solar forcing. That forcing not only drives migration of the ITCZ (Schneider et al., 2014) but also, more importantly, variation in the intensity of the PWC. During the Little Ice Age, solar irradiance was at its lowest over the past millennium, which

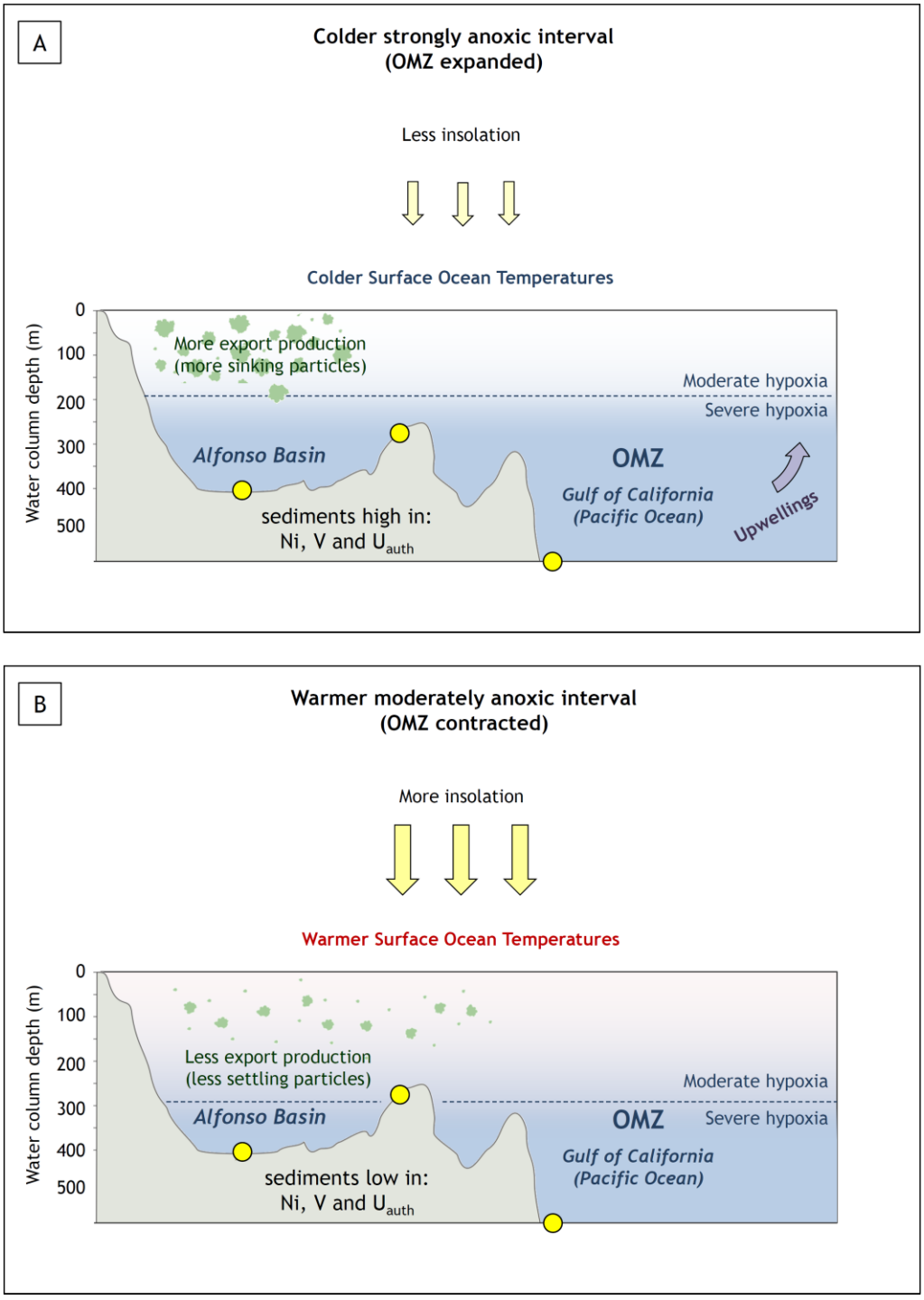


**Figure 1.9.** Two dominating oceanographic regimes: (A) high productivity and enhanced anoxia during colder periods, (B) low productivity and reoxygenation during warm periods.

strengthened Walker Circulation (Bard et al., 2000; Yan et al., 2011; Griffiths et al., 2016). The result was La Niña-like conditions, which enhanced upwelling of colder nutrient-rich waters and favored elevated productivity and reduced bottom oxygen levels (Figure 1.9A), as seen in Alfonso and La Paz basins and on the Pescadero Slope (Figure 1.8). A smaller-scale form of PWC variability is expressed in changes in the PDO and/or NPGO indices, which control rates of denitrification in OMZ waters of the Eastern Pacific (Di Lorenzo et al., 2010; Tems et al., 2016; Beaufort and Grelaud, 2017). As indicated by Tems et al. (2016) and confirmed by our findings, despite a decline in measured $O_2$ values in the Eastern Pacific over the last few decades (Bograd et al., 2003, 2008; Levin, 2018), sedimentary records of the ETNP do not indicate increasing anoxia. Our geochemical proxy data from Alfonso from this study, Pescadero (Tems et al., 2016), and Mazatlan Margin (Ontiveros-Cuadras et al., 2019) also confirm that despite the recent warming trend and related anthropogenically triggered ocean-scale $O_2$ decline (Bograd et al., 2003, 2008; Breitburg et al., 2018; Levin, 2018), the sedimentary records of benthic foraminifera, $\delta^{15}N$, Cd, Mo, $U_{auth}$, and V do not suggest a significant increase in anoxia after the mid-1800s (Figures 1.4, 1.8). Our evidence for gradually increasing dissolved oxygen levels are also supported by a decline in export production toward the beginning of the twenty-first century, evidenced by our $C_{org}$ and Ni data from Alfonso and La Paz, as well as biogenic silica from Guaymas Basin (Barron and Bukry, 2007).

Despite a longstanding decrease of productivity and redox during the last century (Figure 1.8), a subtle regime change toward increased anoxia could have begun around the 1990s but is represented only by a few data points for the redox proxies (this study; Dean et al., 2004; IPCC, 2014; Tems et al., 2016). Remarkably, this relationship is only evidenced by $\delta^{15}N$, V, and Mo and not by productivity proxies, pointing at the global decline of $O_2$ (Tems et al., 2016; Breitburg et al., 2018; Levin, 2018). Rather than reflecting global warming, reoxygenation and deoxygenation scenarios of the last millennium in the ETNP are primarily controlled by coastal productivity and

dominated by long-term persistence of La Niña conditions more often occurring during stronger PWC. Deutsch et al. (2014) proposed another mechanism for the apparent OMZ contraction despite declining $O_2$ trends in the North Pacific. The authors argued that global warming is resulting in a weakening of easterly trade winds and will continue to do so, leading to contraction of the ETNP OMZ rather than the previously predicted expansion (Deutsch et al., 2014; Tems et al., 2016). Regardless of the dominant mechanisms, our results (Figure 1.8) also support the interpretation that OMZ expansion occurred during cooling periods rather than being a consequence of warming—at least over the last millennium (Figure 1.9).

A clear distinction should be made between the dominant mechanisms that control oxygenation in the ETNP over decadal-centennial timescales (Deutsch et al., 2014; Tems et al., 2015, 2016) and those that govern long-term glacial-interglacial variability (Ganeshram and Pedersen, 1998; Nameroff et al., 2004; Hendy and Pedersen, 2006; Ivanochko et al., 2008; Pichevin et al., 2012, 2014; Cartapanis et al., 2014; Umling and Thunell, 2017). High-amplitude variability (such as the one described in our results) is superimposed over the long-term millennial-multimillennial $O_2$ trends (Nameroff et al., 2004; Cartapanis et al., 2014; Chang et al., 2014; Moffitt et al., 2015; Praetorius et al., 2015; Tetard et al., 2017). In contrast, the long-term tendencies (e.g., transition from the Last Glacial Maximum toward the Holocene) are driven by global changes in temperature and circulation that control intermediate and deep-water oxygenation (Ganeshram and Pedersen, 1998; Hendy and Pedersen, 2006; Cartapanis et al., 2014; Praetorius et al., 2015; Lu et al., 2016; Choumiline et al., 2017; Breitburg et al., 2018; Levin, 2018). In other words, short-term decreases in anoxia during warm times in response to the weakening of the Walker Circulation and increase abundance of ENSO years can counteract long-term warming of the upper ocean, which causes stratification and reduced ventilation and $O_2$ concentration on the global scale ocean.

1.3.8.2. Lagged response of the ocean to climate change and future scenarios

The effect of global warming on the world ocean is not expected to be spatially uniform. For example, latitudinal differences in the change of $O_2$ volume have been observed, with faster declines near the equator (0–20°N) compared to higher latitudes (20–90°N) (Schmidtko et al., 2017). Some vulnerable regions have experienced a rapid response (e.g., ETSP), while others (e.g., ETNP) show a lag of several decades (Chavez et al., 2011; Howes et al., 2015; Long et al., 2016). It has been suggested that the response time of the OMZs to ocean deoxygenation caused by a decrease in $O_2$ solubility and enhanced stratification linked to global warming (Praetorius et al., 2015) could be quicker than 25 years (Tems et al., 2016). However, the effects of climate change on OMZ oxygenation seem to only begin toward the end of the 20th century as preserved in multiple sediment records (Dean et al., 2004; Tems et al., 2016)—including ours—wherein the gradual oxygen increase in the beginning of the twentieth century shifts to a decline in $O_2$ toward the twenty-first century. The observed lagged response in $O_2$ trends to warming is consistent with current estimates of oceanic oxygen volume (Chavez et al., 2011; Long et al., 2016; Schmidtko et al., 2017).

Overall, there is still no consensus in the community about predicted OMZ behavior for the near future due to differences in the volume estimates among the models (Cocco et al., 2013; Long et al., 2016; Battaglia and Joos, 2018). A more recent study concludes that after the gradual increase of anoxia, the trend will be reversed globally, and the overall volume of OMZs will start declining (Fu et al., 2018). The mechanism proposed by Fu et al. (2018) involves a reduction of biological export linked to surface warming.

## 1.4. SYNTHESIS

### 1.4.1. Lessons learned about the utility of productivity and redox proxies from our ETNP OMZ records

Our findings indicate that the efficacy of productivity and redox proxies in modern OMZs depends somewhat on the supply of non-detrital trace elements via settling due to biological uptake or scavenging, as well as their preservation potential during diagenetic overprinting. We conclude that Ni, U, and V are the most reliable, while Ba and Mo should be used with caution in OMZ-type settings. Barium is significantly enriched in sediment trap material, which could elevate its proxy potential in the region (Table 1.5; Rodríguez-Castañeda, 2008; Choumiline, 2011). However, its long-term preservation in sedimentary records is an important issue. For La Paz Basin, we can confirm that $Ba_{excess}$ did not behave as a reliable productivity proxy—showing trends that differ significantly from those of the other indicators (Table 1.3). However, our $Ba_{excess}$ record in Alfonso Basin does mirror other productivity proxies ($C_{org}$ and Ni) and is statistically associated with them (Figure 1.5). This agreement could be because our Alfonso Basin core was not exposed to diagenetic remobilization of sedimentary barite as severe as that experienced by the La Paz basin core (McManus et al., 1998; Riedinger et al., 2006). Despite the good agreement between proxy records and $Ba_{excess}$ in Alfonso Basin, long-term preservation of the Ba fraction remains a concern (Schoepfer et al., 2015).

In our studied cores, Ni shows good temporal agreement with both the productivity ($C_{org}$ and $Ba_{excess}$) and water column redox proxies (V and $U_{auth}$). In Alfonso Basin, this element served as the best indicator for productivity—mirroring an independent biogenic $SiO_2$ record from Guaymas Basin generated by Barron and Bukry (2007) (Figure 1.8). Nickel does not follow Mo and Cd, which are bottom water and/or diagenetic redox proxies (Figure 1.5), which could be explained by

a significant contribution of particulate Ni (Table 1.5), enriched in settling matter by biological uptake (Böning et al., 2015) and potentially related to diatom export (Twining et al., 2012).

In our sediment cores from Alfonso and La Paz basins, Mo covaries with Cd (Figure 1.5) and reaches high values. However, due to the low, transient, or even absent concentrations of water column $H_2S$ in most modern OMZs, it is unlikely that Mo enrichments are related to bottom water euxinia in such settings (Scott and Lyons, 2012; McKay and Pedersen, 2014; Costa et al., 2018). Nevertheless, Mo is commonly elevated in ETNP sediment cores, reaching maxima several times higher than the average crustal value of 1.4 mg/kg (Wedepohl, 1995) (Figure 1.7; Table 1.5). These values are likely linked to the presence of sulfide only in the pore waters, leading to diagenetic enrichments (Zheng et al., 2000; Scholz et al., 2017; Hardisty et al., 2018). Because of this diagenetic enrichment, Mo is a less sensitive indicator of very low and transient sulfide in the water column.

We confirm the utility of V as a water column redox proxy as expressed through strong correlation with water column denitrification records reconstructed from sedimentary $\delta^{15}N$ in the ETNP OMZ (Tems et al., 2016). Moreover, V is sensitive to $O_2$ changes occurring not only at upper OMZ depths but also those closer to the OMZ-core, which have less pronounced redox variations. It is worth noting that, as for $U_{auth}$, there is evidence for an important contribution of V through settling matter (Rodríguez-Castañeda, 2008; Hakspiel-Segura et al., 2016; Bauer et al., 2017; Ho et al., 2018). The source of such enrichments is yet unknown, but we hypothesize that it could be related to redox processes causing authigenic V enrichment in organic matter aggregates (Ho et al., 2018).

An important methodological distinction needs to be made for proper numerical treatment of sediments with highly variable $CaCO_3$ and biogenic silica contents. As previously suggested (Pichevin et al., 2012, 2014), proxy records can, in some cases, be significantly impacted by

dilution with major components. In this study we have $CaCO_3$ values for the studied sediment cores, so CFB fraction calculations were possible. By comparing elemental concentrations against CFB-corrected values, no substantial differences were found. Most importantly, the paleoceanographic and paleoclimatic trends described in this chapter also prevailed for the carbonate-corrected values. We have no data to corroborate the dilution effect with biogenic opal, as it was not measured for the cores studied here. The consequences of the dilution effects with biogenic detritus need to be further investigated for Alfonso Basin and similar marine settings.

#### 1.4.1.1. New insights on uranium biogeochemistry in OMZs

In our study, uranium shows a consistently good correlation with $C_{org}$ and the micronutrient Ni in both the deeper (mid OMZ) and shallow cores (upper OMZ) (Figure 1.4 and Supplementary Figure 1.3). We attribute this observation to seasonal variation in dissolved $O_2$ and to a particulate authigenic U contribution during settling (Rodríguez-Castañeda, 2008; Choumiline, 2011). As particles settle deeper, there is more reaction time for dissolved U (+6) to be reduced to its particulate phase U (+4) and/or for adsorption to occur. This relationship is a consistent feature of vertical sediment trap moorings—that is, higher authigenic U enrichment in the particles collected in deeper waters (Zheng et al., 2002; Rodríguez-Castañeda, 2008; Huang and Conte, 2009; Choumiline, 2011). The extent to which $U_{auth}$ enrichments are microbially mediated remains unknown, but evidence suggests that these biological interactions could be among the principal controls (Lovley et al., 1991; Cumberland et al., 2016). There is growing evidence that anaerobic metabolism can occur within aggregates of settling matter if conditions are energetically favorable (Wright et al., 2012; Lehto et al., 2014; Bianchi et al., 2018). Authigenic U formation is favored after the ferruginous (Fe reduction) and sulfidic ($SO_4^{2-}$ reduction) chemical zones (Zheng et al., 2002; Canfield and Thamdrup, 2009). This range of redox conditions is common in marine

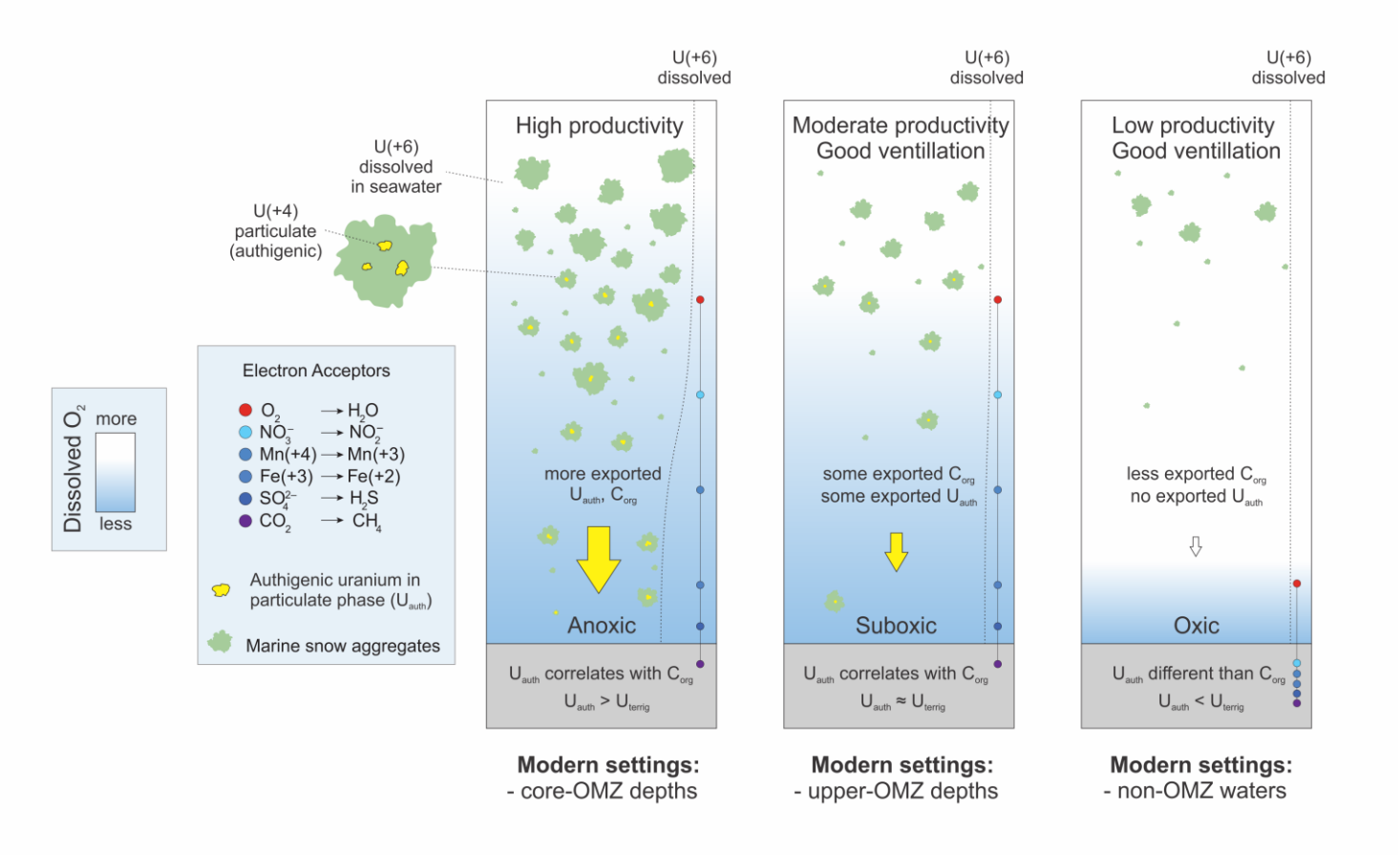


**Figure 1.10.** Hypothetic scenarios of uranium biogeochemistry in modern OMZs.

aggregates of modern OMZs (Bianchi et al., 2018), which could explain the strong authigenic U enrichments in settling matter of the Gulf of California and California Margin (Zheng et al., 2002; Choumiline, 2011). Other marine settings, such as Saanich Inlet, also reveal the possibility of water column authigenic U enrichments, where up to one third of the estimated authigenic fraction is captured in particles in the water column (Holmden et al., 2015). It is worth mentioning that while ideal microenvironments for particulate-$U_{auth}$ formation exist in strongly reducing and restricted settings in the Black and Baltic seas, as well as the Cariaco Basin (Dellwig et al., 2010; Calvert et al., 2015; Bauer et al., 2017), significant $U_{auth}$ enrichments have not been detected (Anderson et al., 1989; Calvert et al., 2015). Perhaps the necessary conditions for authigenic U enrichments are favored in coastal upwelling sites, where high productivity and thus abundant particulate organic matter formation are common.

We propose an updated model for $U_{auth}$ enrichments (Figure 1.10). This model points to a significant contribution of $U_{auth}$, beyond that linked to diagenesis, via settling matter in regions of high productivity and upwelling—such as the coastal regions of the ETNP.

In summary, the current understanding of U geochemistry in OMZs supports a significant contribution via settling particulates during times of high productivity. The actual enrichment mechanism could either be linked to localized reduction within organic-rich microenvironments or simply adsorption to organic matter. Both processes could explain the correlation with $C_{org}$ and Ni and excessive U enrichments during well-ventilated times. Improved understanding of the details of U uptake will enhance its utility as a paleoproxy.

### 1.4.2. Suggestions for future work

This research highlights the importance of comparing high-resolution OMZ records of both modern and past oceanic conditions with global climatic trends. We have demonstrated it is

possible to reconstruct high-resolution OMZ variability using a multiproxy approach. However, there are multiple caveats when interpreting deoxygenation and productivity trends because of the complex mechanisms by which trace elements are transferred to sedimentary records. We encourage particular caution for elements that demand an understanding of the relative contributions from diagenetic vs. water column processes and how specifically those inputs translate to regional patterns of redox and productivity. The importance of particulate supply of scavenged non-detrital trace elements in OMZ-type settings is clear, and further research, when possible, should include isotopic data as a source of additional mechanistic perspective.

## 1.5. CONCLUSIONS

In the modern Eastern Tropical North Pacific, marine sediments are mostly enriched in Cd, Mo, V at sites underlying severely hypoxic and anoxic waters—in contrast to shallower and oxygenated sites where these elements are present in low, mostly crustal, abundances. The exception is U, which is found to be enriched not only in sediments underlying anoxic waters but also in those of well-ventilated regions, suggesting a strong contribution of authigenic uranium through settling of marine snow aggregates.

Most of the sites located at present Oxygen Minimum Zone depths remained anoxic over the last millennium. The Eastern Tropical North Pacific Oxygen Minimum Zone expanded throughout the Little Ice Age, with the most anoxic events during the Spörer, Maunder, and Dalton insolation minima. Reoxygenation in the Eastern Tropical North Pacific occurred during warm periods around late 1300s, early 1700s, and late 1900s AD.

There is no clear effect of the temperature increase of twentieth century on the intensification of the Eastern Tropical North Pacific Oxygen Minimum Zone. The prevailing trend shows an

increase in dissolved oxygen from the 1900s AD toward present time, with a subtle decrease in the beginning of the twenty-first century.

Redox and productivity changes reconstructed for the last millennium from marine basins of the Eastern Tropical North Pacific indicate a strong relationship with insolation fluctuations and the Pacific Walker Circulation that drive upwelling rates, productivity, and oceanic anoxia at Oxygen Minimum Zone depths.

The most reliable redox proxies for water column oxygenation in Oxygen Minimum Zones are vanadium and uranium. Uranium also shows strong potential to serve as a productivity proxy because it can be exported from the water column to sediments through settling particulate matter during periods of high primary productivity. Molybdenum is the least useful proxy for Oxygen Minimum Zone oxygenation because it is not sensitive to small redox variations and can be enriched diagenetically when pore water sulfide is present.

## 1.6. ACKNOWLEDGMENTS

The authors acknowledge financial support granted by UC MEXUS - CONACYT Collaborative Research Grant “High resolution geochemical reconstructions of recent climate and oxygenation history in La Paz Bay, Gulf of California” that covered travel and analytical costs. The authors express gratitude to Coordinación de Plataformas Oceanográficas (UNAM, Mexico) for funding the PALEOMAR-I campaign and the crew members of R/V “El Puma” for exceptional support during the field stage. KC was thankful for the UC MEXUS – CONACYT Doctoral Fellowship for a fully funded scholarship during his Ph.D. studies and for the 2016 UC MEXUS Dissertation Grant award for analytical expenses. Partial support was received by TL, KC, and SB from the NASA Astrobiology Institute, and AG from the USDA NIFA Hatch program (project # CA-R-ENS-5120-H).

## 1.7. REFERENCES


Algeo, T. J., and Lyons, T. W. (2006). Mo-total organic carbon covariation in modern anoxic marine environments: implications for analysis of paleoredox and paleohydrographic conditions. Paleoceanogr. Paleoclimatol. 21:PA1016 doi: 10.1029/2004PA001112

Algeo, T. J., and Rowe, H. (2012). Paleoceanographic applications of trace-metal concentration data. Chem. Geol. 324–325, 6–18. doi: 10.1016/j.chemgeo.2011.09.002

Algeo, T. J., and Tribovillard, N. (2009). Environmental analysis of paleoceanographic systems based on molybdenum–uranium covariation. Chem. Geol. 268, 211–225. doi: 10.1016/j.chemgeo.2009.09.001

Anderson, R. F., Fleisher, M. Q., and Lehuray, A. P. (1989). Concentration, oxidation state, and particulate flux of uranium in the Black Sea. Geochim. Cosmochim. Acta 53, 2215–2224. doi: 10.1016/0016-7037(89)90345-1

Anderson, R. F., and Winckler, G. (2005). Problems with paleoproductivity proxies. Paleoceanogr. Paleoclimatol. 20:PA3012. doi: 10.1029/2004PA0 01107

Atwood, A. R., Wu, E., Frierson, D. M. W., Battisti, D. S., and Sachs, J. P. (2016). Quantifying climate forcings and feedbacks over the Last Millennium in the CMIP5-PMIP3Models. J. Clim. 29, 1161–1178. doi: 10.1175/JCLI-D-15-0063.1

Badan-Dangon, A., Dorman, C. E., Merrifield, M. A., and Winant, C. D. (1991). The lower atmosphere over the Gulf of California. J. Geophys. Res. 96, 16887–16896. doi: 10.1029/91JC01433

Bard, E., Raisbeck, G., Yiou, F., and Jouzel, J. (2000). Solar irradiance during the last 1200 years based on cosmogenic nuclides. Tellus B 52, 985–992. doi: 10.3402/tellusb.v52i3.17080

Barron, J. A., and Bukry, D. (2007). Solar forcing of Gulf of California climate during the past 2000 yr suggested by diatoms and silicoflagellates. Mar. Micropaleontol. 62, 115–139. doi: 10.1016/j.marmicro.2006.08.003

Battaglia, G., and Joos, F. (2018). Hazards of decreasing marine oxygen: the near term and millennial-scale benefits of meeting the Paris climate targets. Earth Syst. Dyn. 9, 797–816. doi: 10.5194/esd-9-797-2018

Bauer, S., Blomqvist, S., and Ingri, J. (2017). Distribution of dissolved and suspended particulate molybdenum, vanadium, and tungsten in the Baltic Sea. Mar. Chem. 196, 135–147. doi: 10.1016/j.marchem.2017.08.010

Beaufort, L., and Grelaud, M. (2017). A 2700-year record of ENSO and PDO variability from the Californian margin based on coccolithophore assemblages and calcification. Prog. Earth Planet. Sci. 4:5. doi: 10.1186/s40645-017-0123-z

Bianchi, D.,Weber, T. S., Kiko, R., and Deutsch, C. (2018). Global niche of marine anaerobic metabolisms expanded by particle microenvironments. Nat. Geosci. 11, 263–268. doi: 10.1038/s41561-018-0081-0

Bianchi, T. S., Schreiner, K. M., Smith, R. W., Burdige, D. J., Woodard, S., and Conley, D. J. (2016). Redox effects on organic matter storage in coastal sediments during the holocene: a biomarker/proxy perspective. Annu. Rev. Earth Planet. Sci. 44, 295–319. doi: 10.1146/annurev-earth-060614-105417

Bograd, S. J., Castro, C. G., Di Lorenzo, E., Palacios, D. M., Bailey, H., Gilly, W., et al. (2008). Oxygen declines and the shoaling of the hypoxic boundary in the California Current. Geophys. Res. Lett. 35:L12607. doi: 10.1029/2008GL034185

Bograd, S. J., Checkley, D. A., and Wooster, W. S. (2003). CalCOFI: a half century of physical, chemical, and biological research in the California Current System. Deep Sea Res. Part II Top. Stud. Oceanogr. 50, 2349–2353. doi: 10.1016/S0967-0645(03)00122-X

Böning, P., Shaw, T., Pahnke, K., and Brumsack, H.-J. (2015). Nickel as indicator of fresh organic matter in upwelling sediments. Geochim. Cosmochim. Acta 162, 99–108. doi: 10.1016/j.gca.2015.04.027

Borreggine, M., Myhre, S. E., Mislan, K. A. S., Deutsch, C., and Davis, C. V. (2017). A database of paleoceanographic sediment cores from the North Pacific, 1951-2016. Earth Syst. Sci. Data 9, 739–749. doi: 10.5194/essd-9-739-2017

Breitburg, D., Levin, L. A., Oschlies, A., Grégoire, M., Chavez, F. P., Conley, D. J., et al. (2018). Declining oxygen in the global ocean and coastal waters. Science 359:eaam7240. doi: 10.1126/science.aam7240

Brumsack, H.-J., and Gieskes, J. (1983). Interstitial water trace-metal chemistry of laminated sediments from the Gulf of California, Mexico. Mar. Chem. 14, 89–106. doi: 10.1016/0304-4203(83)90072-5

Burdige, D. J. (2007). Preservation of organic matter in marine sediments: controls, mechanisms, and an imbalance in sediment organic carbon budgets? Chem. Rev. 107, 467–485. doi: 10.1021/cr050347q

Bustos-Serrano, H., and Castro-Valdez, R. (2006). Flux of nutrients in the Gulf of California: geostrophic approach. Mar. Chem. 99, 210–219. doi: 10.1016/j.marchem.2005.09.012

Calvert, S. E., Bustin, R. M., and Ingall, E. D. (1996). Influence of water column anoxia and sediment supply on the burial and preservation of organic carbon in marine shales. Geochimica Cosmochimica Acta 60, 1577–1593.

Calvert, S. E., and Pedersen, T. (1993). Geochemistry of recent oxic and anoxic marine sediments: implications for the geological record. Mar. Geol. 113, 67–88. doi: 10.1016/0025-3227(93)90150-T

Calvert, S. E., Piper, D. Z., Thunell, R. C., and Astor, Y. (2015). Elemental settling and burial fluxes in the Cariaco Basin. Mar. Chem. 177, 607–629. doi: 10.1016/j.marchem.2015.10.001

Canfield, D. E., and Thamdrup, B. (2009). Towards a consistent classification scheme for geochemical environments, or, why we wish the term 'suboxic' would go away. Geobiology 7, 385–392. doi: 10.1111/j.1472-4669.2009.00214.x

Carpenter, J. H. (1965). The Chesapeake Bay Institute technique for the Winkler dissolved oxygen method. Limnol. Oceanogr. 10, 141–143. doi: 10.4319/lo.1965.10.1.0141

Cartapanis, O., Tachikawa, K., Romero, O. E., and Bard, E. (2014). Persistent millennial-scale link between Greenland climate and northern Pacific Oxygen Minimum Zone under interglacial conditions. Clim. Past 10, 405–418. doi: 10.5194/cp-10-405-2014

Chang, A. S., Bertram, M. A., Ivanochko, T., Calvert, S. E., Dallimore, A., and Thomson, R. E. (2013). Annual record of particle fluxes, geochemistry and diatoms in Effingham Inlet, British Columbia, Canada, and the impact of the 1999 La Niña event. Mar. Geol. 337, 20–34. doi: 10.1016/j.margeo.2013.01.003

Chang, A. S., Pedersen, T. F., and Hendy, I. L. (2014). Effects of productivity, glaciation, and ventilation on late Quaternary sedimentary redox and trace element accumulation on the Vancouver Island margin, western Canada. Paleoceanography 29, 730–746. doi: 10.1002/2013PA002581

Chappaz, A., Lyons, T. W., Gregory, D. D., Reinhard, C. T., Gill, B. C., Li, C., et al. (2014). Does pyrite act as an important host for molybdenum in modern and ancient euxinic sediments? Geochim. Cosmochim. Acta 126, 112–122. doi: 10.1016/j.gca.2013.10.028

Chavez, F. P., Messié, M., and Pennington, J. T. (2011).Marine primary production in relation to climate variability and change. Ann. Rev. Mar. Sci. 3, 227–260. doi: 10.1146/annurev.marine.010908.163917

Choumiline, K. (2011). Geoquímica de la materia particulada en hundimiento y de los sedimentos recientes de Cuenca Alfonso, Bahía de La Paz. (Master's thesis). Centro Interdisciplinario de Ciencias Marinas – Instituto Politécnico Nacional, La Paz, Mexico.

Choumiline, K., Lyons, T. W., Pérez-Cruz, L., Carriquiry, J. D., Raiswell, R., and Beaufort, L. (2017). "Sensitivity of redox proxies to rapid variability in Oxygen Minimum Zones. Goldschmidt 2017," in Abstract Retrieved from Goldschmidt Conference Archive (Paris).

Choumiline, K., Rodríguez-Castañeda, A. P., Silverberg, N., Shumilin, E., Aguirre- Bahena, F., Sapozhnikov, D., et al. (2010). "Arsenic and uranium in the settling particulate matter and sediments of Alfonso Basin, La Paz Bay," in Proceedings of the 13th International Conference on Water-Rock Interaction. Reviewed Extended Abstract (Guanajuato).

Cocco, V., Joos, F., Steinacher,M., Frölicher, T. L., Bopp, L., Dunne, J., et al. (2013). Oxygen and indicators of stress for marine life in multi-model global warming projections. Biogeosciences 10, 1849–1868. doi: 10.5194/bg-10-1849-2013

Conte, M. H., Carter, A. M., Koweek, D. A., Huang, S., and Weber, J. C. (2019). The elemental composition of the deep particle flux in the Sargasso Sea. Chem. Geol. 511, 279–313. doi: 10.1016/j.chemgeo.2018.11.001

Coria-Monter, E., Monreal-Gómez, M. A., Salas-de-León, D. A., Aldeco-Ramírez, J., and Merino-Ibarra, M. (2014). Differential distribution of diatoms and dinoflagellates in a cyclonic eddy confined in the Bay of La Paz, Gulf of California. J. Geophys. Res. 119, 6258–6268. doi: 10.1002/2014JC009916

Costa, K. M., Anderson, R. F., McManus, J. F., Winckler, G., Middleton, J. L., and Langmuir, C. H. (2018). Trace element (Mn, Zn, Ni, V) and authigenic uranium (aU) geochemistry reveal sedimentary redox history on the Juan de Fuca Ridge, North Pacific Ocean. Geochim. Cosmochim. Acta 236, 79–98. doi: 10.1016/j.gca.2018.02.016

Cumberland, S. A., Douglas, G., Grice, K., and Moreau, J. W. (2016). Uranium mobility in organic matter-rich sediments: a review of geological and geochemical processes. Earth Sci. Rev. 159, 160–185. doi: 10.1016/j.earscirev.2016.05.010

Dean, W., Pride, C., and Thunell, R. (2004). Geochemical cycles in sediments deposited on the slopes of the Guaymas and Carmen Basins of the Gulf of California over the last 180 years. Quat. Sci. Rev. 23, 1817–1833. doi: 10.1016/j.quascirev.2004.03.010

Dean, W. E. (2007). Sediment geochemical records of productivity and oxygen depletion along the margin of western North America during the past 60,000 years: teleconnections with Greenland Ice and the Cariaco Basin. Quat. Sci. Rev. 26, 98–114. doi: 10.1016/j.quascirev.2006.08.006

Dellwig, O., Leipe, T., März, C., Glockzin, M., Pollehne, F., Schnetger, B., et al. (2010). A new particulate Mn–Fe–P-shuttle at the redoxcline of anoxic basins. Geochim. Cosmochim. Acta 74, 7100–7115. doi: 10.1016/j.gca.2010.09.017

Deutsch, C., Berelson, W., Thunell, R., Weber, T., Tems, C., McManus, J., et al. (2014). Oceanography. Centennial changes in North Pacific anoxia linked to tropical trade winds. Science 345, 665–668. doi: 10.1126/science.1252332

Di Lorenzo, E., Cobb, K.M., Furtado, J. C., Schneider, N., Anderson, B. T., Bracco, A., et al. (2010). Central Pacific El Niño and decadal climate change in the North Pacific Ocean. Nat. Geosci. 3, 762–765. doi: 10.1038/ngeo984

Di Lorenzo, E., Schneider, N., Cobb, K. M., Franks, P. J. S., Chhak, K., Miller, A. J., et al. (2008). North Pacific Gyre Oscillation links ocean climate and ecosystem change. Geophys. Res. Lett. 35:L08607. doi: 10.1029/2007GL032838

Dickens, G. R., Koelling, M., Smith, D. C., and Schnieders, L. (2007). Rhizon sampling of pore waters on scientific drilling expeditions: an example from the IODP Expedition 302, Arctic Coring Expedition (ACEX). Sci. Drilling 4, 22–25. doi: 10.5194/sd-4-22-2007

Dunk, R. M., Mills, R. A., and Jenkins, W. J. (2002). A reevaluation of the oceanic uranium budget for the Holocene. Chem. Geol. 190, 45–67. doi: 10.1016/S0009-2541(02)00110-9

Dupont, C. L., Buck, K. N., Palenik, B., and Barbeau, K. (2010). Nickel utilization in phytoplankton assemblages from contrasting oceanic regimes. Deep Sea Res. Part I Oceanogr. Res. Pap. 57, 553–566. doi: 10.1016/j.dsr.2009.12.014

Durand, A., Chase, Z., Townsend, A. T., Noble, T., Panietz, E., and Goemann, K. (2016). Improved methodology for the microwave digestion of carbonate-rich environmental samples. Int. J. Environ. Anal. Chem. 96, 119–136. doi: 10.1080/03067319.2015.1137904

Durazo-Arvizu, R., and Gaxiola-Castro, G. (2010). Dinámica del ecosistema pelágico frente a Baja California, 1997–2007. Diez años de investigaciones mexicanas de la Corriente de California. Mexico, Distrito Federal: INE/CICESE/UABC/SEMARNAT.

Dymond, J., Suess, E., and Lyle, M. (1992). Barium in deep-sea sediment. A geochemical proxy for paleoproductivity. Paleoceanography Paleoclimatol. 7, 163–181. doi: 10.1029/92PA00181

Eagle, M., Paytan, A., Arrigo, K. R., van Dijken, G., and Murray, R. W. (2003). A comparison between excess barium and barite as indicators of carbon export. Paleoceanogr. Paleoclimatol. 18:1021. doi: 10.1029/2002PA000793

Erickson, B. E., and Helz, G. R. (2000). Molybdenum(VI) speciation in sulfidic waters:: Stability and lability of thiomolybdates. Geochim. Cosmochim. Acta 64, 1149–1158. doi: 10.1016/S0016-7037(99)00423-8

Foster, I. D. L., and Walling, D. E. (1994). Using reservoir deposits to reconstruct changing sediment yields and sources in the catchment of the Old Mill Reservoir, South Devon, UK, over the past 50 years. Hydrol. Sci. J. 39, 347–368. doi: 10.1080/02626669409492755

Fu,W., Primeau, F.,Moore, J. K., Lindsay, K., and Randerson, J. T. (2018). Reversal of increasing tropical ocean hypoxia trends with sustained climate warming. Global Biogeochem. Cycles 32, 551–564. doi: 10.1002/2017GB005788

Ganeshram, R. S., and Pedersen, T. F. (1998). Glacial-interglacial variability in upwelling and bioproductivity off NW Mexico: implications for quaternary paleoclimate. Paleoceanography Paleoclimatol. 13, 634–645. doi: 10.1029/98PA02508

Garcia, H. E., Locarnini, R. A., Boyer, T. P., and Antonov, J. I. (2006).World Ocean Atlas 2005, Volume 3: Dissolved Oxygen, Apparent Oxygen Utilization, and Oxygen Saturation. S. Levitus, Ed. NOAA Atlas NESDIS 63, U.S. Government Printing Office, Washington, D.C., 342 pp.

Gilly, W. F., Beman, J. M., Litvin, S. Y., and Robison, B. H. (2013). Oceanographic and biological effects of shoaling of the oxygen minimum zone. Ann. Rev. Mar. Sci. 5, 393–420. doi: 10.1146/annurev-marine-120710-1 00849

Griffiths, M. L., Kimbrough, A. K., Gagan, M. K., Drysdale, R. N., Cole, J. E., Johnson, K. R., et al. (2016). Western Pacific hydroclimate linked to global climate variability over the past two millennia. Nat. Commun. 7:11719. doi: 10.1038/ncomms11719

Hakspiel-Segura, C., Martínez-López, A., Pinedo-González, P., Verdugo-Díaz, G., and Acevedo-Acosta, J. D. (2016). Composition of metals in suspended particulate matter of Alfonso basin, southern Gulf of California. Reg. Stud.Mar. Sci. 3, 144–153. doi: 10.1016/j.rsma.2015.07.001

Hardisty, D. S., Lyons, T. W., Riedinger, N., Isson, T. T., Owens, J. D., Aller, R. C., et al. (2018). An evaluation of sedimentary molybdenum and iron as proxies for pore fluid paleoredox conditions. Am. J. Sci. 318, 527–556. doi: 10.2475/05.2018.04

Helz, G. R., Bura-Naki´c, E., Mikac, N., and Ciglenec̆ki, I. (2011). New model for molybdenum behavior in euxinic waters. Chem. Geol. 284, 323–332. doi: 10.1016/j.chemgeo.2011.03.012

Helz, G. R.,Miller, C. V., Charnock, J.M.,Mosselmans, F.W., Pattrick, R., Garner, D., et al. (1996). Mechanism of molybdenum removal from the sea and its concentration in black shales: EXAFS evidence. Geochim. Cosmochim. Acta 60, 3631–3642. doi: 10.1016/0016-7037(96)00195-0

Hendy, I. L., and Kennett, J. P. (2000). Dansgaard-Oeschger cycles and the California current system: Planktonic foraminiferal response to rapid climate change in Santa Barbara Basin, Ocean Drilling Program Hole 893A. Paleoceanogr. Paleoclimatol. 15, 30–42. doi: 10.1029/1999PA000413

Hendy, I. L., and Pedersen, T. F. (2006). Oxygen minimum zone expansion in the eastern tropical North Pacific during deglaciation. Geophys. Res. Lett. 33:L20602. doi: 10.1029/2006GL025975

Ho, P., Lee, J.-M., Heller, M. I., Lam, P. J., and Shiller, A.M. (2018). The distribution of dissolved and particulate Mo and V along the U.S. GEOTRACES East Pacific Zonal Transect (GP16): the roles of oxides and biogenic particles in their distributions in the oxygen deficient zone and the hydrothermal plume. Mar. Chem. 201, 242–255. doi: 10.1016/j.marchem.2017.12.003

Hofmann, A. F., Peltzer, E. T., Walz, P. M., and Brewer, P. G. (2011). Hypoxia by degrees: establishing definitions for a changing ocean. Deep Sea Res. Part I Oceanogr. Res. Pap. 58, 1212–1226. doi: 10.1016/j.dsr.2011.09.004

Holmden, C., Amini, M., and Francois, R. (2015). Uranium isotope fractionation in Saanich Inlet: a modern analog study of a paleoredox tracer. Geochim. Cosmochim. Acta 153, 202–215. doi: 10.1016/j.gca.2014.11.012

Hoogakker, B. A. A., Lu, Z., Umling, N., Jones, L., Zhou, X., Rickaby, R. E.M., et al. (2018). Glacial expansion of oxygen-depleted seawater in the eastern tropical Pacific. Nature 562, 410–413. doi: 10.1038/s41586-018-0589-x

Howes, E. L., Joos, F., Eakin, C. M., and Gattuso, J.-P. (2015). An updated synthesis of the observed and projected impacts of climate change on the chemical, physical and biological processes in the oceans. Front. Mar. Sci. 2:36. doi: 10.3389/fmars.2015.00036

Huang, S., and Conte, M. H. (2009). Source/process apportionment of major and trace elements in sinking particles in the Sargasso sea. Geochim. Cosmochim. Acta 73, 65–90. doi: 10.1016/j.gca.2008.08.023

IPCC (2014). Climate Change 2014: Synthesis Report. Contribution of Working Groups I, II and III to the Fifth Assessment Report of the Intergovernmental Panel on Climate Change [Core Writing Team, R.K. Pachauri and L.A. Meyer (eds.)]. IPCC, Geneva, Switzerland, 151pp.

Ivanochko, T. S., Calvert, S. E., Southon, J. R., Enkin, R. J., Baker, J., Dallimore, A., et al. (2008). Determining the post-glacial evolution of a northeast Pacific coastal fjord using a multiproxy geochemical approach. Can. J. Earth Sci. 45, 1331–1344. doi: 10.1139/E08-030

Ivanochko, T. S., and Pedersen, T. F. (2004). Determining the influences of Late Quaternary ventilation and productivity variations on Santa Barbara Basin sedimentary oxygenation: a multi-proxy approach. Quat. Sci. Rev. 23, 467–480. doi: 10.1016/j.quascirev.2003.06.006

Keeling, R. E., Kortzinger, A., and Gruber, N. (2010). Ocean deoxygenation in a warming world. Ann. Rev. Mar. Sci. 2, 199–229. doi: 10.1146/annurev.marine.010908.163855 Klinkhammer, G. P., and Palmer, M. R. (1991). Uranium in the oceans: where it goes and why. Geochim. Cosmochim. Acta 55, 1799–1806. doi: 10.1016/0016-7037(91)90024-Y

Ku, T.-L., Knauss, K. G., and Mathieu, G. G. (1977). Uranium in open ocean: concentration and isotopic composition. Deep Sea Res. 24, 1005–1017. doi: 10.1016/0146-6291(77)90571-9

Lavín, M. F., Castro, R., Beier, E., and Godínez, V. M. (2013). Mesoscale eddies in the southern Gulf of California during summer: characteristics and interaction with the wind stress. J. Geophys. Res. Oceans 118, 1367–1381. doi: 10.1002/jgrc.20132

Lehto, N., Glud, R. N., Á., Norð*i, G., Zhang, H., and Davison, W. (2014). Anoxic microniches in marine sediments induced by aggregate settlement: biogeochemical dynamics and implications. Biogeochemistry 119, 307–327. doi: 10.1007/s10533-014-9967-0

Levin, L. A. (2018). Manifestation, drivers, and emergence of open ocean deoxygenation. Ann. Rev. Mar. Sci. 10, 229–260. doi: 10.1146/annurev-marine-121916-063359

Long, M. C., Deutsch, C., and Ito, T. (2016). Finding forced trends in oceanic oxygen. Global Biogeochem. Cycles 30, 381–397. doi: 10.1002/2015GB 005310

Lovley, D. R., Phillips, E. J. P., Gorby, Y. A., and Landa, E. R. (1991). Microbial reduction of uranium. Nature 350, 413–416. doi: 10.1038/350413a0

Lu, Z., Hoogakker, B. A. A., Hillenbrand, C.-D., Zhou, X., Thomas, E., et al. (2016). Oxygen depletion recorded in upper waters of the glacial Southern Ocean. Nat. Commun. 7:11146. doi: 10.1038/ncomms11146

Lynn, R. J., and Simpson, J. J. (1987). The California Current system: the seasonal variability of its physical characteristics. J. Geophys. Res. Atmos. 92, 12947–12966. doi: 10.1029/JC092iC12p12947

Lyons, T. W., and Berner, R. A. (1992). Carbon-sulfur-iron systematics of the uppermost deep-water sediments of the Black Sea. Chem. Geol. 99, 1–27. doi: 10.1016/0009-2541(92)90028-4

Lyons, T. W., Reinhard, C. T., and Scott, C. (2009). Redox redux. Geobiology 7, 489–494. doi: 10.1111/j.1472-4669.2009.00222.x

Lyons, T.W., and Severmann, S. (2006). A critical look at iron paleoredox proxies: new insights from modern euxinic marine basins. Geochim. Cosmochim. Acta 70, 5698–5722. doi: 10.1016/j.gca.2006.08.021

Mantua, N. J., and Hare, S. R. (2002). The Pacific decadal oscillation. J. Oceanogr. 58, 35–44. doi: 10.1023/A:1015820616384

McKay, J. L., and Pedersen, T. F. (2014). Geochemical response to pulsed sedimentation: implications for the use of Mo as a paleo-proxy. Chem. Geol. 382, 83–94. doi: 10.1016/j.chemgeo.2014.05.009

McManus, J., Berelson, W. M., Coale, K. H., Johnson, K. S., and Kilgore, T. E. (1997). Phosphorus regeneration in continental margin sediments. Geochim. Cosmochim. Acta 61, 2891–2907. doi: 10.1016/S0016-7037(97)00138-5

McManus, J., Berelson, W. M., Klinkhammer, G. P., Johnson, K. S., Coale, K. H., Anderson, R. F., et al. (1998). Geochemistry of barium in marine sediments: implications for its use as a paleoproxy. Geochim. Cosmochim. Acta 62, 3453–3473. doi: 10.1016/S0016-7037(98)00248-8

McManus, J., Berelson, W. M., Severmann, S., Poulson, R. L., Hammond, D. E., Klinkhammer, G. P., et al. (2006). Molybdenum and uranium geochemistry in continental margin sediments: paleoproxy potential. Geochim. Cosmochim. Acta 70, 4643–4662. doi: 10.1016/j.gca.2006.06.1564

McPhaden, M. J. (2004). Evolution of the 2002/03 El Niño∗. Bull. Am. Meteorol. Soc. 85, 677–695. doi: 10.1175/BAMS-85-5-677 Metcalfe, S. E., Barron, J. A., and Davies, S. J. (2015). The Holocene history of the North American Monsoon: 'known knowns' and 'known unknowns' in understanding its spatial and temporal complexity. Quat. Sci. Rev. 120, 1–27. doi: 10.1016/j.quascirev.2015.04.004

Moffitt, S. E., Moffitt, R. A., Sauthoff, W., Davis, C. W., Hewett, K., and Hill, T. M. (2015). Paleoceanographic insights on recent oxygen minimum zone expansion: lessons for modern oceanography. PLoS ONE 10: e0115246. doi: 10.1371/journal.pone.0115246

Monreal-Gómez, M. A., Molina-Cruz, A., and Salas-de-León, D. A. (2001).Water masses and cyclonic circulation in Bay of la Paz, Gulf of California, during June 1998. J. Mar. Syst. 30, 305–315. doi: 10.1016/S0924-7963(01)00064-1

Morford, J. L., and Emerson, S. (1999). The geochemistry of redox sensitive trace metals in sediments. Geochim. Cosmochim. Acta 63, 1735–1750. doi: 10.1016/S0016-7037(99)00126-X

Morse, J. W., and Luther, G. W. III. (1999). Chemical influences on trace metal-sulfide interactions in anoxic sediments. Geochim. Cosmochim. Acta 63, 3373–3378. doi: 10.1016/S0016-7037(99)00258-6

Moy, C. M., Seltzer, G. O., Rodbell, D. T., and Anderson, D. M. (2002). Variability of El Niño/Southern Oscillation activity at millennial timescales during the Holocene epoch. Nature 420, 162–165. doi: 10.1038/nature01194

Nameroff, T. J., Calvert, S. E., and Murray, J. W. (2004). Glacial-interglacial variability in the eastern tropical North Pacific oxygen minimum zone recorded by redox-sensitive trace metals. Paleoceanogr. Paleoclimatol. 19:PA1010. doi: 10.1029/2003PA000912

Nava-Sánchez, E. H., Gorsline, D. S., and Molina-Cruz, A. (2001). The Baja California peninsula borderland: structural and sedimentological characteristics. Sediment. Geol. 144, 63–82. doi: 10.1016/S0037-0738(01)00135-X

Ontiveros-Cuadras, J. F., Thunell, R., Ruiz-Fernández, A. C., Benitez-Nelson, C., Machain-Castillo, M. L., Tappa, E., et al. (2019). Centennial OMZ changes in the NW Mexican Margin from geochemical and foraminiferal sedimentary records. Cont. Shelf Res. 176, 64–75. doi: 10.1016/j.csr.2019.02.009

Oschlies, A., Schulz, K. G., Riebessel, U., Schmittner, A. (2008). Simulated 21st century's increase in oceanic suboxia by $CO_2$-enhanced biotic carbon export. Global Biogeochem. Cycles 22:GB4008. doi: 10.1029/2007GB003147

Pérez-Cruz, L. (2013). Hydrological changes and paleoproductivity in the Gulf of California during middle and late Holocene and their relationship with ITCZ and North American Monsoon variability. Quat. Res. 79, 138–151. doi: 10.1016/j.yqres.2012.11.007

Pichevin, L., Ganeshram, R. S., Reynolds, B. C., Prahl, F., Pedersen, T. F., Thunell, R., et al. (2012). Silicic acid biogeochemistry in the Gulf of California: Insights from sedimentary Si isotopes. Paleoceanogr. Paleoclimatol. 27:PA2201. doi: 10.1029/2011PA002237

Pichevin, L. E., Ganeshram, R. S., Geibert,W., Thunell, R., and Hinton, R. (2014). Silica burial enhanced by iron limitation in oceanic upwelling margins. Nat. Geosci. 7, 541–546. doi: 10.1038/ngeo2181

Praetorius, S. K., Mix, A. C., Walczak, M. H., Wolhowe, M. D., Addison, J. A., and Prahl, F. G. (2015). North Pacific deglacial hypoxic events linked to abrupt ocean warming. Nature 527, 362–366. doi: 10.1038/nature15753

Raiswell, R., and Canfield, D. E. (2012). The iron biogeochemical cycle past and present. Geochem. Perspect. 1, 1–220. doi: 10.7185/geochempersp.1.1

Reck, B. K.,Müller,D. B., Rostkowski, K., and Graedel, T. E. (2008). Anthropogenic nickel cycle: insights into use, trade, and recycling. Environ. Sci. Technol. 42, 3394–3400. doi: 10.1021/es072108l

Reimer, P. J., Bard, E., Bayliss, A., Beck, J.W., Blackwell, P. G., Ramsey, C. B., et al. (2013). IntCal13 and Marine13 Radiocarbon Age Calibration Curves 0–50,000 Years cal BP. Radiocarbon 55, 1869–1887. doi: 10.2458/azu_js_rc.55.16947

Riedinger, N., Brunner, B., Krastel, S., Arnold, G. L., Wehrmann, L. M., Formolo, M. J., et al. (2017). Sulfur cycling in an iron oxide-dominated, dynamic marine depositional system: the Argentine continental margin. Front. Earth Sci. 5:33. doi: 10.3389/feart.2017.00033

Riedinger, N., Formolo, M. J., Lyons, T. W., Henkel, S., Beck, A., and Kasten, S. (2014). An inorganic geochemical argument for coupled anaerobic oxidation of methane and iron reduction in marine sediments. Geobiology 12, 172–181. doi: 10.1111/gbi.12077

Riedinger, N., Kasten, S., Gröger, J., Franke, C., and Pfeifer, K. (2006). Active and buried authigenic barite fronts in sediments fromthe Eastern Cape Basin. Earth Planet. Sci. Lett. 241, 876–887. doi: 10.1016/j.epsl.2005.10.032

Rodríguez-Castañeda, A. P. (2008). Variación de flujos de los elementos particulados en Cuenca Alfonso, Bahía de La Paz, en el periodo 2002–2005. [Ph.D. dissertation]. [La Paz, Mexico]: Centro Interdisciplinario de Ciencias Marinas – Instituto Politécnico Nacional

Ruiz-Fernández, A. C., Hillaire-Marcel, C., De Vernal, A., Machain-Castillo, M. L., Vásquez, L., Ghaleb, B., et al. (2009). Changes of coastal sedimentation in the Gulf of Tehuantepec, South Pacific Mexico, over the last 100 years from short-lived radionuclide measurements. Estuar. Coast. Shelf Sci. 82, 525–536. doi: 10.1016/j.ecss.2009.02.019

Schmidtko, S., Stramma, L., and Visbeck, M. (2017). Decline in global oceanic oxygen content during the past five decades. Nature 542, 335–339. doi: 10.1038/nature21399

Schneider, T., Bischoff, T., and Haug, G. H. (2014).Migrations and dynamics of the intertropical convergence zone. Nature 513, 45–53. doi: 10.1038/nature13636

Schoepfer, S. D., Shen, J., Wei, H., Tyson, R. V., Ingall, E., and Algeo, T. J. (2015). Total organic carbon, organic phosphorus, and biogenic barium fluxes as proxies for paleomarine productivity. Earth Sci. Rev. 149, 23–52. doi: 10.1016/j.earscirev.2014.08.017

Scholz, F. (2018). Identifying oxygen minimum zone-type biogeochemical cycling in Earth history using inorganic geochemical proxies. Earth Sci. Rev. 184, 29–45. doi: 10.1016/j.earscirev.2018.08.002

Scholz, F., Hensen, C., Noffke, A., Rohde, A., Liebetrau, V., and Wallmann, K. (2011). Early diagenesis of redox-sensitive trace metals in the Peru upwelling area – response to ENSO-related oxygen fluctuations in the water column. Geochim. Cosmochim. Acta 75, 7257–7276. doi: 10.1016/j.gca.2011.08.007

Scholz, F., Siebert, C., Dale, A. W., and Frank, M. (2017). Intense molybdenum accumulation in sediments underneath a nitrogenous water column and implications for the reconstruction of paleo-redox conditions based on molybdenum isotopes. Geochim. Cosmochim. Acta 213, 400–417. doi: 10.1016/j.gca.2017.06.048

Scott, C., and Lyons, T. W. (2012). Contrasting molybdenum cycling and isotopic properties in euxinic versus non-euxinic sediments and sedimentary rocks: refining the paleoproxies. Chem. Geol. 324–325, 19–27. doi: 10.1016/j.chemgeo.2012.05.012

Shaffer, G., Olsen, S. M., and Pedersen, J. O. P. (2009). Long-term ocean oxygen depletion in response to carbon dioxide emissions from fossil fuels. Nat. Geosci. 2, 105–109. doi: 10.1038/ngeo420

Silverberg, N., Aguirre-Bahena, F., and Mucci, A. (2014). Time-series measurements of settling particulate matter in Alfonso Basin, La Paz Bay, southwestern Gulf of California. Cont. Shelf Res. 84, 169–187. doi: 10.1016/j.csr.2014.05.005

Staines-Urías, F., González-Yajimovich, O., and Beaufort, L. (2015). Reconstruction of past climate variability and ENSO-like fluctuations in the southern Gulf of California (Alfonso Basin) since the last glacial maximum. Q. Res. 83, 488–501. doi: 10.1016/j.yqres.2015.03.007

Tems, C. E., Berelson, W. M., and Prokopenko, M. G. (2015). Particulate $\delta^{15}N$ in laminated marine sediments as a proxy for mixing between the California Undercurrent and the California Current: a proof of concept. Geophys. Res. Lett. 42, 419–427. doi: 10.1002/2014GL061993

Tems, C. E., Berelson,W.M., Thunell, R., Tappa, E., Xu, X., Khider,D., et al. (2016). Decadal to centennial fluctuations in the intensity of the eastern tropical North Pacific oxygen minimum zone during the last 1200 years. Paleoceanography Paleoclimatol. 31, 1138–1151. doi: 10.1002/2015PA002904

Tetard, M., Licari, L., and Beaufort, L. (2017). Oxygen history off Baja California over the last 80 kyr: a new foraminiferal-based record. Paleoceanography Paleoclimatol. doi: 10.1002/2016PA003034

Thunell, R. (1998). Seasonal and annual variability in particle fluxes in the Gulf of California. A response to climate forcing. Deep Sea Res. Part I Oceanogr. Res. Pap. 45, 2059–2083. doi: 10.1016/S0967-0637(98) 00053-3

Trasviña-Castro, A., Gutierrez De Velasco, G., Valle-Levinson, A., González- Armas, R., Muhlia, A., and Cosio, M. A. (2003). Hydrographic observations of the flow in the vicinity of a shallow seamount top in the Gulf of California. Estuar. Coast. Shelf Sci. 57, 149–162. doi: 10.1016/S0272-7714(02) 00338-4

Tribovillard, N., Algeo, T. J., Lyons, T., and Riboulleau, A. (2006). Trace metals as paleoredox and paleoproductivity proxies: an update. Chem. Geol. 232, 12–32. doi: 10.1016/j.chemgeo.2006.02.012

Tribovillard, N., Bout-Roumazeilles, V., Algeo, T., Lyons, T. W., Sionneau, T., Montero-Serrano, J. C., et al. (2008). Paleodepositional conditions in the Orca Basin as inferred from organic matter and trace metal contents. Mar. Geol. 254, 62–72. doi: 10.1016/j.margeo.2008.04.016

Twining, B. S., Baines, S. B., Vogt, S., and Nelson, D. M. (2012). Role of diatoms in nickel biogeochemistry in the ocean. Glob. Biogeochem. Cycles 26. doi: 10.1029/2011GB004233 Umling, N. E., and Thunell, R. C. (2017). Synchronous deglacial thermocline and deep-water ventilation in the eastern equatorial Pacific. Nat. Commun. 8:14203. doi: 10.1038/ncomms14203

Wedepohl, K. H. (1995). The composition of the continental crust. Geochim. Cosmochim. Acta 59, 1217–1232. doi: 10.1016/0016-7037(95)00038-2

Wignall, P. B., and Myers, K. J. (1988). Interpreting benthic oxygen levels in mudrocks: a new approach. Geology 16:452–455. doi: 10.1130/0091- 7613(1988)016<0452:IBOLIM>2.3.CO;2

World Ocean Atlas (2005). http://www.nodc.noaa.gov/OC5/WOA05/pr_woa05.html

Wright, J. J., Konwar, K. M., and Hallam, S. J. (2012). Microbial ecology of expanding oxygen minimum zones. Nat. Rev. Microbiol. 10, 381–394. doi: 10.1038/nrmicro2778

Yan, H., Sun, L.,Wang, Y., Huang,W., Qiu, S., and Yang, C. (2011). A record of the Southern Oscillation Index for the past 2,000 years from precipitation proxies. Nat. Geosci. 4, 611–614. doi: 10.1038/ngeo1231

Zheng, Y., Anderson, R. B., Van Geen, A., and Fleisher, M. Q. (2002). Preservation of particulate non-lithogenic uranium in marine sediments. Geochim. Cosmochim. Acta 66, 3085–3092. doi: 10.1016/S0016-7037(01) 00632-9

Zheng, Y., Anderson, R. B., Van Geen, A., and Kuwabara, J. (2000). Authigenic molybdenum formation in marine sediments: a link to pore water sulfide in Santa Barbara Basin. Geochim. Cosmochim. Acta 64, 4165–4178. doi: 10.1016/S0016-7037(00)00495-6

## 1.8. SUPPLEMENTARY MATERIALS

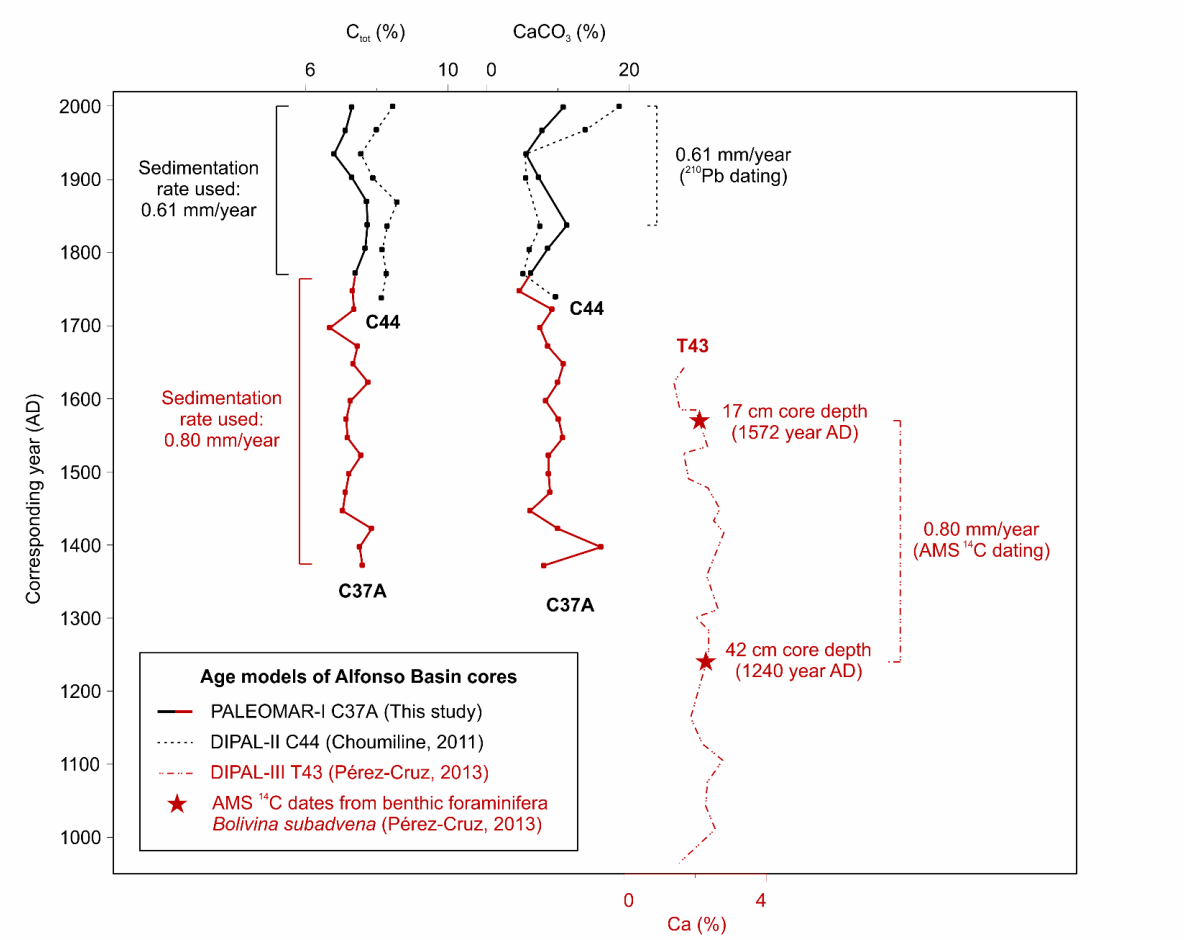


**Supplementary Figure 1.1.** Comparison of age models produced for the following sediment cores collected in Alfonso Basin: DIPAL-II C44 (Choumiline, 2011), DIPAL-III T43 (Pérez-Cruz, 2013) and PALEOMAR-I C37A (this study). To demonstrate that the cores represent the same sedimentary layers and can be properly correlated we show how total carbon ($C_{tot}$), $CaCO_3$ and Ca plotted against time covary for every age model (Choumiline et al., 2010; Choumiline, 2011; Pérez-Cruz, 2013; Choumiline et al., 2017). In our age model for core PALEOMAR-I C37A we extrapolate the sedimentation rate of 0.61 mm/year to the uppermost core section (0 to 15 cm) and use 0.8 mm/year for the lowermost segment (15 to 50 cm).

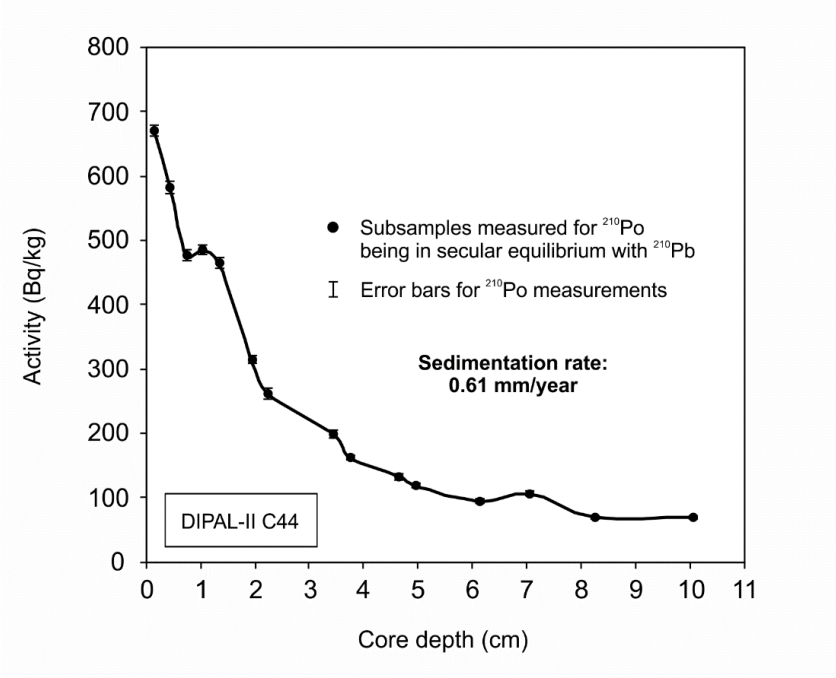


**Supplementary Figure 1.2.** Dating results of the $^{210}$Pb method applied to sedimentary material from core DIPAL-II C44 collected in Alfonso Basin (modified from Choumiline, 2011).

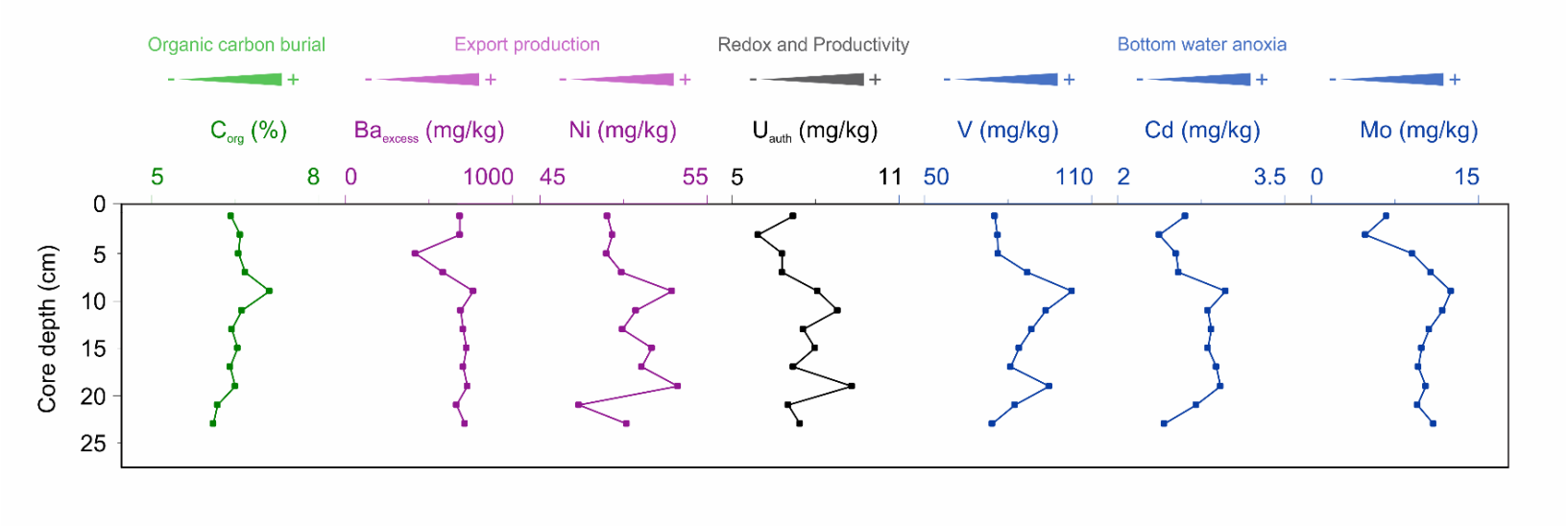


**Supplementary Figure 1.3.** Geochemical profiles of the solid phase from core C52A from La Paz Basin collected during PALEOMAR-I expedition to the Gulf of California.

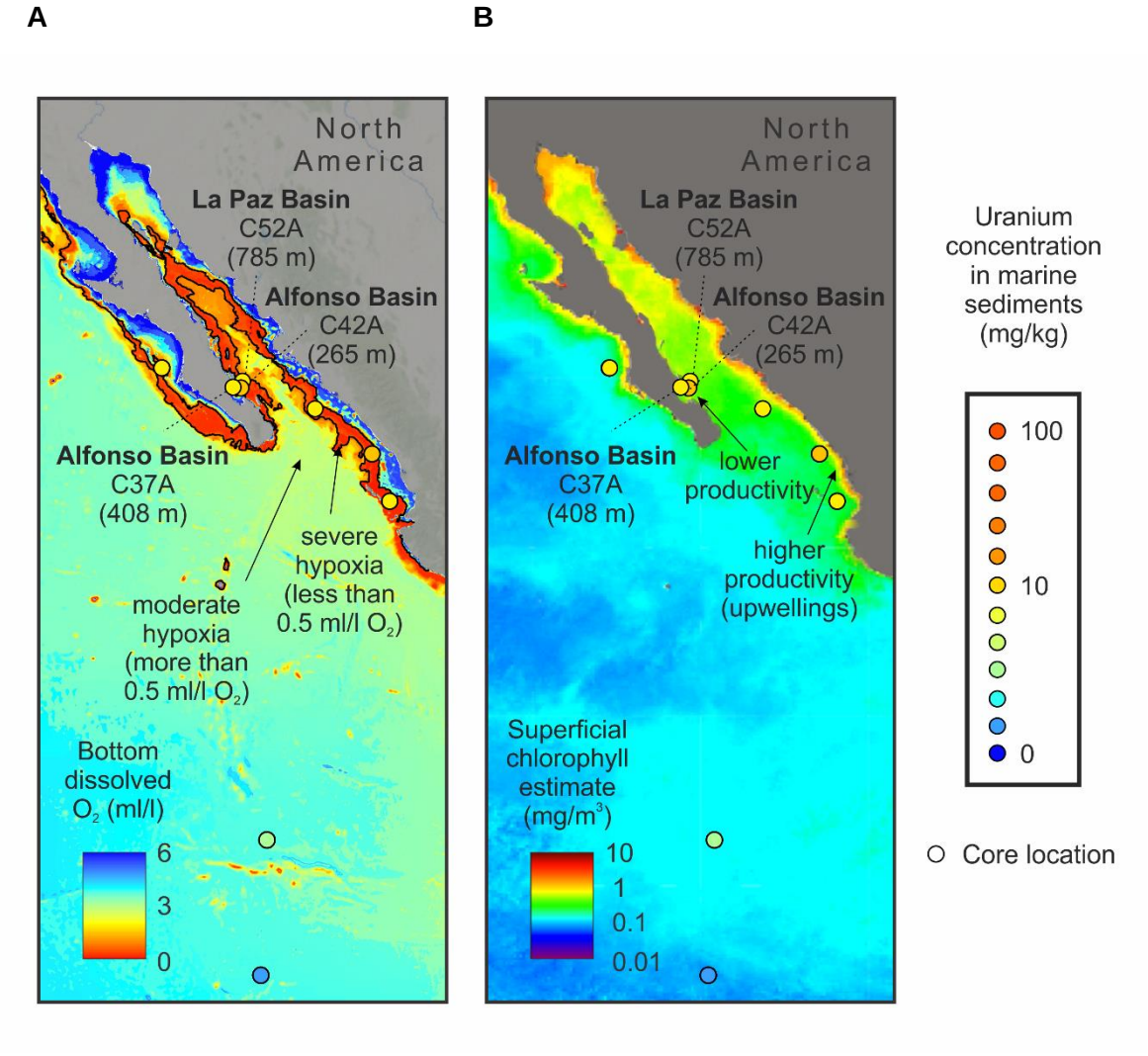


**Supplementary Figure 1.4.** Uranium concentration in various core tops of the Gulf of California and adjacent Pacific, (A) bottom dissolved oxygen, and (B) superficial chlorophyll estimate from the studied marine OMZ settings of ETNP (Alfonso Basin and La Paz Basin), (Oxygen based on World Ocean Atlas, 2005, Garcia et al., 2006; superficial chlorophyll estimates by SeaWIFS satellite sensor published by OBPG/NASA; core top U data from EarthChem SedDB database).

**Supplementary Table 1.1.** Dissolved Fe and Mn in pore water profiles of cores C37A and C52A collected during PALEOMAR-I expedition to the Gulf of California.

| Core | Depth range (cm) | Depth midpoint (cm) | Fe | Mn |
|---|---|---|---|---|
| | | | (µM) | |
| C37A (Alfonso Basin) | 0-2 | 1 | 8.77 | 0.47 |
| | 2-4 | 3 | 15.79 | 0.47 |
| | 4-6 | 5 | 15.58 | 0.44 |
| | 6-8 | 7 | 13.42 | 0.47 |
| | 8-10 | 9 | 12.41 | 0.50 |
| | 10-12 | 11 | 9.93 | 0.51 |
| | 12-14 | 13 | 7.05 | 0.42 |
| | 14-16 | 15 | 5.90 | 0.40 |
| | 16-18 | 17 | 4.32 | 0.40 |
| | 18-20 | 19 | 2.27 | 0.46 |
| | 20-22 | 21 | 1.74 | 0.40 |
| | 22-24 | 23 | 1.03 | 0.35 |
| | 24-26 | 25 | 1.08 | 0.34 |
| | 26-28 | 27 | 0.58 | 0.32 |
| | 28-30 | 29 | 0.41 | 0.30 |
| | 30-32 | 31 | 0.93 | 0.31 |
| | 32-34 | 33 | 0.37 | 0.22 |
| | 34-36 | 35 | 0.33 | 0.22 |
| | 36-38 | 37 | 1.53 | 0.26 |
| | 38-40 | 39 | 0.62 | 0.24 |
| | 40-42 | 41 | 1.11 | 0.16 |
| | 42-44 | 43 | 0.35 | 0.15 |
| | 44-46 | 45 | 1.04 | 0.15 |
| | 46-48 | 47 | 0.36 | 0.09 |
| | 48-50 | 49 | 0.59 | 0.11 |
| C52A (La Paz Basin) | 0-2 | 1 | 9.38 | 0.85 |
| | 2-4 | 3 | 8.15 | 1.01 |
| | 4-6 | 5 | 2.55 | 1.10 |
| | 6-8 | 7 | 0.95 | 1.05 |
| | 8-10 | 9 | 0.81 | 1.12 |
| | 10-12 | 11 | 1.09 | 1.13 |
| | 12-14 | 13 | 0.43 | 1.08 |
| | 14-16 | 15 | 0.50 | 1.04 |
| | 16-18 | 17 | 1.03 | 0.96 |
| | 18-20 | 19 | 0.71 | 0.94 |
| | 20-22 | 21 | 1.08 | 0.93 |
| | 22-24 | 23 | 0.91 | 0.77 |

**Supplementary Table 1.2.** Elemental composition of the solid phase from cores C37A, C42A and C52A collected during PALEOMAR-I expedition to the Gulf of California. Corresponding age is presented for each horizon only for core C37A.

| Core | Depth range (cm) | Depth midpoint (cm) | Age in years AD | $C_{org}$ | Al | Fe | Ba | Cd | Mo | Ni | U | V | $Ba_{excess}$ | $U_{auth}$ |
|---|---|---|---|---|---|---|---|---|---|---|---|---|---|---|
| | | | | (%) | | | (mg/kg) | | | | | | | |
| C37A (Alfonso Basin) | 0-2 | 1 | 1999 | 6.01 | 4.9 | 2.5 | 406.4 | 2.5 | 6.3 | 40.3 | 9.9 | 124.7 | 406.4 | 8.1 |
| | 2-4 | 3 | 1967 | 6.18 | 5.1 | 2.6 | 419.3 | 2.6 | 6.4 | 41.9 | 10.1 | 115.8 | 419.2 | 8.3 |
| | 4-6 | 5 | 1934 | 6.13 | 5.1 | 2.6 | 440.0 | 3.4 | 9.3 | 41.3 | 9.7 | 133.4 | 439.9 | 7.9 |
| | 6-8 | 7 | 1902 | 6.42 | 5.0 | 2.5 | 454.3 | 3.4 | 10.2 | 44.2 | 10.1 | 137.1 | 454.3 | 8.4 |
| | 8-10 | 9 | 1870 | | 4.7 | 2.3 | 439.9 | 3.5 | 9.9 | 44.0 | 11.3 | 139.6 | 439.9 | 9.6 |
| | 10-12 | 11 | 1837 | 6.39 | 4.8 | 2.3 | 430.4 | 3.8 | 9.0 | 45.3 | 13.0 | 150.6 | 430.4 | 11.3 |
| | 12-14 | 13 | 1805 | 6.65 | 5.0 | 2.5 | 476.6 | 4.1 | 9.5 | 47.9 | 13.5 | 156.8 | 476.6 | 11.7 |
| | 14-16 | 15 | 1772 | 6.66 | 5.3 | 2.6 | 479.3 | 3.8 | 9.2 | 48.3 | 12.4 | 141.8 | 479.3 | 10.6 |
| | 16-18 | 17 | 1747 | 6.76 | 4.3 | 2.1 | 416.0 | 3.8 | 9.2 | 41.2 | 9.2 | 117.0 | 415.9 | 7.7 |
| | 18-20 | 19 | 1722 | 6.26 | 4.9 | 2.4 | 458.0 | 3.9 | 8.7 | 45.8 | 11.6 | 149.7 | 458.0 | 9.9 |
| | 22-24 | 23 | 1672 | 6.43 | 5.0 | 2.6 | 480.5 | 4.8 | 12.7 | 49.5 | 10.9 | 167.1 | 480.5 | 9.1 |
| | 24-26 | 25 | 1647 | 6.05 | 4.8 | 2.4 | 458.3 | 4.6 | 11.2 | 46.3 | 12.9 | 157.0 | 458.3 | 11.2 |
| | 26-28 | 27 | 1622 | 6.56 | 4.9 | 2.4 | 459.1 | 4.7 | 8.2 | 50.4 | 12.4 | 154.9 | 459.1 | 10.7 |
| | 28-30 | 29 | 1597 | 6.25 | 5.0 | 2.5 | 461.5 | 5.4 | 13.4 | 46.9 | 10.8 | 160.0 | 461.4 | 9.0 |
| | 30-32 | 31 | 1572 | 5.93 | 5.0 | 2.5 | 485.5 | 5.0 | 13.0 | 46.4 | 11.2 | 164.2 | 485.5 | 9.5 |
| | 32-34 | 33 | 1547 | 5.89 | 4.9 | 2.5 | 468.1 | 4.8 | 11.2 | 47.7 | 11.8 | 160.6 | 468.1 | 10.1 |
| | 34-36 | 35 | 1522 | 6.53 | 5.1 | 2.6 | 488.8 | 5.3 | 12.9 | 51.6 | 11.9 | 172.4 | 488.7 | 10.1 |
| | 36-38 | 37 | 1497 | 6.18 | 5.1 | 2.5 | 470.3 | 4.3 | 10.7 | 48.9 | 11.1 | 167.5 | 470.3 | 9.4 |
| | 38-40 | 39 | 1472 | 6.04 | 5.1 | 2.5 | 441.8 | 3.7 | 9.3 | 46.1 | 11.3 | 146.4 | 441.8 | 9.5 |
| | 40-42 | 41 | 1447 | 6.30 | 5.1 | 2.5 | 472.7 | 4.7 | 13.5 | 48.9 | 10.1 | 161.0 | 472.7 | 8.3 |
| | 42-44 | 43 | 1422 | 6.65 | 4.7 | 2.4 | 481.5 | 7.0 | 14.2 | 51.4 | 14.2 | 170.8 | 481.5 | 12.5 |
| | 44-46 | 45 | 1397 | 5.60 | 4.6 | 2.4 | 372.2 | 2.9 | 6.8 | 42.8 | 14.0 | 124.0 | 372.2 | 12.3 |
| | 46-48 | 47 | 1372 | 6.62 | 4.6 | 2.3 | 440.1 | 5.0 | 13.3 | 46.3 | 9.9 | 148.5 | 440.1 | 8.2 |
| | 48-50 | 49 | 1347 | | 4.8 | 2.4 | 491.6 | 5.2 | 15.2 | 50.0 | 12.9 | 165.9 | 491.5 | 11.2 |
| C52A (La Paz Basin) | 0-2 | 1 | - | 6.41 | 4.3 | 1.8 | 682.8 | 2.6 | 6.7 | 49.1 | 8.8 | 75.0 | 682.8 | 7.2 |
| | 2-4 | 3 | - | 6.58 | 4.3 | 1.9 | 681.1 | 2.4 | 4.9 | 49.4 | 7.5 | 76.0 | 681.1 | 6.0 |
| | 4-6 | 5 | - | 6.55 | 4.3 | 1.9 | 419.8 | 2.5 | 9.1 | 49.0 | 8.3 | 76.5 | 419.8 | 6.8 |
| | 6-8 | 7 | - | 6.68 | 4.3 | 1.9 | 580.4 | 2.5 | 10.7 | 49.9 | 8.4 | 86.8 | 580.4 | 6.8 |
| | 8-10 | 9 | - | 7.12 | 4.6 | 1.9 | 763.3 | 3.0 | 12.6 | 52.9 | 9.7 | 102.8 | 763.2 | 8.1 |
| | 10-12 | 11 | - | 6.61 | 4.4 | 1.8 | 689.6 | 2.8 | 11.8 | 50.7 | 10.4 | 93.4 | 689.5 | 8.8 |
| | 12-14 | 13 | - | 6.43 | 4.4 | 1.9 | 704.3 | 2.8 | 10.6 | 49.9 | 9.2 | 88.4 | 704.3 | 7.6 |
| | 14-16 | 15 | - | 6.54 | 4.6 | 1.9 | 723.0 | 2.8 | 9.9 | 51.7 | 9.6 | 83.9 | 722.9 | 8.0 |
| | 16-18 | 17 | - | 6.40 | 4.6 | 1.9 | 703.2 | 2.9 | 9.6 | 51.1 | 8.8 | 80.9 | 703.2 | 7.2 |
| | 18-20 | 19 | - | 6.49 | 4.8 | 2.0 | 728.1 | 2.9 | 10.3 | 53.2 | 11.1 | 94.7 | 728.1 | 9.3 |
| | 20-22 | 21 | - | 6.17 | 4.3 | 1.9 | 661.3 | 2.7 | 9.5 | 47.3 | 8.6 | 82.2 | 661.3 | 7.0 |
| | 22-24 | 23 | - | 6.10 | 4.5 | 2.0 | 714.1 | 2.4 | 10.9 | 50.2 | 9.1 | 74.3 | 714.1 | 7.5 |
| C42A | Superficial | | - | 2.96 | 2.3 | 1.0 | 175.7 | 5.3 | 0.8 | 26.8 | 14.3 | 26.0 | 175.7 | 13.2 |

**Supplementary Table 1.3.** Al-normalized concentration values (mg/kg / %) in the solid phase from cores C37A, C42A and C52A collected during PALEOMAR-I expedition to the Gulf of California. Corresponding age is presented for each horizon only for core C37A.

| Core | Depth range (cm) | Depth midpoint (cm) | Age in years AD | Ba/Al | Cd/Al | Mo/Al | Ni/Al | U/Al | V/Al |
|---|---|---|---|---|---|---|---|---|---|
| C37A (Alfonso Basin) | 0-2 | 1 | 1999 | 83.14 | 0.51 | 1.30 | 8.24 | 2.02 | 25.51 |
| | 2-4 | 3 | 1967 | 82.48 | 0.52 | 1.26 | 8.25 | 1.99 | 22.78 |
| | 4-6 | 5 | 1934 | 86.33 | 0.67 | 1.83 | 8.10 | 1.91 | 26.18 |
| | 6-8 | 7 | 1902 | 91.02 | 0.67 | 2.03 | 8.86 | 2.02 | 27.47 |
| | 8-10 | 9 | 1870 | 92.84 | 0.75 | 2.09 | 9.29 | 2.39 | 29.45 |
| | 10-12 | 11 | 1837 | 90.32 | 0.80 | 1.90 | 9.51 | 2.72 | 31.60 |
| | 12-14 | 13 | 1805 | 94.71 | 0.82 | 1.88 | 9.52 | 2.67 | 31.16 |
| | 14-16 | 15 | 1772 | 90.57 | 0.72 | 1.74 | 9.12 | 2.35 | 26.80 |
| | 16-18 | 17 | 1747 | 96.88 | 0.89 | 2.14 | 9.60 | 2.15 | 27.25 |
| | 18-20 | 19 | 1722 | 93.21 | 0.80 | 1.77 | 9.32 | 2.36 | 30.46 |
| | 22-24 | 23 | 1672 | 95.64 | 0.95 | 2.54 | 9.85 | 2.17 | 33.26 |
| | 24-26 | 25 | 1647 | 95.36 | 0.97 | 2.32 | 9.64 | 2.68 | 32.66 |
| | 26-28 | 27 | 1622 | 93.93 | 0.97 | 1.68 | 10.31 | 2.55 | 31.69 |
| | 28-30 | 29 | 1597 | 92.34 | 1.09 | 2.69 | 9.39 | 2.17 | 32.01 |
| | 30-32 | 31 | 1572 | 98.07 | 1.01 | 2.63 | 9.36 | 2.26 | 33.16 |
| | 32-34 | 33 | 1547 | 95.05 | 0.98 | 2.28 | 9.69 | 2.40 | 32.61 |
| | 34-36 | 35 | 1522 | 96.30 | 1.05 | 2.55 | 10.17 | 2.35 | 33.97 |
| | 36-38 | 37 | 1497 | 92.50 | 0.85 | 2.10 | 9.62 | 2.19 | 32.95 |
| | 38-40 | 39 | 1472 | 86.89 | 0.73 | 1.83 | 9.06 | 2.22 | 28.79 |
| | 40-42 | 41 | 1447 | 92.52 | 0.91 | 2.63 | 9.57 | 1.97 | 31.51 |
| | 42-44 | 43 | 1422 | 102.28 | 1.49 | 3.02 | 10.92 | 3.01 | 36.29 |
| | 44-46 | 45 | 1397 | 81.11 | 0.62 | 1.47 | 9.33 | 3.04 | 27.03 |
| | 46-48 | 47 | 1372 | 95.33 | 1.09 | 2.89 | 10.03 | 2.13 | 32.17 |
| | 48-50 | 49 | 1347 | 101.68 | 1.08 | 3.14 | 10.34 | 2.67 | 34.31 |
| C52A (La Paz Basin) | 0-2 | 1 | - | 157.16 | 0.60 | 1.55 | 11.29 | 2.03 | 17.27 |
| | 2-4 | 3 | - | 158.79 | 0.55 | 1.14 | 11.51 | 1.74 | 17.72 |
| | 4-6 | 5 | - | 97.84 | 0.59 | 2.12 | 11.42 | 1.94 | 17.83 |
| | 6-8 | 7 | - | 136.07 | 0.60 | 2.51 | 11.69 | 1.96 | 20.35 |
| | 8-10 | 9 | - | 167.21 | 0.65 | 2.75 | 11.59 | 2.13 | 22.52 |
| | 10-12 | 11 | - | 158.07 | 0.64 | 2.70 | 11.63 | 2.38 | 21.42 |
| | 12-14 | 13 | - | 160.97 | 0.65 | 2.41 | 11.41 | 2.09 | 20.20 |
| | 14-16 | 15 | - | 158.64 | 0.62 | 2.17 | 11.34 | 2.12 | 18.41 |
| | 16-18 | 17 | - | 152.24 | 0.63 | 2.08 | 11.06 | 1.91 | 17.52 |
| | 18-20 | 19 | - | 150.30 | 0.60 | 2.12 | 10.99 | 2.29 | 19.54 |
| | 20-22 | 21 | - | 152.81 | 0.63 | 2.20 | 10.94 | 1.99 | 19.00 |
| | 22-24 | 23 | - | 159.54 | 0.54 | 2.44 | 11.21 | 2.03 | 16.60 |
| C42A | Superficial | | - | 77.96 | 2.37 | 0.33 | 11.91 | 6.35 | 11.56 |

**Supplementary Table 1.4.** Carbonate free basis (CFB) concentration values (mg/kg) in the solid phase from cores C37A, C42A and C52A collected during PALEOMAR-I expedition to the Gulf of California. Corresponding age is presented for each horizon only for core C37A.

| Core | Depth range (cm) | Depth midpoint (cm) | Age in years AD | $Ba_{CFB}$ | $Cd_{CFB}$ | $Mo_{CFB}$ | $Ni_{CFB}$ | $U_{CFB}$ | $V_{CFB}$ |
|---|---|---|---|---|---|---|---|---|---|
| C37A (Alfonso Basin) | 0-2 | 1 | 1999 | 362.65 | 2.21 | 5.66 | 35.92 | 8.79 | 111.25 |
| | 2-4 | 3 | 1967 | 386.55 | 2.41 | 5.91 | 38.65 | 9.31 | 106.78 |
| | 4-6 | 5 | 1934 | 415.62 | 3.21 | 8.79 | 38.98 | 9.20 | 126.06 |
| | 6-8 | 7 | 1902 | 421.20 | 3.12 | 9.41 | 40.98 | 9.35 | 127.14 |
| | 8-10 | 9 | 1870 | 439.83 | 3.54 | 9.92 | 44.01 | 11.31 | 139.53 |
| | 10-12 | 11 | 1837 | 382.03 | 3.37 | 8.03 | 40.22 | 11.51 | 133.66 |
| | 12-14 | 13 | 1805 | 435.86 | 3.76 | 8.66 | 43.80 | 12.31 | 143.38 |
| | 14-16 | 15 | 1772 | 449.50 | 3.58 | 8.62 | 45.26 | 11.64 | 133.02 |
| | 16-18 | 17 | 1747 | 397.00 | 3.65 | 8.76 | 39.32 | 8.81 | 111.66 |
| | 18-20 | 19 | 1722 | 415.90 | 3.58 | 7.88 | 41.60 | 10.53 | 135.91 |
| | 22-24 | 23 | 1672 | 439.17 | 4.37 | 11.65 | 45.25 | 9.95 | 152.71 |
| | 24-26 | 25 | 1647 | 409.02 | 4.14 | 9.96 | 41.36 | 11.51 | 140.07 |
| | 26-28 | 27 | 1622 | 413.10 | 4.26 | 7.40 | 45.35 | 11.20 | 139.37 |
| | 28-30 | 29 | 1597 | 423.03 | 4.98 | 12.33 | 43.04 | 9.93 | 146.66 |
| | 30-32 | 31 | 1572 | 436.60 | 4.51 | 11.69 | 41.69 | 10.07 | 147.64 |
| | 32-34 | 33 | 1547 | 417.88 | 4.31 | 10.04 | 42.61 | 10.57 | 143.36 |
| | 34-36 | 35 | 1522 | 446.46 | 4.87 | 11.82 | 47.14 | 10.90 | 157.48 |
| | 36-38 | 37 | 1497 | 429.42 | 3.97 | 9.76 | 44.65 | 10.15 | 152.97 |
| | 38-40 | 39 | 1472 | 402.72 | 3.40 | 8.48 | 42.00 | 10.28 | 133.43 |
| | 40-42 | 41 | 1447 | 444.02 | 4.38 | 12.64 | 45.92 | 9.46 | 151.22 |
| | 42-44 | 43 | 1422 | 433.39 | 6.33 | 12.78 | 46.26 | 12.74 | 153.76 |
| | 44-46 | 45 | 1397 | 312.58 | 2.40 | 5.68 | 35.94 | 11.73 | 104.16 |
| | 46-48 | 47 | 1372 | 404.73 | 4.64 | 12.25 | 42.57 | 9.06 | 136.60 |
| | 48-50 | 49 | 1347 | 434.84 | 4.62 | 13.41 | 44.23 | 11.42 | 146.75 |
| C52A (La Paz Basin) | 0-2 | 1 | - | 559.55 | 2.13 | 5.53 | 40.20 | 7.24 | 61.50 |
| | 2-4 | 3 | - | 558.52 | 1.95 | 4.01 | 40.48 | 6.12 | 62.32 |
| | 4-6 | 5 | - | 348.17 | 2.09 | 7.55 | 40.65 | 6.92 | 63.43 |
| | 6-8 | 7 | - | 485.87 | 2.13 | 8.96 | 41.76 | 7.01 | 72.67 |
| | 8-10 | 9 | - | 640.95 | 2.49 | 10.54 | 44.42 | 8.16 | 86.33 |
| | 10-12 | 11 | - | 562.77 | 2.29 | 9.62 | 41.42 | 8.47 | 76.26 |
| | 12-14 | 13 | - | 558.21 | 2.25 | 8.37 | 39.57 | 7.26 | 70.04 |
| | 14-16 | 15 | - | 585.57 | 2.28 | 8.02 | 41.85 | 7.82 | 67.94 |
| | 16-18 | 17 | - | 570.95 | 2.35 | 7.80 | 41.48 | 7.18 | 65.72 |
| | 18-20 | 19 | - | 592.74 | 2.38 | 8.36 | 43.35 | 9.02 | 77.06 |
| | 20-22 | 21 | - | 527.38 | 2.16 | 7.59 | 37.75 | 6.85 | 65.57 |
| | 22-24 | 23 | - | 573.38 | 1.95 | 8.79 | 40.29 | 7.31 | 59.67 |
| C42A | Superficial | | - | 78.94 | 2.40 | 0.34 | 12.06 | 6.43 | 11.70 |

# CHAPTER 2:

# ENHANCED ANOXIA IN THE EASTERN TROPICAL NORTH PACIFIC OXYGEN MINIMUM ZONE DURING THE MARINE ISOTOPE STAGE 3

**ABSTRACT**

The Marine Isotope Stage (MIS) 3 is one of the most enigmatic times of the last glacial period, often described as a transition known for superior insolation and greater climatic instability. Paleoproxy and model evidence indicate that the shift from the cold glacial MIS 4 toward MIS 3 was accompanied by increased submillennial climatic variability manifested by stronger Dansgaard-Oeschger (D-O) and Heinrich oscillations. Due to their location, the sedimentary records from the Gulf of California are exceptionally sensitive to climatic changes, allowing them to preserve paleoceanographic variability of the Eastern Tropical North Pacific (ETNP). This region is characterized by a prominent Oxygen Minimum Zone (OMZ).

We studied changes in the productivity and oxygenation based on geochemical proxies to evaluate the impact of rapid global warming events (such as D-O) on the productivity and oxygenation in the basin at submillennial and millennial time scales.

High-resolution reconstruction of productivity ($C_{org}$, Cu, Ni, Zn) and redox conditions (Fe/Al, Cd, Mo, V) was performed for the last glacial period with special emphasis on the MIS 4 - MIS 3 transition between 70 and 30 cal kyr BP. During this period the OMZ fluctuated from well oxygenated to strongly anoxic waters. Our results show that the OMZ achieved its peak strength (in other words more persistent oxygen-deficient conditions at the sampled site) during 45-60 cal kyr BP, highlighted by the highest concentrations of Mo (35 mg/kg), V (120 mg/kg), and U (13 mg/kg). Such enhanced anoxia could either indicate a vertical displacement or expansion of the OMZ, subjecting the basin to less-oxygenated waters. It later began to weaken and contract towards the LGM (26 cal kyr BP). Marine productivity was also high during the MIS 3, mirroring most of the redox signals. In contrast, MIS 4 was well-oxygenated and depleted in redox proxies (e.g., as low as 4 mg/kg of Mo, 60 mg/kg of V, and 4 mg/kg of U). In spite of enhanced anoxia or even euxinia during MIS 3, the climatic signal of short-term D-O and Heinrich events were

superimposed over the multimillennial variability. Most of these perturbations corresponded to periods of decreased productivity (low $C_{org}$, Cu/Al, Ni/Al, and Zn/Al) and well oxygenated waters in the ETNP (near-crustal Fe/Al, Mn/Al, Cd/Al, V/Al, and Mo/Al). The returns to anoxic conditions were relatively quick, within hundreds of years.

While there is no definitive explanation for the drivers of enhanced anoxia during the MIS3 or the mechanisms by which D-O and Heinrich events exert changes in the intensity of the ETNP OMZ, a consensus is building. In this regard, we discuss the current hypotheses that involve changes in atmospheric and thermohaline circulation, as well as variability in deep-sea nutrient and dissolved oxygen availability.

## 2.1. INTRODUCTION

Primary productivity and oxygenation in marine basins are tightly controlled by global climatic cycles, patterns of global circulation, nutrient availability, and the rates of organic matter remineralization (Keeling et al., 2010; Chavez et al., 2011; Gilly et al., 2013; Levin, 2018; Breitburg et al., 2018). When studying paleorecords, it is often hard to decouple changes in productivity from oceanic redox conditions. In such cases, a multiproxy approach combined with a multi-core comparison may help (Jaccard et al., 2014; Moffitt et al., 2015; Schoepfer et al., 2015). A delicate balance between primary productivity in the photic zone and remineralization/respiration in the aphotic waters is usually responsible for the abundance of dissolved $O_2$. The lack of oxygenation can lead to the establishment of an Oxygen Minimum Zone (OMZ) (Levin, 2018). Marine productivity is often one of the primary triggers for changes in the redox conditions of OMZs. However, growing evidence suggests that other mechanisms can differentially impact fluctuations of its upper and lower boundaries (Stramma et al., 2008; Moffitt et al., 2015; Gilly et al., 2013; Oschlies et al., 2018). Some of these drivers that are known for influencing OMZ variability with no direct relationship to primary production are local stratification, basin restriction, and changes in dissolved oxygen content as a function of temperature-dependent solubility (Yarincik et al., 2000; Jaccard et al., 2014; Praetorius et al., 2015; Oschlies et al., 2018). Proper reconstruction of the upper and lower depth boundaries of the OMZ is essential for a full mechanistic understanding of the causes of expansion and contraction (Moffitt et al., 2015; Praetorius et al., 2015).

The world's oceans, as we know them, have already been directly or indirectly impacted by climate change. It is hypothesized that human-caused global warming will lead to a decrease in dissolved $O_2$ in the world oceans due to solubility changes, leading to OMZ expansion (Stramma et al., 2008; Praetorius et al., 2015). However, not all marine basins have responded to the warming

of the last centuries with decreases in oxygenation, and some regions such as the coastal Eastern Tropical North Pacific (ETNP) and Eastern Tropical South Pacific (ETSP) instead show increases in oxygenation (Tems et al., 2016; Levin, 2018; Breitburg et al., 2018; Cardich et al., 2019; Choumiline et al., 2019). Finding the best analog for oceanic responses to rapid warming is essential to estimating future trends in anoxia. Multimillennial climatic variability is well defined by Marine Isotope Stages (MIS) and is known to influence water column oxygenation trends of marine basins at OMZ depths (Ivanochko, 2011; Ivanochko and Pedersen, 2004; Cartapanis et al., 2011, 2014; Carriquiry and Sanchez, 2014; Tetard et al., 2017). Numerous lines of evidence in the ETNP confirm that strong, yet intermittent, anoxia followed the last deglaciation when the cold world of the Last Glacial Maximum (LGM) transitioned into overall warmer conditions (Ganeshram and Pedersen, 1998; Nameroff et al., 2004; Jaccard and Galbraith, 2011; Jaccard et al., 2014; Tetard et al., 2017). On a similar note, pronounced warming and sea-level rise accompanied another significant climatic transition at the MIS 4 - MIS 3 boundary (Agosta and Compagnucci, 2016; Pico et al., 2017). Most importantly, during MIS 3, several abrupt climatic shifts occurred, which may serve as analogs for human-induced global warming scenarios. In this chapter, we will discuss the effect of such sporadic cooling-to-warming regime changes on marine productivity and oxygenation during the MIS 3 interstadials (Van Meerbeeck et al., 2009; Dalton et al., 2019) in the Eastern Tropical North Pacific.

### 2.1.1. Marine Isotope Stage 3

Marine Isotope Stage 3 (MIS 3) occurred between 30 cal kyr and 60 cal kyr BP (29 kyr and 57 BP, based on Lisiecki and Raymo, 2005) and was characterized by frequent Dansgaard-Oeschger (D-O) warming events that followed the cold MIS 4 glaciation. This stage was also affected by increased global climatic instability (Agosta and Compagnucci, 2016) manifested in

high amplitude climate and oceanographic fluctuations. One of them is the enhancement of Northern Hemisphere seasonality, caused by increase in summer insolation, in comparison to the LGM and MIS 4 (Van Meerbeeck et al., 2009; Agosta and Compagnucci, 2013; Dalton et al., 2019). During global intensification of D-O climatic cycles (Schmidt and Hertzberg, 2011), the amplitude of $\delta^{18}O$ oscillations in ice cores (Svensson et al., 2008) and foraminiferal calcite (Lisiecki and Raymo et al., 2005) were among the highest of the last 100,000 years. Model and proxy evidence suggest that the extent of both ice sheets and sea ice during MIS 3 was smaller than during the LGM and MIS 4 (Van Meerbeeck et al., 2009). The volume of ice sheets during MIS 4 was 80% of the LGM volume, while during MIS 3 it was about 60% (Van Meerbeeck et al., 2009; Henry et al., 2016). Ice volumes directly impact sea-level, which can also spatially drive the extent of anoxia in OMZs by displacing the exposure of marine sediments to dissolved oxygen. Sea level during the MIS 3 was 40 to 90 meters lower than it is today (Rohling et al., 2009; Grant et al., 2012).

### 2.1.2. Paleoxygenation of the Eastern Tropical North Pacific

Published proxy records suggest that most OMZ-type basins of the ETNP experienced reoxygenation during MIS 4 and LGM, while the Holocene was characterized by oxygen decrease (Ganeshram and Pedersen, 1998; Nameroff et al., 2004; Hendy and Pedersen, 2006; Cartapanis et al., 2014; Chang et al., 2014; Moffitt et al., 2015; Praetorius et al., 2015; Tetard et al., 2017). Some records have shown that during the MIS 3, the ETNP was characterized by an expanded (in other words a more oxygen deficient) OMZ, which was significantly less oxygenated than during the contracted MIS 4 and LGM. More importantly, as previously stated, short-term climatic instabilities of the MIS 3 related to D-O and Heinrich events also impose quick changes in the oxygenation of marine basins, with the stadials (e.g., Heinrich events) having more ventilated conditions than warm interstadials (Cartapanis et al., 2011; Tetard et al., 2017). However, most

available paleorecords either lack temporal resolution or do not provide multiproxy reconstructions. Additionally, there is a need to compare core records across a range of water column depths with different degrees of restriction to accurately recreate three-dimensional changes at the upper and lower OMZ boundaries.

To achieve this goal, we present a new millennial-scale reconstruction of fluctuations in the ETNP OMZ inferred from multiple proxies for productivity and redox. We provide a detailed paleorecord from a sediment core collected in a semi-restricted basin in the Gulf of California, which we then compare with geochemical and sedimentological records from other ETNP basins. Our primary objective is to assess the abrupt productivity and oxygenation changes that took place during the onset of the MIS 3 immediately after the MIS 4 glaciation. Furthermore, we will discuss the potential utility of MIS 3 as an analog for modern OMZ variability and possible future scenarios due to the multiple rapid transitions associated with this time of instability.

## 2.2. MATERIALS AND METHODS

### 2.2.1. Study area

Alfonso Basin is located on the southwestern part of the Gulf of California. At this location, the current dissolved $O_2$ level at the bottom (410 m) reaches values lower than 0.1 ml/l (Figure 2.1). Bottom circulation is semi-restricted by the presence of a bathymetric sill reaching a depth of 250 m (Nava-Sánchez et al., 2001) This basin has remained anoxic throughout most of the Holocene with short intervals of reoxygenation (Choumiline, 2011; Staines-Urias et al., 2015; Choumiline et al., 2019). Bottom oxygen data used in the map was taken from World Ocean Atlas (2005) and Garcia et al., (2006).

In order to approximate the mechanisms of OMZ variability through time, we need to rely on our understanding of modern-day oceanography of the ETNP and its relationship with the

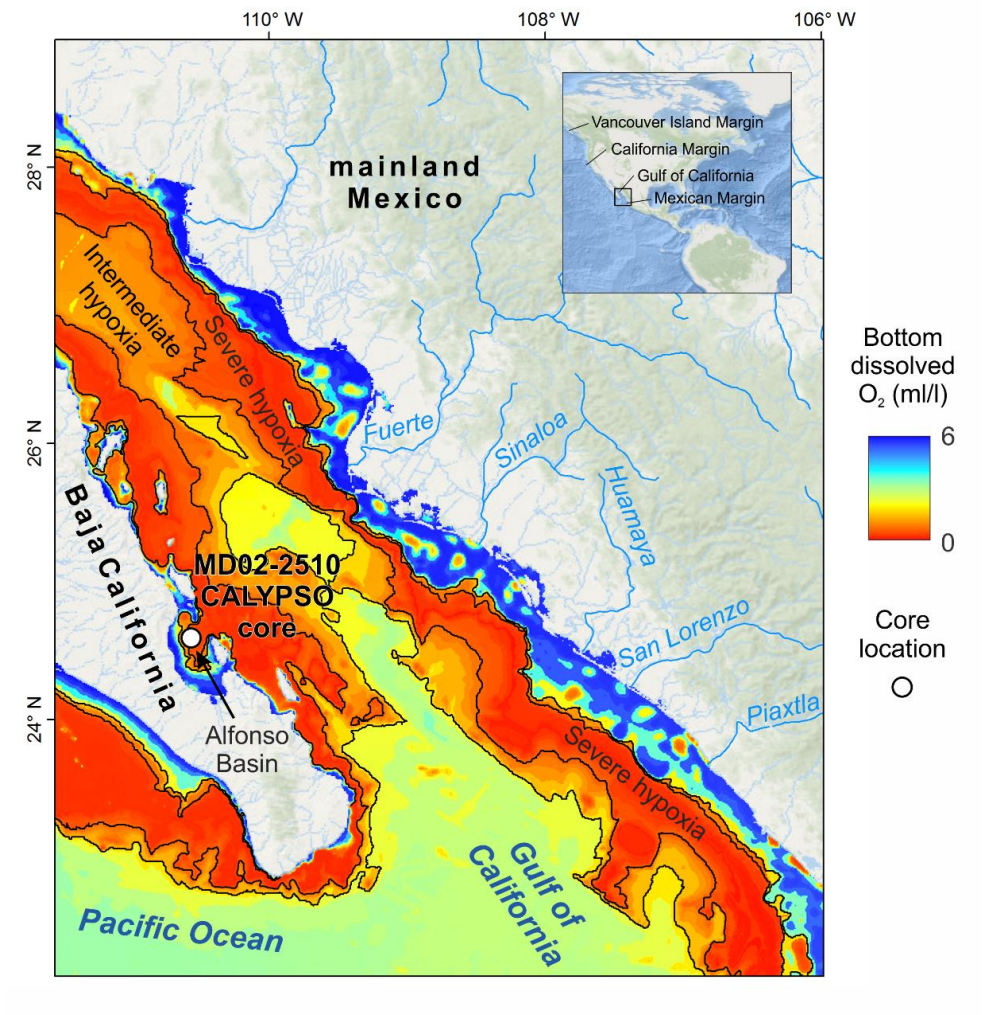


**Figure 2.1.** Study area and location of CALYPSO core MD02-2510 from Alfonso Basin, Gulf of California (Bottom oxygen data based on World Ocean Atlas, 2005 and Garcia et al., 2006).

Alfonso Basin. Many of the features of the Gulf of California are driven by the Pacific Ocean that hosts the following water types: Tropical Surface Water, Subtropical Subsurface Water, North Pacific Intermediate Water (NPIW), and North Pacific Deep Water (NPDW) (Wyrtki, 1966; Lavín et al., 2013). The Gulf of California has the same water types with the addition of the locally formed Gulf of California Water (GCW) (Lavín and Marinone, 2003). The GCW has greater salinity and

is produced in the Gulf of California by evaporative processes that transform Tropical Surface Water. Similar to the Pacific Ocean, the Gulf of California has a well-defined OMZ between 600 and 1200 m depth, mainly due to oxygen-depleted NPIW waters. While Alfonso Basin shares near-surface water masses with the Gulf of California, its water column does not have the presence of the oxygen-depleted NPIW due to its bottom restriction. The anoxic conditions at the bottom of Alfonso Basin are almost entirely controlled by local productivity and stagnation (Monreal-Gómez et al., 2001; Coria-Monter et al., 2014).

### 2.2.2. Sampling

A giant CALYPSO piston core MD02-2510 was obtained at 410 m depth from Alfonso Basin, in the southern Gulf of California, during the "IMAGES VIII / MD126 MONA" expedition on the R/V Marion Dufresne (Figure 2.1). The recovered core spans 47.34 m and is mostly characterized by laminated sediments interbedded with homogeneous intervals (Beaufort et al., 2003). The complete core sections were preserved and subsampled onshore. The subsamples were dried and homogenized before geochemical analyses.

### 2.2.3. Age model

The age model was based on several $^{14}C$ Accelerator Mass Spectrometry (AMS) dates measured in planktic foraminifera *Globigerina bulloides* (Staines-Urias et al., 2015) and in bulk organic matter (produced by J.D. Carriquiry) (Table 2.1). Radiocarbon ages were calibrated using the software Calib 7.0.4. (Stuiver et al., 2019) and Marine 13 curve (Reimer et al., 2013). Due to limitations of the radiocarbon method, ages older than ~40 kyr were extrapolated applying a regression model of the last six reliable $^{14}C$-data points (Figure 2.2). In such model a linear sedimentation rate is assumed, which could compromise the ability to interpret shorter-term processes to an unknown

**Table 2.1.** Age model data for core MD02-2510 produced by Accelerator Mass Spectrometry (AMS) $^{14}C$ dating of foraminifera (Staines-Urias et al., 2015) and organic matter (provided by Jose D. Carriquiry). The radiocarbon ages (cal yr BP) were calibrated using Calib 7.0.4. with Marine 13 curve (Reimer et al., 2013). Please note that Staines-Urias et al. (2015) added 20 cm to the core depth for better stratigraphic correlation of core MD02-2510 with previously published gravity core NH01-15GC3 (Gonzalez-Yajimovich et al., 2007). For sediments older than 33,712 cal yr BP, we produced the age model using an extrapolated average sedimentation rate of the last measurements.

| Core top depth (cm) | Calibrated age ± 1σ uncertainty (cal yr BP) | Dated material | Laboratory and analysis reference code | Reference |
|---|---|---|---|---|
| 252 | 5879 ± 40 | *Globigerina bulloides* | AAR15198 | Staines-Urias et al. (2015) |
| 300 | 7879 ± 36 | Bulk Organic Matter | Keck Lab at University of California Irvine | This study |
| 366 | 8886 ± 110 | *Globigerina bulloides* | AA92440 | Staines-Urias et al. (2015) |
| 638 | 16,797 ± 120 | *Globigerina bulloides* | NZA0280 | Staines-Urias et al. (2015) |
| 953 | 22,413 ± 86 | *Globigerina bulloides* | AA92442 | Staines-Urias et al. (2015) |
| 1510 | 33,712 ± 146 | Bulk Organic Matter | Beta Analytic | This study |

degree. According to this, the upper sediment section spanning 1510 cm reaches 33,712 ± 146 cal yr BP (Table 2.1). The estimated sedimentation rate is around 0.45 mm/year and is in good agreement with previously reported estimates for the Holocene of Alfonso Basin (González-Yajimovich et al., 2007; Choumiline et al., 2010; Pérez-Cruz, 2000; Pérez-Cruz, 2013; Staines-Urias et al., 2015; Silverberg et al., 2014).

The age model allowed for a millennial and submillennial scale resolution in the resulting core record. In this chapter, we focus on the time range spanning 30-70 cal kyr BP in order to include the MIS 3 in high resolution.

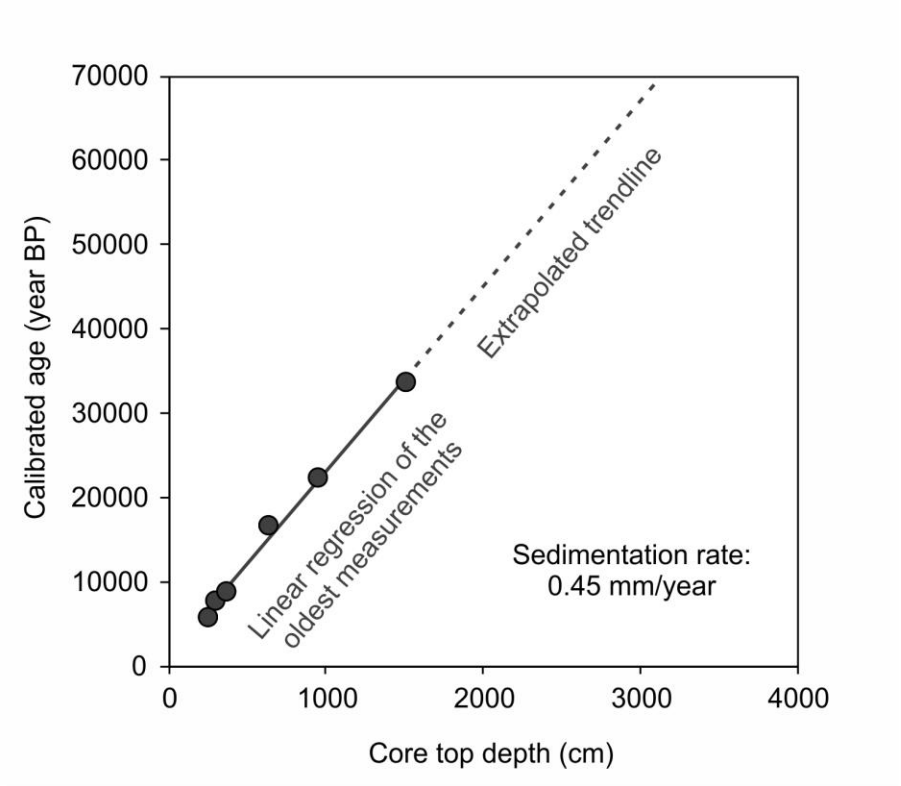


**Figure 2.2.** Age model of core MD02-2510 based on data from Staines-Urias et al. (2015) and Jose D. Carriquiry (this study). Detailed data for the oldest six measurements used to generate the age model for the sediment core, are also presented in Table 2.1.

### 2.2.4. Geochemistry

Total carbon ($C_{tot}$) and total inorganic carbon ($C_{inorg}$) were measured on sediment samples using an ELTRA CS-500. For $C_{tot}$ determination, dry sample splits were placed in ceramic boats and combusted at 1350°C in a furnace. In order to measure $C_{inorg,}$ new sample aliquots were acidified in of Erlenmeyer flasks by carefully adding 20% HCl while spinning and heating inside of a TIC module. Both methods produced $CO_{2,}$ which was independently measured by an infrared analyzer inside of the ELTRA CS-500, allowing to quantify $C_{tot}$ and $C_{inorg}$. The organic carbon ($C_{org}$) fraction was calculated by numerical difference as follows: $C_{org} = C_{tot} - C_{inorg}$.

In order to determine the elemental composition, dry sediment splits weighting 100 mg were transferred to ceramic vessels and were ashed for 8 hours at 550°C in a high-temperature oven. The resulting material was digested in Teflon beakers using a mixture of $HNO_3$, HCl, and HF over several cycles of acidification/drying. The final splits were diluted in 2% $HNO_3$ and measured for major and trace elements (Al, Ba, Cd, Cu, Fe, Mo, Ni, U, V, Zn) on an Agilent 7900 Inductively Coupled Mass Spectrometer (ICP-MS).

The quality of data was tested by analyzing certified reference material USGS SGR-1b, USGS SDO-1, NIST 2702, AR4007, and AR4024, as well as sample duplicates. Analytical precision was always better than 3%. Accuracy of the measured sample relative to certified standard value ranged in recoveries between 96% and 105%.

### 2.2.5. Numerical and statistical approaches

Elemental records were normalized to a crustal indicator (in this case, Al) in order to mitigate the effect of detrital inputs on the concentration values. Likewise, in order to establish the correlation between redox and productivity proxies, we calculated ratios for selected elements.

Excess barium ($Ba_{excess}$) was calculated numerically (Eagle et al., 2003; Anderson and Winkler, 2005), as follows: $Ba_{excess} = Ba_{total} - (Ba/Al_{terrigenous}) \times Al_{total}$. The Ba/Al ratio of 0.0045 was used because it represents the detrital Ba input appropriate for the study area (Dymond et al., 1992; Eagle et al., 2003).

R-mode Factor Analysis with Varimax rotation using the software STATISTICA by StatSoft was applied in order to define proxy associations. The analysis included the following variables: $C_{org}$, $CaCO_3$, Cd, Cu, Mn, Mo, Ni, V, Zn, as well as an authigenic U estimation ($U_{auth}$) taken from Choumiline et al. (2017) and Choumiline et al. (in prep). The location map was constructed using

the ArcGIS Desktop 10.6 software by ESRI. Bottom oxygen data used in the map was taken from World Ocean Atlas (2005) and Garcia et al. (2006).

### 2.2.6. Geochemical proxies used in this study

Organic carbon ($C_{org}$) records were used as a proxy for organic carbon burial (Schoepfer et al., 2015; Bianchi et al., 2016) and $CaCO_3$ as indicator of calcareous sedimentation. Ratios of Cu/Al, Ni/Al, and Zn/Al were used as proxies of productivity (Boyle, 1981; Böning e al., 2015; Tribovillard et al., 2006); meanwhile Fe/Al, Mn/Al, Cd/Al, V/Al, and Mo/Al were used as indicators of redox conditions in bottom waters (Calvert and Pedersen, 1993; Morford and Emerson, 1999; Tribovillard et al., 2006; Scholz et al., 2018).

Barite and its analog $Ba_{excess}$ are commonly used paleoproxies that have been used successfully in the study area to reconstruct changes in productivity (Choumiline et al., 2019). Multiple studies have warned about post-burial remobilization of barite, especially in regions with fluctuating bottom and pore water redox (McManus et al., 1998; Riedinger et al., 2006; Schoepfer et al., 2015). Despite its limitations, we present $Ba_{excess}$ values for this sediment core for discussion purposes.

## 2.3. RESULTS AND DISCUSSION

### 2.3.1. Variability of productivity during the MIS 4 - MIS 3 transition in Alfonso Basin, Gulf of California

Here we present a multi-millennial productivity reconstruction of the 30-70 kyr BP period in core MD02-2510 from Alfonso Basin, which covers the transition from the cold MIS 4 sea-level low stand to the warmer MIS 3 stage (Figure 2.3). Due to transient anoxia in the study area, we focus on the more refractory proxies such as organic carbon ($C_{org}$),

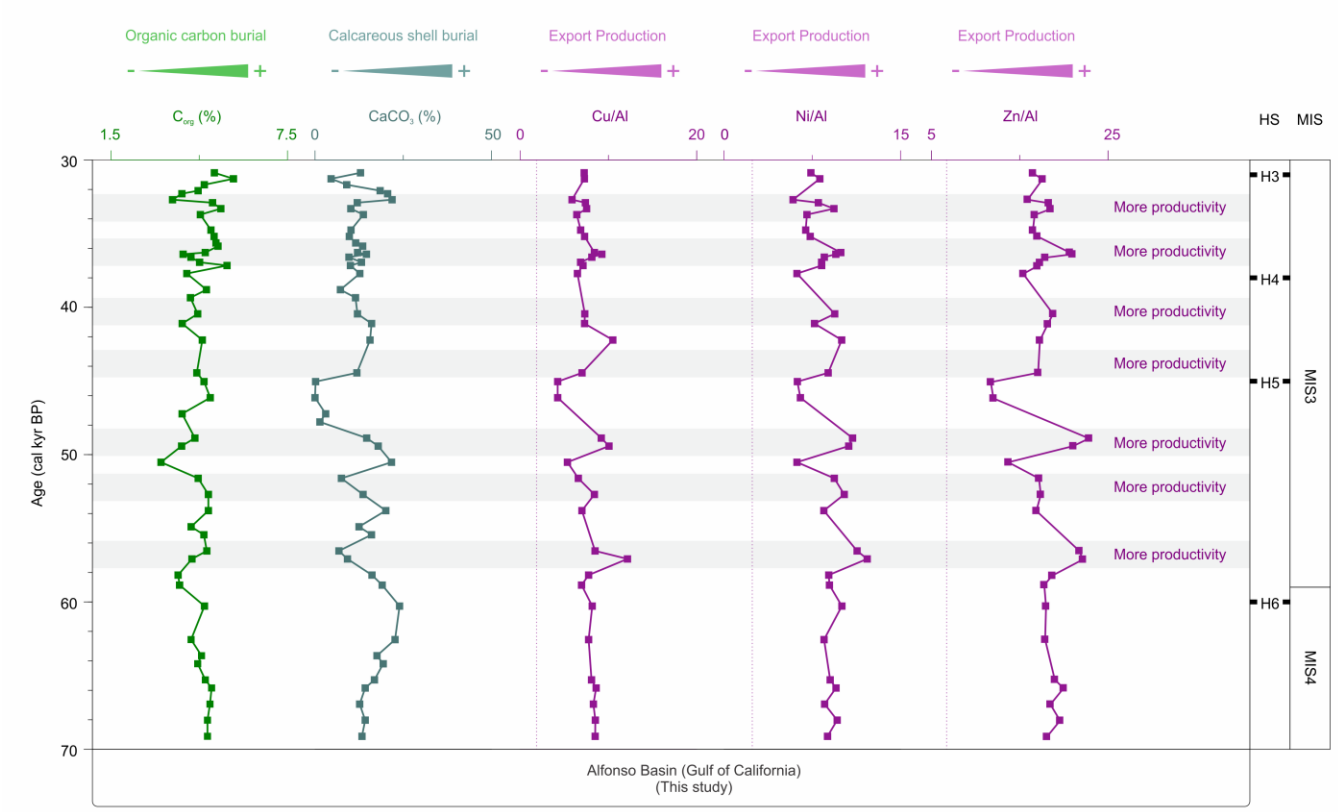


**Figure 2.3.** Productivity proxies in core MD02-2510 from Alfonso Basin, Gulf of California during the 30-70 cal kyr BP period. Vertical dotted lines represent upper continental crust average values (Wedepohl, 1995). Periods of enhanced productivity are highlighted as grey horizontal bars. The approximate timing of Heinrich events (Hemming, 2004) and the hypothetical boundaries between Marine Isotope Stages (Lisiecki and Raymo, 2005) are presented in the figure for reference only. Please note that only the timing of the peak Heinrich events is specified, not the duration (Hemming, 2004).

calcium carbonate content ($CaCO_3$), Cu, Ni, and Zn to assess productivity (Tribovillard et al., 2006; Marchitto, 2007; Böning et al., 2015; Defforey and Paytan, 2018), rather than relying on those involving barium and barite (Ba/Al, $Ba_{excess}$), which are potentially prone to post-burial dissolution and re-precipitation, as discussed by Anderson and Winckler (2005) and Riedinger et al. (2006). The drawbacks of the $Ba_{excess}$ proxy in OMZ-type settings have been debated extensively (Schoepfer et al., 2015). While some sedimentary records from Alfonso might still have usable $Ba_{excess}$ signals, such as those from shallow sediments corresponding to the last few millennia (Choumiline et al., 2019), we believe that $Ba_{excess}$ enrichments in core MD02-2510 are not a primary signal (Supplementary Figure 2.1). The downcore Ba enrichments extending further in time than a few millennia are very likely affected by diagenesis, invalidating its use as productivity proxy in our record. Despite the latter, we still present $Ba_{excess}$ reconstruction compared to productivity (Ni/Al) and redox (Mo/Al) proxies in Supplementary Figure 2.1. The figure shows potential barite redissolution and reprecipitation fronts (McManus et al., 1998; Riedinger et al., 2006; Schoepfer et al., 2015).

The proxy record from Alfonso Basin displays high variability in the concentration and Al-normalized values, ranging from minimum to maximum (in parenthesis) as follows: $C_{org}$ (3.21 - 5.67 %), $CaCO_3$ (0 - 23.94 %), Cu (22.91 - 43.82 mg/kg), Cu/Al (4.25 - 12.16),
Ni (26.53 - 48.13 mg/kg), Ni/Al (5.86 - 12.16), Zn (58.57 - 100.88), Zn/Al (11.72 - 22.87), and $Ba_{excess}$ (230.74 - 435.92).

Low maximum values of $C_{org}$ (4.23 %), $CaCO_3$ (23.94 %), Cu/Al (8.61), Ni/Al (10.01), and Zn/Al (19.94) in the oldest part of the section (70 - 60 cal kyr BP) suggest that productivity was low towards the end of MIS 4 (around 60 cal kyr BP), followed by an increase in values from 60 to 45 cal kyr BP in the MIS 3 (Figure 2.3). This interval displays some of the highest values for the studied core section: 4.88 % $C_{org}$, 21.66 % $CaCO_3$, Cu/Al of 12.16, Ni/Al of 12.16, and Zn/Al of

22.87. Between 45 and 30 cal kyr BP in the MIS 3, productivity slightly decreased with maximum values of 5.67 % $C_{org}$, 21.84 $CaCO_3$, Cu/Al of 10.50, Ni/Al of 10.00, and Zn/Al of 20.92. This trend prevailed until 30 kyr BP that marks the beginning of the LGM when values suddenly decreased to levels similar to those of MIS 4.

It is worth noting that in Alfonso Basin, $Ba_{excess}$ does not correlate with any of the productivity indicators mentioned earlier, revealing the limits of the usage of this proxy in similar OMZ settings, as discussed above (Supplementary Figure 2.1).

### 2.3.2. Oxygen in bottom waters throughout the MIS 4 - MIS 3 transition in Alfonso Basin, Gulf of California

To provide a first-order qualitative assessment of multi-millennial changes in oxygenation during the period of time studied, we used a lithologic description of the sediments, which shows mostly laminated intervals with few short layers of massive sediments (based on the IMAGES VIII / MD126 MONA Cruise Report from Beaufort et al., 2003).

Throughout the core, redox proxies show the following ranges: Fe/Al (0.41 - 0.54), Mn (185.44 - 287.71 mg/kg), Mn/Al (36.21 - 63.82), Cd (3.05 - 10.72 mg/kg), Cd/Al (0.60 - 3.25), V (56.33-121.44 mg/kg), V/Al (12.10-32.87), Mo (4.14-35.12 mg/kg), and Mo/Al (0.99-10.63).

The paleoredox reconstruction (Figure 2.4) indicates well-oxygenated conditions at the end of the MIS 4 evidenced by detrital-like values similar in composition to the average upper crust (Wedepohl, 1995; McLennan, 2001). Between 70 and 60 cal kyr BP, the values maintained very low maximums of Fe/Al (0.52), Mn/Al (56.57), Cd/Al (1.65), V/Al (20.59), and Mo/Al (2.93). Around 60 kyr BP, marked by the beginning of the MIS 3, anoxia commenced abruptly, highlighted by the highest Fe/Al (0.54) and Mo (35.13 mg/kg), as well as elevated Mn (268.42),

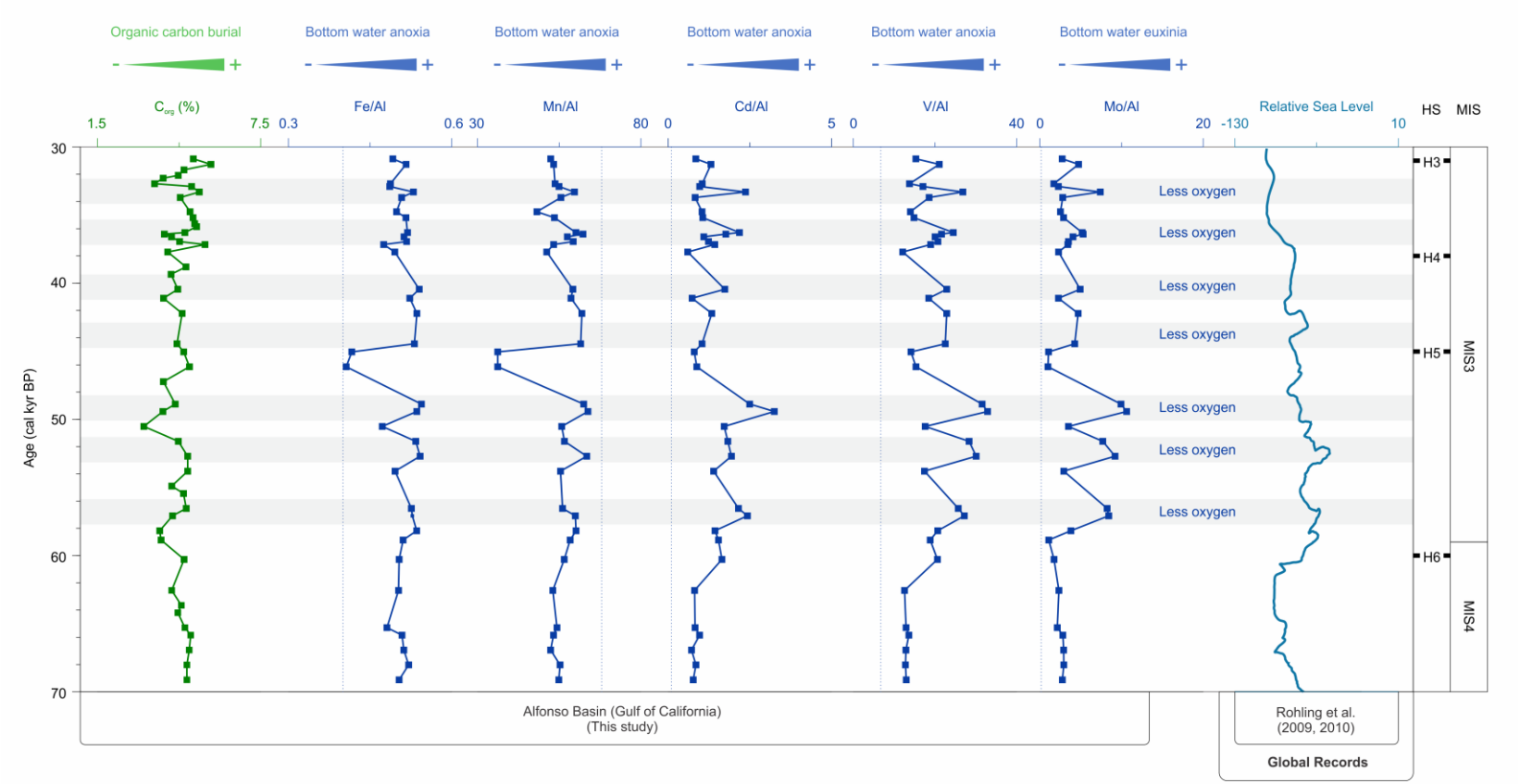


**Figure 2.4.** Redox proxies in core MD02-2510 from Alfonso Basin, Gulf of California during the 30-70 cal kyr BP period. Vertical dotted lines represent upper continental crust average values (Wedepohl, 1995). Periods of stronger deoxygenation are marked as grey horizontal bars. Relative Sea Level reconstruction data taken from Rohling et al., 2009, 2010. The approximate timing of Heinrich events (Hemming, 2004) and the hypothetical boundaries between Marine Isotope Stages (Lisiecki and Raymo, 2005) are presented in the figure for reference only.

Cd (10.32 mg/kg), and V (117.94 mg/kg) values during the first half of this Marine Isotope Stage (60 to 45 cal kyr BP). The normalized values were the highest of the entire dataset during this MIS 3 onset: for Mn/Al (63.82), Cd/Al (3.25), V/Al (32.87), and Mo/Al (10.63). Values for Mo and Mo/Al reach high values in particular (35.12 mg/kg and a ratio of 10.63, respectively), indicating elevated $H_2S$ levels, either in the bottom waters of the basin at the time of deposition or in pore fluids (Zheng et al., 2000; Scott and Lyons, 2012; Scholz et al., 2017; Hardisty et al., 2018). After anoxic (or possibly euxinic) time, bottom waters of Alfonso Basin became intermittently more oxygenated in the interval from 45 to 30 cal kyr in the MIS 3, with values reaching 0.54 of the Fe/Al ratio, 287.71 mg/kg Mn, 10.72 mg/kg Cd, 121.44 mg/kg V, and 33.48 mg/kg Mo in marine sediments. The Al-normalized values were lower than those during the beginning of the MIS 3: Mn/Al (62.29), Cd/Al (2.37), V/Al (26.83), and Mo/Al (7.40).

### 2.3.3. Effect of Dansgaard–Oeschger oscillations and Heinrich events on OMZ variability in Alfonso Basin, Gulf of California

Despite the predominance of enhanced anoxia at the bottom of Alfonso Basin during the MIS 3 (evidenced by high V and Mo), the effect of short submillennial cold climatic events caused a dropdown in productivity and sudden increase in dissolved oxygen. The interplay between warm and cold D-O oscillations is strongly superimposed on both the productivity (Figure 2.3) and the dissolved oxygen records (Figure 2.4). Our record from Alfonso spanned the following Heinrich events with corresponding timing as previously reported by Bond et al. (1992, 1993) and Hemming (2004): H3 (31 cal kyr BP), H4 (38 cal kyr BP), H5 (45 cal kyr BP), and H6 (60 cal kyr BP). There are some dating uncertainties, so that Heinrich event timing is used with caution in paleoceanographic correlations (Hemming, 2004).

Marine productivity and/or amount of exported organic matter were usually low during cold D-O phases, often equivalent to the levels observed during Heinrich events. Throughout the entire MIS 3 (30-60 cal kyr BP), these cold events registered the lowest amounts of $C_{org}$ (3.21 %), $CaCO_3$ (< 0.00 %), Cu (22.91 mg/kg), Ni (26.53 mg/kg), and Zn (58.57 mg/kg) in marine sediments. There is good agreement between the Ni and Cd; however, $C_{org}$ follows a slightly different trend. The $C_{org}$ does not always quantitatively represent exported organic matter, as its burial could be a complex interplay between remineralization, diagenetic overprinting, and organic matter reactivity (Schoepfer et al., 2015; Bianchi et al., 2016). Importantly, despite overall stronger productivity during the first half of the MIS 3 based on Cu/Al, Ni/Al, and Zn/Al the effect of these cold oxygenated periods was enough to lower primary productivity to the same level as that of the second less productive half of the MIS 3 (Figure 2.3). The relatively consistent correlation between Ni and $C_{org}$ for both the Heinrich and non-Heinrich episodes provides evidence for the good preservation of Ni in OMZ-type settings and speaks about the reliability of its use as a productivity indicator (Böning et al., 2015).

In order to evaluate the preservation/remineralization of organic matter during the MIS 3, we compared the correlation coefficients between $C_{org}$ and less refractory proxies Cu, Ni, and Zn (Figure 2.5). Interestingly, stronger correlations were revealed during less-productive Heinrich events (0.511 between $C_{org}$:Cu, 0.6497 for $C_{org}$:Ni and 0.6567 for $C_{org}$:Zn) contrasting with those marked by higher-productivity during non-Henrich periods (0.1937, 0.5686 and 0.2985 respectively). The differences between the $R^2$ values during Heinrich and non-Heinrich events could be due to the source, preservation, and remineralization of each productivity proxy under different oxygenation states. For instance, Heinrich events represent times of lower productivity and slower remineralization, leading to more efficient particulate export of trace elements into the sediments.

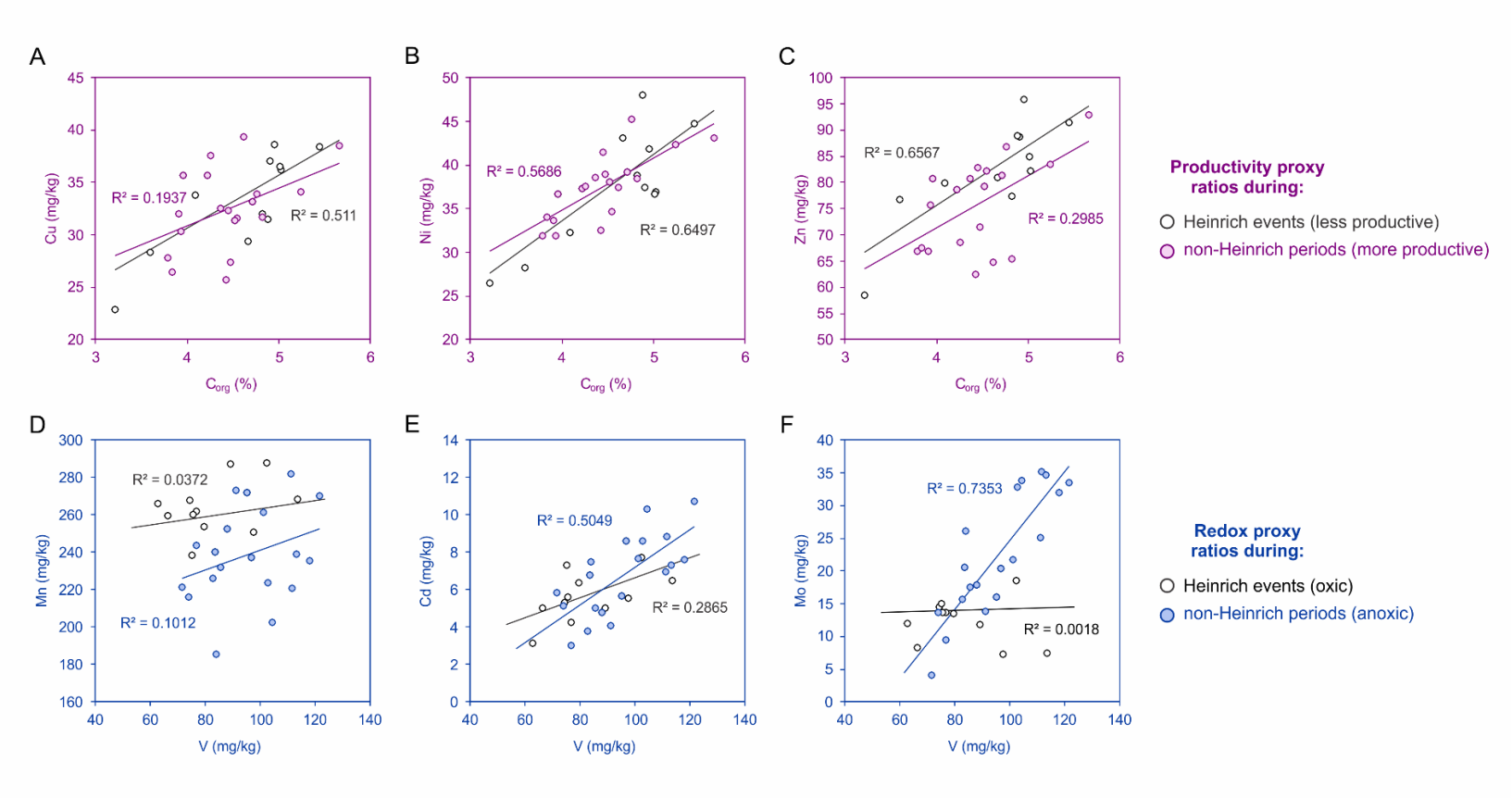


**Figure 2.5.** Comparison of element ratio correlations between Heinrich and non-Heinrich events recorded in core MD02-2510 from Alfonso Basin, Gulf of California during the Marine Isotope Stage 3. We used an approximate correlation of our sedimentary horizons to well-known Heinrich event peaks (Bond et al., 1992, 1993; Hemming, 2004).

Submillennial-scale variability in oxygenation was also revealed during D-O oscillations (Dansgaard et al., 1984; Schmidt and Hertzberg, 2011). For the cold D-O phases and corresponding Heinrich events, the sediments did not preserve a clear laminated structure, while redox proxies showed lower Fe/Al values (0.51) and near-detrital concentrations of redox-sensitive trace elements – all pointing to well-oxygenated bottom waters. The reported proxy values in sediments of Alfonso Basin were low for Mn (185.44 mg/kg), Cd (3.05 mg/kg), V (71.52 mg/kg), and Mo (4.14 mg/kg) during Heinrich events.

To assess how multiple redox indicators compare to vanadium, one of the most reliable redox proxy (Emerson and Huested, 1991; Morford and Emerson, 1999), we show the correlation coefficient between this element and the other oxygenation proxies Mn, Cd, and Mo (Figure 2.5). The stronger correlations always accompany the most anoxic non-Heinrich periods, with $R^2$ values of 0.1012 for V:Mn, 0.5049 for V:Cd, and 0.7353 for V:Mo. The highest correlation during anoxic non-Heinrich events was found for Mo and V and can be attributed to a more substantial dependence of these two proxies on bottom water redox conditions rather than on the particulate trace element supply or scavenging during particulate transport downwards into the sediments (Scholz et al., 2011; Scholz et al., 2017). The weaker redox proxy relationships correspond to well-ventilated Heinrich events (or cold D/O oscillations), exhibiting low $R^2$ values of 0.0372 for V:Mn, 0.2865 for V:Cd and 0.0018 for V:Mo (Figure 2.5). We attribute this lack of correlation to an absence of the authigenic enrichment of redox proxies under oxygenated conditions and the high variability of near-detrital values of Mn, Cd, and Mo. This non-authigenic material was mainly supplied fluvially or by wind-blown dust to the basin through sedimentary inputs, composed mainly of reworked rock material from land.

### 2.3.4. Statistical associations between productivity and redox proxies during the MIS 3 – MIS 4 transition in Alfonso Basin, Gulf of California

Here we present the results of an R-mode Factor Analysis with Varimax rotation for the dataset of the time interval between 30-70 cal kyr BP. We excluded Fe/Al to avoid biasing the results with a normalization artifact and added authigenic U ($U_{auth}$) values from Choumiline et al. (2017) and Choumiline (in prep). The results of the analysis (Table 2.2, Figure 2.6) allowed us to distinguish two leading associations between Factor 1 (42.36 % variance) and Factor 2 (28.85 % variance). The "Productivity" association encompassed $C_{org}$, Ni, Cu, $U_{auth}$, Zn, and potentially Mn, while the "Redox" association included Cd, Mo, V. In this analysis, $CaCO_3$ seem to be independent of the redox and productivity associations. Remarkably, $U_{auth}$ has a stronger statistical connection

**Table 2.2.** Factor loadings of the R-mode Factor Analysis with Varimax rotation performed on the 30-70 cal kyr BP dataset from Alfonso Basin.

| Proxy | Factor 1 | Factor 2 |
|---|---|---|
| $C_{org}$ | 0.858408 | -0.288678 |
| $CaCO_3$ | -0.439062 | 0.531029 |
| Cu | 0.837480 | 0.181691 |
| Ni | 0.858000 | -0.236201 |
| Zn | 0.907623 | 0.131260 |
| Mn | 0.726247 | 0.251412 |
| Cd | -0.133991 | -0.857868 |
| V | 0.029213 | -0.942153 |
| Mo | -0.021614 | -0.822204 |
| $U_{auth}$ | 0.706122 | 0.225497 |
| **Explained Variance** | 4.236272 | 2.885024 |
| **Proportion of Total Variance** | 42.36 % | 28.85 % |

with productivity proxies than with paleoredox indicators. This link could be due to the possible supply of significant amounts of authigenic U via settling during high productivity events discussed in Zheng et al. (2002), Choumiline et al. (2010), Choumiline (2011), and Choumiline et al. (2019). The mechanisms by which $U_{auth}$ is either adsorbed to organic matter or reduced from its dissolved U(+6) form inside of marine snow aggregates are described in depth in Choumiline et al. (2019). The potential association of Mn to productivity proxies could also provide additional evidence for water column processes related to scavenging of trace elements by (oxyhydr)oxides, common in many modern OMZ-type settings (Scholz et al., 2011; 2017).

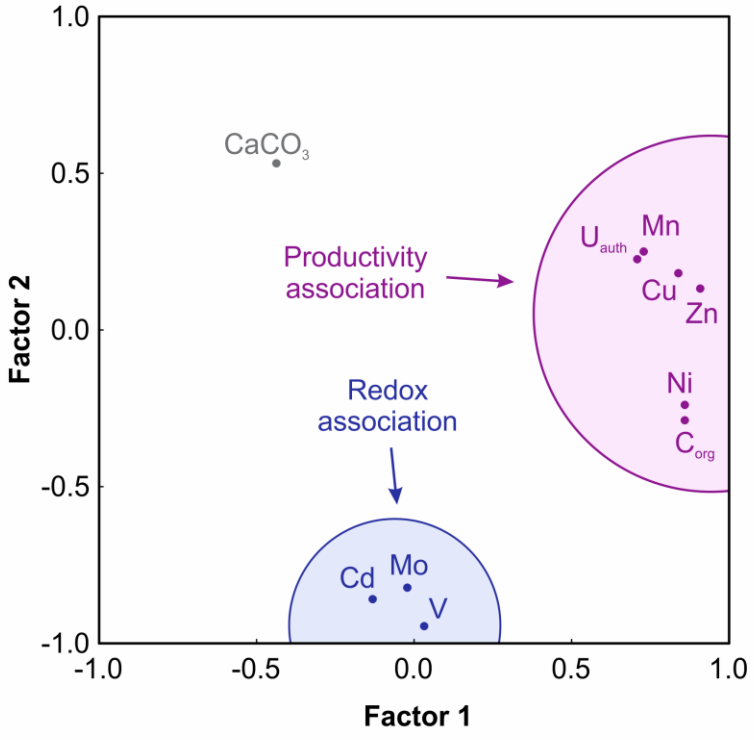


**Figure 2.6.** Productivity and redox proxy associations defined by R-mode Factor Analysis during the 30-70 cal kyr BP interval from Alfonso Basin

### 2.3.5. History of Oxygen Minimum Zone variability in the ETNP during 30-70 cal kyr BP

Our interpretation of the multiproxy paleoceanographic record in Alfonso Basin suggests that there were three main stages of multimillennial OMZ variability overprinted by submillennial Heinrich events and D-O oscillations. During the studied period from 70 to 30 cal kyr BP, the OMZ in Alfonso Basin evolved in three main stages. The first stage was the cold MIS 4 characterized by decreased productivity (low Ni/Al) and abundant bottom water oxygen (low Mo/Al) (Figure 2.7). During this stage, the OMZ was vertically contracted, which is indicated by our redox proxy data showing low Mn/Al, Cd/Al, V/Al, and Mo/Al (Figure 2.4). The following episode occurred during the onset of the MIS 3 and involved elevated productivity (high Ni/Al) and strongly anoxic water conditions based on elevated Cd/Al, V/Al, and Mo/Al values. Abundant Mo during the MIS 3 could either indicate euxinic conditions in bottom waters or the presence of abundant sulfide in pore fluids below the sediment-water interface (Zheng et al., 2000; Scott and Lyons, 2012; Scholz et al., 2017; Hardisty et al., 2018). The limits of the Mo proxy do not allow us to distinguish between the presence of sulfide in the water column or only to the sediments, but high abundance of pore water sulfide is more likely the reason for Mo enrichments in OMZ-type settings than bottom water euxinia (Zheng et al., 2000; Scholz et al., 2017; Hardisty et al., 2018). Elevated Mo could also represent the vertical displacement of the OMZ exposing the basin to the most reducing middle OMZ part, usually hosting the most reducing water masses. The next stage towards the end of MIS 3 involved a slight collapse in marine productivity based on Cu/Al, Ni/Al, and Zn/Al and a subtle increase in oceanic oxygenation based on Cd/Al, V/Al, and Mo/Al, while maintaining a significantly expanded OMZ dominated by anoxia (Figure 2.7). Remarkably, if we compare the end of MIS 3 with MIS 4, productivity remained similar for those two stages based on Cu/Al, Ni/Al, and Zn/Al, while oxygenation drastically differed (Figures 2.3 and 2.4). This relationship could provide insight into the different mechanisms that controlled both episodes: one upwelling-based

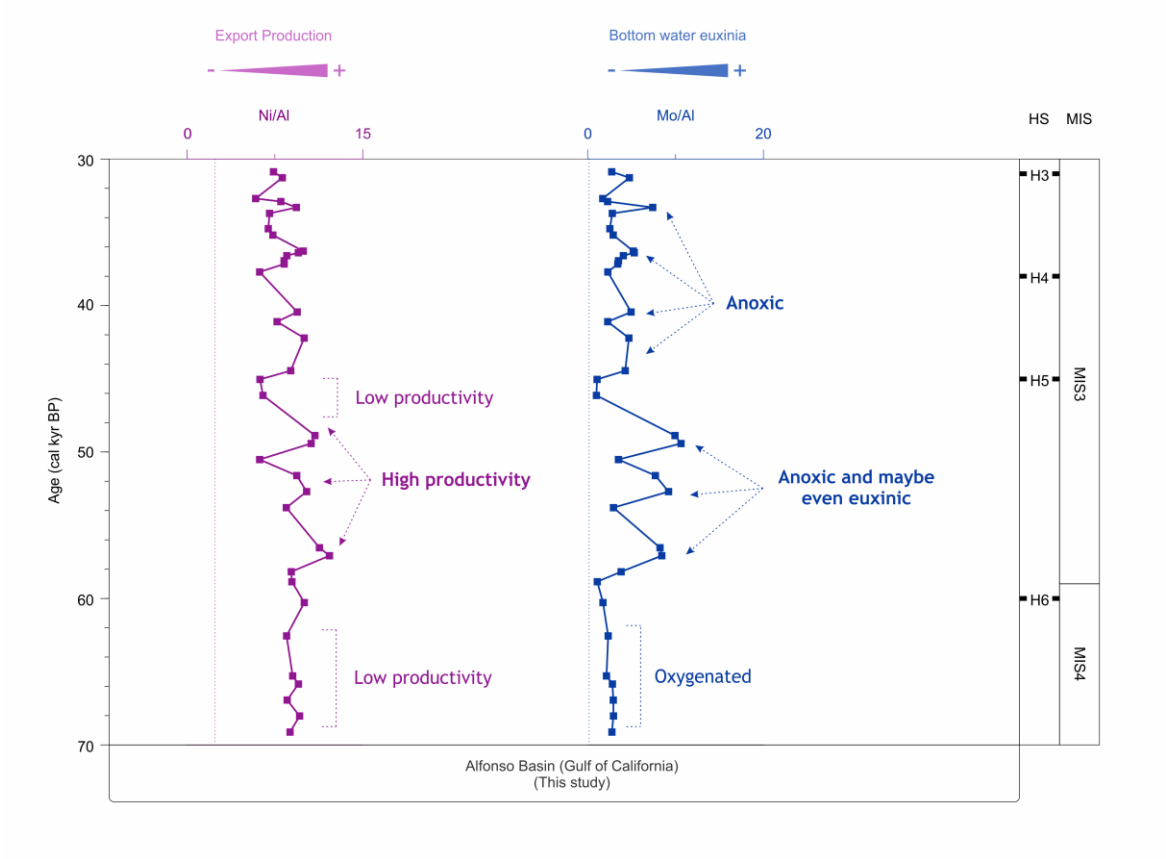


**Figure 2.7.** Interpretation of changes in productivity and redox in core MD02-2510 from Alfonso Basin, Gulf of California during the 30-70 cal kyr BP period. The approximate timing of Heinrich events (Hemming, 2004) and the hypothetical boundaries between Marine Isotope Stages (Lisiecki and Raymo, 2005) are presented in the figure for reference only.

involving a productivity-controlled OMZ shift due to the availability of nutrients (MIS3 onset), while the other occurred via actual changes in deep water oxygenation despite overall abundant nutrient accessibility (MIS3 termination). After the establishment of anoxia during the MIS 3, the long-term multimillennial trend in Mn/Al, Cd/Al, V/Al, and Mo/Al shows that the ETNP did not return to the well-oxygenated conditions of the MIS 4 until the beginning of MIS 2 (Choumiline et al., 2017; Cartapanis et al., 2014; Nameroff et al., 2004; Tetard et al., 2017). Only Heinrich and/or cold D/O events could have potentially driven the OMZ to suboxic/oxic conditions. This short-term Heinrich variability is consistent for both productivity and redox records as shown in Figure 2.7. This relationship probably represents a similarity between the mechanisms that drive each Heinrich (cold D/O) event and a tight relationship between a shutdown in productivity and reduced ventilation at OMZ depths (Cartapanis et al., 2012; Cartapanis et al., 2014; Tetard et al., 2017). On a broader oceanic scale, the productivity and redox of marine basins of the ETNP are tightly controlled by global climatic events that drive the oxygenation in the Pacific by upwelling-induced productivity changes especially crucial for the western margin of North America, including Gulf of California, Baja California, and California coastline (Herbert et al., 2001; Tetard et al., 2017).

To explore these relationships, we compare the results of our OMZ reconstruction (this study) to those of other locations in the Eastern Pacific, emphasizing published productivity ($C_{org}$, biogenic $SiO_2$, Ag, Cu, Ni, Zn) and redox (benthic foraminifera, Cd, Mo, U, V) proxy records. Note that the values and variability of each proxy often depend on local oceanographic effects, terrigenous inputs, and even age model differences.

Most ETNP records agree that productivity reached the highest level of the studied interval 30-70 cal kyr BP during the MIS 3, as evidenced by elevated Ni, Cu, and Zn values in Alfonso Basin (this study); high biogenic $SiO_2$ in Magdalena Margin (Carriquiry and Sanchez, 2014); high $C_{org}$, Ni, and Cu in W. Baja California (Cartapanis et al., 2011, 2014; Baturin et al., 2016); and

elevated $C_{org}$ and Cu in sediments off Mazatlan (Nameroff et al., 2004). Moreover, the extent of MIS 3 is not limited to the ETNP because a comprehensive compilation shows evidence for enhanced organic carbon burial during the MIS 3 compared to MIS 4 (Cartapanis et al., 2016) beyond the Pacific.

For a broad reconstruction of paleoxygenation, we compare the Mo concentration in our sediment record from Alfonso Basin (this study) with other sediment cores of the ETNP OMZ (Figure 2.8) off Mazatlan (Nameroff et al., 2004), W. Baja California (Dean et al., 2006; Cartapanis et al., 2011), Guaymas Basin (Chang et al., 2015), and Santa Barbara Basin (Ivanochko, 2001; Ivanochko and Pedersen, 2004). However, there is a general agreement between most records of paleoxygenation in the ETNP (Figure 2.8), with the exception of the Guaymas Basin record published by Chang et al. (2015). Chang and co-authors were aware of these discrepancies and explore whether their record can be compared to that of the open Pacific margin. To explain the differences with previously published records (e.g., Nameroff et al., 2004), the authors invoke a mechanism of direct Mo removal from seawater (Chang et al., 2015). We also hypothesize that active hydrothermal inputs well known for the Guaymas Basin could also have impacted the differential preservation of proxy records but also compromised the age model by bringing older "dead" $^{14}C$ to the marine basin (Patrick Rafter, personal communication). Despite the latter, based on most published ETNP records (Figure 2.8), the MIS 3 had enhanced organic matter preservation, higher export productivity, and overall stronger deoxygenation (Ivanochko, 2001; van Geen et al., 2003; Nameroff et al., 2004; Cartapanis et al., 2014; Chang et al., 2014; 2015) when compared to MIS 4. Other redox proxies also confirm enhanced anoxia during MIS 3 represented by high Cd and Mn in Alfonso Basin (this study); high Cd in sediments of W. Baja California (Cartapanis et al., 2011, 2014; Baturin et al., 2016); elevated V, Mn, and U in sediments off Mazatlan (Nameroff et al., 2004), and Cd in Santa Barbara Basin (Ivanochko and Pedersen, 2004).

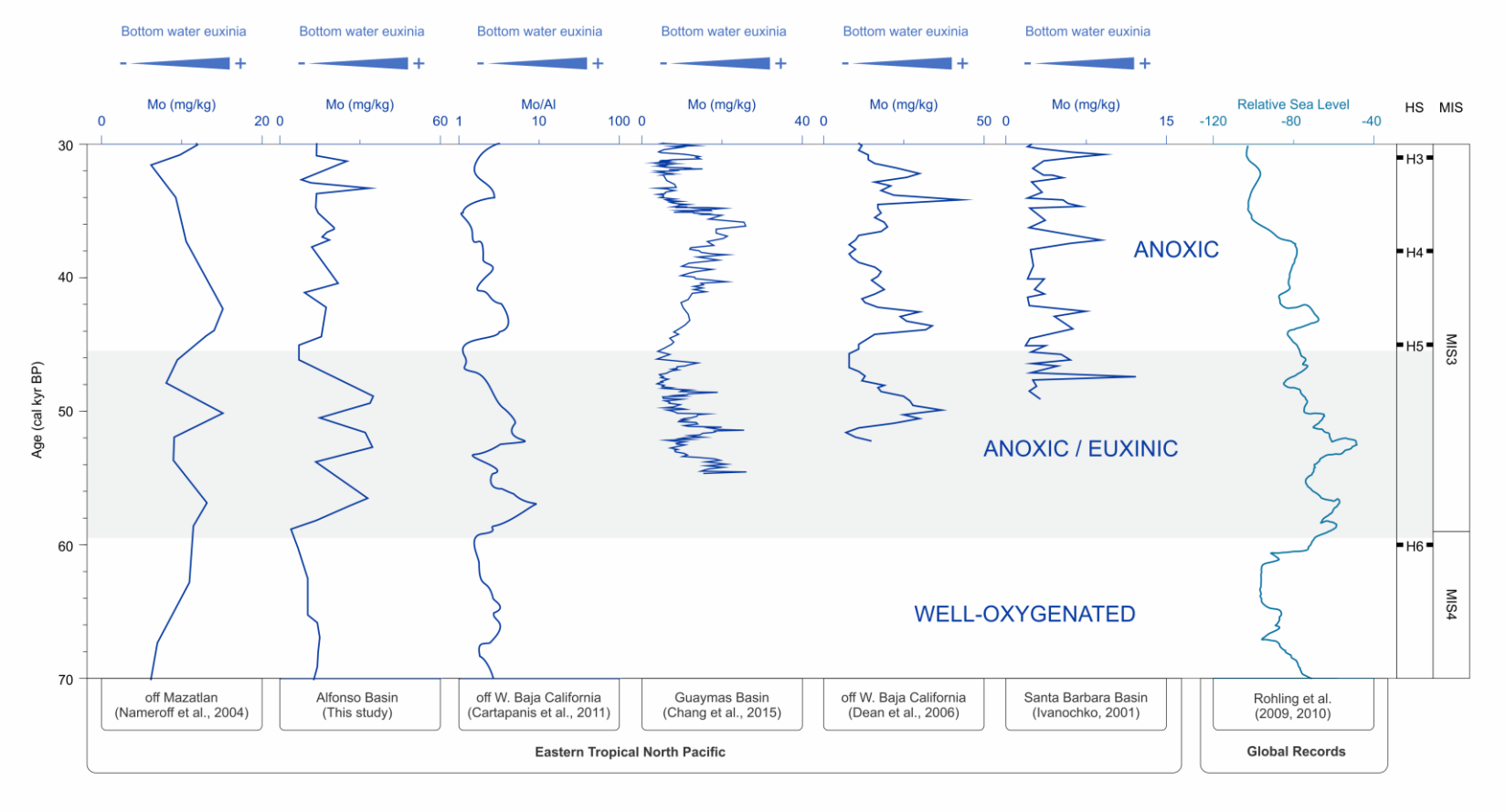


**Figure 2.8.** Comparison of Redox proxies in core MD02-2510 from Alfonso Basin, Gulf of California during the 30-70 cal kyr BP period. Relative Sea Level reconstruction data taken from Rohling et al., 2009, 2010. The approximate timing of Heinrich events (Hemming, 2004) and the hypothetical boundaries between Marine Isotope Stages (Lisiecki and Raymo, 2005) are presented in the figure for reference only.

Non-geochemical proxies also indicate strong bottom water anoxia during the MIS 3 based on the lamination index (Ivanochko and Pedersen, 2004) and microfossil data (Tetard et al., 2017). Reconstructed $O_2$ estimates based on foraminiferal assemblages confirm the findings of our study by also suggesting strongest anoxia in the ETNP throughout the beginning of the MIS3 (Tetard et al., 2017). According to Tetard et al. (2017), the lowest estimated $O_2$ of the last 80 kyr would have been 0.1 ml/l, and the highest reaching 2 ml/l.

Remarkably, the upper (200-500 m), mid (500-800 m), and low (800-1200 m) OMZ depths record both multimillennial and submillennial OMZ variability, registered not only in Alfonso Basin (410 m), Mazatlan Margin (420 m), Santa Barbara Basin (576 m), W. Baja California (705 m), but also in the deep Vancouver Island Margin (1243 m). Despite being part of the Gulf of California, Alfonso Basin is recording the paleoceanographic variability of the open ETNP (Nameroff et al., 2004; Cartapanis et al., 2011). Moreover, MIS 3 also represents times of enhanced anoxia in other core records, including the Eastern Tropical South Pacific (ETSP), such as along the Peru margin (Scholz et al., 2017).

Both the reconstructed productivity and redox signals in most ETNP cores are impacted by submillennial variability of Heinrich events and D/O cycles. As mentioned for Alfonso Basin (this study), productivity was typically lowest during cold Heinrich events, which are equivalent to cold D/O phases (Ivanochko, 2001; Ivanochko and Pedersen, 2004; Carriquiry and Sanchez, 2014; Cartapanis et al., 2011, 2014; Baturin et al., 2016). Redox proxies suggest the most ventilated conditions during such cold Heinrich events (Ivanochko, 2001; van Geen et al., 2003; Ivanochko and Pedersen, 2004; Cartapanis et al., 2011, 2014; Chang et al., 2014; 2015).

### 2.3.6. Climatic drivers and palaeoceanographic mechanisms of changes in the ETNP OMZ

The causes for past changes in oxygenation in the ETNP are still under debate (Ganeshram and Pedersen, 1998; Hendy and Kennett, 2003; Cartapanis et al., 2011; Ohkushi et al., 2013; Cartapanis et al., 2014; Carriquiry and Sanchez, 2014; Tetard et al., 2017). Classic explanations for OMZ fluctuations in the ETNP invoke a direct change in oxygenation of the NPIW, which travels through the Bering and Okhotsk seas (Durazo and Baumgartner, 2002; Hendy and Kennett, 2003). As this water mass moves toward the ETNP (off California and Mexico), it decreases its $O_2$ content due to microbially activated remineralization of organic matter (Cartapanis et al., 2011; Paulmier and Ruiz-Pino, 2009; Wright et al., 2012; Levin, 2018). By the time the NPIW reaches the ETNP, it is further depleted in oxygen, maintaining an expanded OMZ at intermediate depths. One of the leading causes for better oxygenation could have been reduced microbial respiration in the water column, leaving more $O_2$ in the NPIW. Another mechanism could have been enhanced mixing between similarly cold superficial waters and deeper NPIW due to a lower vertical temperature gradient (Cartapanis et al., 2011; Tetard et al., 2017). Some authors hypothesize that colder superficial ocean temperatures could enhance NPIW production, with more $O_2$-rich waters being transported to the ETNP (Cartapanis et al., 2011; Okazaki et al., 2010). Additionally, the direct and indirect climatic effects of changes in the Southern Ocean are likely also affecting the multimillennial ETNP OMZ variability (Mix et al. 1999; Hendy et al., 2004; Marchitto et al., 2007).

Primary productivity has recently been suggested as the dominant control of OMZ variability in the ETNP (Cartapanis et al., 2014; Carriquiry and Sanchez, 2014; Tetard et al., 2017). For example, proxy evidence suggests that MIS 4 had a deep NPIW and well-ventilated OMZ, similar to what has been reported for the LGM (Herguera et al., 2010; Nameroff et al., 2004; Cartapanis et al., 2011; Ohkushi et al., 2013). Due to decreased productivity in the North Pacific, the NPIW was carrying more $O_2$ along the coasts of California all the way south toward the coasts of western Baja

California and Mainland Mexico (Schmittner et al., 2007; Chang et al., 2015). Moreover, colder D/O phases (Dansgaard et al., 1984), frequently corresponding to Heinrich events, were also manifested by low productivity and high oxygen content in many ETNP OMZ records (Cartapanis et al., 2011; Ohkushi et al., 2013; Cartapanis et al., 2014; Tetard et al., 2017). On the contrary, the warm MIS 3 period would have been characterized by increased productivity, which would deplete NPIW oxygen, thus expanding the OMZ (Cartapanis et al., 2011; Cartapanis et al., 2014; Carriquiry and Sanchez, 2014; Tetard et al., 2017).

Our new data from Alfonso Basin shed important light on the controls on OMZ variability explained above. Our $O_2$ paleorecord from Alfonso Basin covaries well with OMZ variability in other locations of the ETNP (Figure 2.8). As mentioned early in the text, deoxygenation in Alfonso is not constrained by NPIW (Monreal-Gómez et al., 2001; Coria-Monter et al., 2014), as this water does not enter the basin. There must be other connections responsible for the $O_2$ variability of the basin other than changes in the NPIW. One hypothesis involves the stagnating effect of the bathymetric sill, reducing bottom $O_2$ content during the MIS 3. The existing covariation between sea level changes and redox proxies Mo, V, and C in the ETNP records off Mazatlan and off W. Baja California (Nameroff et al., 2004; Rohling et al., 2009; 2010) (Figure 2.8) could support the idea of enhanced restriction of circulation during the MIS 3. Other causes could be related to similarities in climatic and atmospheric triggers of primary productivity in both Alfonso and other basins of the ETNP that cause shifts in the upper-OMZ boundaries. Due to covariance between open OMZ records in the Eastern Pacific off Mazatlan (Ganeshram and Pedersen, 1998; Nameroff et al., 2004) and off W. Baja California (Cartapanis et al., 2011), it is reasonable to assume that the Alfonso Basin record (this study) can be confidently used to reconstruct not only local but global paleoceanographic variability.

Our research provides insights into how the OMZ of the Gulf of California responds to global submillennial and multimillennial climatic changes. Our findings from Alfonso Basin show that biologically active trace elements (Ni, Cu, Zn) are often coupled to redox indicators, confirming the importance of primary productivity for the ETNP oxygenation. However, productivity does not explain all the recorded variability, so a complex interaction between organic matter production, remineralization, and mixing of water masses is causing expansion or contraction of the ETNP OMZ.

### 2.3.7. Using MIS 3 as an analog for modern and future OMZ transition scenarios

As previously described, long-lasting climatic trends play a dominant role in controlling dissolved $O_2$ in the ocean (Levin, 2018). Models for future conditions predict that abrupt warming will impact the $O_2$ levels of the entire ocean due to changes in solubility and warming-induced stratification (Stramma et al., 2010; Praetorius et al., 2015; Long et al., 2016). Several events of OMZ variability over the past 70 kyr could serve as analogs for recent human-induced climate change. Here, we discuss one of the possible analogs of climate-related OMZ expansion preserved in the ETNP records: the MIS 4 – MIS 3 transition. The climatic and oceanographic transition from the MIS 4 stadial to the unfinished termination of MIS 3 involved a global sea surface temperature change of approximately 0.5°C towards warmer climates and an increase in 25 ppmv $CO_2$ (Luthi et al., 2008; Shakun et al., 2015). The change from MIS 4 to MIS 3 was accompanied by a global sea level rise of at least 50 m (Rohling et al., 2009, 2010) (Figure 2.8). The $O_2$ decrease during the transition was estimated to roughly be 1.5 ml/l (Tetard et al., 2017); however, precise estimates remain elusive due to uncertainties in proxy reconstruction and interpretation. In Alfonso Basin, this transition is responsible for a relative change of 65% in Cd, 59% in Mn, 85% in Mo, and 52% in V, calculated from the maximum range of the past 70 kyr (Choumiline et al., 2017; in prep).

When comparing MIS 3 to the pre-industrial recent times, we see a clear difference: the pre-industrial Holocene is more oxygenated than MIS 3, reflected in overall higher Mo concentrations compared to V (Figure 2.9). This is a trend seen not only in Alfonso Basin but also in many other ETNP regions (Nameroff et al., 2004; Cartapanis et al., 2001, 2004; Tetard et al., 2017).

Shorter climatic events can also serve as good examples of rapid re-oxygenation and de-oxygenation. Each Heinrich (cold D/O) event represented a shutdown in productivity that was followed by warming episodes with quick recoveries of both productivity and redox. During MIS 3, the amplitude of OMZ change during D/O cycles was the highest of the last 70 kyr (this study; Cartapanis et al., 2011, 2014; Nameroff et al., 2014). The relative changes during the recoveries from Heinrich events were up to 33% in Cd, 35% in Mn, 64% in Mo, and 29%in V, compared to the entire range of data for the period from 0 to 70 kyr (our data; Choumiline et al., 2017; in prep).

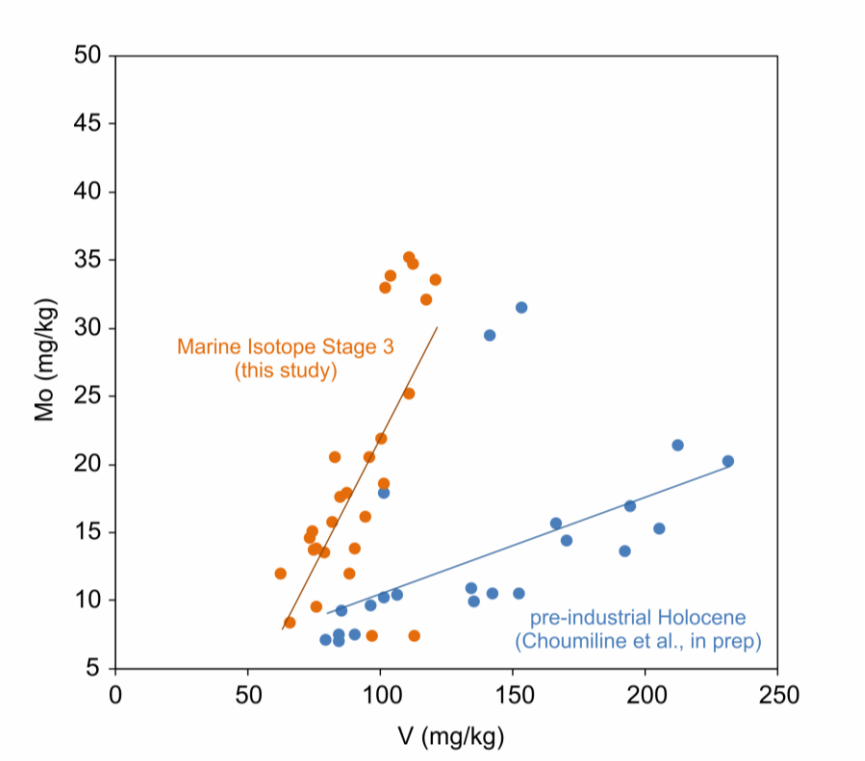


**Figure 2.9.** Comparison of V-Mo relationships for Marine Isotope Stage 3 with pre-industrial Holocene (Data: Choumiline et al., 2017; Choumiline et al., in prep).

## 2.4. CONCLUSIONS

Marine Isotope Stage 3 was distinctive in the Eastern Tropical North Pacific for being a period with strong marine productivity evidenced by high values of $C_{org}$, $CaCO_3$, Cu, Ni, Zn, along with enhanced anoxia demonstrated by high enrichments of Cd, Mn, Mo, and V.

Regardless of the climatic triggers of cold phases of Dansgaard-Oeschger oscillations often manifested as Heinrich events, both the shallow and deep sediment core records of the Eastern Tropical North Pacific Oxygen Minimum Zone indicate increased ventilation and decreased productivity. Such variability could be explained by decreased marine productivity and global changes in water mass circulation that would manifest in low $O_2$ in the Eastern Pacific.

Peak Oxygen Minimum Zone expansion was reached between 60 and 45 cal kyr BP, corresponding to the onset of the Marine Isotope Stage 3, not only suggesting widespread anoxia but potentially even sulfidic conditions in marine basins of the Eastern Tropical North Pacific either in the pore waters or in overlying seawater.

During MIS 3, the water column of the ETNP OMZ reached oxygen levels potentially lower than those of the pre-industrial Holocene. Rapid submillennial events often reoxygenated the otherwise oxygen-deficient waters of the ETNP. Such transient periods of brief deoxygenation and reoxygenation provide a useful framework for post-industrial and future redox predictions.

Our spatiotemporal reconstruction shows that the geographic extent of deoxygenation during the MIS3 encompassed the Gulf of California (Alfonso, La Paz, and Guaymas Basin) but also the Pacific margin off Mazatlan and Baja California (Soledad Basin), as well as California (Santa Barbara Basin) and western Canadian margins. This distribution highlights that global climatic and circulation patterns are the most important controlling factors of the availability of oxygen in the ETNP.

## 2.5. ACKNOWLEDGMENTS

The authors acknowledge the UC MEXUS - CONACYT Collaborative Research Grant "High resolution geochemical reconstructions of recent climate and oxygenation history in La Paz Bay, Gulf of California" for providing funds to cover travel and analytical costs. The authors express gratitude to the scientific team of IMAGES VIII / MD126 MONA expedition and the crew members of Marion Dufresne. K.C is grateful for the UC MEXUS – CONACYT Doctoral Fellowship that sponsored his graduate studies and for the 2016 UC MEXUS Dissertation Grant award for analytical expenses. Partial support was provided to T.L., K.C., and S.B. by the NASA Astrobiology Institute.

## 2.6. REFERENCES


Agosta, E.A., and Compagnucci, R.H. (2016). Abrupt Climate Changes During the Marine Isotope Stage 3 (MIS 3). 81-106.

Anderson, R.F., and Winckler, G. (2005). Problems with paleoproductivity proxies. Paleoceanography 20, PA3012.

Baturin, G.N., Murdmaa, I.O., Beaufort, L., and Alekhina, G.N. (2016). Comparative geochemistry of Quaternary carbonaceous sediments from the continental slope of the Baja California and the Miocene Monterey Formation. Lithology and Mineral Resources 51, 93-106.

Beaufort, L., et al. (2002), Cruise report MD126 MONA (Marges Ouest Nord Américaines) – IMAGESVIII, 452 pp., Inst. Polaire Fr. Paul-Emile Victor, Plouzaneé, France.

Bianchi, T.S., Schreiner, K.M., Smith, R.W., Burdige, D.J., Woodard, S., and Conley, D.J. (2016). Redox effects on organic matter storage in coastal sediments during the Holocene: a biomarker/proxy perspective. Annual Review of Earth and Planetary Sciences 44, 295-319.

Bond, G., Broecker, W., Johnsen, S., McManus, J., Labeyrie, L., Jouzel, J., and Bonani, G. (1993). Correlations between climate records from North Atlantic sediments and Greenland ice. Nature 365, 143-147.

Bond, G., Heinrich, H., Broecker, W., Labeyrie, L., McManus, J., Andrews, J., Huon, S., Jantschik, R., Clasen, S., Simet, C., Tedesco, K., Klas, M., Bonani, G., and Ivy, S. (1992). Evidence for massive discharges of icebergs into the North Atlantic ocean during the last glacial period. Nature 360, 245-249.

Böning, P., Shaw, T., Pahnke, K., and Brumsack, H.-J. (2015). Nickel as indicator of fresh organic matter in upwelling sediments. Geochimica et Cosmochimica Acta 162, 99-108.

Boyle, E.A. (1981). Cadmium, zinc, copper and barium in foraminifera tests. Earth and Planetary Science Letters 53, 11-35.

Breitburg, D., Levin, L.A., Oschlies, A., Grégoire, M., Chavez, F.P., Conley, D.J., Garçon, V., Gilbert, D., Gutiérrez, D., Isensee, K., Jacinto, G.S., Limburg, K.E., Montes, I., Naqvi, S.W.A., Pitcher, G.C., Rabalais, N.N., Roman, M.R., Rose, K.A., Seibel, B.A., Telszewski, M., Yasuhara, M., and Zhang, J. (2018). Declining oxygen in the global ocean and coastal waters. Science 359.

Calvert, S.E., and Pedersen, T.F. (1993). Geochemistry of Recent oxic and anoxic marine sediments: Implications for the geological record. Marine Geology 113, 67-88.

Cardich, J., Sifeddine, A., Salvatteci, R., Romero, D., Briceño-Zuluaga, F., Graco, M., Anculle, T., Almeida, C., and Gutiérrez, D. (2019). Multidecadal Changes in Marine Subsurface Oxygenation Off Central Peru During the Last ca. 170 Years. Frontiers in Marine Science 6.

Carriquiry, J.D., and Sanchez, A. (2014). "Productivity changes in the Magdalena margin, Mexico Baja California peninsula during the past 50,000 years," in Synthesis Series: Environmental Status of The Ecosystems of Northwestern Mexico, eds. E.V. Wehncke, J.R. Lara-Lara, S. Alvarez-Borrego & E. Ezcurra. (Mexico City: UC-MEXUS, SEMARNAT and INECC).

Cartapanis, O., Bianchi, D., Jaccard, S.L., and Galbraith, E.D. (2016). Global pulses of organic carbon burial in deep-sea sediments during glacial maxima. Nature Communications 7, 10796.

Cartapanis, O., Tachikawa, K., and Bard, E. (2011). Northeastern Pacific oxygen minimum zone variability over the past 70 kyr: Impact of biological production and oceanic ventilation. Paleoceanography 26.

Cartapanis, O., Tachikawa, K., and Bard, E. (2012). Latitudinal variations in intermediate depth ventilation and biological production over northeastern Pacific Oxygen Minimum Zones during the last 60 ka. Quaternary Science Reviews 53, 24-38.

Cartapanis, O., Tachikawa, K., Romero, O.E., and Bard, E. (2014). Persistent millennial-scale link between Greenland climate and northern Pacific Oxygen Minimum Zone under interglacial conditions. Climate of the Past 10, 405-418.

Chang, A.S., Pedersen, T.F., and Hendy, I.L. (2014). Effects of productivity, glaciation, and ventilation on late Quaternary sedimentary redox and trace element accumulation on the Vancouver Island margin, western Canada. Paleoceanography 29, 730-746.

Chang, A.S., Pichevin, L., Pedersen, T.F., Gray, V., and Ganeshram, R. (2015). New insights into productivity and redox-controlled trace element (Ag, Cd, Re, and Mo) accumulation in a 55 kyr long sediment record from Guaymas Basin, Gulf of California. Paleoceanography 30, 77-94.

Chavez, F.P., Messié, M., and Pennington, J.T. (2011). Marine primary production in relation to climate variability and change. Ann Rev Mar Sci 3, 227-260.

Choumiline, K. (2011). Geoquímica de la materia particulada en hundimiento y de los sedimentos recientes de Cuenca Alfonso, Bahía de La Paz. Master's Thesis, Centro Interdisciplinario de Ciencias Marinas - Instituto Politécnico Nacional.

Choumiline, K., Lyons, T. W., Pérez-Cruz, L., Carriquiry, J. D., Raiswell, R., and Beaufort, L. (2017). “Sensitivity of redox proxies to rapid variability in Oxygen Minimum Zones. Goldschmidt 2017,” in Abstract Retrieved from Goldschmidt Conference Archive (Paris).

Choumiline, K., Pérez-Cruz, L., Gray, A.B., Bates, S.M., and Lyons, T.W. (2019). Scenarios of Deoxygenation of the Eastern Tropical North Pacific During the Past Millennium as a Window Into the Future of Oxygen Minimum Zones. Frontiers in Earth Science 7.

Choumiline, K., Rodríguez-Castañeda, A.P., Silverberg, N., Aguirre-Bahena, F., Sapozhnikov, D., and Pérez-Cruz, L. (2010). "Arsenic and uranium in the settling particulate matter and sediments of Alfonso Basin, La Paz Bay", in: Proceedings of the 13th International Conference on Water-Rock Interaction. (Guanajuato).

Coria-Monter, E., Monreal-Gómez, M.A., Salas-De-León, D.A., Aldeco-Ramírez, J., and Merino-Ibarra, M. (2014). Differential distribution of diatoms and dinoflagellates in a cyclonic eddy confined in the Bay of La Paz, Gulf of California. Journal of Geophysical Research: Oceans 119, 6258-6268.

Dalton, A.S., Finkelstein, S.A., Forman, S.L., Barnett, P.J., Pico, T., and Mitrovica, J.X. (2019). Was the Laurentide Ice Sheet significantly reduced during Marine Isotope Stage 3? Geology 47, 111-114.

Dansgaard, W., Johnsen, S.J., Clausen, H.B., Dahl-Jensen, D., Gundestrup, N., Hammer, C.U., and Oeschger, H. (1984). North Atlantic climatic oscillations revealed by deep Greenland ice cores. 29, 288-298.

Dean, W.E., Zheng, Y., Ortiz, J.D., and van Geen, A. (2006). Sediment Cd and Mo accumulation in the oxygen-minimum zone off western Baja California linked to global climate over the past 52 kyr. Paleoceanography 21.

Defforey, D., and Paytan, A. (2018). Phosphorus cycling in marine sediments: Advances and challenges. Chemical Geology 477, 1-11.

Durazo, R., and Baumgartner, T.R. (2002). Evolution of oceanographic conditions off Baja California: 1997–1999. Progress in Oceanography 54, 7-31.

Dymond, J., Suess, E., and Lyle, M. (1992). Barium in deep-sea sediment. A geochemical proxy for paleoproductivity. Paleoceanography 7, 163-181.

Eagle, M., Paytan, A., Arrigo, K.R., Van Dijken, G., and Murray, R.W. (2003). A comparison between excess barium and barite as indicators of carbon export. Paleoceanography 18, 1021.
Emerson, S.R., and Huested, S.S. (1991). Ocean anoxia and the concentrations of molybdenum and vanadium in seawater. Marine Chemistry 34, 177-196.

Ganeshram, R.S., and Pedersen, T.F. (1998). Glacial-interglacial variability in upwelling and bioproductivity off NW Mexico: Implications for Quaternary paleoclimate. Paleoceanography 13, 634-645.

Garcia, H. E., Locarnini, R. A., Boyer, T. P., and Antonov, J. I. (2006).World Ocean Atlas 2005, Volume 3: Dissolved Oxygen, Apparent Oxygen Utilization, and Oxygen Saturation. S. Levitus, Ed. NOAA Atlas NESDIS 63, U.S. Government Printing Office,Washington, D.C., 342 pp.

Gilly, W.F., Beman, J.M., Litvin, S.Y., and Robison, B.H. (2013). Oceanographic and biological effects of shoaling of the oxygen minimum zone. Ann Rev Mar Sci 5, 393-420.

Gonzalez-Yajimovich, O.E., Gorsline, D.S., and Douglas, R.G. (2007). Frequency and sources of basin floor turbidites in Alfonso Basin, Gulf of California, Mexico: Products of slope failures. Sedimentary Geology 199, 91-105.

Grant, K.M., Rohling, E.J., Bar-Matthews, M., Ayalon, A., Medina-Elizalde, M., Ramsey, C.B., Satow, C., and Roberts, A.P. (2012). Rapid coupling between ice volume and polar temperature over the past 150,000 years. Nature 491, 744-747.

Hardisty, D.S., Lyons, T.W., Riedinger, N., Isson, T.T., Owens, J.D., Aller, R.C., Rye, D.M., Planavsky, N.J., Reinhard, C.T., Gill, B.C., Masterson, A.L., Asael, D., and Johnston, D.T. (2018). An evaluation of sedimentary molybdenum and iron as proxies for pore fluid paleoredox conditions. American Journal of Science 318, 527-556.

Hemming, S.R. (2004). Heinrich events: Massive late Pleistocene detritus layers of the North Atlantic and their global climate imprint. Reviews of Geophysics 42.

Hendy, I.L., and Kennett, J.P. (2003). Tropical forcing of North Pacific intermediate water distribution during Late Quaternary rapid climate change? Quaternary Science Reviews 22, 673-689.

Hendy, I.L., and Pedersen, T.F. (2006). Oxygen minimum zone expansion in the eastern tropical North Pacific during deglaciation. Geophysical Research Letters 33, L20602.

Hendy, I.L., Pedersen, T.F., Kennett, J.P., and Tada, R. (2004). Intermittent existence of a southern Californian upwelling cell during submillennial climate change of the last 60 kyr. Paleoceanography 19.

Henry, L.G., McManus, J.F., Curry, W.B., Roberts, N.L., Piotrowski, A.M., and Keigwin, L.D. (2016). North Atlantic ocean circulation and abrupt climate change during the last glaciation. Science 353, 470-474.

Herbert, T.D., Schuffert, J.D., Andreasen, D., Heusser, L., Lyle, M., Mix, A., Ravelo, A.C., Stott, L.D., and Herguera, J.C. (2001). Collapse of the California Current during glacial maxima linked to climate change on land. Science 293, 71-76.

Herguera, J.C., Herbert, T., Kashgarian, M., and Charles, C. (2010). Intermediate and deep water mass distribution in the Pacific during the Last Glacial Maximum inferred from oxygen and carbon stable isotopes. Quaternary Science Reviews 29, 1228-1245.

Ivanochko, T. (2001). Productivity influences on oxygenation of the Santa Barbara Basin, California, during the late quaternary. Master's Thesis, The University of British Columbia.

Ivanochko, T.S., and Pedersen, T.F. (2004). Determining the influences of Late Quaternary ventilation and productivity variations on Santa Barbara Basin sedimentary oxygenation: a multi-proxy approach. Quaternary Science Reviews 23, 467-480.

Jaccard, S., Galbraith, E., Frölicher, T., and Gruber, N. (2014). Ocean (De)oxygenation Across the Last Deglaciation: Insights for the Future. Oceanography 27, 26-35.

Jaccard, S.L., and Galbraith, E.D. (2011). Large climate-driven changes of oceanic oxygen concentrations during the last deglaciation. Nature Geoscience 5, 151-156.

Keeling, R.E., Kortzinger, A., and Gruber, N. (2010). Ocean deoxygenation in a warming world. Ann Rev Mar Sci 2, 199-229.

Lavín, M.F., and Marinone, S.G. (2003). An overview of the physical oceanography of the gulf of California. Nonlinear Processes in Geophysical Fluid Dynamics, 173-204.

Lavín, M.F., Castro, R., Beier, E., and Godínez, V.M. (2013). Mesoscale eddies in the southern Gulf of California during summer: Characteristics and interaction with the wind stress. Journal of Geophysical Research: Oceans 118, 1367-1381.

Levin, L.A. (2018). Manifestation, Drivers, and Emergence of Open Ocean Deoxygenation. Annual Review of Marine Science.

Lisiecki, L.E., and Raymo, M.E. (2005). A Pliocene-Pleistocene stack of 57 globally distributed benthic δ18O records. Paleoceanography 20.

Long, M.C., Deutsch, C., and Ito, T. (2016). Finding forced trends in oceanic oxygen. Global Biogeochemical Cycles 30, 381-397.

Luthi, D., Le Floch, M., Bereiter, B., Blunier, T., Barnola, J.M., Siegenthaler, U., Raynaud, D., Jouzel, J., Fischer, H., Kawamura, K., and Stocker, T.F. (2008). High-resolution carbon dioxide concentration record 650,000-800,000 years before present. Nature 453, 379-382.

Marchitto, T.M. (2007). PALEOCEANOGRAPHY, PHYSICAL AND CHEMICAL PROXIES | Nutrient Proxies. Encyclopedia of Quaternary Science, 1732-1740.

Marchitto, T.M., Lehman, S.J., Ortiz, J.D., Fluckiger, J., and van Geen, A. (2007). Marine radiocarbon evidence for the mechanism of deglacial atmospheric CO2 rise. Science 316, 1456-1459.

McLennan, S.M. (2001). Relationships between the trace element composition of sedimentary rocks and upper continental crust. Geochemistry, Geophysics, Geosystems 2.

McManus, J., Berelson, W.M., Klinkhammer, G.P., Johnson, K.S., Coale, K.H., Anderson, R.F., Kumar, N., Burdige, D.J., Hammond, D.E., Brumsack, H.J., Mccorkle, D.C., and Rushdi, A. (1998). Geochemistry of barium in marine sediments: implications for its use as a paleoproxy. Geochimica et Cosmochimica Acta 62, 3453-3473.

Mix, A.C., Lund, D.C., Pisias, N.G., Bodén, P., Bornmalm, L., Lyle, M., and Pike, J. (1999). Rapid climate oscillations in the Northeast Pacific during the last deglaciation reflect Northern and Southern Hemisphere sources. 112, 127-148.

Moffitt, S.E., Hill, T.M., Ohkushi, K., Kennett, J.P., and Behl, R.J. (2014). Vertical oxygen minimum zone oscillations since 20 ka in Santa Barbara Basin: A benthic foraminiferal community perspective. Paleoceanography 29, 44-57.

Moffitt, S.E., Moffitt, R.A., Sauthoff, W., Davis, C.W., Hewett, K., and Hill, T.M. (2015). Paleoceanographic Insights on Recent Oxygen Minimum Zone Expansion: Lessons for Modern Oceanography. PLOS ONE.

Monreal-Gómez, M.A., Molina-Cruz, A., and Salas-De-León, D.A. (2001). Water masses and cyclonic circulation in Bay of La Paz, Gulf of California, during June 1998. Journal of Marine Systems 30, 305-315.

Morford, J.L., and Emerson, S. (1999). The geochemistry of redox sensitive trace metals in sediments. Geochimica et Cosmochimica Acta 63, 1735-1750.

Nameroff, T.J., Calvert, S.E., and Murray, J.W. (2004). Glacial-interglacial variability in the eastern tropical North Pacific oxygen minimum zone recorded by redox-sensitive trace metals. Paleoceanography 19, PA1010.

Nava-Sánchez, E.H., Gorsline, D.S., and Molina-Cruz, A. (2001). The Baja California peninsula borderland: structural and sedimentological characteristics. Sedimentary Geology 144, 63-82.

Ohkushi, K., Kennett, J.P., Zeleski, C.M., Moffitt, S.E., Hill, T.M., Robert, C., Beaufort, L., and Behl, R.J. (2013). Quantified intermediate water oxygenation history of the NE Pacific: A new benthic foraminiferal record from Santa Barbara basin. Paleoceanography 28, 453-467.

Okazaki, Y., Timmermann, A., Menviel, L., Harada, N., Abe-Ouchi, A., Chikamoto, M.O., Mouchet, A., and Asahi, H. (2010). Deepwater formation in the North Pacific during the Last Glacial Termination. Science 329, 200-204.

Oschlies, A., Brandt, P., Stramma, L., and Schmidtko, S. (2018). Drivers and mechanisms of ocean deoxygenation. Nature Geoscience 11, 467-473.

Paulmier, A., and Ruiz-Pino, D. (2009). Oxygen minimum zones (OMZs) in the modern ocean. Progress in Oceanography 80, 113-128.

Paytan, A., Kastner, M., Martin, E.E., Macdougall, J.D., and Herbert, T. (1993). Marine barite as a monitor of seawater strontium isotope composition. Nature 366, 445-449.

Pérez-Cruz, L. (2000). Estudio paleoceanográfico y sedimentológico holocénico de la Bahía de La Paz, Golfo de California. Ph.D. Thesis, Universidad Nacional Autónoma de México.

Pérez-Cruz, L. (2013). Hydrological changes and paleoproductivity in the Gulf of California during middle and late Holocene and their relationship with ITCZ and North American Monsoon variability. Quaternary Research 79, 138-151.

Pico, T., Creveling, J.R., and Mitrovica, J.X. (2017). Sea-level records from the U.S. mid-Atlantic constrain Laurentide Ice Sheet extent during Marine Isotope Stage 3. Nature Communications 8, 15612.

Praetorius, S.K., Mix, A.C., Walczak, M.H., Wolhowe, M.D., Addison, J.A., and Prahl, F.G. (2015). North Pacific deglacial hypoxic events linked to abrupt ocean warming. Nature 527, 362-366.

Reimer, P.J., Bard, E., Bayliss, A., Beck, J.W., Blackwell, P.G., Ramsey, C.B., Buck, C.E., Cheng, H., Edwards, R.L., Friedrich, M., Grootes, P.M., Guilderson, T.P., Haflidason, H., Hajdas, I., Hatté, C., Heaton, T.J., Hoffmann, D.L., Hogg, A.G., Hughen, K.A., Kaiser, K.F., Kromer, B., Manning, S.W., Niu, M., Reimer, R.W., Richards, D.A., Scott, E.M., Southon, J.R., Staff, R.A., Turney, C.S.M., and Van Der Plicht, J. (2013). IntCal13 and Marine13 Radiocarbon Age Calibration Curves 0–50,000 Years cal BP. Radiocarbon 55, 1869-1887.

Riedinger, N., Kasten, S., Gröger, J., Franke, C., and Pfeifer, K. (2006). Active and buried authigenic barite fronts in sediments from the Eastern Cape Basin. Earth and Planetary Science Letters 241, 876-887.

Rohling, E.J., Braun, K., Grant, K., Kucera, M., Roberts, A.P., Siddall, M., and Trommer, G. (2010). Comparison between Holocene and Marine Isotope Stage-11 sea-level histories. Earth and Planetary Science Letters 291, 97-105.

Rohling, E.J., Grant, K., Bolshaw, M., Roberts, A.P., Siddall, M., Hemleben, C., and Kucera, M. (2009). Antarctic temperature and global sea level closely coupled over the past five glacial cycles. Nature Geoscience 2, 500-504.

Schmidt, M.W., and Hertzberg, J.E. (2011) Abrupt Climate Change During the Last Ice Age. Nature Education Knowledge 3, 11

Schmittner, A., Galbraith, E.D., Hostetler, S.W., Pedersen, T.F., and Zhang, R. (2007). Large fluctuations of dissolved oxygen in the Indian and Pacific oceans during Dansgaard-Oeschger oscillations caused by variations of North Atlantic Deep Water subduction. Paleoceanography 22.

Schoepfer, S.D., Shen, J., Wei, H., Tyson, R.V., Ingall, E., and Algeo, T.J. (2015). Total organic carbon, organic phosphorus, and biogenic barium fluxes as proxies for paleomarine productivity. Earth-Science Reviews 149, 23-52.

Scholz, F. (2018). Identifying oxygen minimum zone-type biogeochemical cycling in Earth history using inorganic geochemical proxies. Earth-Science Reviews 184, 29-45.

Scholz, F., Hensen, C., Noffke, A., Rohde, A., Liebetrau, V., and Wallmann, K. (2011). Early diagenesis of redox-sensitive trace metals in the Peru upwelling area – response to ENSO-related oxygen fluctuations in the water column. Geochimica et Cosmochimica Acta 75, 7257-7276.

Scholz, F., Siebert, C., Dale, A.W., and Frank, M. (2017). Intense molybdenum accumulation in sediments underneath a nitrogenous water column and implications for the reconstruction of paleo-redox conditions based on molybdenum isotopes. Geochimica et Cosmochimica Acta 213, 400-417.

Scott, C., and Lyons, T.W. (2012). Contrasting molybdenum cycling and isotopic properties in euxinic versus non-euxinic sediments and sedimentary rocks: Refining the paleoproxies. Chemical Geology 324-325, 19-27.

Shakun, J.D., Lea, D.W., Lisiecki, L.E., and Raymo, M.E. (2015). An 800-kyr record of global surface ocean $\delta^{18}O$ and implications for ice volume-temperature coupling. Earth and Planetary Science Letters 426, 58-68.

Silverberg, N., Aguirre-Bahena, F., and Mucci, A. (2014). Time-series measurements of settling particulate matter in Alfonso Basin, La Paz Bay, southwestern Gulf of California. Continental Shelf Research 84, 169-187.

Staines-Urías, F., González-Yajimovich, O., and Beaufort, L. (2015). Reconstruction of past climate variability and ENSO-like fluctuations in the southern Gulf of California (Alfonso Basin) since the last glacial maximum. Quaternary Research 83, 488-501.

Stramma, L., Johnson, G.C., Sprintall, J., and Mohrholz, V. (2008). Expanding oxygen-minimum zones in the tropical oceans. Science 320, 655-658.

Stramma, L., Schmidtko, S., Levin, L.A., and Johnson, G.C. (2010). Ocean oxygen minima expansions and their biological impacts. Deep Sea Research Part I: Oceanographic Research Papers 57, 587-595.

Stuiver, M., Reimer, P.J., and Reimer, R.W. (2019). CALIB 7.1 [WWW program] at http://calib.org, accessed 2019-11-18

Svensson, A., Andersen, K.K., Bigler, M., Clausen, H.B., Dahl-Jensen, D., Davies, S.M., Johnsen, S.J., Muscheler, R., Parrenin, F., Rasmussen, S.O., Röthlisberger, R., Seierstad, I., Steffensen, J.P., and Vinther, B.M. (2008). A 60 000 year Greenland stratigraphic ice core chronology. Climate of the Past 4, 47-57.

Tems, C.E., Berelson, W.M., Thunell, R., Tappa, E., Xu, X., Khider, D., Lund, S., González-Yajimovich, O., and Hamann, Y. (2016). Decadal to centennial fluctuations in the intensity of the eastern tropical North Pacific oxygen minimum zone during the last 1200 years. Paleoceanography 31, 1138-1151.

Tetard, M., Licari, L., and Beaufort, L. (2017). Oxygen history off Baja California over the last 80 kyr: A new foraminiferal-based record. Paleoceanography.

Tribovillard, N., Algeo, T.J., Lyons, T., and Riboulleau, A. (2006). Trace metals as paleoredox and paleoproductivity proxies: An update. Chemical Geology 232, 12-32.

van Geen, A., Zheng, Y., Bernhard, J.M., Cannariato, K.G., Carriquiry, J., Dean, W.E., Eakins, B.W., Ortiz, J.D., and Pike, J. (2003). On the preservation of laminated sediments along the western margin of North America. Paleoceanography 18.

Van Meerbeeck, C.J., Renssen, H., and Roche, D.M. (2009). How did Marine Isotope Stage 3 and Last Glacial Maximum climates differ? – Perspectives from equilibrium simulations. Climate of the Past 5, 33-51.

Wedepohl, K.H. (1995). The composition of the continental crust. Geochimica et Cosmochimica Acta 59, 1217-1232.

World Ocean Atlas (2005). http://www.nodc.noaa.gov/OC5/WOA05/pr_woa05.html

Wright, J.J., Konwar, K.M., and Hallam, S.J. (2012). Microbial ecology of expanding oxygen minimum zones. Nature Reviews Microbiology 10, 381-394.
Wyrtki, K. (1966). Oceanography of the eastern equatorial Pacific Ocean. Oceanogr. Mar. Biol. Ann. Rev. 33, 33-68.

Yarincik, K.M., Murray, R.W., Lyons, T.W., Peterson, L.C., and Haug, G.H. (2000). Oxygenation history of bottom waters in the Cariaco Basin, Venezuela, over the past 578,000 years: Results from redox-sensitive metals (Mo, V, Mn, and Fe). Paleoceanography 15, 593-604.

Zheng, Y., Anderson, R.F., van Geen, A., and Kuwabara, J. (2000). Authigenic molybdenum formation in marine sediments: a link to pore water sulfide in the Santa Barbara Basin. Geochimica et Cosmochimica Acta 64, 4165-4178.

## 2.7. SUPPLEMENTARY MATERIALS

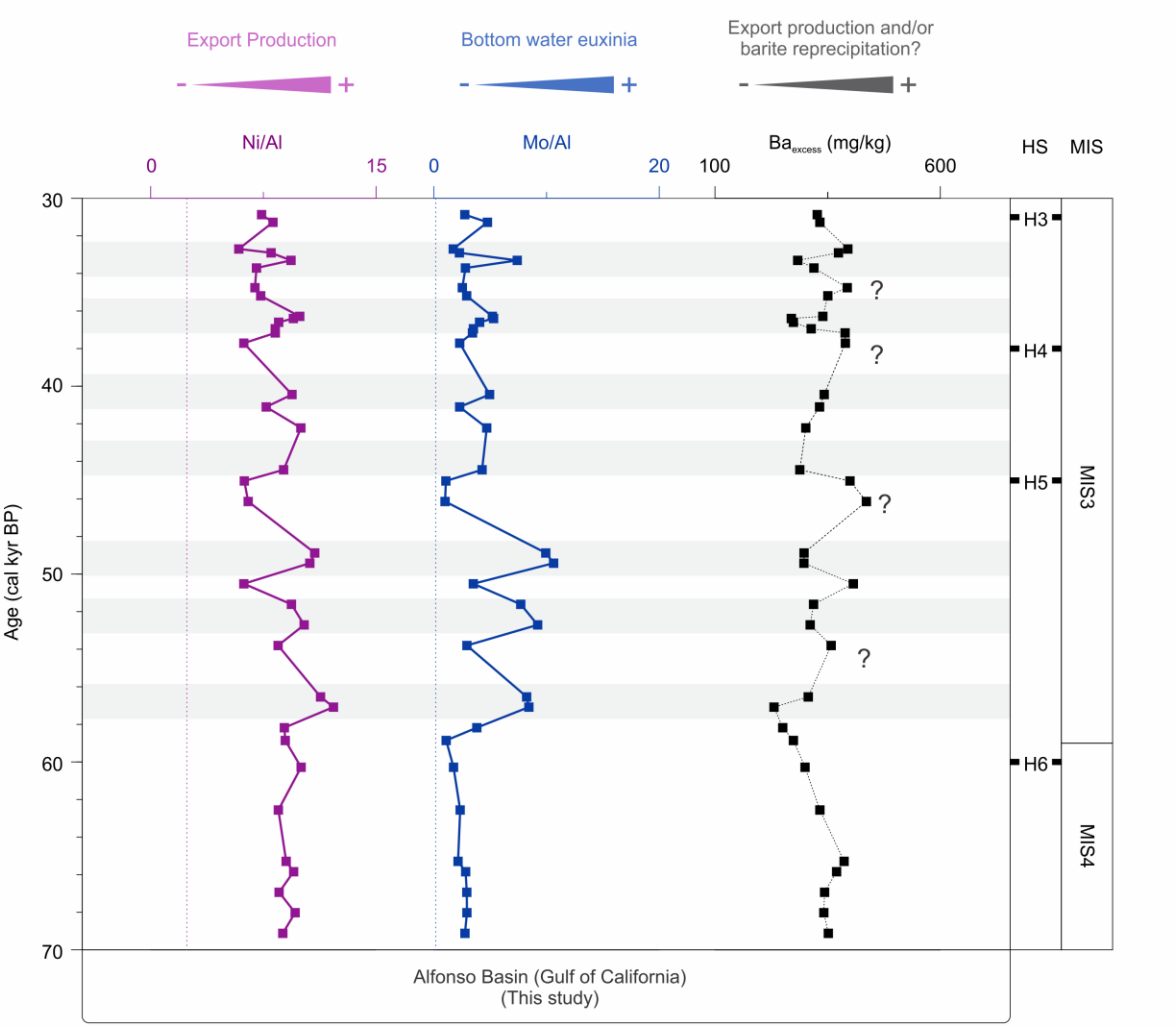


**Supplementary Figure 2.1.** Comparison of productivity (Ni/Al) and redox (Mo/Al) to evaluate the usability of $Ba_{excess}$ in core MD02-2510 from Alfonso Basin, Gulf of California during the 30-70 cal kyr BP period. Periods of enhanced productivity established with more reliable geochemical proxies are highlighted as grey horizontal bars. The approximate timing of Heinrich events (Hemming, 2004) and the hypothetical boundaries between Marine Isotope Stages (Lisiecki and Raymo, 2005) are presented in the figure for reference only.

# CHAPTER 3:

# MECHANISMS FOR AUTHIGENIC URANIUM ENRICHMENTS AND RELATED ISOTOPIC FRACTIONATION WITHIN MARINE SNOW AGGREGATES OF MODERN OXYGEN MINIMUM ZONES

**ABSTRACT**

Our ability to reconstruct past marine oxygenation relies on authigenic enrichment of redox-sensitive elements like uranium (U). While most of the authigenic U ($U_{auth}$) is formed diagenetically, some authigenesis can occur within marine snow aggregates in highly productive regions of the ocean. Here we discuss the first U isotope sediment trap data from the Eastern Tropical North Pacific Oxygen Minimum Zone (Alfonso Basin, Gulf of California). Our goals were to quantify the authigenic and detrital components of the total U in sinking particles while deciphering the processes that cause $U_{auth}$ enrichments and changes in $\delta^{238}U$.

Our data show that the $\delta^{234}U$ composition of the settling particulate matter is highly variable (-7 to 98 ‰) and strongly event dependent. Assuming that $\delta^{234}U$ values reflect a mixture of $U_{auth}$ (seawater 146 ‰) and detrital U (-10 ‰), we use a two-component mixing model to demonstrate that the authigenic fraction of most samples ranges roughly from 30 to 70 %, although storm-related events sometimes produce settling particles with extremely low $\delta^{234}U$ and almost no $U_{auth}$. These outliers are fully dominated by detrital inputs and can produce significant total U increases, despite very low $U_{auth}$.

The $\delta^{238}U$ signature varies from -0.49 to 0.16 ‰, often strongly deviating from the seawater value of -0.39 ‰. Shifts toward high $\delta^{238}U$ are generally linked to the microbially mediated reduction of U(+6) to U(+4). Some samples show evidence for such a process reaching $\delta^{238}U$ values as high as -0.06 ‰ with only moderate elevation of $U_{auth}$ (2.13 mg/kg). We attribute the highest observed $U_{auth}$ enrichment (7.34 mg/kg) to adsorption to organic matter, which is high in the sample (7.65 % $C_{org}$), with no significant $\delta^{238}U$ fractionation (-0.32 ‰).

Our paired $\delta^{234}U$ and $\delta^{238}U$ results allow us to unmix the contribution of U via sinking particles. We conclude that the U sources in marine coastal settings, like Alfonso Basin, represent a mixture between detrital and authigenic components. The detrital components are mostly coming

from relatively constant dust supply and sporadic fluvial events. The authigenic U scavenged in the water column is potentially stimulated by redox conditions caused by microbial niche partitioning in marine snow aggregates. Other processes that are less likely influencing the U composition and isotopic signatures of settling particles from Alfonso Basin are resuspension, turbidity flow, and human-induced transport from mining activities when U-rich rocks are present.

## 3.1. INTRODUCTION

Uranium is used commonly as a tracer of past conditions in the ocean because its cycling is tightly coupled to changes in oxygen levels (Anderson, 1987; Wignall and Myers, 1988; Anderson et al. 1989; Klinkhammer and Palmer, 1991; Calvert and Pedersen, 1993). Indeed, patterns of U concentrations reveal trends of oxygenation in the ocean over billions of years of Earth's history as a backdrop for the evolution of the earliest life on our planet (Partin et al., 2013; Lyons et al., 2014; Lau et al., 2019). From previous work on marine geochemistry of U, we know that most of the dissolved U(+6) is present in seawater as uranyl carbonate complexes $(UO_2)^{2+}$ (typically as uranyl tricarbonates $[UO_2(CO_3)_3]^{4-}$) that are reduced under anoxic conditions to the insoluble U(+4) form by inorganic and microbially mediated processes (Ku et al., 1977; Anderson, 1987; Klinkhammer and Palmer, 1991; McKee et al, 1993; Dunk et al., 2002)—resulting in formation of solid particles. An essential mechanism of particle formation is through adsorption/desorption and organic complexation (Klinkhammer and Palmer, 1991; Cumberland et al., 2016). It is worth noting that dissolved U(+6) does not disappear entirely but rather coexists with U(+4) in different proportions, even under anoxic conditions. While this reduction and the associated increase in particulate U are thought to mostly happen diagenetically in porewaters within sediments underlying strongly anoxic and sulfidic (euxinic) waters (Klinkhammer and Palmer, 1991), some particulate non-lithogenic U can form very slowly in the water column (Zheng et al., 2002). The extent to which non-lithogenic (authigenic) U can be enriched in marine particles is not yet well established and could be more common in highly productive oxygen-deficient settings than previously thought (Choumiline et al., 2019). The usability of U as paleoproxy relies on its authigenic U ($U_{auth}$) enrichments, so finding a proper way to numerically quantify this fraction is of essential importance. Uranium isotopes are rapidly becoming a method that allows us to separate the non-lithogenic component from the

detrital fraction, but importantly that also provide additional environmental and mechanistic details of first-order importance.

Studies of modern and ancient marine oxygenation have only recently added U isotope relationships to the mix, providing insights on the preferential involvement of either the lighter $^{235}U$ or the heavier $^{238}U$ isotope in abiotic, biotic, and redox processes (Noordmann et al., 2015; Stirling et al., 2015; Stylo et al., 2015a,b; Holmden et al., 2015; Andersen et al., 2015; Lau et al., 2019). Uranium has no stable isotopes, but we can explore its properties using the delta (δ) notation typically reserved for stable isotope systems due to its long-lived, quasi-stable behavior. There is no established agreement on which reference standard to use in order to calculate the $\delta^{238}U$ value, but a consensus is building around CRM-112a or (CRM-145, a solution made of CRM-112 metal). A compilation of U isotope values for various types of terrestrial material is published in Weyer et al. (2008), Tissot and Dauphas (2015), Andersen et al. (2015, 2017). The values are presented as using the standard delta nomenclature:

$$\delta^{238}U\ (‰) = \left( \frac{(^{238}U/^{235}U)_{sample}}{(^{238}U/^{235}U)_{CRM\text{-}112a}} - 1 \right) \text{ x } 10^3 ;$$

$$\delta^{234}U\ (‰) = \left( \frac{(^{234}U/^{238}U)_{sample}}{(^{234}U/^{238}U)_{sec.eq.}} - 1 \right) \text{ x } 10^3$$

Despite major advances in our understanding of the biogeochemistry and global budget of U and the individual processes that can lead to the fractionation of its isotopes, most previous research has focused on classic marine systems such as Black Sea and Cariaco Basin famous for strongly reducing bottom waters and limited connectivity to the open ocean (Andersen et al., 2014; Rolison et al., 2017). The shortage of inclusive studies focusing on the complete isotopic cycle of U isotopes ($\delta^{234}U$ and $\delta^{238}$ U) in the water column, settling matter, bottom sediments, and porewaters create

gaps in the understanding of abiotic and biotic mechanisms that can lead to isotopic fractionation favoring either light $^{235}U$ or heavy $^{238}U$ isotope. Importantly, the behavior of U isotopes in highly productive settings as Oxygen Minimum Zones (OMZs) along continental margins has not been studied in detail—despite reflecting the dominant settings of marine oxygen deficiency in past, present, and future oceans. The latter prevents this novel paleoproxy from unleashing its full potential as an indicator of redox and productivity.

### 3.1.1. Processes that control the $\delta^{234}U$ composition of sedimentary material

Modern $\delta^{234}U$ values for seawater are known to be ~146 ‰ (Andersen et al., 2010). Authigenically formed U would typically have a very similar $\delta^{234}U$ signature. The older the material, the lower the $\delta^{234}U$ value. The $\delta^{234}U$ composition is often compared to known records of seawater $^{234}U/^{238}U$ variability (Henderson, 2002; Andersen et al., 2010; Chen et al., 2016), which helps to approximate the authigenic U fraction of target sedimentary material. This approach was used successfully by Holmden et al. (2015) and Andersen et al. (2016). Importantly, this method only applies to modern paleoceanography because its utility is limited to timescales of several hundred years or shorter (Henderson and Anderson, 2003).

### 3.1.2. Processes that fractionate $\delta^{238}U$ ratios in the modern ocean

The compiled $\delta^{238}U$ composition of modern seawater is -0.39±0.01‰ (Tissot and Dauphas, 2015). Both abiotic and biotic processes are responsible for the isotopic fractionation of $\delta^{238}U$ in marine environments (Andersen et al., 2017). The mechanisms linked to the reduction of U(+6) to U(+4) and authigenic U formation are relatively well understood (Ku et al., 1977; Anderson et al., 1987; Klinkhammer and Palmer, 1991), while the associated causes of $\delta^{238}U$ fractionations remain underexplored. Experimental work confirmed that redox processes drive most of the $\delta^{238}U$

fractionation compared to those linked to no redox change (Chen et al., 2016; Andersen et al., 2017). In modern marine systems, the tight connection between abiotic and biotic reduction of U through authigenic U formation makes it particularly hard to disentangle each process individually (Andersen et al., 2017). Experimental work, on the other hand, confirms a significant difference between abiotic and microbially driven U reduction (Stirling et al., 2015). Here, we present the current understanding of the processes that can cause U isotope fractionation in both aqueous or particulate/sedimentary media towards heavier or lighter values when compared to the $\delta^{238}U$ of initial aqueous medium (e.g. seawater). Microbially driven reduction of U(+6) to U(+4) by *Geobacter sulfurreducens, Anaeromyxobacter dehalogenans,* and *Shewanella oneidensis* metal-reducing bacteria is known to cause a shift towards lighter isotopic values in the aqueous medium (Stylo et al., 2015a,b; Stirling et al., 2015). In most cases (except Rademacher et al., 2006), there is a preferential removal of the heavy ($^{238}U$) isotope from solution, making the $\delta^{238}U$ value of aqueous medium 1 to 2 ‰ lighter, while the particulate/solid phase becomes heavier (Stirling et al., 2015). Abiotic adsorption of dissolved U(+6) into Mn-oxyhydroxides also causes a shift towards lighter isotopic values, in which the adsorbed U is 0.2‰ lower than the aquatic medium (Brennecka et al., 2011; Dang et al., 2016). One process that cause a shift towards higher isotopic values is U accumulation in suboxic and anoxic sediments due to diagenetic processes. Such post-depositional accumulation drives $\delta^{238}U$ in porewaters towards lighter values while making sediments heavier isotopically (Weyer et al., 2008; Montoya-Pino et al., 2010; Romaniello et al., 2013). Some processes are known to cause no $\delta^{238}U$ fractionation. Importantly, adsorption to organic matter, which is known to be one of the processes to accumulate U, produces no measurable fractionation. The rates at which each process dominates over the others dictate the final $\delta^{238}U$ composition of the sedimentary records.

### 3.1.3. Uranium isotope data in modern marine settings

There are only few studies that thoroughly address the composition of $\delta^{234}U$ and $\delta^{238}U$ in modern marine settings (Weyer et al., 2008; Andersen et al., 2014; Holmden et al., 2015; Noordmann et al., 2015; Hinojosa et al., 2016; Abshire et al., 2020) with almost no data for the Eastern Tropical North Pacific (ETNP). Uranium isotope measurements in settling particles are very scarce, with only one published sediment trap dataset from the Saanich Inlet (Holmden et al., 2015). Elevated U enrichments were found in the settling particulate matter of Alfonso Basin, with values as high as 40 mg/kg compared to an average of 5 mg/kg throughout a ten-year sediment trap time series (Rodriguez-Castañeda, 2008; Choumiline, 2011; Choumiline et al., 2019). One of the proposed mechanisms is authigenic accumulation in marine snow aggregates, likely associated with micro-redox niches (Wright et al., 2012; Lehto et al., 2014; Bianchi et al., 2018; Choumiline et al., 2019). While the enrichments are significant, the real sources of variability and mechanisms of accumulation can only be established through the combined use of $\delta^{238}U$ and $\delta^{234}U$ isotopic systems. Other mechanisms that are also able to fractionate U isotope values or enrich its total concentration in the particulate matter could be related to the increased supply of land-derived material or the resuspension of marine sediments. Thus, to build a proper understanding U variability in marine settings, all the potential causes of U fractionation need to be investigated, which is the key objective of this chapter.

Here we present U isotope data from settling particles collected in a modern marine OMZ basin of the ETNP under well-constrained levels of dissolved oxygen and estimated primary productivity (Figure 3.1). By emphasizing settling particles, we will define the main sources that control the $\delta^{238}U$ and $\delta^{234}U$ composition in marine snow aggregates, as well as establish the potential transformation pathways of U before it reaches its diagenetic fate within marine sediments.

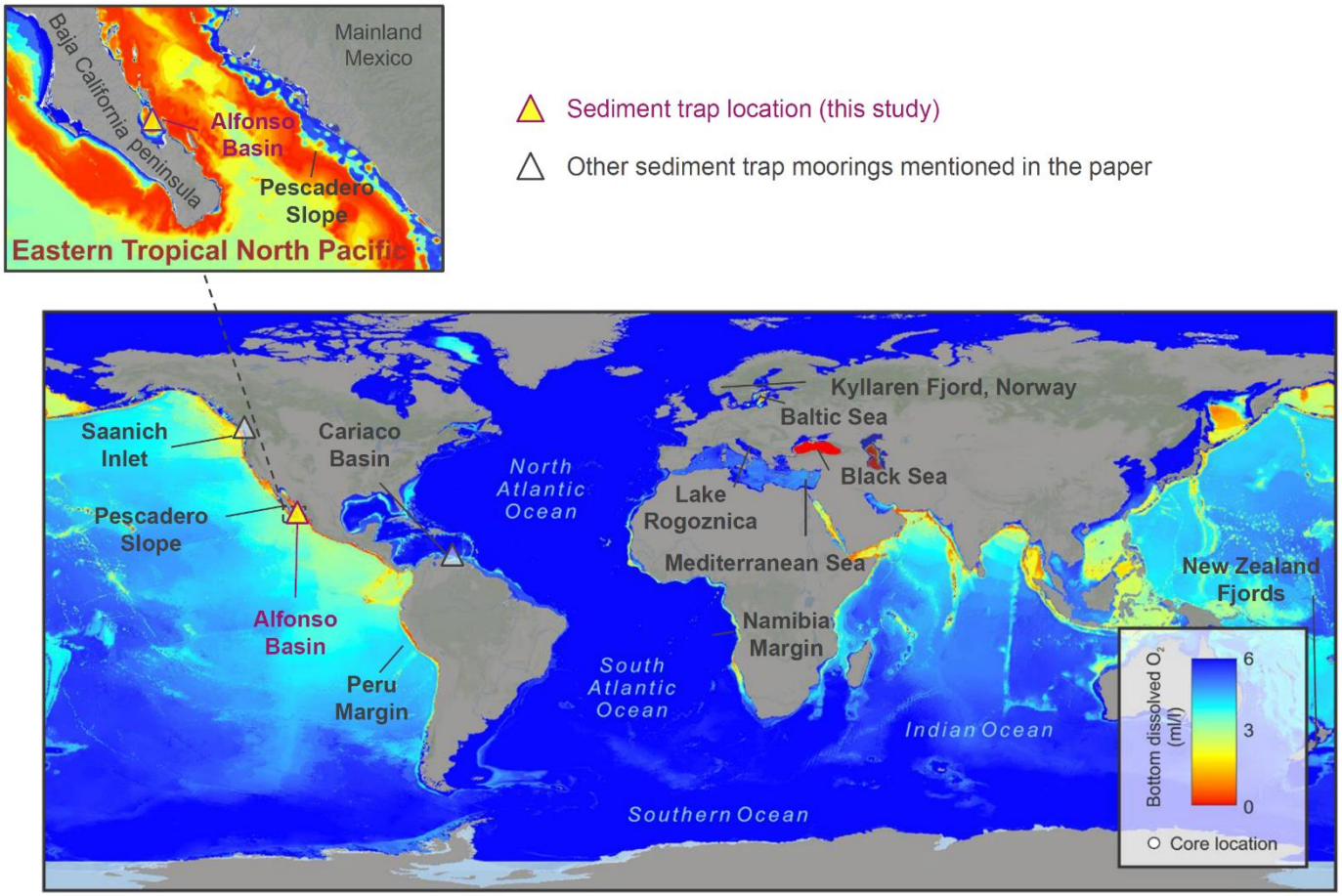


**Figure 3.1.** Locations of the sediment trap studied here (Alfonso Basin) and position of other moorings and sites mentioned in this study.

## 3.2. MATERIALS AND METHODS

### 3.2.1. Sampling and in-situ measurements

We use settling particulate matter collected with a Technicap PPS 3/3 sediment trap at 360 m water depth (50 m above the seafloor) in the anoxic Alfonso Basin (La Paz Bay, Gulf of California) located within the ETNP OMZ (Figure 3.1). The sediment trap mooring was installed and retrieved during multiple research cruises to La Paz Bay aboard the Mexican ships R/V Francisco de Ulloa and R/V Alpha Helix (Figure 3.2).

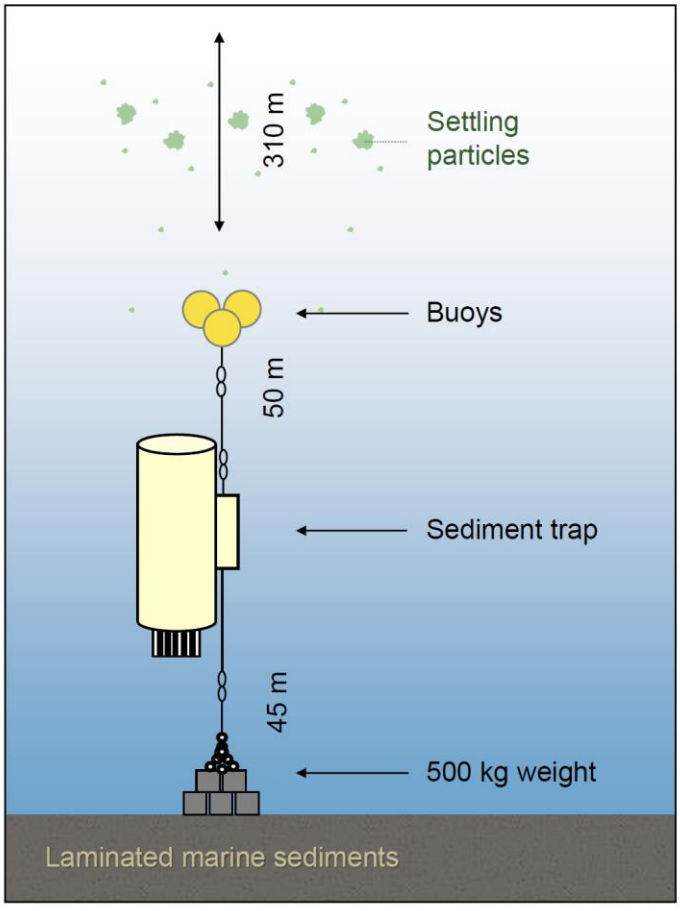


**Figure 3.2.** Simplified schematic of the installation of the sediment trap moored at 360 m depth in Alfonso Basin, Gulf of California.

Vertical water column dissolved oxygen profiles of Alfonso Basin were obtained during several cruises during routine sediment trap installation/retrieval procedures, as well as a complete survey aboard R/V CICIMAR XV, which helped us assess the current state of basin deoxygenation (Figure 3.3). Continuous in-situ measurements were performed using an $O_2$ sensor installed on an SBE 911plus CTD (Sea-Bird Scientific) and calibrated with discrete analyses of water samples collected with Niskin bottles in which dissolved $O_2$ was measured with the Winkler method (Carpenter, 1965).

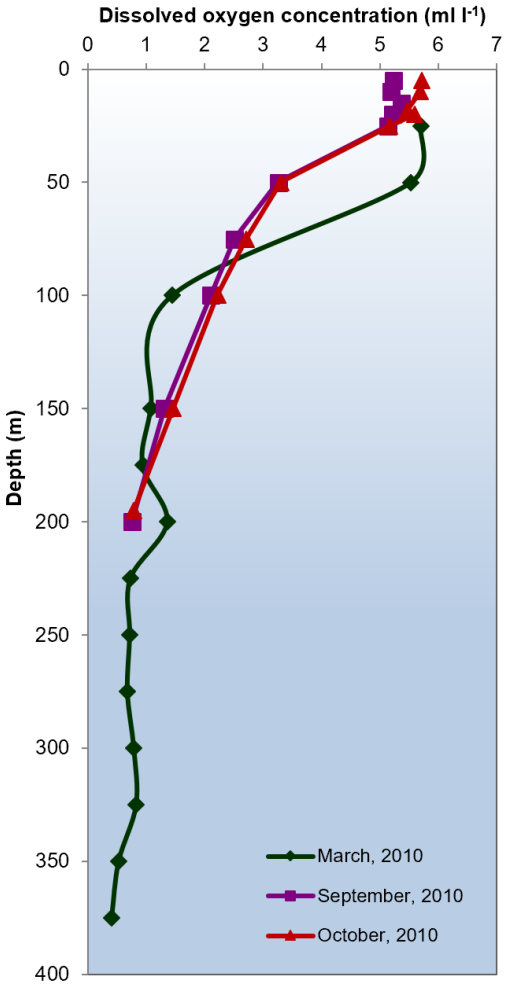


**Figure 3.3.** Dissolved oxygen profiles in the water column above Alfonso Basin measured in La Paz Bay during March, September and October 2010 surveys (Modified from Choumiline, 2011).

**Table 3.1.** Sediment trap samples used in this study and their detailed description (Data: Aguirre-Bahena, 2007; Rodriguez-Castañeda, 2008, Choumiline, 2011; Rochín-Bañaga, 2014, Silverberg et al., 2014).

| Sample Code | Sample ID | Range of collection dates | Resolution (days of collection) | Identified Special Events | |
|---|---|---|---|---|---|
| | | | | Rain | Hurricane |
| A | IX-6 | 15 - 24 Dec 2004 | 10 | | |
| B | XII-2 | 02 - 15 Dec 2005 | 14 | | |
| C | XIV-2 | 02 - 13 Oct 2006 | 12 | X | |
| D | XIV-5 | 07 Nov 2006 - 17 Feb 2007 | 103 | X | |
| E | XV-4 | 11 - 17 Mar 2007 | 7 | | |
| F | XVI-8 | 28 Aug - 12 Sep 2007 | 16 | X | X |
| G | XVII-5 | 18 - 25 Dec 2007 | 8 | | |
| H | XVII-6 | 26 Dec 2007 - 02 Jan 2008 | 8 | X | |
| I | XVII-9 | 18 - 24 Jan 2008 | 7 | | |
| J | XXV-2 | 17 Oct - 16 Nov 2011 | 31 | | |
| K | XXV-3 | 17 Nov - 16 Dec 2011 | 30 | | |
| L | XXV-4 | 17 Dec 2011 - 16 Jan 2012 | 31 | | |
| M | XXV-5 | 17 Jan 2012 - 16 Feb 2012 | 31 | | |
| N | XXV-6 | 17 Feb 2012 - 16 Mar 2012 | 29 | | |

The settling particulate matter samples used in this study were selected based on aliquot availability and U concentration. Since most samples did not have enough material left for proper analytical determination, we used samples that had at least 20 mg left. We present more detailed information on the selected samples in Table 3.1.

### 3.2.2. Analytical determinations

3.2.2.1. Uranium isotopes

Sample size availability for settling particulate matter was limited due to previously performed analytical determinations. Only some samples had enough material remaining to ensure

proper detection of uranium isotopes. All preparation procedures were performed under class-100 clean laboratory conditions at Cardiff University (Cardiff, United Kingdom).

The bulk fraction was extracted from dry and homogenized settling particulate matter by a digestion procedure involving a mixture of isotope-grade purity acids (HF, $HNO_3$, HCl) with conventional protocols in an ultraclean laboratory to avoid contamination (Andersen et al., 2014). We followed the detailed method described by Andersen et al. (2014, 2015). Proper amounts of double spike solution IRMM-3636 $^{233}U$-$^{236}U$ were added to each sample to correct for instrumental mass bias (Richter et al., 2008; Verbruggen et al., 2008). Uranium was separated using the column chromatography technique involving a UTEVA resin over several cleaning and elution steps, as described in Andersen et al. (2015) (Figure 3.4). The U isotope composition was measured on a Nu Plasma 2 MC-ICP-MS at Cardiff University (Cardiff, United Kingdom). The methods were checked against the in-house uraninite standard CZ-1 (Andersen et al., 2016; 2018) and Certified Reference Materials including USGS SDO-1 and USGS SGR-1 with well-known, but unofficial U isotope values (Tissot and Dauphas, 2015). Selected standards and samples were repeated for lab

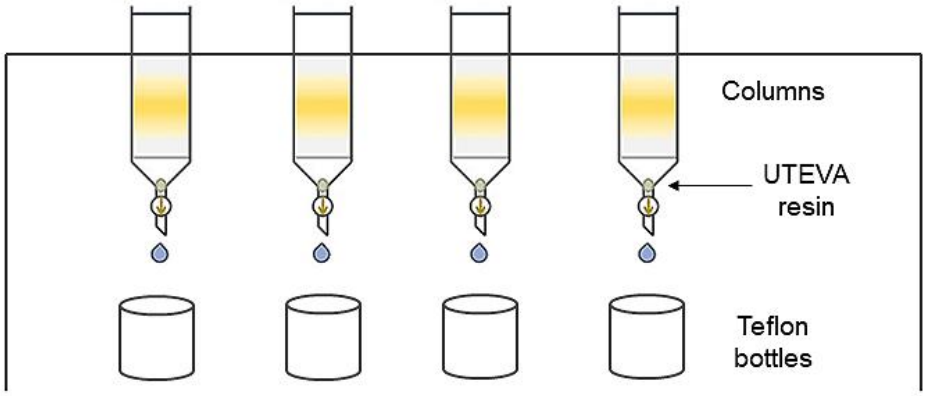


**Figure 3.4.** Column chromatography schematic during the last step in which pure U is eluded from the UTEVA resin and collected in the Teflon bottles.

intercalibration purposes. Sample and method blanks were used often during the analytical and preparation steps to check for contamination. The measured versus expected values for the in-house standard and certified reference material are presented in Table 3.2. The accuracy and reproducibility are in good agreement with previous determinations reported by Tissot and Dauphas (2015); Andersen et al., (2015, 2016 and 2018).

**Table 3.2.** Measured and expected values in reference materials used to check analytical quality of the data with errors presented as ±2SD.

| Standard | $\delta^{238}U$ (‰) | $\delta^{234}U$ (‰) | Reference |
|---|---|---|---|
| Expected USGS-SGR1b | -0.17 ± 0.05 | 4.5 ± 6.5 | Tissot and Dauphas, 2015 |
| Measured USGS-SGR1b | -0.19 ± 0.09 | 1 ± 11 | This study |
| Expected USGS-SDO-1 | -0.07 ± 0.05 | 0.3 ± 0.2 | Tissot and Dauphas, 2015 |
| Measured USGS-SDO-1 | -0.02 ± 0.09 | 4 ± 13 | This study |
| Expected CZ-1 (Uraninite) | -0.05 ± 0.03 | - | Andersen et al., 2016; 2018 |
| Measured CZ-1 (Uraninite) | -0.04 ± 0.09 | -1 ± 13 | This study |

### 3.2.3. Supporting analytical data

In order to provide better context for interpretation of $\delta^{234}U$ and $\delta^{238}U$ isotopic relationships, we include previously published data analyzed by our extended group members and collaborators. The organic carbon ($C_{org}$) data from the same sediment trap material with methodological details are described in Aguirre-Bahena (2007) and Silverberg et al., (2014). Biogenic silica or $SiO_{2(biog)}$ values are taken from Aguirre-Bahena (2007) and Rochín-Bañaga, (2014). Selected trace elements

were determined by Instrumental Neutron Activation Analysis (INAA) and Inductively Coupled Plasma Mass Spectrometry (ICP-MS) at ActLabs (Lancaster, Canada). The U and $U_{auth}$ data for such samples were taken from Rodriguez-Castañeda (2008), Choumiline et al. (2010), and Choumiline (2011).

### 3.2.4. Numerical and statistical approaches

The authigenic U ($U_{auth}$) calculations are done using the following equation by Wignall and Myers (1988) plugging in measured total U ($U_{sample}$) and Th values:

$$U_{auth} = U_{sample} - (Th/3).$$

Another common way to obtain $U_{auth}$ is by subtracting an estimated detrital U component from the total measured U ($U_{sample}$). A detrital indicator (El) such as Al is required. The calculation is as follows:

$$U_{auth} = U_{sample} - [(U/El)_{detrital} \times El_{sample}],$$

In this chapter, we use the approach of Holmden et al. (2015), which involve the measured $\delta^{234}U$ values for each sample ($\delta^{234}U_{sample}$) compared to both an authigenic ($\delta^{234}U_{auth}$) and a detrital ($\delta^{234}U_{detrital}$) end member. The choice of which value to use differ slightly depending on the region and the isotopic composition of the surrounding lithologies. We decided to use a typical (based on modern seawater) $\delta^{234}U_{auth}$ value of 146 ‰ for the authigenic end member and -10 ‰ for the detrital end member. The actual authigenic concentration values are then calculated multiplying the fraction of authigenic U by the measured total U ($U_{sample}$) concentration (Table 3.4):

$$\% \text{ fraction of isotopically-calculated } U_{auth} = \frac{\delta^{234}U_{sample} - \delta^{238}U_{detrital}}{\delta^{234}U_{auth}/^{234}U_{detrital}}$$

In order to assess the degree of organic matter degradation and mixture of organic sources into the basin, we assumed C:N (also $C_{org}$:N) ratios of sedimentary material (Meyers, 1994; Bianchi and Bauer, 2011). According to the classic Redfield ratio, marine biomass should have a C:N ratio

of 106:16 (Redfield, 1934). A more recent estimate indicates an updated ratio of 163:22 (Martiny et al., 2014). The latter means that C:N values close to 6 or 7 would indicate marine organic matter as the dominating source, while higher values would represent a terrestrial source for the organics (Meyers, 1994; Martiny et al., 2014). To establish the statistical relationships between major components and U isotopes, we calculated the coefficient of determination ($R^2$) correlations for selected elements.

We estimated regional average values for the surrounding lithologies of La Paz Bay (Alfonso Basin) from the rock geochemistry database GeoInfoMex provided by Servicio Geológico Mexicano (https://www.sgm.gob.mx/GeoInfoMexGobMx/) using ArcGIS 10.6 by ESRI. The geochemistry datapoints (n=62) were selected based on the rocks that are intersected with drainage basins that flow into La Paz Bay. These selected rocks represent an important source of the fluvial material supplied to Alfonso Basin.

## 3.3. RESULTS AND DISCUSSION

### 3.3.1. Uranium isotopic composition of settling particles from Alfonso Basin

We present uranium concentrations for selected sinking particle samples from the Alfonso Basin sediment trap in Figure 3.5 (full dataset presented in Supplementary Figure 3.1). The U concentration of the sample set ranges from 0.5 to 17.3 mg/kg and averages 4.79 mg/kg (Rodriguez-Castañeda, 2008; Choumiline, 2011). The $\delta^{238}U$ composition changes from -0.49 to 0.16 and averages -0.25 ‰ (Table 3.3, Figure 3.5). The $\delta^{234}U$ composition varies from -7 to 98 ‰, averaging 54 ‰ (Table 3.3, Figure 3.5).

When plotting U against $\delta^{238}U$ (Figure 3.6), a clear pattern can be observed in which the samples are either heavier (A, F, J, K, L, I) or lighter (M, N, B) in $\delta^{238}U$ than the average seawater composition. Most of these samples very likely represent normal marine sedimentation without the

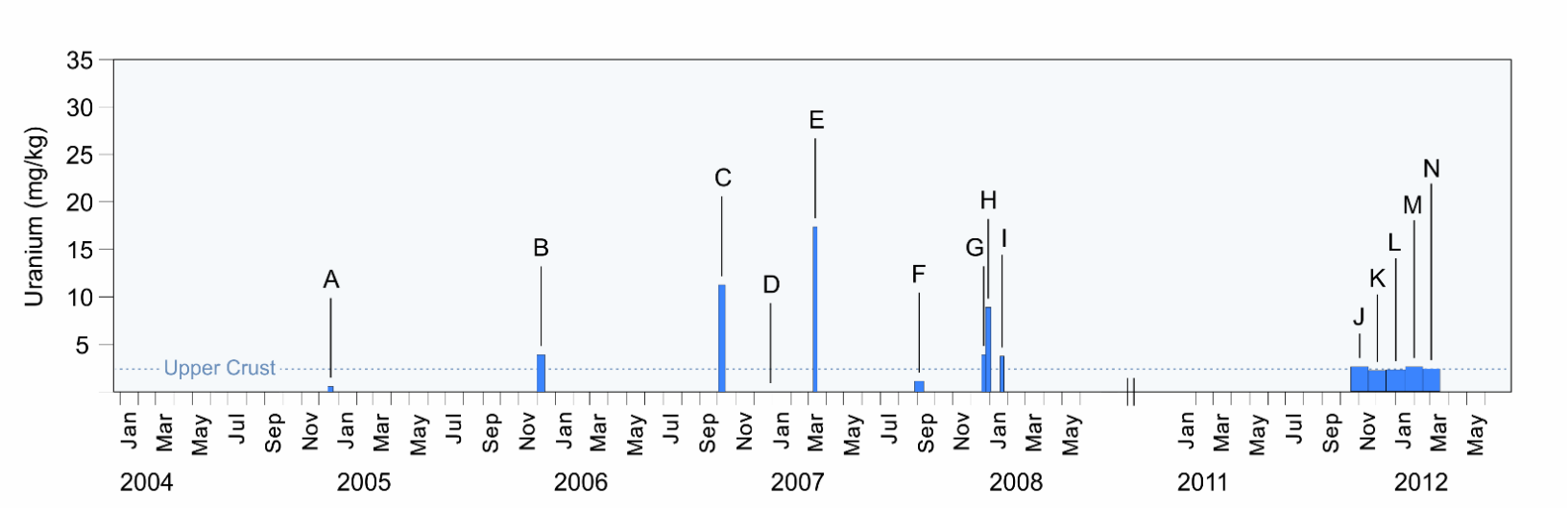


**Figure 3.5.** Uranium concentrations and sample codes of the selected settling particulate matter samples analyzed for $\delta^{238}U$ and $\delta^{234}U$ collected with a sediment trap moored at 360 m depth in Alfonso Basin, Gulf of California (Data from: Rodriguez-Castañeda, 2008; Choumiline, 2011). The horizontal dotted line represents average Upper Continental Crust concentration values for U (Wedepohl, 1995).

**Table 3.3.** Composition of select settling particulate matter samples from Alfonso Basin. The assigned ±2SD for the measurements was 0.13 ‰ for $\delta^{238}U$ and 16 ‰ for $\delta^{234}U$ (Data from: Aguirre-Bahena, 2007; Rodriguez-Castañeda, 2008, Choumiline, 2011; Rochín-Bañaga, 2014; Silverberg et al., 2014).

| Sample Code | Sample ID | Total mass flux (g/m2/d) | $C_{org}$ (%) | $SiO_{2(biog)}$ (%) | N (%) | U (mg/kg) | $\delta^{238}U$ (‰) | $\delta^{234}U$ (‰) |
|---|---|---|---|---|---|---|---|---|
| A | IX-6 | 1.07 | 6.85 | 59.51 | 0.87 | 0.50 | -0.25 | 42 |
| B | XII-2 | 1.86 | 4.99 | 49.91 | 0.64 | 3.84 | -0.42 | 49 |
| C | XIV-2 | 0.78 | 8.50 | 24.59 | 1.07 | 11.20 | 0.16 | -7 |
| D | XIV-5 | 0.43 | 4.80 | 34.91 | 0.59 | - | -0.08 | 35 |
| E | XV-4 | 0.70 | 7.65 | 41.92 | 0.99 | 17.30 | -0.32 | 56 |
| F | XVI-8 | 1.95 | 7.48 | 25.30 | 0.92 | 1.02 | -0.29 | 45 |
| G | XVII-5 | 4.54 | 3.88 | 44.63 | 0.55 | 3.79 | -0.06 | 78 |
| H | XVII-6 | 2.92 | 4.14 | 52.13 | 0.56 | 8.79 | -0.11 | 34 |
| I | XVII-9 | 1.20 | 5.29 | 53.85 | 0.71 | 3.75 | -0.34 | 97 |
| J | XXV-2 | 0.73 | 8.84 | 28.57 | 1.13 | 2.60 | -0.23 | 61 |
| K | XXV-3 | 1.43 | 5.97 | 29.82 | 0.91 | 2.20 | -0.29 | 52 |
| L | XXV-4 | 1.98 | 4.08 | 39.58 | 0.60 | 2.30 | -0.30 | 42 |
| M | XXV-5 | 0.69 | 6.04 | 45.24 | 0.99 | 2.60 | -0.49 | 98 |
| N | XXV-6 | 0.65 | 6.25 | 28.57 | 0.98 | 2.40 | -0.46 | 75 |

influence of strong U contributions during special events (Table 3.1). Additionally, at least four clear outliers were found: C, E, G, and H. These samples are up to 0.50 ‰ heavier in $\delta^{238}U$ than seawater and multiple times higher in U than the average crustal composition of 2.5 mg/kg (Wedepohl, 1995). These samples represent extreme climatic events and could be essential to giving us insights into the end members of the mixture of marine snow material that is trapped in Alfonso Basin. For instance, particularly H and C were deposited under increased precipitation, so they most likely have detrital inputs.

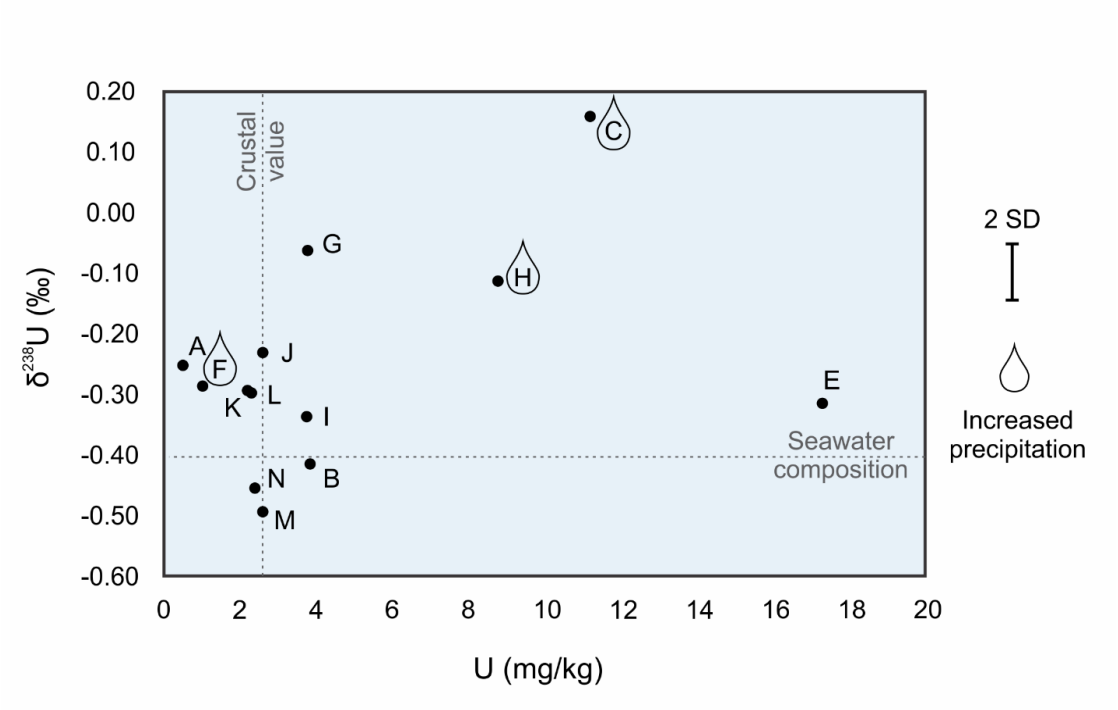


**Figure 3.6.** Total U plotted against $\delta^{238}U$ in settling particles collected with a sediment trap moored at 360 m depth in Alfonso Basin, Gulf of California from 2004 to 2012 (Data: Choumiline, 2011; Silverberg et al., 2014).

In order to provide a concentration-independent assessment of $\delta^{234}U$ and $\delta^{238}U$ in settling particles from Alfonso Basin, we present the variability of both components in Figure 3.7. A first order evaluation of $\delta^{234}U$ provides insights into the dominance of fresh authigenic U in the sample ($\delta^{234}U \approx 146$ ‰) over old or reworked $\delta^{234}U$ ($\delta^{234}U$ around 0 ‰). With slight deviations, most samples fall on a two end-member mixing line. One end member represents the detrital component defined by near-zero $\delta^{234}U$ and heavy $\delta^{238}U$ values. The samples that most likely represent this end member are C, D, and H. On the other side of the spectrum, the authigenic end member is most likely exemplified by samples M, N, and I. The remainder of the sinking particle samples fall in the middle of the hypothetical mixture between the two end members, potentially indicating a constant mixture of both fractions (Figure 3.7).

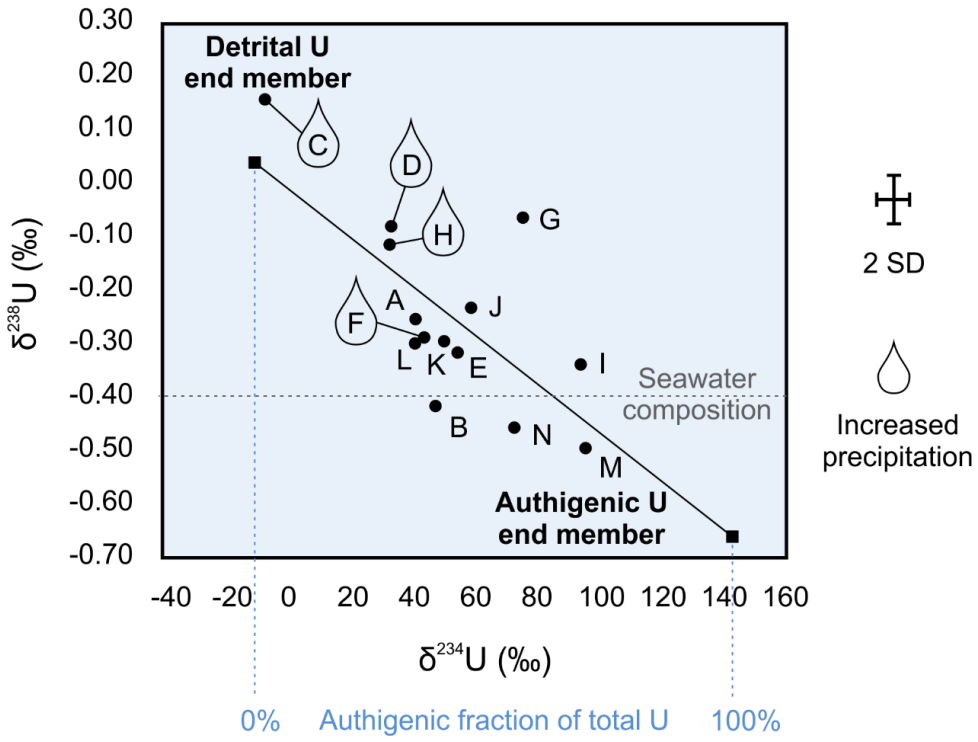


**Figure 3.7.** Plot of $\delta^{234}U$ vs $\delta^{238}U$ of settling particles from Alfonso Basin, Gulf of California. The two end members shown are: authigenic U and detrital U. The proximity to each end member on the $\delta^{234}U$ axis represents the estimated percentage (%) of authigenic U in each sample.

### 3.3.2. Authigenic uranium fraction

Here we show the $U_{auth}$ fraction and concentration values calculated using the equation of Holmden et al. (2015) as described earlier in this chapter (Table 3.4, Figure 3.8). The calculated authigenic U values range from 2 % to 69 % with an average of 41 %. The fractions translate into concentration values from 0.17 mg/kg to 7.34 mg/kg, averaging 1.74 mg/kg for $U_{auth}$. Most of the detrital deposition in Alfonso Basin is dominated by dust (Silverberg et al., 2014), which accounts for the resulting non-authigenic U. The samples deposited under sporadic pluvial events, such as C, H, and D (Aguirre-Bahena, 2007; Silverberg et al., 2014) tend to have the lowest authigenic fraction as shown in Figure 3.8.

**Table 3.4.** Isotopically-calculated concentration, fraction and percentage fraction of authigenic uranium ($U_{auth}$) in settling particulate matter samples from Alfonso Basin (Uranium data used for calculation taken from: Rodriguez-Castañeda, 2008, Choumiline, 2011).

| Sample Code | Sample ID | U (mg/kg) | $U_{auth}$ (mg/kg) | $U_{auth}$ (fraction) | $U_{auth}$ (percentage fraction) |
|---|---|---|---|---|---|
| A | IX-6 | 0.50 | 0.17 | 0.34 | 34% |
| B | XII-2 | 3.84 | 1.45 | 0.38 | 38% |
| C | XIV-2 | 11.20 | 0.24 | 0.02 | 2% |
| D | XIV-5 | - | - | 0.29 | 29% |
| E | XV-4 | 17.30 | 7.34 | 0.42 | 42% |
| F | XVI-8 | 1.02 | 0.36 | 0.36 | 36% |
| G | XVII-5 | 3.79 | 2.13 | 0.56 | 56% |
| H | XVII-6 | 8.79 | 2.49 | 0.28 | 28% |
| I | XVII-9 | 3.75 | 2.56 | 0.68 | 68% |
| J | XXV-2 | 2.60 | 1.18 | 0.45 | 45% |
| K | XXV-3 | 2.20 | 0.87 | 0.40 | 40% |
| L | XXV-4 | 2.30 | 0.77 | 0.34 | 34% |
| M | XXV-5 | 2.60 | 1.80 | 0.69 | 69% |
| N | XXV-6 | 2.40 | 1.31 | 0.54 | 54% |

### 3.3.3. Relationships between $\delta^{238}U$, $C_{org}$, and N in settling particles from Alfonso Basin and potential differences of organic matter source

We determine correlations between elemental ratios of $\delta^{238}U$ versus either $C_{org}$ or N for sediment trap samples. We found a lack of correlation for most components based on coefficients of determination ($R^2$) for the full set of sediment samples (Table 3.3). The $R^2$ values were 0.00 for $\delta^{238}U$:$C_{org}$, and 0.02 for $\delta^{238}U$:$C_{org}$. Due to the heterogeneity of our settling matter, which is comprised of both marine-dominated (modern-seawater-like $\delta^{234}U$) and detrital-sourced sinking

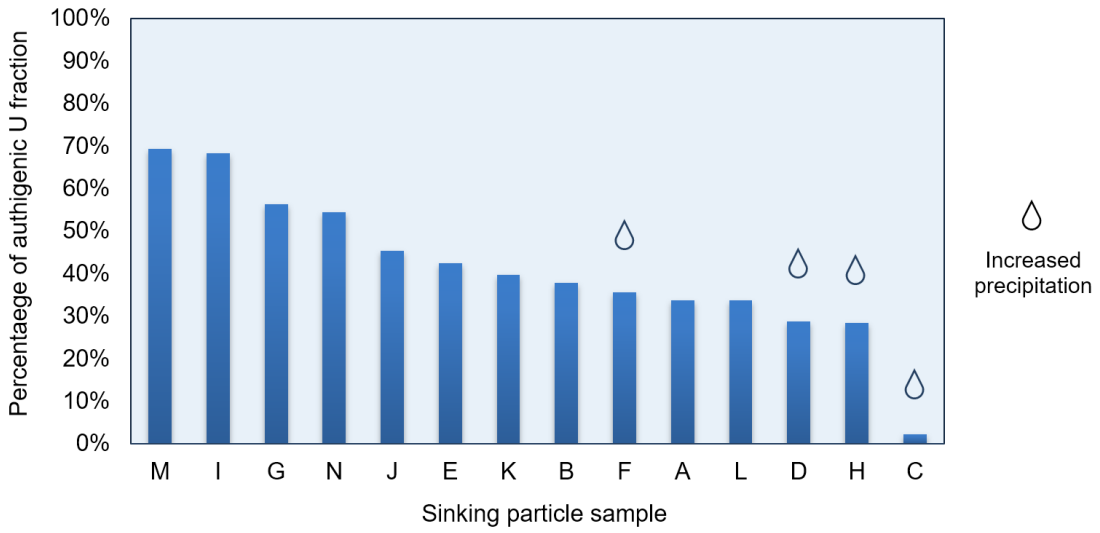


**Figure 3.8.** Percentage of calculated authigenic U as a fraction of the total U concentration in settling particulate matter samples from Alfonso Basin, Gulf of California.

particles ($\delta^{234}$U lighter than modern seawater) (Figure 3.7), we classified our samples based on their $C_{org}$:N ratio. The resulting two groups represent samples with more (Figure 3.9A) and less abundant (Figure 3.9B) marine organic matter carefully chosen by $C_{org}$:N ratios below or above 7.5, respectively. The $C_{org}$:N ratios of sediment trap samples from Alfonso Basin range from 6.08 to 8.15 – all pointing toward a predominantly marine organic matter source (Meyers, 1994; Martiny et al., 2014). We hypothesize that slightly elevated values indicate a somewhat higher contribution of terrestrial (also called pedogenic) organic matter.

3.3.3.1. Settling particles with more abundant organic matter ($C_{org}$:N ratios below 7.5)

The first group of sediment trap material with more abundant marine organic matter (Figure 3.9A) encompassed samples with $C_{org}$:N ratios sorted from low (6.08) to high (7.44) in the

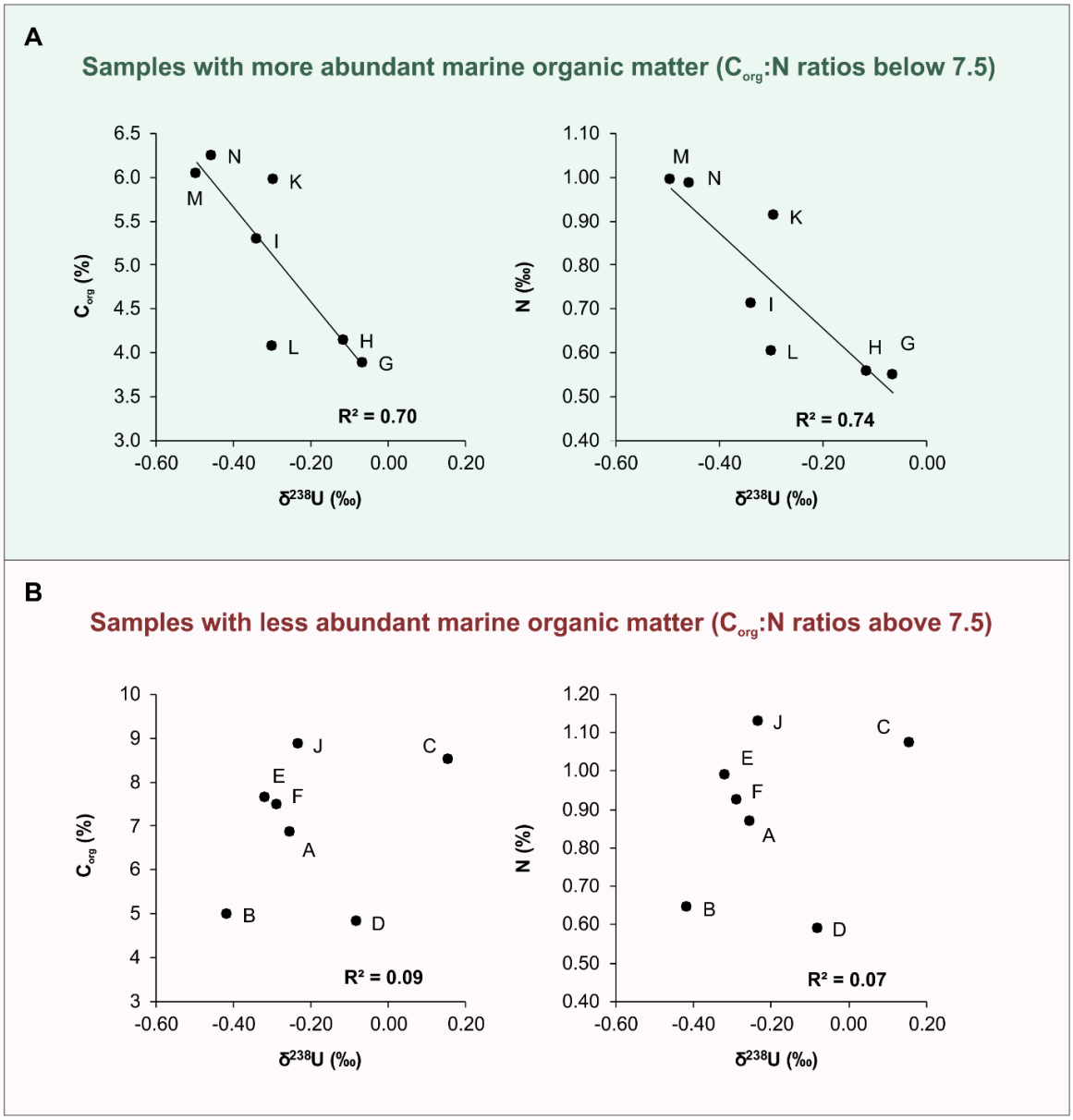


**Figure 3.9.** Elemental ratios of $\delta^{238}U$ vs $C_{org}$ and N for sediment trap samples with: (A) consistently abundant marine organic matter; and (B) scattered detrital inputs supplied during rain and dust storms. Stronger correlations could indicate mechanistical relationships between primary productivity and U chemistry (Data from: Aguirre-Bahena, 2007; Rodriguez-Castañeda, 2008, Choumiline, 2011; Rochín-Bañaga, 2014; Silverberg et al., 2014).

following order: M, N, K, L, G, I, and H. The average $\delta^{238}U$ for this sample group is -0.29, with a range of -0.49 to -0.06 ‰. When comparing the $R^2$ coefficients for this dataset, we found good correlation between $\delta^{238}U$ and both $C_{org}$ ($R^2$ = 0.70) and N ($R^2$ = 0.74) as shown in Figure 3.9A. The correlation improves further for the four samples (M, N, K, and L) with the lowest $C_{org}$:N ratios of 6.08, 6.34, 6.55, and 6.75, respectively. We found $R^2$ values for this group as high as 0.97 for the $\delta^{238}U$:$C_{org}$ correlation and 0.91 for $\delta^{238}U$:N. Both groups very likely represent normal marine sedimentation with less detrital inputs (Figure 3.9A), showing a mixture between plankton-like low $\delta^{238}U$ values (Holmden et al., 2015) and elevated $\delta^{238}U$ often corresponding to reduced U(+4). While this heavy $\delta^{238}U$ is very likely driven by the rock-derived end member previously explained (Figure 3.7) and evidenced by lower-than-seawater $\delta^{234}U$ values, some process could still be fractionating $\delta^{238}U$ within the marine snow aggregates. For instance, sample G is not the lowest in terms of $\delta^{238}U$ (78 ‰) but reaches a very heavy $\delta^{238}U$ value of -0.09 ‰ that could be associated to U(+6) reduction. Adsorption to organic matter usually leads to no fractionation, so even if this process is actively happening during normal marine sedimentation, it is nearly impossible to track when no significant $U_{auth}$ enrichments are to be found.

The average U concentration values found for samples associated with marine-sourced organic matter (Figure 3.9A) were 3.69 mg/kg for $U_{tot}$ and 1.70 mg/kg for $U_{auth}$. Even the samples with the lowest $C_{org}$:N ratios (M, N, K, and L) that represent normal marine sedimentation have relatively low U concentrations compared to the maximum $U_{tot}$ value of 17.3 mg/kg for the same data series (Rodriguez-Castañeda, 2008; Choumiline, 2011). This result could indicate water column authigenic enrichments that might not be a dominating source in coastal regions.

3.3.3.2. Settling particles with less abundant organic matter ($C_{org}$:N ratios above 7.5)

For the second group of samples with less abundant marine organic matter (Figure 3.9B), the $C_{org}$:N ratios ranged from 7.74 to 8.15 in the following order: E, B, J, A, C, F, and D. There is no correlation between $\delta^{238}U$ and $C_{org}$ and N. We found $R^2$ coefficients as low as 0.09 for $\delta^{238}U$:$C_{org}$ and 0.07 $\delta^{238}U$:N Most of the fluvially dominated samples fall within this group. We suggest that this group is dominated by events, which overprint the regular normal marine sedimentation with detrital fluvial inputs, turbidity flows, and potentially resuspension.

We found a somewhat elevated average $U_{tot}$ of 6.08 mg/kg for this group of samples with less abundant marine organic matter (Figure 3.9B). An $U_{auth}$ average of 1.79 mg/kg, with light $\delta^{234}U$ (40 ‰ on average), is reported for the second group of samples with less abundant marine organic matter (Figure 3.9B). During deposition of these samples, the detrital input could have been overprinting the total concentrations and $\delta^{238}U$ composition of settling particulate matter deposited under normal marine conditions not dominated by sporadic events.

The mixture between marine and terrestrial (pedogenic) organic matter and their implications in the paleorecords is a subject of interest in modern biogeochemistry (Calvert et al., 1996; Burdige, 2007; Bianchi et al., 2016; Blattmann et al., 2019). While we cannot fully exclude the possibility of a correlation between U, $C_{org,}$ and N in rocks surrounding the basin, such a relationship was not reported previously in those lithologies (Piper et al., 1994; Hausback, 1984; Choumiline, 2011). Moreover, if the correlations shown in Figure 3.9A were due to dust sedimentation, it would very likely impact most samples and correlate with other detrital components. Instead, there is little to no correlation between the biogenically sourced $C_{org}$ and N and $\delta^{238}U$ for samples deposited during rainy events C, D, and F (Figure 3.9).

## 3.4. SYNTHESIS

### 3.4.1. Potential sources of U isotopic variability in settling particles from Alfonso Basin

Marine snow aggregates are complex microsystems that can host a variety of particles of detrital, authigenic, and biogenic origin. We present the potential sources and mechanisms of isotopic variability in the settling particulate matter (Figure 3.10; Supplementary Figure 3.2). In this section we describe each of these components based on what is known for the region and the isotopic composition of sedimentary material from other, relevant localities (Weyer et al., 2008; Tissot and Dauphas, 2015). We remind the reader that each sediment trap sample can have variable amounts of each component, making definitive interpretations challenging.

#### 3.4.1.1. Detrital contribution

In the sediment trap samples from Alfonso, lithogenic contributions are usually established via Al, Fe, and Sc content, peaking during rainy events, hurricanes, and dust storms (Rodriguez-Castañeda, 2008; Silverberg et al., 2014). While we do find distinct $\delta^{234}U$ and $\delta^{238}U$ patterns for fluvial-dominated events, total U concentrations show no relationship with typical lithogenic indicators (Rodriguez-Castañeda, 2008; Choumiline, 2011). We describe the potential sources for the detrital U fraction in this section.

##### 3.4.1.1.1. Surrounding lithologies

The classic approach to assessing non-lithogenic enrichments is to compare the data for average crustal composition, which is 2.5 mg/kg for U (Wedepohl, 1995), to the values measured in the studied samples (Tables 3.3 and 5). Even better is using regional averages, especially in regions of high U background. We calculated an average U composition for the local drainage basin surrounding La Paz Bay (GeoInfoMex by SGM) as described in the Materials and Methods section.

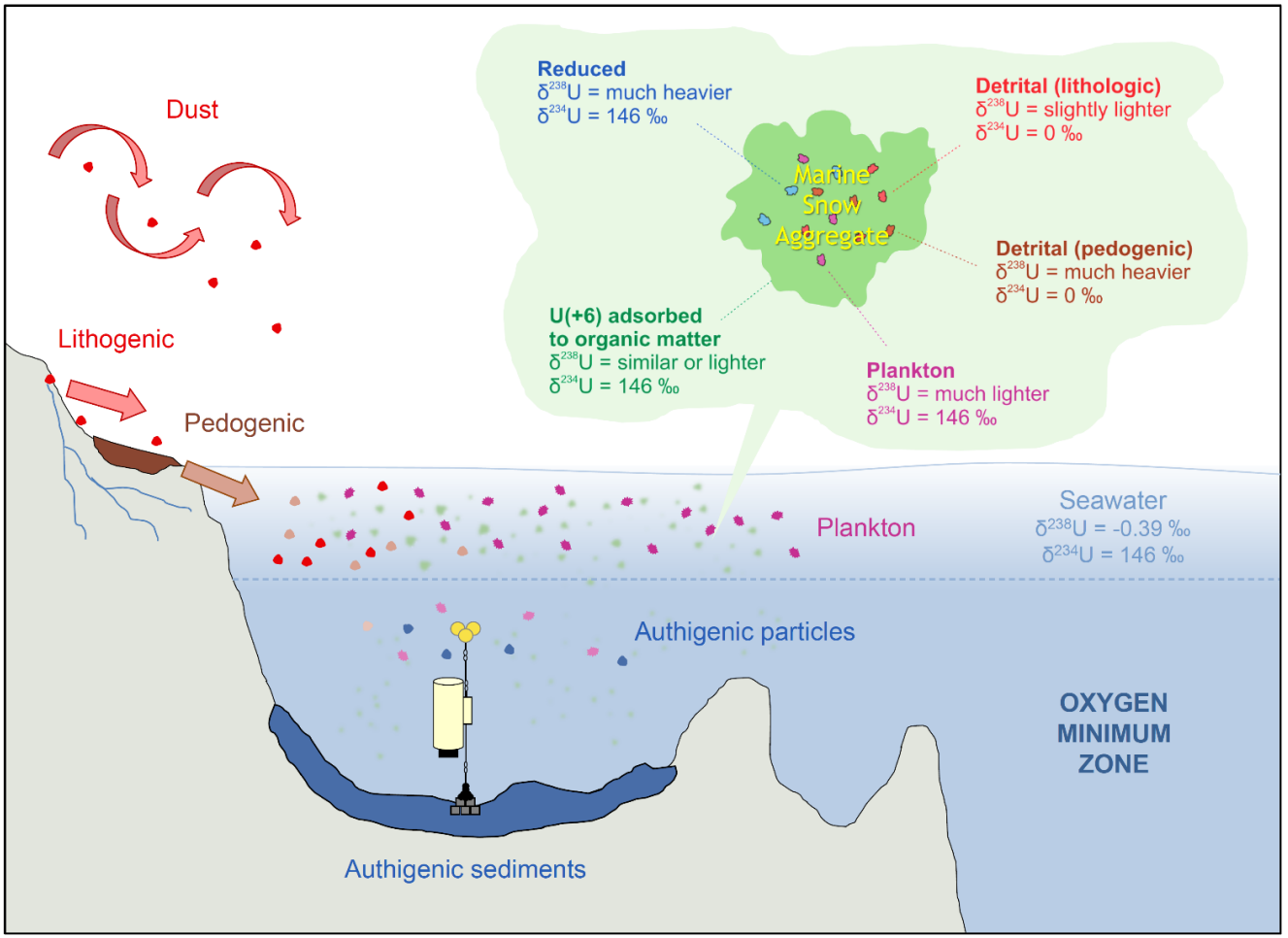


**Figure 3.10.** Schematic representing sources and processes that contribute to the variability of $\delta^{234}U$ and $\delta^{238}U$ in marine snow from Oxygen Minimum Zones. The $\delta^{238}U$ values are presented qualitatively either higher (isotopically heavier) or lower (isotopically lighter) than the average seawater value of -0.39 ‰ suggested by Tissot and Dauphas (2015).

The data range from a minimum of 0.26 mg/kg to a maximum of 4.88 mg/kg, while averaging 2.76 mg/kg. These numbers are consistent with the previously reported regional background average of 2.03 mg/kg (n=11) (Piper, 1991; Choumiline, 2011) if the highly localized phosphorite value of 87 for El Cien Formation (Fischer et al., 1995) is excluded from the calculation. This phosphorite, while high in U, represents only a tiny fraction of the drainage basin and is very unlikely to be contributing significantly to the total U value (and isotopic composition) of settling particles and marine sediments (Choumiline, 2011). As mentioned above, the local detrital background of 2.76 mg/kg (Table 3.5) is very similar to the value of 2.5 mg/kg for average upper continental crust (Wedepohl, 1995). In fact, the highest U concentrations for the sediment trap from Alfonso Basin are several times higher than the background values, for both the complete dataset (42.79 mg/kg) and samples (17.30) reported for the first time in this chapter.

3.4.1.2. Fluvial erosion and transport

The potential fluvial sources could either be due to the erosion of the surrounding lithologies or transport of soil to the marine environment. Most dry stream beds in the drainage basin of La Paz Bay are not enriched in U compared to the average rock concentration of 2.1 mg/kg U other than the dry stream right next to the phosphatic high-U outlier of 15.0 (Choumiline, 2011). Due to similarities in composition between arroyo and regional geology, it is safe to assume that the rock composition would be accurately representing detrital contribution.

Some rocks are identified to have elevated U composition, such as the phosphorite layer of El Cien Formation (Fischer et al., 1995). The issue is that the limited areal extent of this localized sedimentary layer does extend over most of the region, so we do not expect a substantial detrital contribution. We do hypothesize that some of the $\delta^{238}$U-heavy but $\delta^{234}$U-light samples are due to

**Table 3.5**. Comparison of the uranium concentration and isotopic composition of sedimentary material from different regions. The values are presented as averages and (minimum to maximum), unless only one value is used.

| Marine basin and sample type | Water column depth | Redox condition and bottom dissolved $O_2$ (mL/L) | $C_{org}$ | U | $U_{auth}$ | $\delta^{238}U$ | $\delta^{234}U$ |
|---|---|---|---|---|---|---|---|
| | | | (%) | mg/kg | mg/kg | ‰ | ‰ |
| La Paz Bay Lithologies (Alfonso Basin) Regional Background[a] | - | | - | 2.76 (0.26 - 4.88) | - | - | - |
| Alfonso Basin, Gulf of California (all settling particles)[b] | 360 m | Anoxic (< 0.1) | 7.80 (2.96 - 16.37) | 4.65 (0 - 42.79) | 4.16 (0 - 42.70) | - | - |
| Alfonso Basin, Gulf of California (settling particles studied here)[b] | 360 m | Anoxic (< 0.1) | 6.05 (3.88 - 8.84) | 4.79 (0.5 - 17.3) | 1.74 (0.17 - 7.34) | -0.25 (-0.49 to 0.16) | 54 (-7 to 98) |
| Alfonso Basin, Gulf of California (core MD02-2510 10-11)[c] | 410 m | Anoxic (< 0.1) | - | 13.04 | 11.09 | -0.06 | 116 |
| Pescadero Slope, Gulf of California (core DIPAL-III T2 5-6)[c] | 577 m | Anoxic (< 0.1) | 6.76 | 8.09 | 5.05 | -0.21 | 118 |
| Saanich Inlet, Vancouver Island (plankton)[d] | 50 m | Oxic | - | 0.4 | - | -1.24 | 157 |
| Saanich Inlet, Vancouver Island (settling particles)[d] | 50-180 m | | 4.7 (3.6 - 7.1) | 2.11 (1.67 - 2.90) | - | -0.52 (-0.66 to -0.29) | 48 (28 to 63) |
| Saanich Inlet, Vancouver Island (Sediments from shallow stations)[d] | 78-80 m | Oxic | 0.85 (0.8 - 0.9) | 1.96 (1.93 - 1.98) | - | -0.39 (-0.39 to -0.38) | -11 |
| Saanich Inlet, Vancouver Island (Sediments from deep stations)[d] | 187-230 m | Anoxic | 3.63 (3.3 - 3.9) | 5.13 (4.51 - 5.88) | - | -0.21 (-0.29 to -0.05) | 101 (81 to 117) |
| Peru Margin (ODP Leg 112, Site 680A)[e] | 250 m | Suboxic | - | 12.71 (7.30 - 16.20) | - | -0.29 (-0.41 to -0.16) | - |
| Namibia Margin (core 25020)[f] | 116 m | Anoxic (< 0.5) | 9.26 (7.22 - 11.59) | 34.25 (5.18 - 95.82) | - | -0.16 (-0.62 to 0.20) | - |

| | | | | | | | |
|---|---|---|---|---|---|---|---|
| Namibia Margin (core GC 4)[f] | 302 m | Suboxic (1.11) | 3.22 (2.51 - 3.82) | 45.15 (38.69 - 50.36) | - | -0.20 (-0.36 to 0.05) | - |
| Namibia Margin (core GC 5)[f] | 795 m | Oxic (3.36) | 6.80 (5.79 - 7.69) | 8.13 (5.99 - 12.47) | - | -0.11 (-0.38 to 0.17) | - |
| Landsort Deep, Baltic Sea (core 342390-2-7)[g] | 450 m | Euxinic | - | 5.42 (4.40 - 8.10) | - | -0.30 (-0.39 to -0.13) | |
| Black Sea (Sediments from shallow stations 3, 4 and 16)[h] | 85-129 m | Oxic | - | 3.91 (3.31 - 6.24) | 2.82 (2 - 5.2) | -0.02 (-0.36 to 0.12) | 74 (44 to 119) |
| Black Sea (Sediments from deep stations 9 and 14)[h] | 2094-2218 m | Euxinic | - | 15.65 (10.50 - 17.95) | 14.57 (9.1 - 17) | -0.01 (-0.13 to 0.11) | 169 (154 to 177) |
| Cariaco Basin (sediment trap)[i] | 275-1255 m | | 9.15 (2.65 - 17.53) | 3.04 (1.97 - 4.28) | - | - | - |
| Cariaco Basin (ODP Leg 165, Site 1002)[h] | 900 m | Euxinic | 3.56 (0.13 - 6.21) | 8.26 (3.22 - 14.13) | 6.68 (0.6 - 13.00) | -0.09 (-0.32 to 0.05) | 69 (-90 to 119) |
| Kyllaren Fjord, Norway (cores KY09-1 and KY09-3)[j] | 29 m | Euxinic | - | 4.83 (3.80 - 6.00) | - | -0.26 (-0.34 to -0.18) | - |
| New Zealand Fjords[k] | | Anoxic / Euxinic | - | 5.06 (1.9 - 12.4) | - | -0.33 (-0.64 to -0.14) | - |
| Eastern Mediterranean (ODP 967C 1H-5)[l] | 2550 m | Euxinic | - | 22.27 (5.00 - 38.00) | 21.59 (4.60 - 37.00) | -0.13 (-0.35 to 0.11) | - |
| Lake Rogoznica, Adriatic Sea, Croatia[m] | 15 m | Euxinic | - | 4.91 (3.08 - 8.09) | 4.06 (2.37 - 7.25) | -0.31 (-0.41 to -0.24) | |
| Upper Continental Crust Average[n] | - | - | | 2.5 | - | | |

Sources:
[a] average values from the rock geochemistry database GeoInfoMex provided by Servicio Geológico Mexicano (https://www.sgm.gob.mx/GeoInfoMexGobMx/); [b] Sediment trap material with values between 2002–2008 in 173 samples (Rodríguez-Castañeda, 2008; Choumiline, 2011; Silverberg et al., 2014); [c] Choumiline et al., 2018; [d] Holmden et al., 2015; [e] Weyer et al., 2008; [f] Abshire et al., 2020; [g] Noordmann et al., 2015; [h] Lyons et al., 2003; Andersen et al., 2014; [i] Calvert et al., 2015; [j] Noordmann et al., 2015; [k] Hinojosa et al., 2016; [l] Andersen et al. 2018; [m] Bura-Nakić et al., 2018; [n] Wedepohl, 1995

event-driven contribution, potentially leading to the erosion of the U-enriched phosphorite layer. Sample C is the sediment trap material that most likely represents this source (Figure 3.7).

#### 3.4.1.2.1. Aeolian transport

It has been suggested that the Baja California Peninsula could be providing a significant fraction of the aeolian material on a regional scale (Segovia-Zavala et al., 2009; Morales-Acuña et al., 2019). Combined with other distal sources (Sonora Desert), the Baja California Peninsula could be nourishing the aeolian sedimentation of Alfonso Basin and other water masses of the Gulf of California. Unfortunately, there are currently no measured U isotope values for global or local dust sources, but the values are expected to be detrital-like (Lau et al., 2019).

The variability of the contribution of wind-blown material to Alfonso Basin is well documented for the region (Rodriguez-Castañeda, 2008; Aguirre-Bahena, 2007; Choumiline, 2011; Silverberg et al., 2007; Silverberg et al., 2014) The wind pattern is known to fluctuate seasonally in response to monsoon climatic shifts. A good correlation between the number of strong gusts in the region (> 4.5 m/s) and the supply of lithogenic indicators confirm the consistently sustained importance of dust supply into the basin (Silverberg et al., 2014).

#### 3.4.1.2.2. Pedogenic processes and transport

A potential contribution, especially for the samples that seem to be less dominated by marine organic matter input, could be related to soil material transported from land. Increasing evidence shows that terrestrial organics can fractionate $\delta^{238}U$ due to the adsorption of either U(+6) or U(+4) to organics and/or humic acids, which could produce a wide range of $\delta^{238}U$ signatures in soils. This possibility could help explain the extreme outlier values such as sediment trap sample C (Figures 3.6 and 3.7). The addition of moisture to such soils during sporadic rain events (Table 3.1) in a

predominantly dry climate not only creates a flow of water into the bay but can also enhances this adsorption process in the soils. The transport of this local soil source can alternate from fluvial during storms to wind during dry spells, also mixing with the other sources such as dust. This mechanism of soil $\delta^{238}U$ fractionation could explain the high $\delta^{238}U$ values in some of the sediment trap samples, without having to invoke a heavy $\delta^{238}U$ lithogenic background source.

3.4.1.2.3. Anthropogenic sources

The local drainage basin has rather low U values (Source: GeoInfoMex by SGM) compared to the highest reported for the Alfonso Basin sediment trap (42.8 mg/kg) and marine sediment averages (4.8 mg/kg). The only known rock to be strongly enriched in U is a small phosphorite layer in the western part of the bay reaching 87 mg/kg (Choumiline, 2011). As previously found, the tailings dam of Rofomex mine has a U value of 39.0 mg/kg (Choumiline, 2011), and the arroyo next to it reaches 15 mg/kg. Studies have reported a potential link between elevated U (33.3 mg/kg) in macroalgae *Enteromorpha intestinalis* and mining activities of the Rofomex phosphorite enterprise (Rodriguez-Castañeda, 2002). The mine has experienced episodes of flooding during tropical cyclones in which unknown amounts of material were transported to the ocean. Additionally, dust storms or industrial accidents could spread wind-driven particles to Alfonso Basin that could have reached the sediment trap location. While the enrichments and accumulation mechanisms are unknown, long-distance transport of industrially concentrated U-enriched material is possible. This option could explain some of the outlier samples, such as fluvially dominated C. However, we would expect phosphorites to have low rather than high $^{238}U$. The possibility of similar anthropogenic sources needs to be further evaluated in this region and other areas where U-rich tailings are present.

3.4.1.3. Resuspension of marine sediments and turbidity flow

Seismically triggered turbidites have been reported for the tectonic marine basins of the Gulf of California, including Alfonso (Gonzalez-Yajimovich et al., 2007; Gorsline et al., 2000). The bottom U values range from 0.3 to 19.5 mg/kg with an average of 1.6 mg/kg for the entire bay (Rodriguez-Castañeda, 2002). These values are rather high and are partially influenced by the diagenetic U enrichments due to bottom water anoxia (Calvert and Pedersen, 1993; Morford and Emerson, 1999; Rodriguez-Castañeda, 2002; McManus et al., 2005; Choumiline, 2011; Choumiline et al., 2019).

During the sampling period, there was no evidence detected for turbidite fluxes into the sediment trap, which is intentionally positioned at least 50 m above the seafloor to avoid resuspension (Aguirre-Bahena, 2007; Silverberg et al., 2014). Also, there is no prominent enrichment of other trace elements that are also abundant in the bottom sediments. Additional evidence against resuspension or turbidity fluxes are the $\delta^{234}U$ values of the samples that are too low for freshly formed authigenic U ($\delta^{234}U$ of 146 ‰) and would be more characteristic for old detrital material coming from eroded rocks ($\delta^{234}U$ of -10 ‰).

3.4.1.4. Water column authigenesis

A fraction of the authigenic U could be originating in the water column (Zheng et al., 2002; Holmden et al., 2015; Choumiline et al., 2019) and potentially make its way to marine sediments. One of the mechanisms that trigger U authigenesis in the ocean is the reduction of dissolved U(+6) to insoluble U(+4). This microbially mediated process usually leads to $\delta^{238}U$ fractionation (Lovley et al., 1991; Bopp et al., 2010; Murphy et al., 2014; Stirling et al., 2015). If reduction occurs, then the resulting $\delta^{238}U$ in the particulate or sedimentary matter will have higher values (Stylo et al., 2015a,b; Stirling et al., 2015). This possibility was most likely the case for samples H or G.

Uranium adsorption is common in organic-rich material (Bone et al., 2017), but it is known to cause no significant $\delta^{238}U$ fractionation. Due to the high abundance of organic matter, adsorption could be occurring in every sample, especially those that have no significant $\delta^{238}U$ fractionation while having higher $\delta^{234}U$ values. This process could be exemplified by sample E (Figures 3.6 and 3.7).

3.4.1.5. Plankton and productivity

Current understanding indicates that U(VI) can accumulate in plankton, very likely by sorption (Anderson et al., 1989; Fisher et al., 1987). So far, the only values reported for marine plankton reach an extremely low $\delta^{238}U$ value of -1.24 ‰ (Holmden et al., 2015) with a hypothetical seawater-like $\delta^{234}U$. In terms of U concentration, plankton presence will not cause significant U increase, as the concentration in this type of material is low (0.395 mg/kg; Holmden et al., 2015).

The Alfonso Basin sediment trap sample that is most likely influenced by an increased abundance of plankton would be M (Figures 3.6 and 3.7). This sample also has the highest authigenic percentage of the entire dataset, reaching almost 70 %. As expected for plankton-dominated sample, the $\delta^{234}U$ value is authigenic-like (98 ‰) with the lowest $\delta^{238}U$ value of the dataset with -0.49 ‰.

### 3.4.2. Comparison of isotopic U composition of sinking particles with other types of sedimentary material

In this section we compare $\delta^{238}U$ values among relevant components of the marine system: settling particles, seawater, plankton, and marine sediments (Table 3.5). In Figure 3.11 we show a Box Whisker plot (n=69) for the above mentioned materials from the following regions of the ocean: the Gulf of California (This study; Choumiline et al., 2018); Saanich Inlet (Holmden et al.,

2015), Peru Margin (Weyer et al., 2008); Namibia Margin (Abshire et al., 2020), and Arabian Sea (Choumiline et al., in prep). $\delta^{238}U$ values for marine sediments deposited under anoxic and euxinic waters are skewed towards values heavier than the seawater average (Figure 3.11, Supplementary Figure 3.3). Interestingly, the only existing datasets for marine settling particles — from Saanich Inlet (Holmden et al., 2015) and Alfonso Basin (this study) — also fall slightly higher in $\delta^{238}U$ (-0.33 ‰) than seawater on average but range from -0.66 to 0.16 ‰. Most marine sediments from Peru, Namibia, and Saanich Inlet fall within similar $\delta^{238}U$ range from -0.62 to 0.20 ‰ (Weyer et al., 2008; Holmden et al., 2015; Abshire et al., 2020). The heaviest $\delta^{238}U$ value reported so far was for the Namibia Margin (Abshire et al., 2020), which is expected for a highly productive marine OMZ setting. Compared with other types of non-OMZ marine basins, the average values tend to be similar for the Baltic Sea (-0.30 ‰), the lower deep for Cariaco Basin (-0.09 ‰), and the Black Sea (-0.02 ‰), reaching maximum values of -0.13 ‰, 0.05 ‰, and 0.12 ‰, respectively (Andersen et al., 2014; Noordmann et al., 2015). In particular, the deep, strongly reducing euxinic part of the restricted Black Sea has heavy $\delta^{238}U$ values and strong $U_{auth}$ enrichments of 17 mg/kg (Andersen et al., 2014).

Most $U_{auth}$ enrichments and associated $\delta^{238}U$ fractionations happen in marine sediments during microbially mediated diagenetic processes previously discussed (Ku et al., 1977; Anderson, 1987; Anderson et al., 1989; Klinkhammer and Palmer, 1991; Lovley et al., 1991; Calvert and Pedersen, 1993; Morford and Emerson, 1999; Dunk et al., 2002; McManus et al., 2005; Stylo et al., 2015a,b; Andersen et al., 2015, 2016, 2017). The contribution of our research is the idea that a portion of authigenic U enrichments and associated fractionation could be coming from settling particles, which are often ignored or considered non-significant. This type of U enrichment might not be relevant for strongly reducing conditions such as the Black Sea because it will be almost entirely dominated by diagenetic U enrichment. However, in non-coastal open ocean settings,

settling particles can be largely composed of authigenic U formed in marine snow aggregates, as discussed in Choumiline et al. (2019).

When it comes to $\delta^{234}U$, the average for both Saanich Inlet and Alfonso is 52 ‰ (Table 3.3) (Holmden et al., 2015; this study). The range of values (-7 to 98 ‰) represent a wide variety of mixtures between detrital and authigenic/biogenic components. As previously discussed, every deviation from the seawater value could represent authigenic enrichment or a mixture between components. With the help of the $\delta^{234}U$ and $\delta^{238}U$ combo, we were able to produce an updated model for U biogeochemistry and shed more light on U authigenic processes.

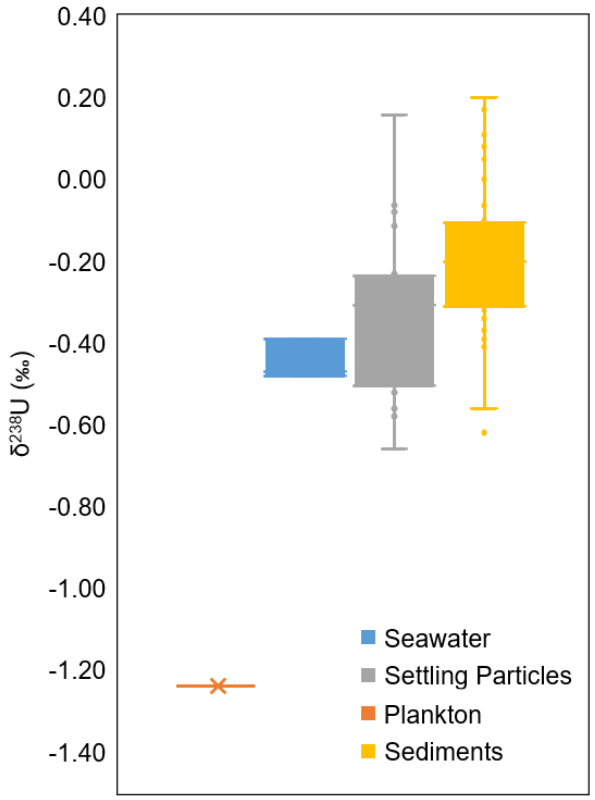


**Figure 3.11.** Box and Whisker Plot comparing $\delta^{238}U$ values in various types of sedimentary material from OMZ-type settings including: Gulf of California, Saanich Inlet, Peru Margin and Namibia Margin (Data: this study, Choumiline et al., 2018; Weyer et al., 2008; Holmden et al., 2015; Abshire et al., 2020).

### 3.4.3. Microbial niches and associated $\delta^{238}U$ fractionation during remineralization of sinking organic matter

A strong correlation of $\delta^{238}U$ for marine-sourced samples with $C_{org}$ and N suggests a tight relationship of authigenic U with primary productivity (Figure 3.9). Emerging microbiota rRNA gene survey, biomarker, and other geochemical evidence show clear gradients in abundances of bacteria and archaea in water columns and marine snow that vary across diverse modern basins and OMZ settings (Wakeham et al., 2007; Pitcher et al., 2011; Ulloa et al., 2012; Wright et al., 2012; Lehto et al., 2014; Bianchi et al., 2018). These microbial niches are responsible for most of the organic matter degradation/respiration, as well as water column and diagenetic transformations (Ulloa et al., 2012). Experimental work suggests different $\delta^{238}U$ fractionations for abiotic and biologically mediated reduction of U(+6) to U(+4) (Stylo et al., 2015a,b; Stirling et al., 2015). In the experiments by Stylo et al. (2015a,b), the authigenic solid U(+4) phase was preferentially enriched in the heavy $^{238}U$ isotope only by biotic transformations.

Such microbially controlled transformations could be occurring in marine snow from the productive Alfonso Basin. For instance, the relationships between $\delta^{238}U$ and $C_{org}$ and N could indicate a varying degree of remineralization in the marine-sourced organic matter samples (Figure 3.9A). For instance, labile organic matter (our samples M or N) shows high $C_{org}$ and N concentrations with a light plankton-like $\delta^{238}U$ value (Holmden et al., 2015). Conversely, sample G potentially underwent stronger remineralization (evidenced by low $C_{org}$ and N) that could have enhanced anoxia within marine snow aggregate, leading to heavier $\delta^{238}U$ in the particulate matter. Differences in remineralization were reported for sinking particles of Alfonso Basin, so variable redox on a microscale is feasible (Aguiñiga et al., 2010; Hakspiel-Segura et al., 2016). The ability to separate between preservation and remineralization processes, as tested by $\delta^{238}U$ vs $C_{org}$ and N, could have important implications for the U paleoproxy in past OMZs. Similarly, unscrambling

the U fractionation associated to biotic and abiotic processes should permit the use of U isotopes as a paleoproductivity proxy not only in the modern oceans but also in ancient environments, where the ability to track the first appearance and proliferation of biotic processes is crucial (Homoky et al., 2016).

### 3.4.4. Our model for the biogeochemistry of uranium isotopes in coastal modern marine settings

Several modern anoxic marine basins (Noordmann et al., 2015; Hinojosa et al., 2016; Rolison et al., 2017) show a considerable export of authigenic U from bottom waters into the particulate phase, long before reaching the sediment-water interface where most of the U(+6) reduction was previously thought to occur (Anderson, 1987; Anderson et al., 1989; Klinkhammer and Palmer, 1991). We provide additional evidence and a specific mechanism for authigenic U enrichment and isotopic fractionation in the water column, specifically relevant for modern high productivity OMZ settings or similar ancient past analogs such as Oceanic Anoxic Events (OAEs) (Montoya-Pino et al., 2010). The classic mechanism attributes the occurrence of authigenic U in marine sediments to early diagenetic processes (Anderson, 1987; Klinkhammer and Palmer, 1991). While this is an important pathway, it fails to fully explain the highly variable isotopic values in settling particles and the strong authigenic contribution in strongly reducing and highly productive basins (Tribovillard et al., 2006).

Our proposed mechanism involves the formation of particulate $U_{auth}$ within marine snow aggregates that, depending on their size, could host a sequence of redox reactions modulated by microbial communities in redox microniches (Lehto et al., 2014; Ulloa et al., 2012; Wright et al., 2012), as depicted in Figure 3.10. Similar to marine sediments, the formation of authigenic U in particles is accomplished either by abiotic adsorption to organic matter and Mn-oxyhydroxides or

microbially mediated reduction (Dang et al., 2016; Stylo et al., 2015a,b; Stirling et al., 2015). This newly formed authigenic U is transported downward as settling particulate matter sink to the seafloor. Highly productive anoxic marine basins have the same sequence of terminal electron acceptors that continues into the sediments. We hypothesize that higher productivity within anoxic basins leads to more exported $U_{auth}$ and $C_{org}$ into marine sediments and results in the heaviest $\delta^{238}U$ in sediments (Hinojosa et al., 2016 and Andersen et al., 2017). Contrastingly, low productivity and better ventilation lead to little or no water column exported $U_{auth}$, so sedimentary $\delta^{238}U$ is drawn towards lighter values (Hinojosa et al., 2016). Importantly, the final isotopic composition of the sedimentary material will be a mixture of authigenic, biogenic, and detrital sources, combining more negative (hydrothermal and metalliferous rocks) or less negative (anoxic sediments) $\delta^{238}U$ fingerprints that can shift the baseline for interpretations of the sedimentary record (Homoky et al., 2016).

### 3.5. FINAL REMARKS

This study has important implications for the biogeochemistry of U in the marine oceanic realm and serves to improve the way we interpret this element in the paleoceanographic record. The main finding of our study challenges the old paradigm of $U_{auth}$ enrichments entirely dominated by diagenetic processes. Our findings confirm that fresh $U_{auth}$ may be formed in marine snow aggregates, evidenced by near-seawater $\delta^{234}U$ composition of settling particles. A wide range of $\delta^{238}U$ values indicates that reduction of U(+6) to U(+4) and adsorption to organic matter are causing these authigenic enrichments. More importantly, due to the heterogeneity of samples in coastal marine settings, especially those rich in ancient U, every sample contains a mixture of different proportions of $U_{auth}$ diluted by varying proportion of detrital non-authigenic U. Additionally, it is

also expected that in the underlying sedimentary record, not only freshly created $U_{auth}$ will be present but also old resuspended $U_{auth}$ with its own $\delta^{234}U$ - $\delta^{238}U$ signatures.

It is logical that some coastal regions with modern OMZ settings also had strong upwelling. For instance, organic-rich Miocene rocks off the coast of California and southern Baja California have elevated U. Since authigenic enrichments are the most critical value for paleoceanographic proxy purposes, it is important to start using the isotopically calculated $U_{auth}$ value, instead of the classic numerical calculations, which fail to make this distinction. In regions with variable detrital components, mixing model corrections in the $\delta^{234}U$ - $\delta^{238}U$ isotopic space should be made to properly estimate authigenic enrichments. Properly assessing $U_{auth}$ is particularly important during times of high productivity, as authigenic U contribution through settling can be significant.

For future studies, it will be essential to separate the detritally derived U from the potentially fresh authigenic U fraction. The latter represents a common challenge for sediment trap material, as separating bedrock-derived grains from the surrounding organic matter is usually complicated. Moreover, physical separation is often not done because the samples are needed for other analyses. Modern field techniques allow the nearly undisturbed collection of sinking aggregates using marine snow samplers (Flintrop et al., 2018). Improvements in analytical methods are making $\delta^{234}U$ and $\delta^{238}U$ determinations in smaller samples possible. In addition to the data presented here, only a true physical separation of marine snow components and precise U isotope measurements in each fraction will fully answer long-vexing questions on the utility of U as paleoproxy — including its greatest value, whether for redox or paleoproductivity or other parameter.

## 3.6. CONCLUSIONS

The $\delta^{234}U$ isotopic composition of sediment trap material from Alfonso Basin averages 54 ‰ and varies from detrital-dominated -7 ‰ to marine-influenced 98 ‰. The average authigenic U portion for all samples represents 41% of the total U concentration. This authigenic fraction ranges from near-zero to almost three-fourths of the total U. The range of values means that every sample has a significant detrital contribution either coming from the local catchment basin or through aeolian dust transport.

The settling particulate matter samples from Alfonso Basin have an average $\delta^{238}U$ of -0.25 ‰ which slightly deviates from the expected seawater composition of -0.39 ‰ towards heavier (0.16 ‰) and lighter (-0.49 ‰) values. Evidence for two mechanisms controlling authigenic uranium enrichments was found: adsorption leading to no $\delta^{238}U$ fractionation, and reduction driving the particulate phase towards heavier $\delta^{238}U$. Significant increases in $\delta^{238}U$ values in particulates are very likely a fingerprint for biotically-controlled authigenic U formation. Marine plankton is known to have smaller $\delta^{238}U$, which most likely explains some lower-than seawater values.

The $\delta^{238}U$ and $\delta^{234}U$ composition of sinking particles show that each particular sample consists of a variable mixture between detrital and authigenic components. A combined assessment using $\delta^{234}U$, $\delta^{238}U$, and $C_{org}$:N ratios allowed to define the main two groups of settling particles in Alfonso Basin: one dominated by the terrestrial inputs and the other by marine-derived organic matter. For the marine-dominated sample groups, the average $\delta^{238}U$ values are -0.29 ‰ which would represent “normal sedimentation”. The relationship of $\delta^{238}U$ with either N or $C_{org}$ in marine-derived samples could indicate differences in remineralization that would create differential redox conditions within marine snow aggregates. This metabolic change in microscale redox probably

leads to the in-situ formation of authigenic U and causes isotopic fractionation of particulate $\delta^{238}U$ towards heavier values.

In coastal regions with abundant background U the potential ranges $\delta^{238}U$ can be significantly variable. If there is high U in the surrounding rocks the $\delta^{234}U$ composition can help to disentangle the authigenic enrichments from local detrital ones. In this study, the contribution of soil, dust, and fluvial material is very likely skewing the bulk $\delta^{238}U$ of the marine snow samples towards isotopically heavier values.

## 3.7. REFERENCES


Abshire, M.L., Romaniello, S.J., Kuzminov, A.M., Cofrancesco, J., Severmann, S., and Riedinger, N. (2020). Uranium isotopes as a proxy for primary depositional redox conditions in organic-rich marine systems. Earth and Planetary Science Letters 529, 115878.

Aguiñiga, S., Sanchez, A., and Silverberg, N. (2010). Temporal variations of C, N, $\delta^{13}C$, and $\delta^{15}N$ in organic matter collected by a sediment trap at Cuenca Alfonso, Bahía de La Paz, SW Gulf of California. Continental Shelf Research 30, 1692-1700.

Aguirre-Bahena, F. (2007). Cambios temporales en los componentes y flujos de la materia en hundimiento en Cuenca Alfonso, Bahía de La Paz, durante el periodo 2002-2005. Master's Thesis, Centro Interdisciplinario de Ciencias Marinas - Instituto Politécnico Nacional.

Andersen, M.B., Matthews, A., Vance, D., Bar-Matthews, M., Archer, C., and De Souza, G.F. (2018). A 10-fold decline in the deep Eastern Mediterranean thermohaline overturning circulation during the last interglacial period. Earth and Planetary Science Letters 503, 58-67.

Andersen, M.B., Romaniello, S., Vance, D., Little, S.H., Herdman, R., and Lyons, T.W. (2014). A modern framework for the interpretation of $^{238}U/^{235}U$ in studies of ancient ocean redox. Earth and Planetary Science Letters 400, 184-194.

Andersen, M.B., Stirling, C.H., and Weyer, S. (2017). Uranium Isotope Fractionation. Reviews in Mineralogy and Geochemistry 82, 799-850.

Andersen, M.B., Stirling, C.H., Zimmermann, B., and Halliday, A.N. (2010). Precise determination of the open ocean 234U/238U composition. Geochemistry, Geophysics, Geosystems 11.

Andersen, M.B., Vance, D., Morford, J.L., Bura-Nakić, E., Breitenbach, S.F.M., and Och, L. (2016). Closing in on the marine $^{238}U/^{235}U$ budget. Chemical Geology 420, 11-22.

Anderson, R.F., Fleisher, M.Q., and Lehuray, A.P. (1989). Concentration, oxidation state, and particulate flux of uranium in the Black Sea. Geochimica et Cosmochimica Acta 53, 2215-2224.

Anderson, R.F. (1987). Redox behavior of uranium in an anoxic marine basin. Uranium 3, 145-164.

Bianchi, D., Weber, T.S., Kiko, R., and Deutsch, C. (2018). Global niche of marine anaerobic metabolisms expanded by particle microenvironments. Nature Geoscience 11, 263-268.

Bianchi, T.S., and Bauer, J.E. (2011). Particulate organic carbon cycling and transformation. 69-117.

Bianchi, T.S., Schreiner, K.M., Smith, R.W., Burdige, D.J., Woodard, S., and Conley, D.J. (2016). Redox effects on organic matter storage in coastal sediments during the Holocene: a biomarker/proxy perspective. Annual Review of Earth and Planetary Sciences 44, 295-319.

Blattmann, T.M., Liu, Z., Zhang, Y., Zhao, Y., Haghipour, N., Montlucon, D.B., Plotze, M., and Eglinton, T.I. (2019). Mineralogical control on the fate of continentally derived organic matter in the ocean. Science 366, 742-745.

Bone, S.E., Dynes, J.J., Cliff, J., and Bargar, J.R. (2017). Uranium(IV) adsorption by natural organic matter in anoxic sediments. Proceedings of the National Academy of Sciences 114, 711-716.

Bopp, C.J., Lundstrom, C.C., Johnson, T.M., Sanford, R.A., Long, P.E., and Williams, K.H. (2010). Uranium $^{238}U/^{235}U$ isotope ratios as indicators of reduction: results from an in situ biostimulation experiment at Rifle, Colorado, U.S.A. Environmental Science & Technology 44, 5927-5933.

Brennecka, G.A., Wasylenki, L.E., Bargar, J.R., Weyer, S., and Anbar, A.D. (2011). Uranium isotope fractionation during adsorption to Mn-oxyhydroxides. Environmental Science & Technology 45, 1370-1375.

Bura-Nakić, E., Andersen, M.B., Archer, C., De Souza, G.F., Marguš, M., and Vance, D. (2018). Coupled Mo-U abundances and isotopes in a small marine euxinic basin: Constraints on processes in euxinic basins. Geochimica et Cosmochimica Acta 222, 212-229.

Burdige, D.J. (2007). Preservation of Organic Matter in Marine Sediments: Controls, Mechanisms, and an Imbalance in Sediment Organic Carbon Budgets? Chemical Reviews 107, 467-485.

Calvert, S.E., Bustin, R.M., and Ingall, E.D. (1996). Influence of water column anoxia and sediment supply on the burial and preservation of organic carbon in marine shales. Geochimica et Cosmochimica Acta 60, 1577-1593.

Calvert, S.E., and Pedersen, T. (1993). Geochemistry of Recent oxic and anoxic marine sediments: Implications for the geological record. Marine Geology 113, 67-88.
Calvert, S.E., Piper, D.Z., Thunell, R.C., and Astor, Y. (2015). Elemental settling and burial fluxes in the Cariaco Basin. Marine Chemistry 177, 607-629.

Carpenter, J.H. (1965). The Chesapeake Bay Institute technique for the Winkler dissolved oxygen method. Limnology and Oceanography 10, 141-143.

Chen, T., Robinson, L.F., Beasley, M.P., Claxton, L.M., Andersen, M.B., Gregoire, L.J., Wadham, J., Fornairi, D.J., and Harpp, K.S. (2016). Ocean mixing and ice-sheet control of seawater $^{234}U/^{238}U$ during the last deglaciation. Science 354, 626-629.
Choumiline, K., Andersen, M.D., Pérez-Cruz, L., Carriquiry, J. D., and Beaufort, L. (2018). "Uranium Isotopes as the Storytellers of Swaying Oxygen Minimum Zones. Goldschmidt 2018," in Abstract Retrieved from Goldschmidt Conference Archive (Boston).

Choumiline, K., Pérez-Cruz, L., Gray, A.B., Bates, S.M., and Lyons, T.W. (2019). Scenarios of Deoxygenation of the Eastern Tropical North Pacific During the Past Millennium as a Window Into the Future of Oxygen Minimum Zones. Frontiers in Earth Science 7.

Choumiline, K., Rodríguez-Castañeda, A.P., Silverberg, N., Aguirre-Bahena, F., Sapozhnikov, D., and Pérez-Cruz, L. (2010). "Arsenic and uranium in the settling particulate matter and sediments of Alfonso Basin, La Paz Bay", in: Proceedings of the 13th International Conference on Water-Rock Interaction. (Guanajuato).

Choumiline, K. (2011). Geoquímica de la materia particulada en hundimiento y de los sedimentos recientes de Cuenca Alfonso, Bahía de La Paz. Master's Thesis, Centro Interdisciplinario de Ciencias Marinas - Instituto Politécnico Nacional.

Cumberland, S.A., Douglas, G., Grice, K., and Moreau, J.W. (2016). Uranium mobility in organic matter-rich sediments: A review of geological and geochemical processes. Earth-Science Reviews 159, 160-185.

Dang, D.H., Novotnik, B., Wang, W., Georg, R.B., and Evans, R.D. (2016). Uranium isotope fractionation during adsorption, (co)precipitation, and biotic reduction. Environmental Science & Technology 50, 12695-12704.

Dunk, R.M., Mills, R.A., and Jenkins, W.J. (2002). A reevaluation of the oceanic uranium budget for the Holocene. Chemical Geology 190, 45-67.

Fischer, R., Galli-Olivier, C., Gidde, A., and Schwennicke, T. (1995). The El Cien Formation of southern Baja California, Mexico: Stratigraphic precisions. Newsletters on Stratigraphy 32, 137-161.

Fisher, N.S., Teyssié, J.L., Krishnaswami, S., and Baskaran, M. (1987). Accumulation of Th, Pb, U, and Ra in marine phytoplankton and its geochemical significance. Limnology and Oceanography 32, 131-142.

Flintrop, C.M., Rogge, A., Miksch, S., Thiele, S., Waite, A.M., and Iversen, M.H. (2018). Embedding and slicing of intact in situ collected marine snow. Limnology and Oceanography: Methods 16, 339-355.

GeoInfoMex by Servicio Geológico Mexicano. https://www.sgm.gob.mx/GeoInfoMexGobMx/

Gonzalez-Yajimovich, O.E., Gorsline, D.S., and Douglas, R.G. (2007). Frequency and sources of basin floor turbidites in Alfonso Basin, Gulf of California, Mexico: Products of slope failures. Sedimentary Geology 199, 91-105.

Gorsline, D.S., De Diego, T., and Nava-Sanchez, E.H. (2000). Seismically triggered turbidites in small margin basins: Alfonso Basin, Western Gulf of California and Santa Monica Basin, California Borderland. Sedimentary Geology 135, 21-35.

Hakspiel-Segura, C., Martínez-López, A., Pinedo-González, P., Verdugo-Díaz, G., and Acevedo-Acosta, J.D. (2016). Composition of metals in suspended particulate matter of Alfonso basin, southern Gulf of California. Regional Studies in Marine Science 3, 144-153.

Hausback, B.P. (1984). "Cenozoic, volcanic and tectonic evolution of Baja California Sur, Mexico," in Geology of the Baja California Peninsula, ed. V.A. Frizzel. (Bakersfield, California), 219-236.

Henderson, G.M. (2002). Seawater ($^{234}U/^{238}U$) during the last 800 thousand years. Earth and Planetary Science Letters 199, 97-110.

Henderson, G.M., and Anderson, R.F. (2003). The U-series Toolbox for Paleoceanography. Reviews in Mineralogy and Geochemistry 52, 493-531.

Hinojosa, J.L., Stirling, C.H., Reid, M.R., Moy, C.M., and Wilson, G.S. (2016). Trace metal cycling and $^{238}U/^{235}U$ in New Zealand's fjords: Implications for reconstructing global paleoredox conditions in organic-rich sediments. Geochimica et Cosmochimica Acta 179, 89-109.

Homoky, W.B., Weber, T., Berelson, W.M., Conway, T.M., Henderson, G.M., Van Hulten, M., Jeandel, C., Severmann, S., and Tagliabue, A. (2016). Quantifying trace element and isotope fluxes at the ocean–sediment boundary: a review. Philosophical Transactions A 374, 20160246.

Klinkhammer, G.P., and Palmer, M.R. (1991). Uranium in the oceans: Where it goes and why. Geochimica et Cosmochimica Acta 55, 1799-1806.

Ku, T.-L., Knauss, K.G., and Mathieu, G.G. (1977). Uranium in open ocean: concentration and isotopic composition. Deep Sea Research 24, 1005-1017.

Lau, K.V., Romaniello, S.J., and Zhang, F. (2019). The Uranium Isotope Paleoredox Proxy. Elements in Geochemical Tracers in Earth System Science.

Lehto, N., Glud, R.N., Á Norði, G., Zhang, H., and Davison, W. (2014). Anoxic microniches in marine sediments induced by aggregate settlement: biogeochemical dynamics and implications. Biogeochemistry.

Lovley, D.R., Phillips, E.J.P., Gorby, Y.A., and Landa, E.R. (1991). Microbial reduction of uranium. Nature 350, 413-416.

Lyons, T.W., Reinhard, C.T., and Planavsky, N.J. (2014). The rise of oxygen in Earth's early ocean and atmosphere. Nature 506, 307-315.

Lyons, T.W., Werne, J.P., Hollander, D.J., and Murray, R.W. (2003). Contrasting sulfur geochemistry and Fe/Al and Mo/Al ratios across the last oxic-to-anoxic transition in the Cariaco Basin, Venezuela. Chemical Geology 195, 131-157.

Martiny, A.C., Vrugt, J.A., and Lomas, M.W. (2014). Concentrations and ratios of particulate organic carbon, nitrogen, and phosphorus in the global ocean. Scientific Data 1, 140048.

McKee, B.A., and Todd, J.F. (1993). Uranium behavior in a permanently anoxic fjord: Microbial control? Limnology and Oceanography 38, 408-414.

McManus, J., Berelson, W.M., Klinkhammer, G.P., Hammond, D.E., and Holm, C. (2005). Authigenic uranium: Relationship to oxygen penetration depth and organic carbon rain. Geochimica et Cosmochimica Acta 69, 95-108.

Meyers, P.A. (1994). Preservation of elemental and isotopic source identification of sedimentary organic matter. Chemical Geology 114, 289-302.

Montoya-Pino, C., Weyer, S., Anbar, A.D., Pross, J., Oschmann, W., Van De Schootbrugge, B., and Arz, H.W. (2010). Global enhancement of ocean anoxia during Oceanic Anoxic Event 2: A quantitative approach using U isotopes. Geology 38, 315-318.

Morales-Acuña, E., Torres, C., Delgadillo-Hinojosa, F., Linero-Cueto, J., Santamaría-Del-Ángel, E., and Castro, R. (2019). The Baja California Peninsula, a significant source of dust in Northwest Mexico. Atmosphere 10, 582.

Morford, J.L., and Emerson, S. (1999). The geochemistry of redox sensitive trace metals in sediments. Geochimica et Cosmochimica Acta 63, 1735-1750.

Murphy, M.J., Stirling, C.H., Kaltenbach, A., Turner, S.P., and Schaefer, B.F. (2014). Fractionation of $^{238}U/^{235}U$ by reduction during low temperature uranium mineralisation processes. Earth and Planetary Science Letters 388, 306-317.

Noordmann, J., Weyer, S., Montoya-Pino, C., Dellwig, O., Neubert, N., Eckert, S., Paetzel, M., and Böttcher, M.E. (2015). Uranium and molybdenum isotope systematics in modern euxinic basins: Case studies from the central Baltic Sea and the Kyllaren fjord (Norway). Chemical Geology 396, 182-195.

Partin, C.A., Lalonde, S.V., Planavsky, N.J., Bekker, A., Rouxel, O.J., Lyons, T.W., and Konhauser, K.O. (2013). Uranium in iron formations and the rise of atmospheric oxygen. Chemical Geology 362, 82-90.

Piper, D.Z. (1991). Geochemistry of a Tertiary sedimentary phosphate deposit: Baja California Sur, Mexico. Chemical Geology 92, 283-316.

Piper, D.Z. (1994). Seawater as the source of minor elements in black shales, phosphorites and other sedimentary rocks. Chemical Geology 114, 95-114.

Pitcher, A., Villanueva, L., Hopmans, E.C., Schouten, S., Reichart, G.J., and Sinninghe Damste, J.S. (2011). Niche segregation of ammonia-oxidizing archaea and anammox bacteria in the Arabian Sea oxygen minimum zone. ISME J 5, 1896-1904.

Rademacher, L.K., Lundstrom, C.C., Johnson, T.M., Sanford, R.A., Zhao, J., and Zhang, Z. (2006). Experimentally determined uranium isotope fractionation during reduction of hexavalent U by bacteria and zero valent iron. Environmental Science & Technology 40, 6943-6948.

Redfield, A.C. (1934). On the proportions of organic derivates in sea water and their relation to the composition of plankton. James Johnstone Memorial Volume, 176-192.

Richter, S., Alonso-Munoz, A., Eykens, R., Jacobsson, U., Kuehn, H., Verbruggen, A., Aregbe, Y., Wellum, R., and Keegan, E. (2008). The isotopic composition of natural uranium samples—Measurements using the new $n(^{233}U)/n(^{236}U)$ double spike IRMM-3636. International Journal of Mass Spectrometry 269, 145-148.

Rochin-Bañaga, H. (2014). Contribución de cocolitóforos y foraminíferos al flujo de carbonato de calcio en Cuenca Alfonso, B.C.S. Master's Thesis, Centro Interdisciplinario de Ciencias Marinas - Instituto Politécnico Nacional.

Rodríguez-Castañeda, A.P. (2002). Elementos mayores y traza en sedimentos y macroalgas de la Bahía de La Paz, Baja California Sur, México. Master's Thesis, Centro Interdisciplinario de Ciencias Marinas - Instituto Politécnico Nacional.

Rodríguez-Castañeda, A.P. (2008). Variación de flujos de los elementos particulados en Cuenca Alfonso, Bahía de La Paz, en el periodo 2002-2005. Ph.D. Thesis, Centro Interdisciplinario de Ciencias Marinas - Instituto Politécnico Nacional.

Rolison, J.M., Stirling, C.H., Middag, R., and Rijkenberg, M.J.A. (2017). Uranium stable isotope fractionation in the Black Sea: Modern calibration of the $^{238}U/^{235}U$ paleo-redox proxy. Geochimica et Cosmochimica Acta 203, 69-88.

Romaniello, S.J., Herrmann, A.D., and Anbar, A.D. (2013). Uranium concentrations and $^{238}U/^{235}U$ isotope ratios in modern carbonates from the Bahamas: Assessing a novel paleoredox proxy. Chemical Geology 362, 305-316.

Segovia-Zavala, J.A., Delgadillo-Hinojosa, F., Lares-Reyes, M.L., Huerta-Diaz, M.A., Muñoz-Barbosa, A., and Torres-Delgado, E.V. (2009). Atmospheric input and concentration of dissolved iron in the surface layer of the Gulf of California. Ciencias Marinas 35, 75-90.

Silverberg, N., Aguirre-Bahena, F., and Mucci, A. (2014). Time-series measurements of settling particulate matter in Alfonso Basin, La Paz Bay, southwestern Gulf of California. Continental Shelf Research 84, 169-187.

Silverberg, N., Shumilin, E., Aguirre-Bahena, F., Rodríguez-Castañeda, A.P., and Sapozhnikov, D. (2007). The impact of hurricanes on sedimenting particulate matter in the semi-arid Bahía de La Paz, Gulf of California. Continental Shelf Research 27, 2513-2522.

Stirling, C.H., Andersen, M.B., Warthmann, R., and Halliday, A.N. (2015). Isotope fractionation of $^{238}U$ and $^{235}U$ during biologically-mediated uranium reduction. Geochimica et Cosmochimica Acta 163, 200-218.

Stylo, M., Neubert, N., Roebbert, Y., Weyer, S., and Bernier-Latmani, R. (2015). Mechanism of uranium reduction and immobilization in Desulfovibrio vulgaris biofilms. Environmental Science & Technology 49, 10553-10561.

Stylo, M., Neubert, N., Wang, Y., Monga, N., Romaniello, S.J., Weyer, S., and Bernier-Latmani, R. (2015). Uranium isotopes fingerprint biotic reduction. Proceedings of the National Academy of Sciences 112, 5619-5624.

Tissot, F.L.H., and Dauphas, N. (2015). Uranium isotopic compositions of the crust and ocean: Age corrections, U budget and global extent of modern anoxia. Geochimica et Cosmochimica Acta 167, 113-143.

Tribovillard, N., Algeo, T.J., Lyons, T., and Riboulleau, A. (2006). Trace metals as paleoredox and paleoproductivity proxies: An update. Chemical Geology 232, 12-32.

Ulloa, O., Canfield, D.E., Delong, E.F., Letelier, R.M., and Stewart, F.J. (2012). Microbial oceanography of anoxic oxygen minimum zones. Proceedings of the National Academy of Sciences 109, 15996-16003.

Verbruggen, A., Alonso-Munoz, A., Eykens, R., Kehoe, F., Kuhen, H., Richter, S., and Arbegbe, Y. (2008). Preparation and certification of IRMM-3636, IRMM-3636a and IRMM-3636b. JRC Scientific and Technical Reports.

Wakeham, S.G., Amann, R., Freeman, K.H., Hopmans, E.C., Jørgensen, B.B., Putnam, I.F., Schouten, S., Sinninghe Damsté, J.S., Talbot, H.M., and Woebken, D. (2007). Microbial ecology of the stratified water column of the Black Sea as revealed by a comprehensive biomarker study. Organic Geochemistry 38, 2070-2097.

Wedepohl, K.H. (1995). The composition of the continental crust. Geochimica et Cosmochimica Acta 59, 1217-1232.

Weyer, S., Anbar, A.D., Gerdes, A., Gordon, G.W., Algeo, T.J., and Boyle, E.A. (2008). Natural fractionation of $^{238}U/^{235}U$. Geochimica et Cosmochimica Acta 72, 345-359.

Wignall, P.B., and Myers, K.J. (1988). Interpreting benthic oxygen levels in mudrocks: A new approach. Geology 16, 452.

Wright, J.J., Konwar, K.M., and Hallam, S.J. (2012). Microbial ecology of expanding oxygen minimum zones. Nature Reviews Microbiology 10, 381-394.

Zheng, Y., Anderson, R.B., van Geen, A., and Fleisher, M.Q. (2002). Preservation of particulate non-lithogenic uranium in marine sediments. Geochimica et Cosmochimica Acta 66, 3085-3092.

## 3.8. SUPPLEMENTARY MATERIALS

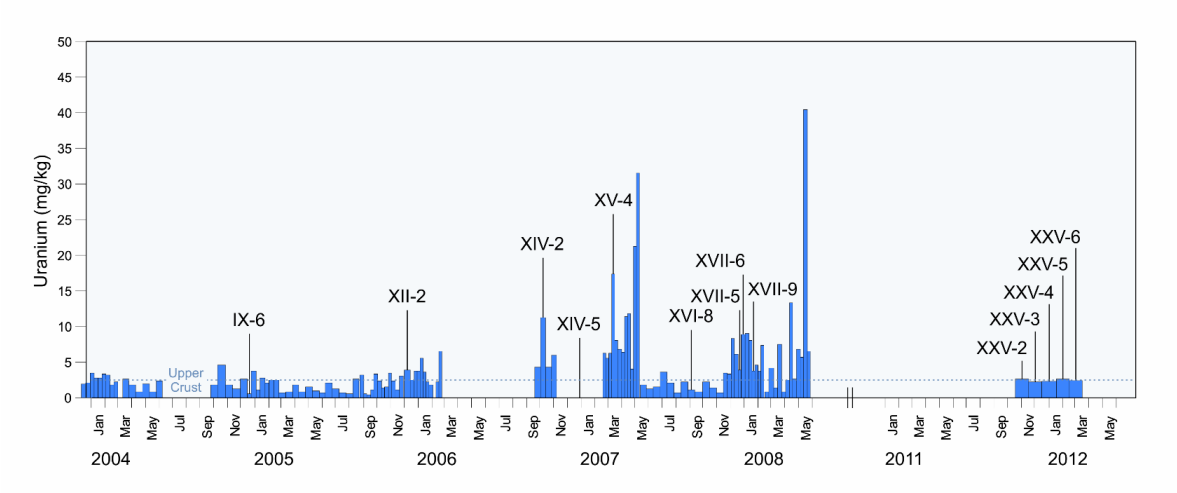


**Supplementary Figure 3.1.** Uranium concentrations and sample codes in settling particulate matter samples selected for $\delta^{234}U$ and $\delta^{238}U$ determinations. The figure shows the entire time span of U concentrations in sinking particles collected by the sediment trap moored at 360 m depth in Alfonso Basin, Gulf of California (Data from: Rodriguez-Castañeda, 2008; and Choumiline, 2011). The horizontal dotted line represents average Upper Continental Crust concentration values for U (Wedepohl, 1995).

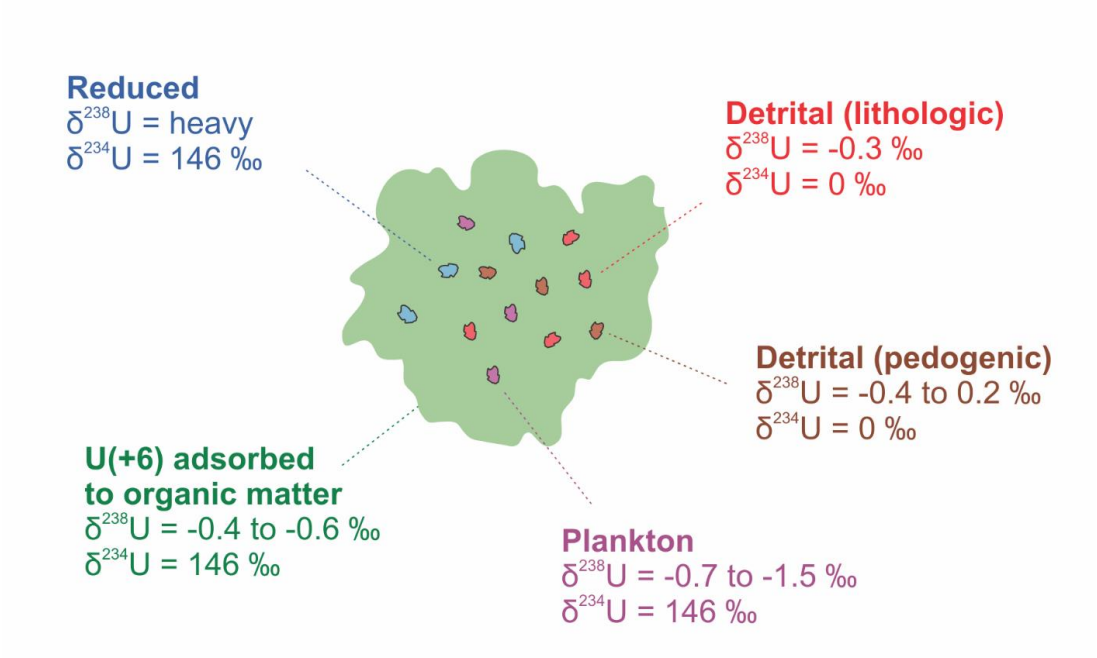


**Supplementary Figure 3.2.** Schematic representing the hypothetical ranges of $\delta^{234}U$ and $\delta^{238}U$ values in marine snow aggregates from Oxygen Minimum Zones

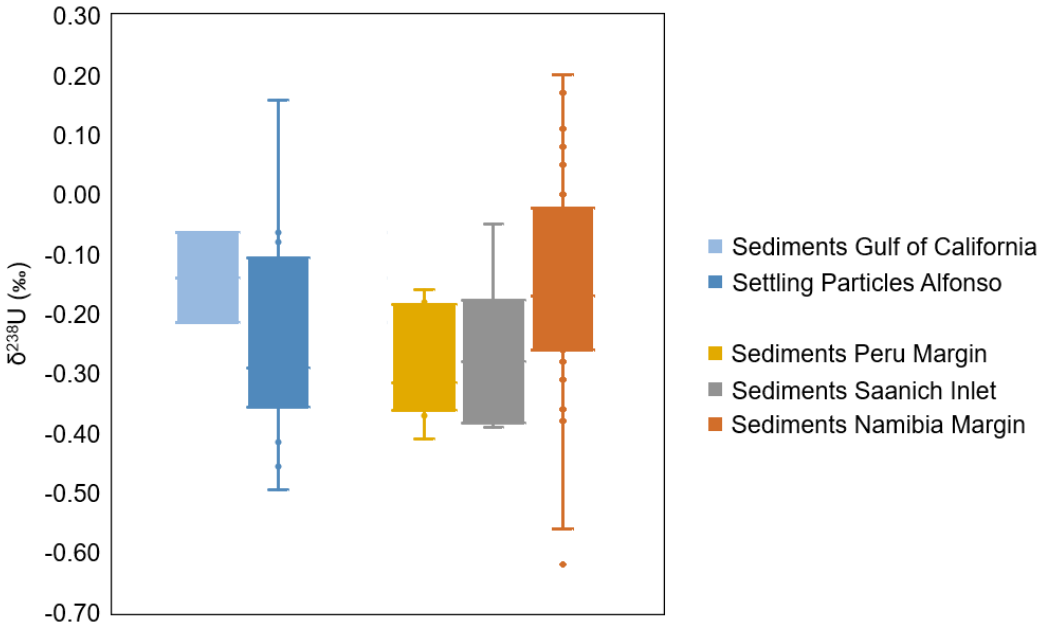


**Supplementary Figure 3.3.** Box and Whisker Plot comparing $\delta^{238}U$ from OMZ-type settings sorted by sediment type and by region (Data from: this study, Choumiline et al., in prep; Weyer et al., 2008; Holmden et al., 2015; Abshire et al., 2020).

# FINAL REMARKS AND SYNTHESIS

The dissertation provided new evidence that trace elements are useful to track not only long-term changes of oxygenation such as glacial-interglacial and millennial variability but also fast-paced OMZ shifts manifested over decadal or even subannual timescales. The major complications for paleoceanographic reconstructions are the reliability of age models (when dating of sedimentary material is out of analytical range), post-depositional remobilization of certain paleoenvironmental indicators ($Ba_{excess}$) and incomplete understanding of the biogeochemistry of classic (U) and novel proxies ($\delta^{238}U$).

Besides generating new sedimentary records of OMZ variability in the ETNP over the Last Glacial Period and into the present recorded in classic (trace elements, Fe-S relationships) and novel proxies (U isotopes), a major outcome of this research was finding a strong covariation between biologically-active element Ni and authigenic U ($U_{auth}$) exclusively during past events of high marine productivity. These periods, characterized by elevated organic carbon burial, were not as enriched in V and Mo as they were in Ni and $U_{auth}$.

There is growing evidence that suggests that in OMZs several trace elements like uranium can actively accumulate in marine snow aggregates as particles sink (Bianchi et al., 2018; Choumiline et al., 2019). Our findings using U isotopes ($\delta^{238}U$ and $\delta^{234}U$) in sediment trap samples have confirmed multiple sources of detrital and authigenic U enrichment mechanisms in coastal OMZs. Additionally, it is now known that redox microniches are very likely responsible for some authigenic enrichments and potential isotopic fractionation in marine snow aggregates.

As for future research, I suggest the community to focus on complementing classic trace element proxies with isotopic measurements. While $\delta^{234}U$ and $\delta^{238}U$ are slowly receiving more acceptance in the paleoceanographic community, other non-traditional isotopic systems remain in the shadows. It is becoming increasingly relevant to provide validation to $\delta^{60}Ni$, $\delta^{65}Cu$, and $\delta^{66}Zn$ as paleoceanographic and environmental proxies. These micronutrients are actively involved in

marine biogeochemistry and are essential for our understanding of past oceanic processes. The importance of such isotopic systems was highlighted by colleagues from the geochemical community. In order to calibrate these proxies in the modern ocean, multidisciplinary efforts bridging isotopic geochemistry with marine biology and microbiology will be key. We need to test these isotopes in various components of the marine realm involving river water, seawater, plankton, suspended and settling particulate matter, as well as marine sediments and pore waters. The study of isotopic biogeochemistry on a broad range of components of the marine system will help providing mechanistical insights to allow deciphering modern OMZ dynamics. Fostering the emergence of non-traditional isotopic toolboxes not limited to $\delta^{234}U$, $\delta^{238}U$, $\delta^{60}Ni$, $\delta^{65}Cu$, and $\delta^{66}Zn$, will allow us to produce more reliable paleoceanographic reconstructions, while at the same time finding proper past analogs for future OMZ changes.